

Robust computational methods to simulate slow-fast dynamical systems governed by predator-prey models

Woinshet D. Mergia



Thesis Submitted for the Degree of **DOCTOR OF PHILOSOPHY** in the
Department of Mathematics and Applied Mathematics at the Faculty of Natural
Sciences

UNIVERSITY OF THE WESTERN CAPE

Supervisor: Prof. Kailash C. Patidar

September 2019

KEYWORDS

Singularly perturbed problems

Slow-fast predator-prey model

Slow-fast eco-evolutionary model

Competition-diffusion models

Geometric singular perturbation theory

Relaxation oscillation

Spatio-temporal pattern

High-order multirate schemes

High-order multi-method schemes

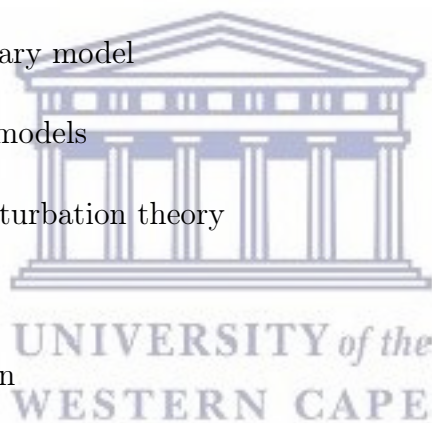
Anderson's acceleration fixed point iterative algorithm

Jacobian-free Newton-Krylov method

Stability analysis

Convergence analysis

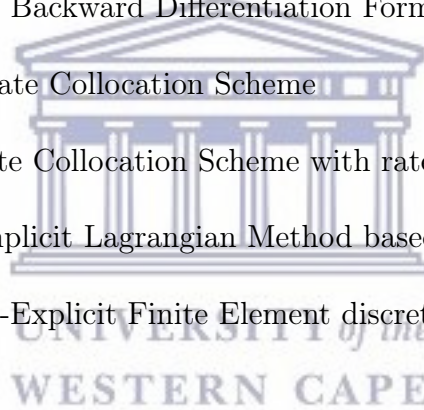
Finite element methods



List of abbreviations

Abbreviations	Descriptions
JFNK	Jacobian-Free Newton-Krylov
AA	Anderson's Acceleration
IVP	Initial Value Problem
CN	Crank-Nicholson
BDF	Backward Differentiation Formula
LF	Leap-Frog
RK	Runge-Kutta
EE	Explicit forward Euler
IE	Implicit backward Euler
FSTS	Fractional-Step θ -Scheme
FSMIMEX	Fractional-Step Mixed Implicit-Explicit
GMRES	Generalized Minimal RESidual
MTS	Monolithic θ -Scheme
CNLF	Crank-Nicholson-Leapfrog
Mrate	Multirate

IMEX-BDF	Implicit-Explicit Backward Differentiation Formula
IMEX-BDF _{<i>k</i>}	Implicit-Explicit Backward Differentiation Formula of order <i>k</i>
IMEX-LG	Implicit-Explicit Lagrange
IMEX-LG _{<i>k</i>}	Implicit-Explicit Lagrange of order <i>k</i>
IM-LG	Implicit Lagrange
EX-LG	Explicit Lagrange
IM-BDF	Implicit Backward Differentiation Formula
EX-BDF	Explicit Backward Differentiation Formula
SCS	Single-rate Collocation Scheme
MCS _{<i>m</i>}	Multirate Collocation Scheme with rate <i>m</i>
SILM-FE	Semi-implicit Lagrangian Method based finite element discretization
IMEX-FE	Implicit-Explicit Finite Element discretization



ABSTRACT

**Robust computational methods to simulate slow-fast dynamical systems
governed by predator-prey models**

by

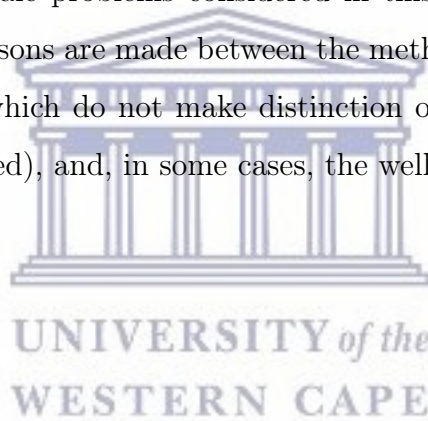
Woinshet D. Mergia

**PhD thesis, Department of Mathematics and Applied Mathematics,
Faculty of Natural Sciences, University of the Western Cape**

Numerical approximations of multiscale problems of important applications in ecology are investigated. One of the class of models considered in this work are singularly perturbed (slow-fast) predator-prey systems which are characterized by the presence of a very small positive parameter representing the separation of time-scales between the fast and slow dynamics. Solution of such problems involve multiple scale phenomenon characterized by repeated switching of slow and fast motions, referred to as *relaxation-oscillations*, which are typically challenging to approximate numerically. Granted with a priori knowledge, various time-stepping methods are developed within the framework of partitioning the full problem into fast and slow components, and then numerically treating each component differently according to their time-scales. Nonlinearities that arise as a result of the application of the implicit parts of such schemes are treated by using iterative algorithms, which are known for their superlinear convergence, such as the Jacobian-Free Newton-Krylov (JFNK) and the Anderson's Acceleration (AA) fixed point methods. The other class of problems considered are competition-diffusion problems in which species diffusion take place at a much slower time-scale than the rate of competition of species. Solutions of these problems exhibit interesting spatio-temporal

coexistence patterns and transient regimes. For their numerical approximations, a conforming finite element method for the spatial discretization is combined with temporal integration techniques in which the linear (and less dominant) diffusion parts are treated implicitly, while, the (more dominant) nonlinear competition terms are discretized by using novel semi-implicit schemes. Considerable attention is focused on the formulation of the methods, and their convergence and stability analysis, needed for their numerical realization applied to complex and nonlinear problems of multiscale nature. A series of numerical experiments are conducted to demonstrate the effectiveness and the capability of these methods in capturing the various essential solution features of the multiscale problems considered in this work, with good stability behaviour. Also, comparisons are made between the methods developed here and related monolithic methods (which do not make distinction on the scale differences between the components involved), and, in some cases, the well-known solvers from literature.

September 2019.



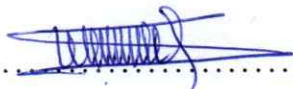
DECLARATION

I declare that *Robust computational methods to simulate slow-fast dynamical systems governed by predator-prey models* is my own work, that it has not been submitted before for any degree or examination at any other university, and that all sources I have used or quoted have been indicated and acknowledged by complete references.

Woinshet D. Mergia

September 2019

Signed



ACKNOWLEDGEMENT

First of all, I would like to thank the almighty God for all He has done for me – for making my dream come true, relieving me from all the burdens, helping me finish this long journey with success.

My deepest gratitude goes to my supervisor Professor Kailash C. Patidar, for his continued support, encouragement, critical direction, friendly approach, politeness and his invaluable advise on academic and non academic issues. This thesis would not have been possible without his continued patience, understanding and support.

I would like to thank the University of the Western Cape (UWC) and African Institute of Mathematical Science (AIMS) for their financial support of this PhD programme.

I have no words to express my gratefulness for my dear husband, Dr. Mebratu Fenta Wakeni, for his endless support, guidance, concern, kindness, amazing and creative ideas. You were sharing all my burdens each and every second throughout this long journey. Because you are by my side, I feel confident to having go through this. You showed me the meaning of true love practically. May God pay you the price by adding more and more to your beautiful and creative mind.

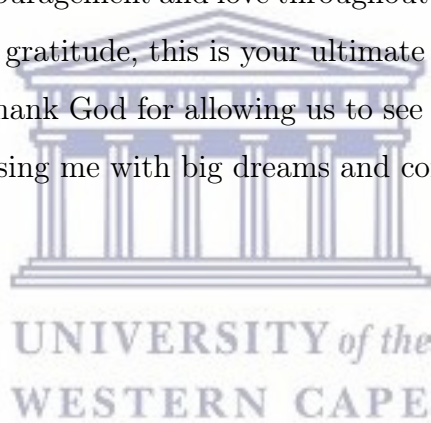
To my bundle of Joy daughter, Hasset Mebratu, you were my reason to keep pushing with all my energy. My only regret is making your initial existence a little unstable because of my study. This is my best gift ever that I can give you and your little brother Milki Mebratu. I hope you will be proud of it. I love you so much, my little angels!

My best friends Yemsrach Zewdu, Abdu Mohammed, Yahya Aly and Hagos Hailu,

thank you for being there for me when I need your encouragement and support during the ups and downs of my study. My special thanks goes to Meaza Fentahun for your great and motivational support, encouragement and advice when I felt lost in those tough times of the journey.

A very special thanks goes to my other family members Yenealem Alemu, Lemlem Fenta, Atsede Fenta and Sinke Alemu for giving your full love and attention to take care of my daughter Hasset during the second year her life.

Last but not least, my special thanks goes to my mother Ayelech Yirgu and my siblings Yemisrach Defar and Aleign Defar and Leta Temesgen for their daily prayer, emotional support, encouragement and love throughout my life. My father Defar Merga you deserve my special gratitude, this is your ultimate dream that you held for me for so long, and I always thank God for allowing us to see this day come true. Thank you for believing in me, raising me with big dreams and confidence to be the person I am.



DEDICATION

Dedicated to my father, my children and my husband.



UNIVERSITY *of the*
WESTERN CAPE

Contents

Keywords	i
Abbreviations	iii
Abstract	v
Declaration	vi
Acknowledgement	viii
Dedication	ix
List of Tables	xvi
List of Figures	xxiii
List of Publications	xxv
1 General introduction	1
1.1 Some background on models of predator-prey population dynamical systems	2
1.1.1 Slow-fast systems	5
1.1.2 A competition-diffusion problem	9
1.2 An overview on geometric method of singular perturbation theory . . .	11
1.3 Literature review on some numerical methods for multiscale problems .	14



1.4	Outline of the thesis	17
2	Efficient simulation of a slow-fast dynamical system using multirate finite difference schemes	20
2.1	Introduction	21
2.2	The mathematical model	23
2.3	Multirate base methods	29
2.4	Stability analysis of the numerical methods	32
2.5	Numerical results	48
2.6	Summary and discussion	54
3	Fractional-step θ-methods for singularly perturbed problems in ecology	55
3.1	Introduction	56
3.2	The mathematical model	59
3.2.1	Analysis via geometric singular perturbation theory	60
3.3	Numerical methods	64
3.3.1	Monolithic θ -method	64
3.3.2	Fractional-step θ -method	65
3.3.3	Fractional-step mixed implicit-explicit method	68
3.4	Iterative treatment of nonlinearities	69
3.4.1	Jacobian-Free Newton-Krylov method	70
3.4.2	Anderson's acceleration method	71
3.5	Stability analysis of the discrete schemes	73
3.6	Numerical results	77
3.7	Summary and discussion	89
4	A class of high-order IMEX linear multistep method for slow-fast model	90
4.1	Introduction	91

4.2	The mathematical model and its qualitative analysis	94
4.2.1	Coupled ecological and evolutionary dynamics	94
4.2.2	Analysis of (4.2.2) using geometric singular perturbation theory	96
4.3	High-order multistep IMEX methods for slow-fast problems	100
4.3.1	The Crank-Nicholson–Leapfrog (CNLF)	101
4.3.2	The Backward Differentiation Formula (BDF)	103
4.3.3	A Multistep Lagrange implicit-explicit (IMEX-LG) scheme	105
4.3.4	Convergence and linear stability analysis of the LG schemes	109
4.4	An order consistent starting solution scheme	114
4.5	Iterative treatment of nonlinearities using Anderson’s acceleration method	117
4.6	Numerical results	118
4.7	Summary and discussion	127
5	A family of fully implicit, high-order, multirate collocation method	129
5.1	Introduction	130
5.2	The mathematical model and its qualitative analysis	132
5.2.1	The eco-evolutionary model	132
5.2.2	Linear stability analysis of the model	133
5.3	A fully-implicit multirate collocation methods for the slow-fast system (5.2.1)	135
5.3.1	Collocation of the slow and fast components	136
5.3.2	Convergence and stability analysis of the scheme	142
5.4	Iterative treatment of nonlinearities: Anderson’s Acceleration method	146
5.5	Numerical results	146
5.6	Summary and discussion	150
6	A semi-implicit multistep methods with finite element for competition- diffusion problems	153
6.1	Introduction	154
6.2	The Lotka-Volterra competition-diffusion model	156

6.3	The numerical method	158
6.3.1	Spatial discretization: Galerkin finite element method	158
6.3.2	Temporal integration: a high-order semi-implicit method	160
6.3.3	Convergence and stability analysis	162
6.4	Numerical results	167
6.5	Summary and discussion	168
7	An asymptotically consistent semi-implicit scheme for competition-diffusion problems	176
7.1	Introduction	177
7.2	A three-species competitive-diffusion model	179
7.3	The numerical method	183
7.3.1	Spatial discretization: Galerkin finite element method	183
7.3.2	Temporal integration	185
7.3.3	Stability analysis	187
7.4	Numerical results	189
7.5	Summary and discussion	190
8	Concluding remarks and scope for future research	195
	Bibliography	200

List of Tables

2.5.1 Comparison of efficiency of single-rate explicit Euler and multirate ($m = 4$) explicit Euler method	49
2.5.2 Comparison of efficiency of single-rate linearly-implicit Euler and multirate ($m = 4$) linearly-implicit Euler method.	49
2.5.3 Comparison of efficiency of single-rate CN and multirate ($m = 4$) CN method.	49
2.5.4 Comparison of the convergence profile of the single-rate ($m = 1$) of the three methods: explicit Euler (M1), linearly-implicit Euler (M2) and CN (M3); LC: Limit Cycle.	50
2.5.5 Comparison of the convergence profile of the multirate ($m = 4$) of the three methods: explicit Euler (M1), linearly-implicit Euler (M2) and CN (M3); LC: Limit Cycle.	50
3.6.1 Comparison of stability profiles of MTS, FSTS and FSMIMEX methods with rates $r = 2$	85
3.6.2 Comparison of stability profiles of MTS, FSTS and FSMIMEX methods with rates $r = 4$	86
4.3.1 Coefficient vectors of the IMEX-LG schemes as given in (4.3.27) for $\theta = 0.5$	108
4.3.2 Coefficient vectors of the IMEX-BDF schemes as given in (4.3.27) for $\theta = 1$	109
4.3.3 Zero-stability of the LG methods for $\theta = 0.5$	110

4.6.1	Maximum errors and order of convergence of the implicit (IM-CN), explicit (EX-LF) and the implicit-explicit (IMEX-CNLF) schemes. Here $\varepsilon = 0.1$, $\text{To1} = 10^{-12}$, and final time $T = 1$	120
4.6.2	Maximum errors and order of convergence of the implicit (IM-BDF2), explicit (EX-BDF2) and the implicit-explicit (IMEX-BDF2) schemes. Here $\varepsilon = 0.1$, $\text{To1} = 10^{-12}$, and final time $T = 1$	120
4.6.3	Maximum errors and order of convergence of the implicit (IM-BDF4), explicit (EX-BDF4) and the implicit-explicit (IMEX-BDF4) schemes. Here $\varepsilon = 0.1$, $\text{To1} = 10^{-12}$, and final time $T = 1$	120
4.6.4	Maximum errors and order of convergence of the implicit (IM-LG2), explicit (EX-LG2) and the implicit-explicit (IMEX-LG2) schemes. Here $\varepsilon = 0.1$, $\text{To1} = 10^{-12}$, and final time $T = 1$	121
4.6.5	Maximum errors and order of convergence of the implicit (IM-LG4), explicit (EX-LG4) and the implicit-explicit (IMEX-LG4) schemes. Here $\varepsilon = 0.1$, $\text{To1} = 10^{-12}$, and final time $T = 1$	121
4.6.6	CPU comparison of the second-order of the IMEX-BDF2, IMEX-LG2 and IMEX-CNLF and their corresponding implicit IM-BDF2, IM-LG2 and IM-CNLF with parameters $\varepsilon = 0.1$, $\text{To1} = 10^{-12}$ and final time $T = 10$	122
4.6.7	CPU comparison of the third-order of the IMEX-BDF3 and IMEX-LG3 and their corresponding implicit IM-BDF3 and IM-LG3 with parameters $\varepsilon = 0.1$, $\text{To1} = 10^{-11}$ and final time $T = 10$	122
4.6.8	CPU comparison of the fourth-order of the IMEX-BDF4 and IMEX-LG4 and their corresponding implicit IM-BDF4 and IM-LG4 with parameters $\varepsilon = 0.1$, $\text{To1} = 10^{-11}$ and final time $T = 10$	122
5.2.1	Summary of the linear stability analysis for the system (5.2.1) (here, v_i , $i = 1, 2$ satisfies (5.2.4)).	134

5.5.1 Maximum error of the single-rate (SCS)and multirate (MCS4) collocation scheme of second-order. Here $\varepsilon = 0.025$; $T = 1$; $To1 = 10^{-10}$	147
5.5.2 Maximum error of the single-rate (SCS)and multirate (MCS4) collocation scheme of third-order. Here $\varepsilon = 0.025$; $T = 1$; $To1 = 10^{-10}$	147
5.5.3 Maximum error of the single-rate (SCS)and multirate (MCS4) collocation scheme of fourth-order. Here $\varepsilon = 0.025$; $T = 1$; $To1 = 10^{-10}$	148
6.3.1 Derivative and extrapolation coefficient vectors.	161



UNIVERSITY *of the*
WESTERN CAPE

List of Figures

1.1.1 Phase portrait for Lotka-Volterra model ($e = 0.5$, $r = 1.2$, $\beta = 0.8$, $m = 0.6$).	4
2.5.1 Simulation results displaying predators and prey over time using extrapolated explicit Euler method with single-rate ($m = 1$) (upper figures) and explicit Euler method with multirate rate ($m = 4$) (lower figures) applied to the system (2.2.3).	51
2.5.2 Simulation results showing trajectories in the phase space (predators over the prey) using extrapolated explicit Euler method with single-rate ($m = 1$) (upper figures) and explicit Euler method with multirate rate ($m = 4$) (lower figures) applied to the system (2.2.3). The amplitude decreases towards a limit cycle.	51
2.5.3 Simulation results displaying predators and prey over time using extrapolated implicit Euler method with single-rate ($m = 1$) (upper figures) and implicit Euler method with multirate ($m = 4$) (lower figures) applied to the system (2.2.3).	52
2.5.4 Simulation results showing trajectories in the phase space (predators over the prey) using extrapolated implicit Euler method with single-rate ($m = 1$) (upper figures) and implicit Euler method with multirate ($m = 4$) (lower figures) applied to the system (2.2.3). The amplitude decreases towards a limit cycle.	52

2.5.5 Simulation results displaying predators and prey over time using extrapolated single-rate ($m = 1$) Crank-Nicholson method (upper figures) and Crank-Nicholson method with multirate ($m = 4$) (lower figures) applied to the system (2.2.3).	53
2.5.6 Simulation results showing the trajectories in the phase space (predators over the prey) using extrapolated Crank-Nicholson method with single-rate ($m = 1$) (upper figures) and Crank-Nicholson method with multirate ($m = 4$) (lower figures) applied to the system (2.2.3). The amplitude decreases towards a limit cycle.	53
3.3.1 Schematic of fractional-step r -rate algorithm. The broken arrows show the input flow, where as, the solid arrow lines represent stepping from one compartment to the other. The algorithmic flow reads from left to right.	66
3.6.1 Rates of convergence of the monolithic θ -methods with Anderson's acceleration method (left) and with JFNK method (right).	80
3.6.2 Rates of convergence of the fractional-step θ -methods with Anderson's acceleration method (left) and with JFNK method (right).	80
3.6.3 Rates of convergence of schemes with $\theta = 0.5$ using Anderson's acceleration method (left) and JFNK method (right).	80
3.6.4 Comparison of efficiency results of the schemes with $\theta = 0.5$ using JFNK method: accuracy level of the schemes (left) and CPU time (right).	82
3.6.5 Comparison of efficiency results of the schemes with $\theta = 0.5$ using Anderson's acceleration method: accuracy level of the schemes (left) and CPU time (right).	82
3.6.6 Comparison of efficiency results of the schemes with $\theta = 1$ using JFNK method: accuracy level of the schemes (left) and CPU time (right).	83
3.6.7 Comparison of efficiency results of the schemes with $\theta = 1$ using Anderson's acceleration method: accuracy level of the schemes (left) and CPU time (right).	83

3.6.8 Comparison results of number of iterations taken by the monolithic θ -schemes with $\theta = 1.0$ (left) and $\theta = 0.5$ (right), using JFNK and Anderson's acceleration methods.	84
3.6.9 Comparison results of number of iterations taken by the fractional θ -schemes with $\theta = 1.0$ (left) and $\theta = 0.5$ (right), using JFNK and Anderson's acceleration methods.	84
3.6.10 Comparison results of number of iterations taken by the mixed fractional implicit-explicit θ -schemes with $\theta = 1.0$ (left) and $\theta = 0.5$ (right), using JFNK and Anderson's acceleration methods.	84
3.6.11 Simulation results displaying predators and prey over time (left) and trajectories in the phase space (right), using $r = 4$; $H = 0.05$; $T = 200$ and $(x_0, y_0, z_0) = (0.28, 0.001, 0.2)$	86
3.6.12 Simulation results displaying predators and prey over time (left) and trajectories in the phase space (right), using $r = 4$; $H = 0.05$; $T = 200$ and $(x_0, y_0, z_0) = (0.001, 0.2, 0.2)$	86
3.6.13 Simulation results displaying predators and prey over time (left) and trajectories in the phase space (right), using <code>MATLAB ode15s</code> , for $T = 200$ and $(x_0, y_0, z_0) = (0.28, 0.001, 0.2)$ (upper), $(x_0, y_0, z_0) = (0.01, 0.2, 0.2)$ (lower).	87
3.6.14 Simulation results displaying predators and prey over time (left) and trajectories in the phase space (right), using <code>MATLAB ode23s</code> , for $T = 200$ and $(x_0, y_0, z_0) = (0.28, 0.001, 0.2)$ (upper), $(x_0, y_0, z_0) = (0.01, 0.2, 0.2)$ (lower).	88
4.3.1 Stability region: (a) Crank-Nicholson scheme, (b) Leapfrog scheme and (c) and the IMEX-CNLF scheme.	103
4.3.2 Stability region of the BDF schemes of order two (BDF2), three (BDF3) and four (BDF4): The shaded region in the first, second and third row indicates the stability regions of the implicit, explicit and IMEX schemes, respectively.	106

4.3.3 Stability region of the Lagrange based schemes of order two (LG2), three (LG3) and four (LG4): The shaded region in the first, second and third row indicates the stability regions of the implicit, explicit and IMEX schemes, respectively.	115
4.6.1 Successive mesh refinement. The open dots denote the common nodes at which maximum errors are computed.	119
4.6.2 Comparison of the maximum error obtained by the second-order schemes IMEX-LG2, IMEX-BDF2 and IMEX-CNLF at various time-steps applied to (4.2.2). Here $\varepsilon = 0.1$, and $To1 = 10^{-12}$	123
4.6.3 Comparison of the maximum error obtained by the third-order schemes IMEX-LG3 and IMEX-BDF3 (a), and fourth-order schemes IMEX-BDF4 and IMEX-LG4 (b), at various time-steps applied to (4.2.2). Here $\varepsilon = 0.1$ and $To1 = 10^{-12}$	123
4.6.4 Comparison of the maximum error obtained by the second-order schemes IMEX-CNLF (a), IMEX-BDF2 (b), and IMEX-LG2 (c), at various time-steps applied to (4.2.2). Here $\varepsilon = 0.5, 0.1, 0.025$, and $To1 = 10^{-11}$	124
4.6.5 Comparison of the maximum error obtained by the third-order schemes IMEX-BDF3 (a), and IMEX-LG3 (b), at various time-steps applied to (4.2.2). Here $\varepsilon = 0.5, 0.1, 0.025$, and $To1 = 10^{-11}$	125
4.6.6 Comparison of the maximum error obtained by the fourth-order schemes IMEX-BDF4 (a), and IMEX-LG4 (b), at various time-steps applied to (4.2.2). Here $\varepsilon = 0.5, 0.1, 0.025$, and $To1 = 10^{-11}$	125
4.6.7 Eco-evolutionary dynamics of predator-trait and predator-prey interaction over time of the system (4.2.2) which is obtained at different value of separation of time-scale ε	126

4.6.8 Phase space of the system (4.2.2) with the dynamics of predator and the two preys interaction (a); predator, predator-trait and prey (p_1) (b); predator, predator-trait and prey p_2 (c); and the interaction of the two preys with respect to the predator-trait (d). Here the value of separation of time-scale ε is taken as 0.001 and $T = 100$	127
5.3.1 Sub-division of the time domain into macro- and micro-steps.	136
5.3.2 Configurations and types of nodes distributed in the macro-step $[t_n, t_{n+1}]$	138
5.3.3 Piecewise polynomial interpolatory functions corresponding to interior and adjacent fast nodes.	139
5.3.4 Stability regions of the single-rate collocation scheme.	145
5.5.1 Comparison of maximum error results of the SCS and MCS of first-order (a), second-order (b), third-order (c) and fourth-order (d). Here $T = 1$; $\text{To1} = 10^{-10}$; $\varepsilon = 0.1$	149
5.5.2 Comparison of efficiency results (CPUtime) of the SCS and MCS of second-order (right) and accuracy level of the schemes (left). Here $T = 1$; $\text{To1} = 10^{-10}$; $\varepsilon = 0.1$	149
5.5.3 Comparison of efficiency results (CPUtime) of the SCS and MCS of third-order (right) and accuracy level of the schemes (left). Here $T = 1$; $\text{To1} = 10^{-10}$; $\varepsilon = 0.1$	150
5.5.4 Comparison of efficiency results (CPUtime) of the SCS and MCS of fourth-order (right) and accuracy level of the schemes (left). Here $T = 1$; $\text{To1} = 10^{-11}$; $\varepsilon = 0.1$	150
5.5.5 Simulation results displaying eco-evolutionary dynamics of predator-trait and predator-prey interaction over time of the system (5.2.1) which is obtained using second-order SCS at different value of separation of time-scale ε . Here $T = 10$; $H = 0.005$; $\text{To1} = 10^{-11}$	151

5.5.6 Simulation results displaying eco-evolutionary dynamics of predator-trait and predator-prey interaction over time of the system (5.2.1) which is obtained using second-order MCS2 scheme at different value of separation of time-scale ε . Here $T = 10$; $H = 0.005$; $\text{To1} = 10^{-11}$	152
6.3.1 Spatial convergence of SILM-FE schemes for the model problem (6.2.1) with parameters in (6.3.13). The horizontal axis label ' N ' refers to the number of elements along each side of the square spatial domain.	164
6.3.2 Temporal convergence of the SILM-FE and IMEX-FE schemes applied to the model problem (6.2.1) with same parameters in Figure 6.3.1. Here the horizontal axis label ' N ' refers to the number of time-steps.	164
6.3.3 Convergence in both space and time of SILM-FE and IMEX-FE schemes applied to the model problem (6.2.1) with parameters same as in Figure 6.3.1. Here the space and time meshes are simultaneously refined so that $\Delta t = 2h_x = 2h_y$ and the horizontal axis N refers to the number of elements either of the sides of the spatial square domain (or twice of the number of time-steps). . .	165
6.3.4 Stability regions of the semi-linear multistep methods applied to the reduced nonlinear problem (6.3.16).	167
6.4.1 Simulation of occurrence of segregation pattern of the three species U, V and W with triple junction at different times. Parameters used for the simulation are $a_{ii} = r_i = d_i = 1$, ($i = 1, 2, 3$), $a_{12} = a_{23} = a_{31} = a_{13} = a_{21} = a_{32} = 3$, $\varepsilon = 0.1$, and $\Delta t = 1$	169
6.4.2 Competitive exclusion patterns of the three species U, V and W at different times. Parameters used for the simulation are $a_{ii} = r_i = d_i = 1$, ($i = 1, 2, 3$), $a_{12} = 2$, $a_{31} = 5$, $a_{13} = a_{21} = a_{23} = 3$, $a_{32} = 4$, $\varepsilon = 0.1$, and $\Delta t = 1$	170
6.4.3 Coexistence pattern ('inward' spiral-like) in the dynamics of the three species U, V and W at different times. Parameters used for the simulation are the transpose of $a_{ii} = r_i = d_i = 1$, $a_{12} = a_{23} = a_{31} = 2$, $a_{13} = a_{21} = a_{32} = 7$, $\varepsilon = 0.1$, and $\Delta t = 0.25$	171

6.4.4	Coexistence pattern ('outward' spiral-like) in the dynamics of the three species U, V and W at different times. Parameters used for the simulation are $a_{ii} = r_i = d_i = 1$, ($i = 1, 2, 3$), $a_{12} = a_{23} = a_{31} = 2$, $a_{13} = a_{21} = a_{32} = 7$, $\varepsilon = 0.1$, and $\Delta t = 0.25$	172
6.4.5	Coexistence pattern in the dynamics of the three species U, V and W at different times. Parameters used for the simulation are $a_{ii} = r_i = d_i = 1$, $a_{12} = a_{23} = a_{31} = 2$, $a_{13} = a_{21} = a_{32} = 7$, $\varepsilon = 0.1$, and $\Delta t = 0.25$	173
6.4.6	A spatio-temporal dynamic coexistence pattern ('cluster' shape) of the three species U, V and W at different times. Parameters used for the simulation are $a_{ii} = r_i = d_i = 1$, ($i = 1, 2, 3$), $a_{12} = 3$, $a_{13} = 6$, $a_{21} = 6.5$, $a_{23} = 3.5$, $a_{31} = 2.9$, $a_{32} = 6.1$, $\varepsilon = 0.1$, and $\Delta t = 0.5$	175
7.2.1	Schematic representation of cyclic competition. The arrows indicate the direction of domination.	183
7.3.1	Stability regions of the semi-linearized scheme applied to the reduced nonlinear problem (7.3.13).	189
7.4.1	Droplet-like pattern of the three species at different times. Parameters used for the simulation are $a = 1$, $b = 2$, $\varepsilon_2 = 0.1$, $\varepsilon_3 = 0.6$, and $\Delta t = 1$	191
7.4.2	Strip-like pattern in the dynamics of the three species at different times. Parameters used for the simulation are $a = 1$, $b = 2$, $\varepsilon_2 = 0.1$, $\varepsilon_3 = 0.9$, and $\Delta t = 1$	192
7.4.3	Spiral-like pattern in the dynamics of the three species at different times. Parameters used for the simulation are $a = 1$, $b = 2$, $\varepsilon_2 = 1.0$, $\varepsilon_3 = 1.0$, and $\Delta t = 1$	193
7.4.4	Glider-like patterns of the three species at various times. Parameters used for the simulation are $a = 1$, $b = 2$, $\alpha = 1.3$, $\varepsilon_2 = 0.55$, $\varepsilon_3 = 0.5$, and $\Delta t = 1$	194

List of Publications

Part of this thesis has been published or submitted for publication in the form of the following research articles to international journals.

1. W.D. Mergia and K.C. Patidar, Efficient simulation of a slow-fast dynamical system using multirate finite difference schemes, *Quaestiones Mathematicae* **39(5)** (2016), 689-714.
2. W.D. Mergia and K.C. Patidar, Fractional-step θ -method for solving singularly perturbed problem in ecology, *Advances in Computational Mathematics* **44(3)** (2018) 645-671.
3. W.D. Mergia and K.C. Patidar, A novel high-order IMEX linear multistep methods for a strongly-coupled and nonlinear slow-fast eco-evolutionary model, Submitted for publication .
4. W.D. Mergia and K.C. Patidar, High-order fully implicit multirate collocation methods for a singularly perturbed eco-evolutionary model, Submitted for publication.
5. W.D. Mergia and K.C. Patidar, High-order semi-implicit linear multistep LG scheme for a three-species competition-diffusion system in two-dimensional spatial domain arising in ecology, Submitted for publication.
6. X. Li, W.D. Mergia and K.C. Patidar, A finite element discretization with semi-implicit nonlinear multistep scheme for a two-dimensional competition-diffusion

system of three competing species with different mobility rates, Submitted for publication.



UNIVERSITY *of the*
WESTERN CAPE

Chapter 1

General introduction

Complex systems of biological as well as ecological importance are the most ubiquitous features of the world we live in. Such systems typically involve the evolution of multiple constituent agents interacting at different time- and length-scales. Differential equations are continued to be used extensively in modelling a broad range of biological and ecological phenomena. Particularly, those differential equations that have important relevance to systems evolving at multiple temporal and/or spatial scales belong to the class of singularly perturbed differential equations.

The multiscale nature of singularly perturbed models requires careful attention in the development of numerical solutions. The standard approach for a numerical solution of multi-component problem (or systems of ordinary/partial differential equations) is to use a single computational framework in which, regardless of scale differences that may exist, each component are treated numerically in exactly same way spatially and/or temporally. Such methods have either to be modified, or it becomes essential to employ extremely small discretization parameters for the entire problem, with a consequent significant increase in computational cost. The need to develop computational procedures for problems of singularly perturbed-type that imitates the nature of the dynamics of the continuous problem is therefore self-evident.

Differential equations modelling systems which are composed of multiple interacting components with different time and/or length-scales are generally complex and

nonlinear. Thus their closed form or exact solutions are rarely obtainable. Moreover, for problems of multiscale nature, standard numerical schemes are often not adequate due to the need for computational efficiency with desirable level of accuracy.

An alternative to standard approaches is the class of multirate methods, in which multiple step-sizes are employed to capture the relative scale differences between the constituent components. Multirate methods are significantly superior in terms of efficiency and accuracy features than standard approaches that use a single step-size for all components involved. However, the derivation of high-order multirate methods can potentially be more complicated, particularly when the singularly perturbed problem is nonlinear.

Motivated in large part by the success of multirate methods to provide efficient and robust numerical algorithms to challenging multiscale problems in various applications, the focus of the work presented here is the use of classes of multirate and multi-methods for solutions of multiscale problems in ecology.

Therefore, this thesis is concerned with the formulation, analysis and implementation of high-order and robust such numerical schemes to efficiently solve multiscale ordinary and partial differential equations arising in ecology. Various ordinary and partial differential equations of multiscale nature that arises in predator-prey population dynamical systems are considered, some of which are summarized in the following section.

1.1 Some background on models of predator-prey population dynamical systems

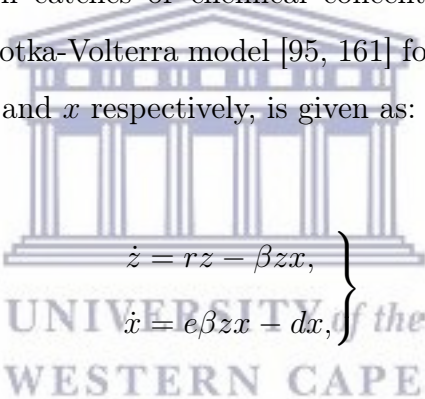
Mathematical models describing the behavior of real-world problems such as population dynamics of predator-prey systems attract the attention of many mathematicians, ecologists as well as biologists, (see for example [16, 102, 151]). The study of predator-prey models is a long existing discipline in mathematical biology [117].

In this section, we present a brief survey of some important classes of predator-prey models considered in the work presented here.

The Lotka-Volterra model

One of the most important and fundamental mathematical models in ecology is the Lotka-Volterra equation which was named after the well-known scientists Alfred Lotka [96] and Vitro Volterra [160]. It is a coupled model representing the nonlinear interaction between different species, for instance, a predator and a prey.

The Lotka-Volterra system was originally developed to explain the oscillatory behaviour observed in fish catches or chemical concentrations in a chemical reaction system [95, 161]. The Lotka-Volterra model [95, 161] for prey and predator population densities, denoted by z and x respectively, is given as:



$$\left. \begin{aligned} \dot{z} &= rz - \beta zx, \\ \dot{x} &= e\beta zx - dx, \end{aligned} \right\} \quad (1.1.1)$$

where the superimposed dots indicate derivative in time, r is the growth rate of the prey, β the death rate of the prey due to predation, e the predator conversion efficiency (which describes what proportion of the prey eaten by the predator yields predator growth), and d the predator death rate.

Since the pioneering Lotka-Volterra model for the temporal evolution of interacting predator and prey population densities [95], exploiter-resource interactions that are described through coupled systems of differential equations have also provided an adaptable modelling approach for applications other than ecology such as epidemiology [17].

The Lotka-Volterra model (1.1.1) exhibits periodic solutions for predator and prey populations. The phase curves form the family of closed curves, as shown in Fig-

Figure 1.1.1, given by

$$U = e\beta z - d \log z + \beta x - r \log x, \quad (1.1.2)$$

around the neutrally stable steady-state $(d/e\beta, r/\beta)$.

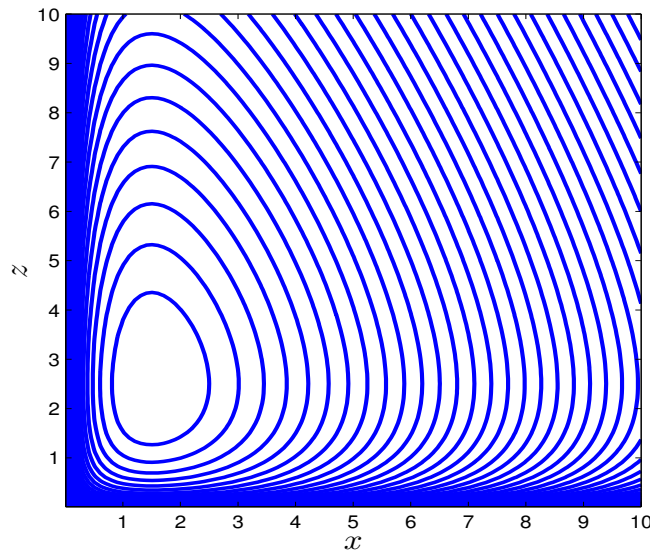


Figure 1.1.1: Phase portrait for Lotka-Volterra model ($e = 0.5$, $r = 1.2$, $\beta = 0.8$, $m = 0.6$).

However, these solutions are structurally unstable, in the sense that a small perturbation in the initial conditions can result in a drastic change in the dynamical system. Although it is not that realistic, the Lotka-Volterra model (1.1.1) has been useful for studying the mechanisms behind oscillatory population behaviour, thereby suggesting further directions to acquire deeper understanding of the observed phenomena.

In 1963, Rosenzweig and MacArthur [131] introduced a modified version of the Lotka-Volterra model with logistic prey growth and a saturating predation term,

$$\left. \begin{aligned} \dot{z} &= z \left[r \left(1 - \frac{z}{K} \right) - \frac{ax}{b+x} \right], \\ \dot{x} &= x \left[\frac{eaz}{b+z} - d \right], \end{aligned} \right\} \quad (1.1.3)$$

where K is the prey carrying capacity, a the maximum consumption rate, and b the half saturation constant for consumption (i.e., the concentration of z at which the predation rate of x reaches half of its maximum value) and d the death rate of the predator.

The Rosenzweig-MacArthur model (1.1.3) reproduces two type of behaviours: co-existence of predator and prey at a steady state, and predator-prey stable limit cycles, which are periodic orbits in phase plane from which small perturbations tend to zero as time $t \rightarrow \infty$. Thus, the amplitude of the predator-prey cycles is independent of the initial conditions (unlike in the Lotka-Volterra model). This model was also reintroduced 20 years later by May [100] and Shimazu et al. [142].

1.1.1 Slow-fast systems

In ecology, some predator-prey population models exhibit oscillatory multiple scale phenomena characterized by repeated switching of slow and fast motions, referred to as relaxation-oscillations. Particularly, models that are considered in this work include systems that evolve in time at two different time-scales, termed as slow-fast systems. Mathematical models of such systems are characterized by the presence of a small parameter $\varepsilon > 0$, often, multiplying the derivative of one of the constituent component, precisely the one with the fastest dynamics.

The behaviour of a slow-fast dynamics can become unexpectedly complex as $\varepsilon \rightarrow 0$, and breaks down at the limiting case, i.e., when $\varepsilon = 0$. Because of this singular property, slow-fast systems fall under the class of singularly perturbed problems. In the following, we briefly discuss some models of predator-prey population dynamics with slow-fast dynamics considered in this work.

Competitive coexistence and exclusion of species

The theory of competition argued by Volterra in his work [160] was that the coexistence of two or more predators competing for fewer resource of prey is not possible, which was later referred to as the principle of competition exclusion. However, in 1974 Koch

[84] re-examined through numerical simulations that the possibility of coexistence of two predators competing exploitatively for a single prey species under a uniform and constant environment, but with the assumption that the predator functional response to the prey density was according to the *Michaelis-Menten kinetics*. This coexistence is appeared to be periodic orbits in the positive octant of a three-dimensional system rather than converging to an equilibrium state. Furthermore, Mc Gehee and Armstrong [103] via numerical experiment showed the possibility of the coexistence of n competing species and fewer than n resources. Unfortunately, these studies do not show clearly the range of the prey and predator parameters guaranteeing coexistence. However, Muratori and Rinaldi [116], using a singular perturbation argument, showed coexistence for the case that the prey has a faster dynamics than the two predators via the reference model,

$$\left. \begin{aligned} \dot{S} &= \gamma S(1 - S/K) - \frac{m_1}{y_1} \frac{x_1 S}{a_1 + S} - \frac{m_2}{y_2} \frac{x_2 S}{a_2 + S}, \\ \dot{x}_i &= \frac{m_i x_i S}{a_i + S} - d_i x_i, \end{aligned} \right\} \quad (1.1.4)$$

where, for $i = 1, 2$, x_i represents the time-varying population density of the i th-predator, S the time-varying population density of the prey, $m_i > 0$ the maximal growth or birth rate of the i th-predator, $d_i > 0$ the death rate of the i th-predator, y_i the yield factor for the i^{th} -predator feeding on the prey, a_i the half-saturation constant for the i th-predator, i.e., the prey density at which the functional response of the predator is half maximal, and $\gamma > 0, K > 0$ are the intrinsic growth rate and the carrying capacity of the prey, respectively. The nonlinear term

$$\frac{m_i}{y_i} \frac{S}{(a_i + S)},$$

is the functional response of the per capita rate at which the predator x_i captures prey S , for $i = 1, 2$.

Muratori and Rinaldi based their analysis on the non-dimensional form of (1.1.4),

that is,

$$\left. \begin{aligned} \varepsilon \dot{z} &= z \left[r \left(1 - \frac{z}{K} \right) - \frac{m_1 x}{\beta_1 + z} - \frac{m_2 y}{\beta_2 + z} \right], \\ \dot{x} &= x \left[\frac{m_1 z}{\beta_1 + z} - d_1 \right], \\ \dot{y} &= y \left[\frac{m_2 z}{\beta_2 + z} - d_2 \right]. \end{aligned} \right\} \quad (1.1.5)$$

Models of predator-prey with an evolutionary trait

Ecological and evolutionary changes occur simultaneously and interact with each other. Inter-specific interactions, which take place between different species in an ecosystem, depend not only on the population densities of the interacting species, but on their phenotypes (which is the interaction of genotype and the environment) as well. On one hand, ecological changes depend on the observable traits of the population, which are directly associated with some specific genes. On the other hand, evolutionary changes, which are mainly driven by natural selection, will change the frequencies of the associated genes in a population from generation to generation. Furthermore, variation in ecologically important species traits yield phenotypic change that occurs at rates comparable to or faster than those of ecological dynamics.

Interactions of a predator and two prey populations, with the two prey species having a limited growth rate, can coexist if they are shared by the predator. However, it has been demonstrated by Geritz et al. [52] that, using the three-dimensional classical Lotka-Volterra model for one predator and two prey with unlimited prey growth, allowing diversity in one type of the prey population leads to extinction of the other prey type with a smaller capacity to survive. In their work the predator-prey interaction of Kiwi-rabbits-stoats were shown as an existing example from New-Zealand.

By considering a case consisting of a predator and multiple preys, one can explicitly examine predator preference towards more abundant prey by constructing models in which, in addition to the densities of the preys and the predator, the predator preference

trait are also included in the list of system variables. It has been demonstrated that adaptive prey switching can promote coexistence of competing prey species [152] or decrease prey competition due to a shared predator [1].

However, adaptivity can also be expressed as an evolutionary change in traits (i.e., properties that affect how well an individual performs as an organism [104]) via genomic changes of a predator and/or prey. If such evolution occurs on a time-scale of about a thousand generations and can be observed in laboratory conditions, it is interpreted to be a rapid evolutionary change of traits [47]. Rapid evolutionary changes have been observed in a wide variety of organisms, ranging from mammals [122] to bacteria [13], and both in predators (for example, in traits that involve resource consumption [58] or the ability to counteract prey defence mechanisms [62]) and in prey (for example, in traits that involve predator avoidance [71, 166]). Understanding the dependencies between rapid evolution and ecological interactions is fundamental for making accurate predictions of a population's ability to adapt to, and persist under, changing environmental conditions [36, 138]. For example, rapid evolutionary change of traits has been observed in a plankton predator-prey system [46, 166], which is a good example for studying the coupling between rapid evolution and predator-prey interaction due to its short generation times and the tractability of genetic studies [71]. Consequently, focusing only on ecological interaction without allowing properties of the interacting populations to undergo changes, which often come with a cost in the population density, does not give a complete picture of the dynamics of an ecosystem, let alone its ability to adapt to changing environmental conditions [149].

One way of describing the effect of rapid evolutionary change of traits on the predator-prey population dynamics is the assumption that ecological and evolutionary dynamics occur on a different time-scales, that is, the situation in which evolutionary change occurs either on a faster [29] or slower [78] time-scale than ecological interaction. When considering the evolutionary trait as a system variables in the model dynamics, it also increases the dimension of the system which leads the analysis of the resulting system challenging.

When the time-scales of the population in ecological dynamics and the evolutionary trait differ, one may use slow-fast dynamical system [88] to exploit and introduce a time-scale separation between them to reduce the dimension of the system of equation.

1.1.2 A competition-diffusion problem

The general Lotka-Volterra competition model representing the interaction of n -species is given by:

$$\frac{dN_i(t)}{dt} = r_i N_i(t) \left[1 - \sum_j \alpha_{ij} N_j(t) \right], \quad (1.1.6)$$

where $N_i(t)$ is the number of individuals in the i th population, r_i the growth rate of the i th species, α_{ij} competition coefficients measuring the extent to which the j th species affects the growth rate of the i th.

Although the dynamics of the Lotka-Volterra competition model is quite interesting, it is structurally unstable in the sense that a small perturbation of the equations often results to a drastic change in the dynamical system. For this reason, the presence of diffusion mechanism changes the behaviour of the whole model and leads to a coupled partial differential equations termed as reaction-diffusion system. In contrast, the Lotka-Volterra competition model for the competition of three species without diffusion leads to the extinction of one or more species (referred to as competitive exclusion), see, for example, [53, 101].

Durrett and Levin [32], Frean and Abraham [45], Reichenbach et al. [126] showed coexistence of three species by considering random dispersion of the interacting species in space. Such possibility of coexistence of three species governed by random dispersal was also theoretically discussed by [3, 124]. In these works, the following 3-species competition-diffusion system of Lotka-Volterra type

$$\left. \begin{aligned} \dot{u} &= d_1 \Delta u + u(r_1 - a_{11}u - a_{12}v - a_{13}w), \\ \dot{v} &= d_2 \Delta v + v(r_2 - a_{21}u - a_{22}v - a_{23}w), \\ \dot{w} &= d_3 \Delta w + w(r_3 - a_{31}u - a_{32}v - a_{33}w), \end{aligned} \right\} \text{ in } \Omega \times \mathbb{R}^+, \quad (1.1.7)$$

was considered. Here Δ is the Laplacian operator; the population densities are denoted by u , v , and w ; the constant d_i , $i = 1, 2, 3$, denote the diffusivities (mobility) of u , v , w respectively.

The system (1.1.7) is supplemented with the homogeneous Neumann boundary conditions

$$\frac{\partial u}{\partial \mathbf{n}} = 0, \quad \frac{\partial v}{\partial \mathbf{n}} = 0, \quad \text{and} \quad \frac{\partial w}{\partial \mathbf{n}} = 0, \quad \text{on } \partial\Omega \times \mathbb{R}^+, \quad (1.1.8)$$

and initial conditions are of the form

$$u(\mathbf{x}, 0) = u_0(\mathbf{x}), \quad v(\mathbf{x}, 0) = v_0(\mathbf{x}), \quad \text{and} \quad w(\mathbf{x}, 0) = w_0(\mathbf{x}). \quad (1.1.9)$$

Here \mathbf{x} represents the coordinate of a point in Ω , \mathbf{n} is a unit vector normal to the boundary $\partial\Omega$, and u_0 , v_0 , w_0 are some prescribed positive functions defined over the spatial domain Ω .

In the absence of the third species w , the qualitative properties of the non-negative solutions of the system have been studied intensively [65]. Kishimoto and Weinger [82] showed that if the domain Ω is convex, any spatially non-constant equilibrium solution (if they exist) are unstable under the assumption that the competition between the two species are strong, which is represented by the relation $a_{11}/a_{21} < r_1/r_2 < a_{12}/a_{22}$. It also means that, the interaction of the two species leads to competitive exclusion. But Matano and Mimura [99] showed that if the domain Ω is not convex, the structure of the solution depends on the shape of the domain. For example, if the domain has a suitable dumb-bell shape, there will exist a stable non-constant equilibrium solution which exhibit spatial segregation of the two competing species, in which the spatial

domain is divided into two where each region is nearly exclusively occupied by one species. This in turn means that coexistence of the two species depends on whether their habitat is convex or not.

The segregation pattern of the competitive mediated coexistence and competitive exclusion of three competing species with a convex shaped habitat has also been studied in [35] under the condition that all the mobility rates are very smaller and inter-specific competition of species are larger.

1.2 An overview on geometric method of singular perturbation theory

The development of analytical study of slow-fast systems and the related relaxation oscillation phenomena have been influenced by several view points from asymptotic techniques [33, 114], for instance, matching asymptotic analysis [77, 91]. The more recently developed theory for qualitative analysis of dynamical systems is the geometric singular perturbation theory. It employs the concept of invariant manifold in phase space to construct orbits with desired properties or to understand the global structure of the phase space [66]. The foundation of the technique was laid by Fenichel [39], and later developed in [66, 88]. For a more comprehensive exposition to applications in biological practice, including several examples, we refer to [66].

The goal in choosing a geometric approach was to create solution trajectories for a parameter $0 < \varepsilon \ll 1$ by suitably glueing together segments of orbits that are determined from the fast time-scaled and the slow time-scaled dynamics at the limiting case $\varepsilon = 0$.

The general formulation of a slow-fast system of ordinary differential equations with m fast and n slow variables (and time as the only independent variable) is expressed as

$$\left. \begin{aligned} \varepsilon \dot{u} &= f(u, v, \varepsilon), \\ \dot{v} &= g(u, v, \varepsilon), \end{aligned} \right\} \quad (1.2.1)$$

where the superposed dot indicates derivative with respect to the slow time-scale t , $(u, v) \in \mathbb{R}^m \times \mathbb{R}^n$ are variables, f and g are sufficiently smooth functions with respect to all the three arguments. Rescaling the slow time t by ε and obtain an equivalent system that evolves on the fast time-scale $\tau = t/\varepsilon$. We thus write

$$\left. \begin{aligned} u' &= f(u, v, \varepsilon), \\ v' &= \varepsilon g(u, v, \varepsilon), \end{aligned} \right\} \quad (1.2.2)$$

where the primes indicate the derivative with respect to the faster time-scale τ .

Due to the slower time-scale t (respectively, the faster time-scale τ) used in the dynamics of equation (1.2.1) (respectively, (1.2.2)), these system of equations are referred to as *slow dynamics* (respectively, *fast dynamics*). We then take the (singular) limit $\varepsilon \rightarrow 0$ in slow system (1.2.1) and obtain

$$\left. \begin{aligned} 0 &= f(u, v, 0), \\ \dot{v} &= g(u, v, 0), \end{aligned} \right\} \quad (1.2.3)$$

which is known as the *reduced problem*. Note that the reduced problem is a differential-algebraic equations (DAE), which represents a dynamical system for the slower variable v subject to $f(u, v, 0) = 0$.

And, similarly taking the limiting case to the fast system (1.2.2) we obtain what is known as the *layer problem*, i.e.,

$$\left. \begin{aligned} u' &= f(u, v, 0), \\ v' &= 0, \end{aligned} \right\} \quad (1.2.4)$$

which represents a dynamic for the fast problem while the slower variable is ‘frozen’ (i.e., an n -parameter dynamics for the fast variable).

The layer and reduced problems are connected through the *critical manifold* $\mathcal{C}_0 = \{(u, v) \in \mathbb{R}^{m+n} : f(u, v, 0) = 0\}$, which is a sufficiently smooth n -dimensional submanifold of \mathbb{R}^{m+n} . The critical manifold \mathcal{C}_0 is the equilibrium points of the layer problem (1.2.4).

By using geometric singular perturbation theory, one can obtain global information about the system (1.2.1) for $\varepsilon \neq 0$, but very small, by joining the two systems together in some suitable manner. The main idea here is as follows. Suppose that an n -dimensional manifold \mathcal{M}_0 contained in \mathcal{C}_0 is compact and *normally hyperbolic*, that is, eigenvalues λ of $\frac{\partial f}{\partial u}|_{\mathcal{M}_0}$ are $\operatorname{Re}(\lambda) \neq 0$ and uniformly bounded away from the imaginary axis. Then the critical manifold persists as a locally invariant *slow manifold*. Moreover, suppose that $\mathcal{W}^s(\mathcal{M}_0)$ (respectively, $\mathcal{W}^u(\mathcal{M}_0)$) is the stable manifold (respectively, the unstable manifold) of \mathcal{M}_0 , that is, the eigenvalues λ such that $\operatorname{Re}(\lambda) < 0$ (respectively, $\operatorname{Re}(\lambda) > 0$). Then they also persists as manifolds $\mathcal{W}^s(\mathcal{M}_\varepsilon)$ and $\mathcal{W}^u(\mathcal{M}_\varepsilon)$.

The theory of geometric singular perturbation is based on three fundamental theorems due to Fenichel [39]. In the following we only state the first two theorems without proofs, and the third one is omitted as its application is out of the scope of the work reported in this thesis. A complete discussion of the theorems with their application in biology can be found in [66].

Theorem 1.2.1 (Fenichel, [39]). *Suppose $\mathcal{M}_0 \subseteq \mathcal{C}_0$ is compact, possibly with boundary, and normally hyperbolic, that is, the eigenvalues λ of the Jacobian $\frac{\partial f}{\partial u}|_{\mathcal{M}_0}$ all satisfy $\operatorname{Re}(\lambda) \neq 0$. Suppose f and g are smooth. Then for $\varepsilon > 0$ and sufficiently small, there exists a manifold \mathcal{M}_ε , $\mathcal{O}(\varepsilon)$ close and diffeomorphic to \mathcal{M}_0 , that is locally invariant under the flow of the full problem (1.2.1).*

Fenichel’s first theorem only gives a very local picture of the system (1.2.1) for small nonzero ε . It guarantees under the conditions indicated in the above theorem the existence of the slow manifold, and gives an approximation for the flow on this slow

manifold. However it does not give a more global picture that, in particular, addresses the interplay between the slow manifold and the surrounding phase space. In general, such interplay takes place via stable and unstable manifolds. Those are the objects of concern in Fenichel's second theorem.

Theorem 1.2.2 (Fenichel, [39]). *Suppose $\mathcal{M}_0 \subseteq \mathcal{C}_0$ is compact, possibly with boundary, and normally hyperbolic, and suppose f and g are smooth. Then for $\varepsilon > 0$ and sufficiently small, there exist manifolds $\mathcal{W}^s(\mathcal{M}_\varepsilon)$ and $\mathcal{W}^u(\mathcal{M}_\varepsilon)$, that are $\mathcal{O}(\varepsilon)$ close and diffeomorphic to $\mathcal{W}^s(\mathcal{M}_0)$ and $\mathcal{W}^u(\mathcal{M}_0)$, respectively, and that are locally invariant under the flow of (1.2.1).*

In the following we present a literature review on numerical methods for multiscale methods relevant to predator-prey systems arising in ecology.

1.3 Literature review on some numerical methods for multiscale problems

The standard approach for numerical solutions of coupled systems of differential equations is to treat the full problem using a single time integration scheme with a single time-step length, without any consideration on the possible variation in dynamics between the involved components. Such methods applied to multiscale problems such as singularly perturbed predator-prey models suffers from a number of issues from numerical instability to computational inefficiency due to the fact that stiffness of the problem is primarily determined by the dynamics of the fastest component.

For the last decade a range of numerical integration schemes beyond the standard approach have been developed to efficiently solve multiscale problems from various applications. A great deal of survey of such methods can be found in the article [153]. In the following we review some important classes of non-standard methods that have been developed over the last decade for slow-fast problems arising in ecology.

Multi-method schemes

Multi-method schemes are based on the idea of operator-splitting methods for initial value problems (IVPs). For slow-fast systems, with some prior information, the problem is split into two subproblems each having a single time-scale, one with fast dynamics which we referred to as *fast subproblem*, and the other with slow dynamics, referred to as *slow subproblem*. Appropriate methods, based on the stiffness, stability and accuracy requirements, may be employed for each subproblem, which will be combined at each time-step to obtain an approximate solution for the full multiscale problem. Typically, implicit schemes such as Crank-Nicholson (CN) and implicit Backward Difference Formula (BDF) are used for the fast subproblem, whereas, explicit methods such as Leap-Frog (LF) and explicitly extrapolated BDF for the slow subproblem.

Various multi-method schemes have been developed in the literature to efficiently solve IVPs involving different time-scales. Andrus [6] proposed a numerical method in which the fourth-order explicit Runge-Kutta (RK4) to discretize the slow sub-system, while the faster one is solved by any sufficiently accurate method or some closed form solution if available. In a later paper [5], Andrus considered a numerical method which consists of integrating the slow and the fast sub-systems with RK4 and third-order implicit Runge-Kutta methods, respectively. He then derived the absolute stability condition of this method and showed that the region of stability is nearly as large as that of the embedded methods if the sub-systems are weakly coupled. Such approaches have also been applied in various fields with varying success [68, 110, 127, 139, 156, 164]. In [164] an algorithm based on the local information of the system Jacobian for dynamic partitioning of the system has been suggested.

A related approach which is based on similar partitioning of the full problem is *multi-order scheme*. Such methods, on the other hand, use methods of same class with same step-size but the order of the schemes considered in the partition are different. Depending on the activity level of the subproblems, the order of the methods used for each partition may be different. That is, the faster the activity level of the subproblem

is, the higher the order of the method used to discretize it. Such methods are efficient only for non-stiff problems, for example in [37] extrapolation and RK schemes are employed.

Multirate schemes

Multirate methods are also based on the view point of treating fast and slow subproblems independently. However, unlike the standard approach or the multi-method/multi-order schemes in which discretization of both the slow and fast subproblems employ a single time step-size, multirate methods use different step-sizes with same or different numerical methods. The idea is that a smaller time-step is used to discretize the faster subproblem while a bigger time-step for the slow subproblem, which leads to a considerable reduction of computational cost and computer memory relative to using the standard method with a single time-size. Furthermore, such methods exhibit a better stability property than the standard approach in which, often, the step-size restriction for the full problem depends on the fastest changing components. In multirate methods, the time-steps for the slow and the fast subproblems are referred to as *macrostep* and *microstep*, respectively [61], for obvious reasons. In order to handle the coupling between the slow and fast components on the microsteps, a multirate method incorporates interpolations or extrapolations which may result in a further interpolation or extrapolation errors. Such methods can be used for both stiff (or slow-fast) and non-stiff problems. In the work presented here, various multirate approaches have been developed coupled with extrapolation algorithms to ensure higher-order accuracy of the solution, moreover, fractional- step algorithms have also been employed for better stability and efficiency. As one of major contributions in this work, we have analyzed the linear stability of the extrapolated multirate schemes applied on a multiscale model problem of predator-prey-type.

In the literature, various multirate methods have been developed. Rice [128] was the first to try to use different step-sizes for each partition. Linearized multirate schemes coupled with extrapolation algorithms have been proposed by Constantanescu

and Sandu [25, 27] to solve multi-physics problems with multi time-scales. Multirate integration schemes based on Runge-Kutta methods have been discussed in [24, 61, 143]. Gear [51] and Socia [148] suggested multirate schemes based on BDF methods. Skelboe [146] also presented the stability properties of multirate schemes based on BDF. A more recent work [10] by Bartel dealt with the coupling between sub-systems by using internal stages instead of interpolation/extrapolation to overcome stability issues that are typical of multirate schemes. Multirate methods have been applied in various areas which include simulations of electric circuit [60], molecular dynamics [86, 155], vehicle models containing flexible tire [143], aero-elastic models of helicopter [146] and planetary problems [37].

In this work, some selected models arising in ecology and evolutionary dynamics have been used to illustrate the performance of multirate or fractional-step algorithms in mimicing the essential qualitative property of the exact solutions of these problems. In addition, the results have revealed that these schemes can significantly reduce the computation time with a comparable level of accuracy relative to corresponding (standard) conventional schemes.

1.4 Outline of the thesis

The rest of this thesis is organized as follows. In Chapter 2, we consider a mathematical model describing two slow predators competing for a single fast prey species in a quite diversified time response. Results of qualitative analysis of the continuous model are discussed based on local stability. The formulation of an efficient multirate scheme based on extrapolation algorithm is detailed. Extensive numerical experiments are produced to demonstrate the efficiency of the method by comparing with corresponding single-rate (conventional) scheme.

In Chapter 3, classes of multirate fractional-step θ -method and multirate fractional-step mixed implicit-explicit method (which we abbreviate them as FSTS and FS-MIMEX, respectively) are developed for an approximate solution of slow-fast predator-

prey model that is considered in Chapter 2. The fractional-step algorithm is developed in such a way that, the full problem is decouple into fast and slow sub-systems, and then we apply suitable sub-algorithms based on a class of θ -methods to discretize each sub-system independently using different time-steps. Then the algorithm for the full problem is obtained by utilizing a higher-order product formula by merging the sub-algorithms at each time-step. We also present the details of the nonlinear solvers employed to treat the resulting (implicitly) nonlinear system, such as Jacobian-Free Newton-Krylov (JFNK) and Anderson's acceleration methods, which are known for their superlinear convergence. Stabilities of the discrete multirate schemes are also analyzed. A thorough numerical experiments have been presented to demonstrate the performance of the multirate schemes considered in this chapter by comparing them with the monolithic-theta method (MTS) and stiff `Matlab` solvers.

In Chapter 4, a coupled ecological and evolutionary dynamics of a 1-predator and 2-prey species in an ecology having a slow dynamics with a fast evolution of predator-trait is presented. Results of qualitative nature, which are obtained with the aid of geometric singular perturbation theory, are presented. A high-order linear multistep implicit-explicit schemes are proposed and analyzed for stability and convergence. The method is based on splitting the model into stiff part (fast component) and non-stiff part (slow components) and applying implicit and explicit schemes to the stiff and non-stiff parts, respectively. The methods are then compared for stability, convergence and efficiency with an existing conventional implicit-explicit schemes.

In Chapter 5, we formulate a high-order implicit multirate collocation methods for the singularly perturbed model considered in Chapter 4. Here the unknown variables are expressed as linear combination of Lagrangian interpolation polynomials which are used as basis functions, by which slow and fast subproblems are collocated at each macro and micro time-steps, respectively. Extensive numerical experiments are also presented to show the superior performance of multirate collocation scheme over single-rate scheme in terms of accuracy, efficiency and replicating the qualitative feature of the continuous model.

Chapter 6 presents a singularly perturbed three species Lotka-Volterra competition-diffusion model. The model problem exhibits internal layer with spatial segregation pattern with the condition that the mobility rate of the species is sufficiently smaller compared to the inter-specific competition of the species. Competitive-mediated coexistence and competitive exclusion can also be exhibited by varying the parameters of the growth rate and inter-specific coefficients of the model. To capture the dynamical behavior of various spatio-temporal patterns, a high-order semi-implicit multistep scheme based on Lagrange temporal interpolation coupled with high-order conforming finite element methods are developed in a two spatial dimensions. Stability and convergence of the developed scheme is analyzed both theoretically and experimentally. Various numerical results have been shown to demonstrate the performance of the scheme in predicting fine features of the solution.

Chapter 7 deals with the numerical simulation of the singularly perturbed three-species Lotka-Volterra competition-diffusion model considered in Chapter 6, but having different spatial mobility rates. The model problem exhibit various interesting spatio-temporal patterns such as droplet, stripe, spiral, glider-like patterns for different values of diffusion coefficients. We develop a high-order semi-implicit linear multistep schemes based on the Crank-Nicholson and Adams-Bashforth methods for the temporal discretization in conjunction with C^0 -conforming finite element method in a 2-dimensional spatial domain. The scheme is second-order in time and have good stability properties and captures the complex dynamics very well, as demonstrated in the numerical experimentation.

Finally, In Chapter 8, we presented some concluding remarks and the scope for future research.

Chapter 2

Efficient simulation of a slow-fast dynamical system using multirate finite difference schemes



In this chapter, a predator-prey model that is highly susceptible to local time variations is considered. It is a three-dimensional model consisting of one prey and two predator species. The model exhibits coexistence in the case where the prey population grows in a much faster rate than that of the predators in quite diversified time response. For certain range of parameters, the solution shows a stable relaxation-oscillation behaviour in the positive octant. The standard approach often fails to capture such important solution features. Hence, the main objective here is to formulate and analyze a class of extrapolated multirate time integration scheme that are capable of efficiently represent solutions of slow-fast models such as the one considered in this chapter for a wide range of parameters. The methods are based on splitting the full problem into fast and slow subproblems, and then applying smaller step-size for the fast subproblem than for the slow subproblem. We present a thorough numerical experiments to demonstrate the efficiency and capability of the schemes in mimicking important solution features of the model, which have been predicted from a theoretical analysis. We also show that

the proposed multirate schemes substantially outperform the corresponding single-rate schemes (which use a single time-step for all components) in CPU times.

2.1 Introduction

In some ecological systems, quantities of interest can vary according to widely differing time-scales. For instance, a predator-prey system with a time diversified response can be modelled as a slow-fast dynamical system. Temporal changes such as collapse (nearly vanishing), explosion (rapid exponential growth), single or multiple stationary states, oscillations and chaos can occur in such models [73]. As a result, mathematical models of such systems can be understood as combinations and interactions of these basic types.

Geometric singular perturbation theory has been continued to be used successfully to analyze slow-fast systems in various fields including ecology. Lenbury [93] studied a model of a predator-prey system invaded by the action of a parasite. The prey population is divided into two classes, susceptible and infected members. whereas, the predator population is assumed to have very fast dynamics with all its members infected by the parasite. The model is rescaled by two small positive dimensionless parameters and the analysis is carried out through the geometric singular perturbation approach. The method allows one to detect the limit cycle in the extreme case of very fast or very slow dynamics and then to identify different transient and attractors which are developed in the system. In [56], Ginoux et al. studied the famous Volterra-Gauss model and its several modifications such as Rosenzweig-MacArthur and Hastings-Powell models. Under certain conditions, these models present slow-fast dynamics which result into singularly perturbed systems. Using geometric singular perturbation theory, they analyzed the nature and stability of fixed points, existence of Hopf-bifurcation and chaotic attractors. In [29], a three-dimensional eco-evolutionary model representing a predator-prey model with fast evolution of the predator was studied using geometric singular perturbation theory. Their work describes how slow-fast dynamical systems

theory offers a clear viewpoint through which the effects of evolution on ecological dynamics can be studied. In [98], the interaction of predator-prey systems having two slow predators competing exploitatively for the same fast prey in a constant environment was considered. By using the geometric singular perturbation theory, they gave conditions which guarantee existence of stable relaxation-oscillations for systems within the class. They showed coexistence in the case where the prey population grows much faster than that of predators.

Due to the presence of different time scales, standard techniques for numerical solutions of slow-fast systems typically lose favour due to a number of issues such as the need for an excessively small time step-size which can quickly become uneconomical both in terms of memory and computational time, especially, when one needs long time simulations. Furthermore, such classical methods often generate oscillations, chaos, and false steady states. To overcome the above mentioned difficulties, in this chapter, we present a multirate numerical method which is based on splitting of the full slow-fast system into two parts referred to as fast and slow sub-systems corresponding to the fast and the slow components, respectively. Then the fast subproblem will be integrated with a small step-size, while, the slow sub-system using a large one.

Multirate methods have been investigated and applied in various fields of science that include modular dynamical simulation [50, 132], electrical network simulation [89], etc. However, the lack of general theoretical results which guarantee absolute stability of a multirate approach has been one of the major problems concerning the use of multirate methods to solve real life problems [90]. However, many results have appeared in the literature concerning with the analysis of absolute stability according to the underlying differential systems to be integrated. The extrapolated multirate method has been explored by many researchers to solve problems having different time-scales. One of the first article to treat numerically problems of this type appears to be by Rice in [128], who proposed multirate Runge-Kutta methods that use different time-steps to integrate fast and slow solution components. More recent works in multirate methods include [10, 61, 69, 134, 135, 165]. Furthermore, a multirate scheme based on

extrapolated forward Euler methods was developed by Engstler and Lubich [37]. The methods presented in this chapter are motivated by the work of Constantinescu and Sandu [25], in which they constructed extrapolated multirate methods for problems that have different dynamics. They also analyzed the linear stability properties of the extrapolated multirate explicit and linearly-implicit methods.

In this chapter, we extend the extrapolated multirate discretization methods proposed by Constantinescu and Sandu [27]) to a three-dimensional slow-fast system describing the interactions of two predators competing for one fast prey. We also present some qualitative results which will be used as basis for the numerical tests used to demonstrate the performance of our method in preserving qualitative property of the continuous problem.

The rest of this chapter is organized as follows. In Section 2.2, we present the governing mathematical model, and some theoretical results concerning it. In Section 2.3, the class of multirate numerical base methods are formulated for solving the model problem discussed in Section 2.3. A detailed stability analysis of these numerical schemes is presented in Section 2.4. Extensive numerical simulations, along with a thorough discussion, are presented in Section 2.5. Finally, summary and some comments are presented in Section 2.6.

2.2 The mathematical model

We consider the mathematical model predator-prey system proposed by [98] to describe the dynamics of two predators competing for the same prey, that is,

$$\left. \begin{aligned} \dot{S} &= \gamma S(1 - S/K) - \frac{m_1}{y_1} \frac{x_1 S}{a_1 + S} - \frac{m_2}{y_2} \frac{x_2 S}{a_2 + S}, \\ \dot{x}_1 &= \frac{m_1 x_1 S}{a_1 + S} - d_1 x_1, \\ \dot{x}_2 &= \frac{m_2 x_2 S}{a_2 + S} - d_2 x_2, \end{aligned} \right\} \quad (2.2.1)$$

where, for $i = 1, 2$, x_i represents the time-varying population density of the i th-predator; S represents the time-varying population density of the prey; $m_i > 0$ is the maximal growth or birth rate of the i th-predator; $d_i > 0$ is the death rate of the i th-predator, y_i is the yield factor for the i th-predator feeding on the prey, a_i is the half-saturation constant for the i th-predator, i.e., the prey density at which the functional response of the predator is half maximal; and $\gamma > 0, K > 0$ are the intrinsic growth rate and the carrying capacity of the prey, respectively. The term

$$\frac{m_i}{y_i} \frac{S}{(a_i + S)},$$

is the functional response of the per capita rate at which the predator x_i captures prey S , for $i = 1, 2$.

To proceed with the qualitative analysis, we non-dimensionalize equation (2.2.1) so that the scaled system contains a minimum number of parameters. Following [98], we consider the scaling

$$\varepsilon = \frac{1}{\gamma}, \beta_1 = \frac{a_1}{K}, \beta_2 = \frac{a_2}{K}, x = \frac{x_1}{\gamma y_1 K}, y = \frac{x_2}{\gamma y_2 K}, z = \frac{S}{K}, \quad (2.2.2)$$

and after some simplifications, we obtain that the governing model (2.2.1) will be described by the following nonlinear and non-dimensional system of ordinary differential equations:

$$\left. \begin{aligned} \dot{x} &= x \left[\frac{m_1 z}{\beta_1 + z} - d_1 \right] =: f(x, y, z), \\ \dot{y} &= y \left[\frac{m_2 z}{\beta_2 + z} - d_2 \right] =: g(x, y, z), \\ \dot{z} &= \frac{1}{\varepsilon} z \left[1 - z - \frac{m_1 x}{\beta_1 + z} - \frac{m_2 y}{\beta_2 + z} \right] =: w(x, y, z), \end{aligned} \right\} \quad (2.2.3)$$

where x, y, z are time-dependant unknown functions and $f(x, y, z), g(x, y, z), w(x, y, z)$ are smooth continuous functions describing the dynamics of the system. Furthermore,

ε is assumed to be a very small positive number ($0 < \varepsilon \ll 1$). Earlier, this model has been studied for one predator by Armstrong and Mc Gehee [7] for $\beta_i = 0$.

In this system, the component z corresponds to the prey population and is much faster than those corresponding to the predator ones, i.e., x, y . To exploit these local time-scale variations, we intend to use multirate methods that use different, local time-steps over the components. In these methods larger (macro) time-steps are used for the slow components and smaller (micro) time-steps are used for the fast ones.

In the following we briefly present some important theoretical results in [98], concerning the existence of stable relaxation oscillations in the positive octant. These qualitative results will be used as a basis to test the performance of the multirate scheme which will be discussed in a later section.

The equilibria of system (2.2.3) are found to be $A(0, 0, 0)$, $B(0, 0, 1)$, $C(a_1, 0, b_1)$, and $D(0, a_2, b_2)$, where for $i = 1, 2$

$$a_i = \frac{\beta_i(d_i(\beta_i + 1) - m_i)}{(d_i - m_i)^2}, \text{ and } b_i = -\frac{\beta_i d_i}{(d_i - m_i)^2},$$

and the Jacobian matrix for system (2.2.3) is given by

$$J(x, y, z) = \begin{bmatrix} \sigma_1 - d_1 & 0 & x\varphi_1 \\ 0 & \sigma_2 - d_2 & y\varphi_2 \\ -\varepsilon^{-1}\sigma_1 & -\varepsilon^{-1}\sigma_2 & -\varepsilon^{-1}\Sigma \end{bmatrix}, \quad (2.2.4)$$

where for $i = 1, 2$

$$\sigma_i = \frac{zm_i}{z + \beta_i}, \quad \varphi_i = \frac{m_i\beta_i}{(z + \beta_i)^2}, \text{ and } \Sigma = 2z + x\varphi_1 + y\varphi_2 - 1.$$

The Jacobian evaluated at the critical point $A(0,0,0)$ gives

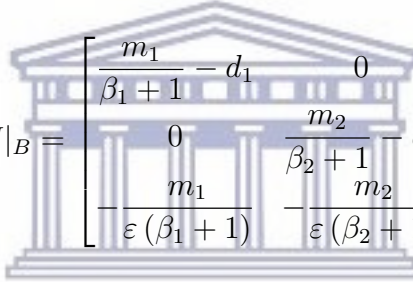
$$J|_A = \begin{bmatrix} -d_1 & 0 & 0 \\ 0 & -d_2 & 0 \\ 0 & 0 & \varepsilon^{-1} \end{bmatrix}, \quad (2.2.5)$$

with eigenvalues

$$\lambda_1 = -d_1, \lambda_2 = -d_2, \text{ and } \lambda_3 = \varepsilon^{-1}. \quad (2.2.6)$$

This implies that equilibrium point $(0,0,0)$ is an unstable equilibrium since $\lambda_3 > 0$.

The Jacobian evaluated at the critical point $B(0,0,1)$ gives



$$J|_B = \begin{bmatrix} \frac{m_1}{\beta_1 + 1} - d_1 & 0 & 0 \\ 0 & \frac{m_2}{\beta_2 + 1} - d_2 & 0 \\ \frac{m_1}{\varepsilon(\beta_1 + 1)} & \frac{m_2}{\varepsilon(\beta_2 + 1)} & -\frac{1}{\varepsilon} \end{bmatrix}, \quad (2.2.7)$$

with eigenvalues

$$\lambda_1 = \frac{m_1}{\beta_1 + 1} - d_1, \lambda_2 = \frac{m_2}{\beta_2 + 1} - d_2, \text{ and } \lambda_3 = -\frac{1}{\varepsilon}. \quad (2.2.8)$$

This implies that the equilibrium point $(0,0,1)$ is stable if,

$$d_1 > \frac{m_1}{\beta_1 + 1} \text{ and } d_2 > \frac{m_2}{\beta_2 + 1},$$

otherwise it is unstable. The Jacobian evaluated at the critical point $C(a_1, 0, b_1)$ gives

$$J|_C = \begin{bmatrix} 0 & 0 & \beta_1(d_1(\beta_1 + 1) - m_1) \\ 0 & -\frac{d_1 m_2 \beta_1}{\tilde{d}_1(\beta_2 - \tilde{d}_1)} - d_2 & 0 \\ \frac{d_1}{\varepsilon} & \frac{d_1 m_2 \beta_1}{\varepsilon \tilde{d}_1(\beta_2 - \tilde{d}_1)} & \frac{\beta_1(d_1(\beta_1 + 1) - m_1) - 2\tilde{d}_1 - 1}{\varepsilon} \end{bmatrix}, \quad (2.2.9)$$

where $\tilde{d}_i = d_i \beta_i / (d_i - m_i)$, $i = 1, 2$; and the Jacobian matrix evaluated at the critical

point $D(0, a_2, b_2)$ is given by

$$J|_D = \begin{bmatrix} -\frac{m_1\beta_2d_2}{\widehat{d_2}(\beta_1-\widehat{d_2})} - d_1 & 0 & 0 \\ 0 & 0 & \beta_2(d_2(\beta_2 + 1) - m_2) \\ \frac{d_2m_1\beta_2}{\varepsilon\widehat{d_2}(\beta_1-\widehat{d_2})} & \frac{d_2}{\varepsilon} & -\frac{\beta_2(d_2(\beta_2+1)-m_2)-2\widehat{d_2}-1}{\varepsilon} \end{bmatrix}. \quad (2.2.10)$$

From (2.2.9) and (2.2.10), we see that it is a highly complicated task to find eigenvalues in a closed form. However, following [98], we consider cases for some typical parameter values, for example, if we take

$$m_1 = 2, d_1 = 0.4, \beta_1 = 0.2, m_2 = 5, d_2 = 0.5, \beta_2 = 0.7, \varepsilon = 0.1, \quad (2.2.11)$$

we see that the critical points are

$$A(0, 0, 0), B(0, 0, 1), C(0.1187, 0, 0.05) \text{ and } D(0, 0.1435, 0.0778). \quad (2.2.12)$$

All these critical points are in the first octant, and therefore are biologically acceptable. The stability of the critical points are then obtained from the eigenvalues of the corresponding Jacobian matrices (2.2.5), (2.2.7), (2.2.9) and (2.2.10) evaluated at the equilibrium points. Then the corresponding eigenvalues are summarized as follows:

$$\left. \begin{aligned} A(0.0000, 0.0000, 0.0000) &\rightarrow \{-0.4, -0.5, 10\}, \\ B(0.0000, 0.0000, 1.0000) &\rightarrow \{1.2667, 2.4412, -10\}, \\ C(0.1187, 0.0000, 0.0500) &\rightarrow \{-1/6, 7/10 \pm \sqrt{255/10i}\}, \\ D(0.0000, 0.1435, 0.0778) &\rightarrow \{4/25, 13/180 \pm \sqrt{134291/180i}\}, \end{aligned} \right\} \quad (2.2.13)$$

where the entries on the right sides of the arrows are the eigenvalues.

Now, we note that the following criteria by Routh-Hurwitz [4] gives a necessary and sufficient condition for all roots of the characteristic polynomial lie in the negative half of the complex plane.

Theorem 2.2.1. *Given the polynomial*

$$P(\lambda) = \lambda^n + a_1\lambda^{n-1} + \dots + a_{n-1}\lambda + a_n, \quad (2.2.14)$$

where the coefficients a_i are real constants, $i = 1, \dots, n$, define the n Hurwitz matrices using the coefficients a_i of the characteristic polynomial as

$$H_1 = (a_1), \quad H_2 = \begin{bmatrix} a_1 & 1 \\ a_3 & a_2 \end{bmatrix}, \quad H_3 = \begin{bmatrix} a_1 & 1 & 0 \\ a_3 & a_2 & a_1 \\ a_5 & a_4 & a_3 \end{bmatrix}, \quad \text{and}$$

$$H_n = \begin{bmatrix} a_1 & 1 & 0 & 0 & \dots & 0 \\ a_3 & a_2 & a_1 & 1 & \dots & 0 \\ a_5 & a_4 & a_3 & a_2 & \dots & 0 \\ \vdots & \vdots & \vdots & \vdots & \ddots & \vdots \\ 0 & 0 & 0 & 0 & \dots & a_n \end{bmatrix},$$

where $a_j = 0$ if $j > n$. Then all roots of the polynomial $P(\lambda)$ will be negative or will have negative real parts iff the determinants of all Hurwitz matrices are positive; i.e.,

$$\det H_j > 0, \quad j = 1, 2, \dots, n. \quad (2.2.15)$$

For example, the Routh-Hurwitz criteria for a polynomial of degree $n = 3$ is,

$$a_1 > 0, \quad a_3 > 0, \quad \text{and } a_1 a_3 > a_2^2. \quad (2.2.16)$$

In view of the above criteria, we see from (2.2.13) that all the critical points do not satisfy the conditions stated and hence they are not asymptotically stable.

In the next section, we present the construction of the multirate integration method to solve the mathematical model considered in this section.

2.3 Multirate base methods

Consider the initial value problem defined by

$$\mathbf{Y}'(t) = \mathbf{F}(t, \mathbf{Y}(t)), \mathbf{Y}(a) = \mathbf{Y}_0, \quad (2.3.1)$$

where the prime “'” denotes the differentiation with respect to time and $F : \mathbb{R} \times \mathbb{R}^N \rightarrow \mathbb{R}^N$.

Recall that, in this work, we consider the case where $N = 3$, i.e.,

$$\mathbf{Y}'(t) = \begin{bmatrix} x' \\ y' \\ z' \end{bmatrix} = \begin{bmatrix} f(t, x, y, z) \\ g(t, x, y, z) \\ w(t, x, y, z) \end{bmatrix}; \mathbf{Y}(a) = \begin{bmatrix} x_0 \\ y_0 \\ z_0 \end{bmatrix}, \quad (2.3.2)$$

where, in view of slow-fast systems, x and y are assumed to be the slow components, and z is a fast component; t is defined in the closed interval $I = [a, b]$, a time interval of interest in which we seek a solution to the problem. Also $f(t, x, y, z)$, $g(t, x, y, z)$, and $w(t, x, y, z)$ are sufficiently smooth in all of their arguments, and satisfy conditions which guarantee a unique solution for IVP (2.3.2). In the present context, the functions f , g and w are the right hand side function in (2.2.3). The solution will be given by $(x(t), y(t), z(t))^T$. We wish to approximate the solution of (2.3.2) by a multirate base methods together with the extrapolation algorithm. The discretization of the base methods are as follows: Let $H = mh$ be the step-size of the slow components x, y , and h that of the fast component z . m is a fixed positive integer termed as a *multirate factor*. We are interested in an approximate solution of (2.3.2) on discrete point sets

$$P_{slow} := a + nH; n = 0, 1, \dots, \frac{(b-a)}{H}, \quad (2.3.3)$$

$$P_{fast} := a + nh; n = 0, 1, \dots, \frac{(b-a)}{h}, \quad (2.3.4)$$

with $0 < H \leq b - a$.

The slow components x, y are integrated on P_{slow} whereas the fast component is integrated on P_{fast} . Note that, P_{slow} and P_{fast} coincide at the macro nodes.

The procedure of integrating the slow components with step-size H is referred to as a macro-stepping and the process of integrating the fast components with step-size h is referred to as a micro-stepping.

The general base method we consider here is a θ -method

$$\mathbf{Y}_{i+1} = \mathbf{Y}_i + \ell[\theta\mathbf{F}(t_i, \mathbf{Y}_i) + (1 - \theta)\mathbf{F}(t_{i+1}, \mathbf{Y}_{i+1})], \quad (2.3.5)$$

which for $\theta = 1, 0$ and $1/2$ becomes the explicit Euler, implicit Euler, and Crank-Nicholson (CN) method, respectively.

Now the linearly-implicit Euler method (i.e., a linearization of the implicit Euler schemes) is given by

$$(\mathbf{I} - \ell J)(\mathbf{Y}_{i+1} - \mathbf{Y}_i) = \ell\mathbf{F}(t_i, \mathbf{Y}_i), \quad \text{where } J = \frac{\partial\mathbf{F}}{\partial\mathbf{Y}_i}(t_i, \mathbf{Y}_i). \quad (2.3.6)$$

Similarly, the linearized Crank-Nicholson method is given by

$$(\mathbf{I} - \frac{\ell}{2}J)(\mathbf{Y}_{i+1} - \mathbf{Y}_i) = \ell\mathbf{F}(t_i, \mathbf{Y}_i), \quad \text{where } J = \frac{\partial\mathbf{F}}{\partial\mathbf{Y}_i}(t_i, \mathbf{Y}_i), \quad (2.3.7)$$

where ℓ is the step-size for the general scheme.

Now the general multirate explicit Euler base method (with rate m) for (2.3.5) can be written as

$$\left. \begin{aligned} x_{n+1} &= x_n + Hf(x_n, y_n, z_n), \\ y_{n+1} &= y_n + Hg(x_n, y_n, z_n), \\ z_{n+\frac{i}{m}} &= z_{n+\frac{i-1}{m}} + hw(x_{n+\frac{i-1}{m}}, y_{n+\frac{i-1}{m}}, z_{n+\frac{i-1}{m}}). \end{aligned} \right\} \quad (2.3.8)$$

The general multirate linearly-implicit method (with rate m) for (2.3.6) is given by

$$\left. \begin{aligned} \begin{bmatrix} 1 - Hf_x(0) & -Hf_y(0) & -Hf_z(0) \\ -Hg_x(0) & 1 - Hg_y(0) & -Hg_z(0) \\ -Hw_x(0) & -Hw_y(0) & 1 - Hw_z(0) \end{bmatrix} \begin{bmatrix} x_{n+1} - x_n \\ y_{n+1} - y_n \\ z_{n+1} - z_n \end{bmatrix} &= H \begin{bmatrix} f(x_n, y_n, z_n) \\ g(x_n, y_n, z_n) \\ w(x_n, y_n, z_n) \end{bmatrix} \\ [1 - hw_z(0)] \left[z_{n+\frac{i}{m}} - z_{n+\frac{(i-1)}{m}} \right] &= hw \left[x_{n+\frac{i-1}{m}}, y_{n+\frac{i-1}{m}}, z_{n+\frac{i-1}{m}} \right]; \end{aligned} \right\} \quad (2.3.9)$$

where $i = 1, \dots, m$.

Finally, the general multirate Crank-Nicholson method (with rate m) for (2.3.7) is defined by

$$\left. \begin{aligned} \begin{bmatrix} 1 - \frac{H}{2}f_x(0) & -\frac{H}{2}f_y(0) & -\frac{H}{2}f_z(0) \\ -\frac{H}{2}g_x(0) & 1 - \frac{H}{2}g_y(0) & -\frac{H}{2}g_z(0) \\ -\frac{H}{2}w_x(0) & -\frac{H}{2}w_y(0) & 1 - \frac{H}{2}w_z(0) \end{bmatrix} \begin{bmatrix} x_{n+1} - x_n \\ y_{n+1} - y_n \\ z_{n+1} - z_n \end{bmatrix} &= H \begin{bmatrix} f(x_n, y_n, z_n) \\ g(x_n, y_n, z_n) \\ w(x_n, y_n, z_n) \end{bmatrix} \\ \left[1 - \frac{h}{2}w_z(0) \right] \left[z_{n+\frac{i}{m}} - z_{n+\frac{(i-1)}{m}} \right] &= \frac{h}{2}w \left[x_{n+\frac{i-1}{m}}, y_{n+\frac{i-1}{m}}, z_{n+\frac{i-1}{m}} \right]; \end{aligned} \right\} \quad (2.3.10)$$

where $i = 1, \dots, m$.

Also note that $f_{[j]}(0)$, $g_{[j]}(0)$ and $w_{[j]}(0)$; $j = x, y, z$ denote the derivatives evaluated at the previous time-step t_n .

It is assumed that there is only a linear change in the output of the slow sub-system each its macro-steps while the fast sub-system is being integrated over several micro-steps within a macro-step. Thus, it may seem natural to interpolate, using a polynomial of order ≥ 1 , the value of the slow sub-system while integrating the fast sub-system thus reducing the approximation error. To this end, we use a first-order interpolation between the slow and fast components and therefore the variables of slow

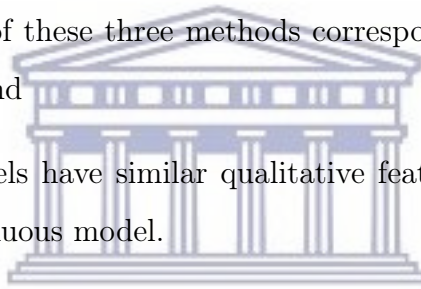
components at the fast nodes will be calculated using the formula

$$\begin{bmatrix} x_{n+\frac{i-1}{m}} \\ y_{n+\frac{i-1}{m}} \end{bmatrix} = \begin{bmatrix} \frac{m-i+1}{m}x_n + \frac{i-1}{m}x_{n+1} \\ \frac{m-i+1}{m}y_n + \frac{i-1}{m}y_{n+1} \end{bmatrix}. \quad (2.3.11)$$

2.4 Stability analysis of the numerical methods

We study the stability property of the multirate methods (2.3.8), (2.3.9) and (2.3.10) and investigate whether

- a. the fixed points of these three methods correspond to the equilibria of the continuous model, and
- b. the discrete models have similar qualitative features near these fixed points as that of the continuous model.



Here, we discuss the stability properties of the fixed points of single-rate ($m = 1$) and multirate ($m = 2$) methods by applying these methods to solve the problem (2.2.3).

Let (x^*, y^*, z^*) be fixed point of the discrete methods, i.e.,

$$\left. \begin{aligned} F(x^*, y^*, z^*) &= x^*, \\ G(x^*, y^*, z^*) &= y^*, \\ W(x^*, y^*, z^*) &= z^*, \end{aligned} \right\} \quad (2.4.1)$$

where F, G and W are the discrete counter parts of the right-hand side functions of the methods when applied to (2.2.3). These functions are obviously different for different base methods. The general right-hand side functions of these three multirate methods (with rate m), where $h = H/m$ are defined as:

(i) For m rate explicit Euler scheme:

$$\left. \begin{aligned} F(x^*, y^*, z^*) &= x^* + Hf(x^*, y^*, z^*), \\ G(x^*, y^*, z^*) &= y^* + Hg(x^*, y^*, z^*), \\ W(x^*, y^*, z^*) &= \underbrace{z^* + hw(x^*, y^*, z^*)}_{z_1} + \tilde{w}_1 + \tilde{w}_2 + \cdots + \tilde{w}_{m-1}, \\ &\quad \underbrace{\hspace{10em}}_{z_2} \\ &\quad \underbrace{\hspace{15em}}_{\vdots} \\ &\quad \underbrace{\hspace{20em}}_{z_{m-1}} \end{aligned} \right\} \quad (2.4.2)$$

where $\tilde{w}_i = hw(x^*, y^*, z_i)$ for $i = 1, 2, \dots, m - 1$.

(ii) For m rate linearly-implicit Euler scheme:

$$\left. \begin{aligned} \begin{bmatrix} F(x^*, y^*, z^*) \\ G(x^*, y^*, z^*) \\ W(x^*, y^*, z^*) \end{bmatrix} &= \begin{bmatrix} x^* \\ y^* \\ z^* \end{bmatrix} + H(\mathcal{H}_I^*)^{-1} \begin{bmatrix} f(x^*, y^*, z^*) \\ g(x^*, y^*, z^*) \\ w(x^*, y^*, z^*) \end{bmatrix}, \\ W(x^*, y^*, z^*) &= \underbrace{z^* + [hw(x^*, y^*, z^*)]}_{z_1} + \tilde{w}_1 + \tilde{w}_2 + \cdots + \tilde{w}_{m-1} / Q_1, \\ &\quad \underbrace{\hspace{10em}}_{z_2} \\ &\quad \underbrace{\hspace{15em}}_{\vdots} \\ &\quad \underbrace{\hspace{20em}}_{z_{m-1}} \end{aligned} \right\} \quad (2.4.3)$$

where, $Q_1 = [1 - hw_{z^*}(0)]$ and

$$\mathcal{H}_I^* = \begin{bmatrix} 1 - Hf_{x^*}(0) & -Hf_{y^*}(0) & -Hf_{z^*}(0) \\ -Hg_{x^*}(0) & 1 - Hg_{y^*}(0) & -Hg_{z^*}(0) \\ -Hw_{x^*}(0) & -Hw_{y^*}(0) & 1 - Hw_{z^*}(0) \end{bmatrix}.$$

(iii) For m -rate linearly CN scheme:

$$\left. \begin{aligned} \begin{cases} \begin{bmatrix} F(x^*, y^*, z^*) \\ G(x^*, y^*, z^*) \\ W(x^*, y^*, z^*) \end{bmatrix} &= \begin{bmatrix} x^* \\ y^* \\ z^* \end{bmatrix} + H (\mathcal{H}_{CN}^*)^{-1} \begin{bmatrix} f(x^*, y^*, z^*) \\ g(x^*, y^*, z^*) \\ w(x^*, y^*, z^*) \end{bmatrix}, \\ W(x^*, y^*, z^*) &= \underbrace{z^* + [hw(x^*, y^*, z^*)]}_{z_1} + \underbrace{\tilde{w}_1 + \tilde{w}_2 + \dots + \tilde{w}_{m-1}}_{z_2}, \\ &\underbrace{\hspace{10em}}_{z_{m-1}} \end{cases} \end{aligned} \right\} \quad (2.4.4)$$

where, $Q_2 = [1 - hw_{z^*}(0)/2]$ and

$$\mathcal{H}_{CN}^* = \begin{bmatrix} 1 - \frac{H}{2} f_{x^*}(0) & -\frac{H}{2} f_{y^*}(0) & -\frac{H}{2} f_{z^*}(0) \\ -\frac{H}{2} g_{x^*}(0) & 1 - \frac{H}{2} g_{y^*}(0) & -\frac{H}{2} g_{z^*}(0) \\ -\frac{H}{2} w_{x^*}(0) & -\frac{H}{2} w_{y^*}(0) & 1 - \frac{H}{2} w_{z^*}(0) \end{bmatrix}.$$

Next, we analyze the stability of the three scheme by considering particular cases, for example, single-rate ($m = 1$) and multirate ($m = 2$).

(i) For explicit Euler method with single-rate ($m = 1$) where $H = h$, (2.4.2) becomes

$$\left. \begin{aligned} \begin{cases} F(x^*, y^*, z^*) = x^* + Hf(x^*, y^*, z^*), \\ G(x^*, y^*, z^*) = y^* + Hg(x^*, y^*, z^*), \\ W(x^*, y^*, z^*) = z^* + Hw(x^*, y^*, z^*). \end{cases} \end{aligned} \right\} \quad (2.4.5)$$

A simple calculation reveals that the fixed points include the equilibrium points of the continuous problem (2.2.3) are $A(0, 0, 0)$, $B(0, 0, 1)$, $C(a_1, 0, b_1)$, and $C(0, a_2, b_2)$. This clearly is one of the desirable properties of the scheme.

Now the associated Jacobian matrix $J(x^*, y^*, z^*)$ is

$$J = \begin{bmatrix} -Hd_1 + \frac{Hzm_1}{z + \beta_1} + 1 & 0 & \frac{Hxm_1\beta_1}{(z + \beta_1)^2} \\ 0 & -Hd_2 + \frac{Hzm_2}{z + \beta_2} + 1 & \frac{Hym_2\beta_2}{(z + \beta_2)^2} \\ -\frac{Hzm_1}{\varepsilon(z + \beta_1)} & -\frac{Hzm_2}{\varepsilon(z + \beta_2)} & J_{33} \end{bmatrix}, \quad (2.4.6)$$

where

$$J_{33} = \frac{-2zH - \frac{xm_1\beta_1H}{(z + \beta_1)^2} - \frac{ym_2\beta_2H}{(z + \beta_2)^2} + H + \varepsilon}{\varepsilon}.$$

Since our interest is to show the extent to which the schemes qualitatively agree with the continuous problem, we consider those equilibrium points (which also happen to be fixed points of the numerical scheme (2.4.5)) which correspond to the set of parameters listed in (2.2.11). Thus, these points are

$$A(0, 0, 0), B(0, 0, 1), C(0.11875, 0, 0.05) \text{ and } D(0, 0.14345, 0.07778). \quad (2.4.7)$$

Calculating the Jacobian matrix at each fixed point, we obtain the corresponding eigenvalues.

For $A(0, 0, 0)$:

$$J_A = \begin{bmatrix} 1 - \frac{2H}{5} & 0 & 0 \\ 0 & 1 - \frac{H}{2} & 0 \\ 0 & 0 & 10H + 1 \end{bmatrix}, \quad (2.4.8)$$

and its eigenvalues are

$$\lambda_1 = 1 - 0.5H, \lambda_2 = 1 - 0.4H \text{ and } \lambda_3 = 1 + 10H. \quad (2.4.9)$$

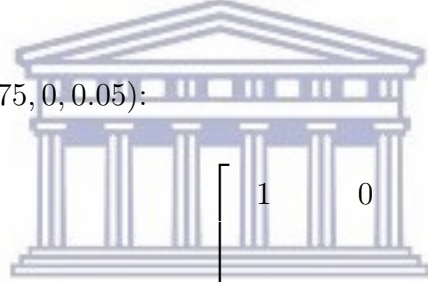
For $B(0, 0, 1)$:

$$J_B = \begin{bmatrix} \frac{19H}{15} + 1 & 0 & 0 \\ 0 & \frac{83H}{34} + 1 & 0 \\ -\frac{50H}{3} & -\frac{500H}{17} & 1 - 10H \end{bmatrix}, \quad (2.4.10)$$

and the eigenvalues are

$$\lambda_1 = 1 - 10H, \quad \lambda_2 \approx 1 + 1.2667H \quad \text{and} \quad \lambda_3 \approx 1 + 2.44118H. \quad (2.4.11)$$

For $C(0.11875, 0, 0.05)$:



UNIVERSITY of the
WESTERN CAPE

$$J_C = \begin{bmatrix} 1 & 0 & \frac{19H}{25} \\ 0 & 1 - \frac{H}{6} & 0 \\ -4H & -\frac{10H}{3} & \frac{7H}{5} + 1 \end{bmatrix}, \quad (2.4.12)$$

and the eigenvalues are

$$\lambda_1 \approx 1 - 0.166667H, \quad (2.4.13)$$

$$\lambda_2 \approx 1.52(0.657895 + (0.460526 - 1.05057I)H), \quad \text{and}$$

$$\lambda_3 \approx 1.52(0.657895 + (0.460526 + 1.05057I)H),$$

Finally, for $D(0., 0.143457, 0.0777778)$:

$$J_D = \begin{bmatrix} \frac{4H}{25} + 1 & 0 & 0 \\ 0 & 1 & \frac{83H}{100} \\ -\frac{28H}{5} & -5H & \frac{13H}{90} + 1 \end{bmatrix}, \quad (2.4.14)$$

and the eigenvalues as

$$\lambda_1 \approx 2.075(0.481928 + (0.0348059 - 0.981144I)H), \quad (2.4.15)$$

$$\lambda_2 \approx 2.075(0.481928 + (0.0348059 + 0.981144I)H), \quad \text{and}$$

$$\lambda_3 = 1 + 0.16H.$$

It can easily be shown, with the aid of symbolic calculation software, that the spectral radius (the maximum of the modulus of the eigenvalues) of all the eigenvalues in each case (2.4.9), (2.4.11), (2.4.13), (2.4.15) are greater than unity in magnitude. Hence, it means that the associated fixed points are not stable for all positive step-size H .

We next analyze stability of the multirate explicit Euler scheme with $m = 2$, i.e., $h = H/2$, in which case, (2.4.2) becomes

$$\left. \begin{aligned} F(x^*, y^*, z^*) &= x^* + Hf(x^*, y^*, z^*), \\ G(x^*, y^*, z^*) &= y^* + Hg(x^*, y^*, z^*), \\ W(x^*, y^*, z^*) &= z^* + \underbrace{hw(x^*, y^*, z^*)}_{z_1} + \tilde{w}_1. \end{aligned} \right\}. \quad (2.4.16)$$

The fixed points corresponding to the chosen values of parameters are

$$A(0, 0, 0), B(0, 0, 1), C(0.11875, 0, 0.05), D(0, 0.14345, 0.07778), \quad (2.4.17)$$

$$E \left(\frac{0.00625H_E}{H^3}, 0, 0.05 \right), \quad (2.4.18)$$

$$F \left(0, 0, \frac{0.1 (5H^2 \pm 1\sqrt{25H^4 - 4H^2 + 2H})}{H^2} \right), \text{ and} \quad (2.4.19)$$

$$G \left(0, \frac{0.000246H_G}{H^3}, 0.0778 \right), \quad (2.4.20)$$

where

$$H_E = \left(19H^3 - 26H^2 \pm 2\sqrt{225H^4 + 784H^3 + 576H^2 - 48H} \right)$$

and

$$H_G = \left(581H^3 - 54H^2 \pm 18\sqrt{100H^4 + 3114H^3 + 9801H^2 - 1782H} \right).$$

For $m = 2$, the discrete scheme has 6 more fixed points than that of the continuous problem. This should not come as a surprise because the trade-off for more accuracy in higher rate numerical schemes is a numerical artefact that merely leads to additional fixed points. Nevertheless, what is important is that all equilibrium points of the continuous problems are also fixed points of its discrete counterpart. Hence, for the remainder of this chapter, attention is focused on the common fixed points of the discrete and continuous problems. In view of this, for the case $m = 2$ with explicit Euler method, the fixed points of interest are the first four fixed points:

$$A(0, 0, 0), B(0, 0, 1), C(0.11875, 0, 0.05) \text{ and } D(0, 0.14345, 0.07778), \quad (2.4.21)$$

corresponds to the equilibria of the continuous model. Therefore we will con-

sider only these fixed points for further analysis, and the corresponding Jacobian matrices are

$$J_A = \begin{bmatrix} 1 - \frac{2H}{5} & 0 & 0 \\ 0 & 1 - \frac{H}{2} & 0 \\ 0 & 0 & (5H + 1)^2 \end{bmatrix}, \quad (2.4.22)$$

$$J_B = \begin{bmatrix} \frac{19H}{15} + 1 & 0 & 0 \\ 0 & \frac{83H}{34} + 1 & 0 \\ \frac{25}{3}H(5H - 2) & \frac{250}{17}H(5H - 2) & (1 - 5H)^2 \end{bmatrix}, \quad (2.4.23)$$

$$J_C = \begin{bmatrix} 1 & 0 & \frac{19H}{25} \\ 0 & 1 - \frac{H}{6} & 0 \\ -\frac{1}{5}H(7H + 20) & -\frac{1}{6}H(7H + 20) & \frac{1}{100}(7H + 10)^2 \end{bmatrix}, \quad (2.4.24)$$

and (2.4.25)

$$J_D = \begin{bmatrix} \frac{4H}{25} + 1 & 0 & 0 \\ 0 & 1 & \frac{83H}{100} \\ -\frac{7}{450}H(13H + 360) & -\frac{1}{72}H(13H + 360) & \frac{(13H+180)^2}{32400} \end{bmatrix}. \quad (2.4.26)$$

Further algebraic calculations showed that the spectral radii of the four Jacobian matrices J_A to J_D (for the explicit Euler scheme with $m = 2$) are each greater than unity in magnitude, and hence all the fixed points are unstable. Hence, we have proved that

Lemma 2.4.1. *The equilibrium points of (2.2.3) are also the fixed points of the Euler explicit multirate schemes (2.3.8) with $m = 1$ and $m = 2$. Furthermore, the dynamics of the discrete problems qualitatively behave in the same way as that of the continuous problem near those equilibrium points.*

- (ii) For single-rate ($m = 1$), i.e., $H = h$, the linearly-implicit Euler scheme (2.4.3) reads

$$\begin{bmatrix} F(x^*, y^*, z^*) \\ G(x^*, y^*, z^*) \\ W(x^*, y^*, z^*) \end{bmatrix} = \begin{bmatrix} x^* \\ y^* \\ z^* \end{bmatrix} + H (\mathcal{H}_I^*)^{-1} \begin{bmatrix} f(x^*, y^*, z^*) \\ g(x^*, y^*, z^*) \\ w(x^*, y^*, z^*) \end{bmatrix}. \quad (2.4.27)$$

Here, we also consider the following fixed points of (2.4.27):

$$A(0, 0, 0), B(0, 0, 1), C(0.11875, 0, 0.05) \text{ and } D(0, 0.14345, 0.07778), (2.4.28)$$

which correspond to (2.2.12).

The Jacobian matrix corresponding to the fixed point $A(0, 0, 0)$ is

$$J_A = \begin{bmatrix} \frac{5}{2H+5} & 0 & 0 \\ 0 & \frac{2}{H+2} & 0 \\ 0 & 0 & \frac{1}{1-10H} \end{bmatrix}. \quad (2.4.29)$$

It can be easily deduced that the spectral radius is less than unity in magnitude for $H > 0.2$. This implies that the fixed point is asymptotically stable for $H > 0.2$ and unstable otherwise. This in turn means that for $H \leq 2$, the scheme renders

that the dynamics of the discrete solution near the fixed point A is unstable, as expected.

The Jacobian matrix corresponding to the fixed point $B(0, 0, 1)$ is

$$J_B = \begin{bmatrix} \frac{15}{15-19H} & 0 & 0 \\ 0 & \frac{34}{34-83H} & 0 \\ -\frac{250H}{-190H^2+131H+15} & -\frac{1000H}{-830H^2+257H+34} & \frac{1}{10H+1} \end{bmatrix}, \quad (2.4.30)$$

in which case the spectral radius is calculated to be less than unity in magnitude for $H > 1.57895$ and therefore the fixed point is asymptotically stable for these values of H . However, for $H < 1.57895$, the dynamics of the discrete solution near this fixed point is unstable, also as required

The Jacobian matrix corresponding to the fixed point $C(0.11875, 0, 0.05)$ is

$$J_C = \begin{bmatrix} \frac{25-35H}{76H^2-35H+25} & -\frac{380H^2}{(H+6)(76H^2-35H+25)} & \frac{19H}{76H^2-35H+25} \\ 0 & \frac{6}{H+6} & 0 \\ -\frac{100H}{76H^2-35H+25} & -\frac{500H}{(H+6)(76H^2-35H+25)} & \frac{25}{76H^2-35H+25} \end{bmatrix}, \quad (2.4.31)$$

Finally, the Jacobian matrix corresponding to the fixed point $D(0, 0.1435, 0.0778)$

is

$$J_D = \begin{bmatrix} \frac{25}{25-4H} & 0 & 0 \\ \frac{20916H^2}{(4H-25)\tilde{H}} & \frac{180-26H}{\tilde{H}} & \frac{747H}{5\tilde{H}} \\ \frac{25200H}{(4H-25)\tilde{H}} & -\frac{900H}{\tilde{H}} & \frac{180}{\tilde{H}} \end{bmatrix}, \quad (2.4.32)$$

where $\tilde{H} = 747H^2 - 26H + 180$.

In these cases also the spectral radii of (2.4.31) and (2.4.32) are greater than unity in magnitude for all positive H . This implies that the fixed points $C(0.11875, 0, 0.05)$ and $D(0, 0.1435, 0.0778)$ are both unstable.

Now, we analyze stability of the multirate linearly-implicit Euler scheme (with $m = 2$), where $h = H/2$. In this case, (2.4.3) becomes,

$$\left. \begin{aligned} \begin{bmatrix} F(x^*, y^*, z^*) \\ G(x^*, y^*, z^*) \\ W(x^*, y^*, z^*) \end{bmatrix} &= \begin{bmatrix} x^* \\ y^* \\ z^* \end{bmatrix} + H (\mathcal{H}_I^*)^{-1} \begin{bmatrix} f(x^*, y^*, z^*) \\ g(x^*, y^*, z^*) \\ w(x^*, y^*, z^*) \end{bmatrix} \\ W(x^*, y^*, z^*) &= \underbrace{z^* + [hw(x^*, y^*, z^*) + \tilde{w}_1]}_{z_1} / (1 - hw_z(0)). \end{aligned} \right\} \quad (2.4.33)$$

The fixed points that we consider are

$$A(0, 0, 0), B(0, 0, 1), C(0.11875, 0, 0.05) \text{ and } D(0, 0.14345, 0.07778), (2.4.34)$$

and their corresponding Jacobian matrices are

$$J_A = \begin{bmatrix} \frac{5}{2H+5} & 0 & 0 \\ 0 & \frac{2}{H+2} & 0 \\ 0 & 0 & \frac{25H^2+5H+1}{1-5H} \end{bmatrix}, \quad (2.4.35)$$

$$J_B = \begin{bmatrix} \frac{15}{15-19H} & 0 & 0 \\ 0 & \frac{34}{34-83H} & 0 \\ \frac{25H(5H-2)}{15H+3} & \frac{250H(5H-2)}{85H+17} & \frac{25H^2-5H+1}{5H+1} \end{bmatrix}, \quad (2.4.36)$$

$$J_C = \begin{bmatrix} \frac{25-35H}{76H^2-35H+25} & \frac{380H^2}{(H+6)(76H^2-35H+25)} & \frac{19H}{76H^2-35H+25} \\ 0 & \frac{6}{H+6} & 0 \\ \frac{2H(7H+20)}{7H-10} & \frac{5H(7H+20)}{21H-30} & \frac{49H^2+70H+100}{100-70H} \end{bmatrix}, \quad \text{and} \quad (2.4.37)$$

$$J_D = \begin{bmatrix} \frac{25}{25-4H} & 0 & 0 \\ \frac{20916H^2}{(4H-25)\tilde{H}} & \frac{180-26H}{\tilde{H}} & \frac{747H}{5\tilde{H}} \\ \frac{14H(13H+360)}{65H-900} & \frac{5H(13H+360)}{26H-360} & \frac{169H^2+2340H+32400}{32400-2340H} \end{bmatrix}. \quad (2.4.38)$$

The eigenvalue calculations in these cases imply that the spectral radii of the multirate implicit Euler scheme (with $m = 2$) are all greater than unity in magnitude and therefore the fixed points are unstable.

Lemma 2.4.2. *The continuous system (2.2.3) and the discrete systems of single-rate ($m = 1$) and multirate ($m = 2$) implicit Euler scheme (2.3.9) have the same equilibria, and the qualitative behaviour of their solutions near these equilibria is*

also similar.

(iii) For the single-rate CN scheme, where $H = h$, scheme (2.4.4) reads

$$\begin{bmatrix} F(x^*, y^*, z^*) \\ G(x^*, y^*, z^*) \\ W(x^*, y^*, z^*) \end{bmatrix} = \begin{bmatrix} x^* \\ y^* \\ z^* \end{bmatrix} + H (\mathcal{H}_{CN}^*)^{-1} \begin{bmatrix} f(x^*, y^*, z^*) \\ g(x^*, y^*, z^*) \\ w(x^*, y^*, z^*) \end{bmatrix}, \quad (2.4.39)$$

whose fixed points under consideration are

$$A(0, 0, 0), B(0, 0, 1), C(0.11875, 0, 0.05) \text{ and } D(0, 0.14345, 0.07778). \quad (2.4.40)$$

The Jacobian matrices corresponding to these fixed points are

$$J_A = \begin{bmatrix} \frac{5-H}{H+5} & 0 & 0 \\ 0 & \frac{4-H}{H+4} & 0 \\ 0 & 0 & \frac{5H+1}{1-5H} \end{bmatrix}, \quad (2.4.41)$$

$$J_B = \begin{bmatrix} \frac{19H+30}{30-19H} & 0 & 0 \\ 0 & \frac{83H+68}{68-83H} & 0 \\ -\frac{500H}{-95H^2+131H+30} & \frac{2000H}{(5H+1)(83H-68)} & \frac{1-5H}{5H+1} \end{bmatrix}, \quad (2.4.42)$$

$$J_C = \begin{bmatrix} \frac{-38H^2-35H+50}{H} & -\frac{760H^2}{(H+12)H} & \frac{38H}{H} \\ 0 & \frac{12-H}{H+12} & 0 \\ -\frac{200H}{H} & -\frac{2000H}{(H+12)H} & \frac{-38H^2+35H+50}{H} \end{bmatrix}, \quad (2.4.43)$$

where $\bar{H} = 38H^2 - 35H + 50$ and

$$J_D = \begin{bmatrix} \frac{2H+25}{25-2H} & 0 & 0 \\ \frac{41832H^2}{(2H-25)H^*} & \frac{-747H^2-52H+720}{H^*} & \frac{2988H}{5H^*} \\ \frac{100800H}{(2H-25)H^*} & \frac{3600H}{H^*} & \frac{-747H^2+52H+720}{H^*} \end{bmatrix}, \quad (2.4.44)$$

with $H^* = 747H^2 - 52H + 720$.

By calculating the eigenvalues of the above four matrices, we found that the spectral radii in each case are strictly greater than unity in magnitude. Therefore all the fixed points are unstable.

Finally, we analyze stability of the multirate CN scheme (with $m = 2$), where $h = H/2$. Scheme (2.4.4) in this case reads

$$\left. \begin{aligned} \begin{bmatrix} F(x^*, y^*, z^*) \\ G(x^*, y^*, z^*) \\ W(x^*, y^*, z^*) \end{bmatrix} &= \begin{bmatrix} x^* \\ y^* \\ z^* \end{bmatrix} + h(\mathcal{H}_{CN}^*)^{-1} \begin{bmatrix} f(x^*, y^*, z^*) \\ g(x^*, y^*, z^*) \\ w(x^*, y^*, z^*) \end{bmatrix} \\ W(x^*, y^*, z^*) &= \underbrace{z^* + [hw(x^*, y^*, z^*) + \tilde{w}_1]}_{z_1} / (1 - \frac{h}{2}w_z(0)). \end{aligned} \right\} \quad (2.4.45)$$

The fixed points of (2.4.45) are

$$A(0, 0, 0), \quad B(0, 0, 1), \quad C(0.11875, 0, 0.05) \quad \text{and} \quad D(0, 0.14345, 0.07778). \quad (2.4.46)$$

The Jacobian matrices corresponding to each fixed points are, respectively,

$$J_A = \begin{bmatrix} \frac{5-H}{H+5} & 0 & 0 \\ 0 & \frac{4-H}{H+4} & 0 \\ 0 & 0 & \frac{25H^2+1}{1-10H} \end{bmatrix}, \quad (2.4.47)$$

$$J_B = \begin{bmatrix} \frac{19H+30}{30-19H} & 0 & 0 \\ 0 & \frac{83H+68}{68-83H} & 0 \\ \frac{25H(5H-2)}{30H+3} & \frac{250H(5H-2)}{170H+17} & \frac{25H^2+1}{10H+1} \end{bmatrix}, \quad (2.4.48)$$

$$J_C = \begin{bmatrix} \frac{-38H^2-35H+50}{H} & \frac{760H^2}{(H+12)H} & \frac{38H}{H} \\ 0 & \frac{12-H}{H+12} & 0 \\ \frac{H(7H+20)}{7H-5} & \frac{5H(7H+20)}{6(7H-5)} & \frac{49H^2+100}{100-140H} \end{bmatrix}, \quad (2.4.49)$$

and

$$J_D = \begin{bmatrix} \frac{2H+25}{25-2H} & 0 & 0 \\ \frac{41832H^2}{(2H-25)H^*} & \frac{-747H^2-52H+720}{H^*} & \frac{2988H}{5H^*} \\ \frac{7H(13H+360)}{65H-450} & \frac{5H(13H+360)}{52H-360} & \frac{169H^2+32400}{32400-4680H} \end{bmatrix}. \quad (2.4.50)$$

Similarly, with the aid of symbolic calculation software, we found that for any positive real value of H , the spectral radii of the corresponding Jacobian matrices are each greater than unity in magnitude and hence the fixed points are unstable. Hence, we have the following result:

Lemma 2.4.3. *The continuous system (2.2.3) and the discrete system of single-rate and multirate (with $m = 2$) Crank-Nicholson scheme (2.3.10) have the same equilibria and behave qualitatively similar near these equilibria.*

In the remaining part of this section, we present a short description of extrapolation of the methods presented above with the multirate methods discussed above used as the basis. It is important to note that, an extrapolation method is a simple way to obtain high-order accuracy by extrapolating lower-order solutions obtained by some basic methods, in our case, these are the multirate methods discussed in the above. This method is introduced in its present form by Gragg and Stetter [57]. The idea behind the method is as follows:

Consider the initial value problem or the system of ordinary differential equations (2.3.1) and $H > 0$ as the basic step-size.

Consider a sequence of positive integers $n_i < n_{i+1}$, $1 \leq i \leq M$ and define the corresponding micro step-sizes $h_1 > h_2 > h_3 > \dots$, by $h_i = H/n_i$. Then choose a numerical approximation of the initial value problem at $x_0 + H$, by performing n_i steps with step-size h_i to obtain,

$$T_{i,1} := y_{h_i}(x_0 + H). \quad (2.4.51)$$

That is, the term defined in equation (2.4.51) comes from a numerical method which in this chapter would be any of the basic methods described by (2.3.8)-(2.3.10). By using M number of approximations to (2.4.51) with different h_i 's, one can eliminate the truncation error terms by using Richardson extrapolation. As a result, we can obtain a high-order approximate solution of our initial value problem by using the Aitken-Neville formula [48],

$$T_{j,k+1} = T_{j,k} + \frac{T_{j,k} - T_{j-1,k}}{(n_j/n_{j-1}) - 1}, \quad j = 1, \dots, k. \quad (2.4.52)$$

This formula provides a simple way of recursively generating high-order accurate approximations from those with lower-orders.

2.5 Numerical results

In this section, we present numerical results obtained by using the proposed multirate schemes for the model under consideration. To compare efficiency of these methods, we also provide results obtained with their single-rate analogues. The interactions of the three species in this model are very sensitive to parameter values and initial data, which can lead to competitive exclusion as well as total extinction of the whole system, coexistence in the form of steady state and coexistence in the form of an oscillatory solution. Using the parameter values (2.2.11) and considering the initial condition $(x_0, y_0, z_0) = (0.28, 0.001, 0.2)$, we demonstrate the capability of the numerical schemes in representing the coexistence of the three species under a stable relaxation oscillation. The simulations are performed with final time $T = 100$, a reasonably long time.

In tables 2.5.1, 2.5.2, and 2.5.3, we present results where comparison is made by taking the slow or inactive component of the dynamics to use a larger time-step in multirate scheme with $m = 4$ (for all three basic schemes) where the fast dynamics being four times faster than the slow dynamics. We can see that the computational costs of the multirates of explicit Euler, implicit Euler and CN schemes are far less than their corresponding single-rate schemes with comparative level of accuracy. Moreover, with the same step-size, the accuracy of multirate methods is better than the corresponding single-rate schemes, see tables, 2.5.4, 2.5.5.

To further corroborate the applicability of the proposed methods, we plotted some results obtained with these methods. Figure 2.5.2, 2.5.4 and 2.5.6 display results in phase space of the three species for single-rate with step-size $H = 0.0025$ and multirate ($m = 4$) with step-size $H = 0.01$ of the three schemes as well as those obtained with the extrapolated ($T_{5,4}$ versions) schemes, respectively. Figure 2.5.1, 2.5.3 and 2.5.5 display the results of the three species over time for single-rate with step-size $H = 0.0025$ and multirate ($m = 4$) with step-size $H = 0.01$ of the three schemes and as well as those obtained with the extrapolated ($T_{5,4}$ versions) schemes, respectively.

Table 2.5.1: Comparison of efficiency of single-rate explicit Euler and multirate ($m = 4$) explicit Euler method

H	explicit Euler ($m = 1$)	CPU	H	explicit Euler ($m = 4$)	CPU
0.025	Converges to LC	0.8145	0.1	Converges to LC	0.3020
0.005	Converges to LC	4.0424	0.02	Converges to LC	1.4628
0.0025	Converges to LC	11.2710	0.01	Converges to LC	2.9606
0.0005	Converges to LC	40.2141	0.002	Converges to LC	14.8274
0.00025	Converges to LC	83.8838	0.001	Converges to LC	29.3732

Table 2.5.2: Comparison of efficiency of single-rate linearly-implicit Euler and multirate ($m = 4$) linearly-implicit Euler method.

H	implicit Euler ($m = 1$)	CPU	H	implicit Euler ($m = 4$)	CPU
0.025	Converges to LC	1.6038	0.1	Converges to LC	0.5147
0.005	Converges to LC	7.9557	0.02	Converges to LC	2.4976
0.0025	Converges to LC	15.7078	0.01	Converges to LC	4.9862
0.0005	Converges to LC	79.2014	0.002	Converges to LC	24.8913
0.00025	Converges to LC	158.4473	0.001	Converges to LC	49.6068

Table 2.5.3: Comparison of efficiency of single-rate CN and multirate ($m = 4$) CN method.

H	Single-rate CN	CPU	H	multirate ($m = 4$) CN	CPU
0.025	Converges to LC	1.6009	0.1	Converges to LC	0.5100
0.005	Converges to LC	7.8744	0.02	Converges to LC	2.5066
0.0025	Converges to LC	15.8151	0.01	Converges to LC	5.0268
0.0005	Converges to LC	78.3874	0.002	Converges to LC	24.8153
0.00025	Converges to LC	158.1450	0.001	Converges to LC	49.8310

Table 2.5.4: Comparison of the convergence profile of the single-rate ($m = 1$) of the three methods: explicit Euler (M1), linearly-implicit Euler (M2) and CN (M3); LC: Limit Cycle.

H	M1	M2	M3
0.1	Diverges Converges to LC	Converges to LC	Diverges
0.05	involving negative values	Converges to LC	Converges to LC



Table 2.5.5: Comparison of the convergence profile of the multirate ($m = 4$) of the three methods: explicit Euler (M1), linearly-implicit Euler (M2) and CN (M3); LC: Limit Cycle.

H	M1	M2	M3
0.1	Converges to LC	Converges to LC	Converges to LC
0.05	Converges to LC	Converges to LC	Converges to LC

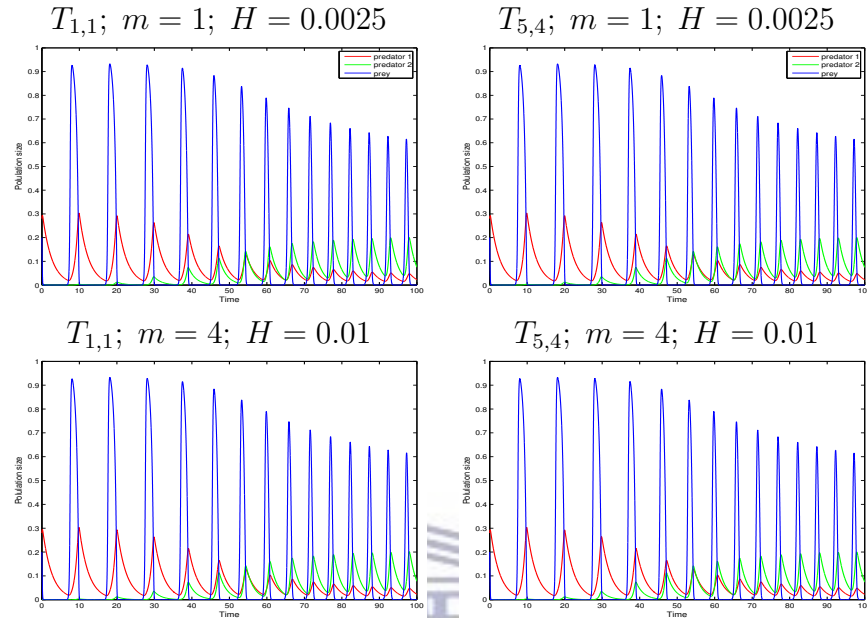


Figure 2.5.1: Simulation results displaying predators and prey over time using extrapolated explicit Euler method with single-rate ($m = 1$) (upper figures) and explicit Euler method with multirate rate ($m = 4$) (lower figures) applied to the system (2.2.3).

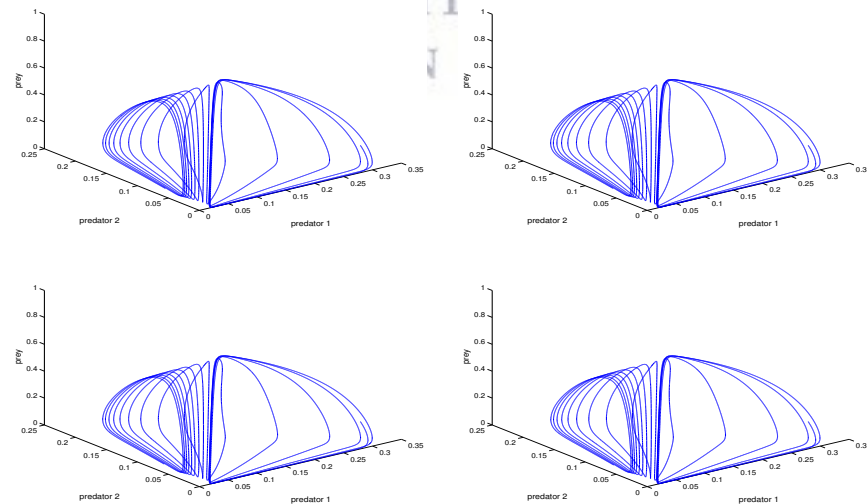


Figure 2.5.2: Simulation results showing trajectories in the phase space (predators over the prey) using extrapolated explicit Euler method with single-rate ($m = 1$) (upper figures) and explicit Euler method with multirate rate ($m = 4$) (lower figures) applied to the system (2.2.3). The amplitude decreases towards a limit cycle.

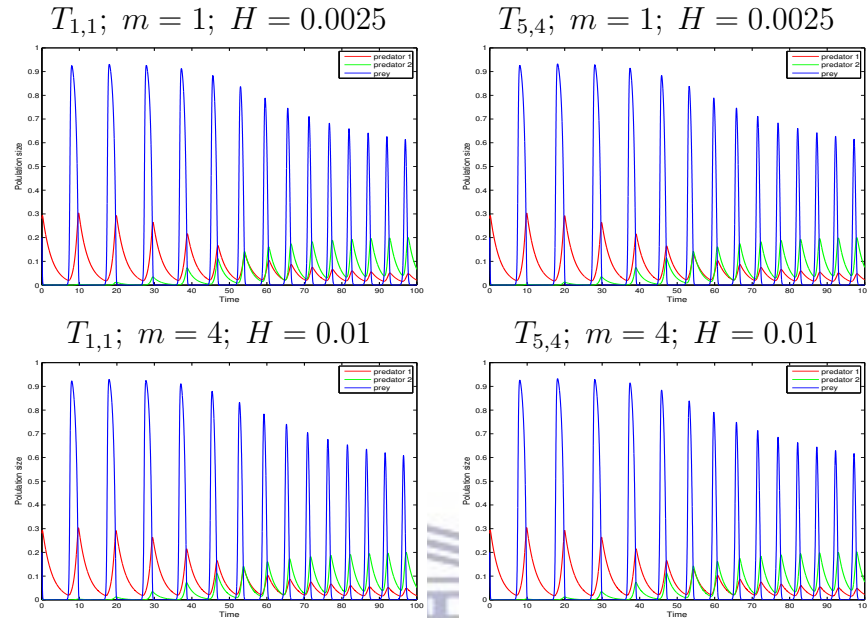


Figure 2.5.3: Simulation results displaying predators and prey over time using extrapolated implicit Euler method with single-rate ($m = 1$) (upper figures) and implicit Euler method with multirate ($m = 4$) (lower figures) applied to the system (2.2.3).

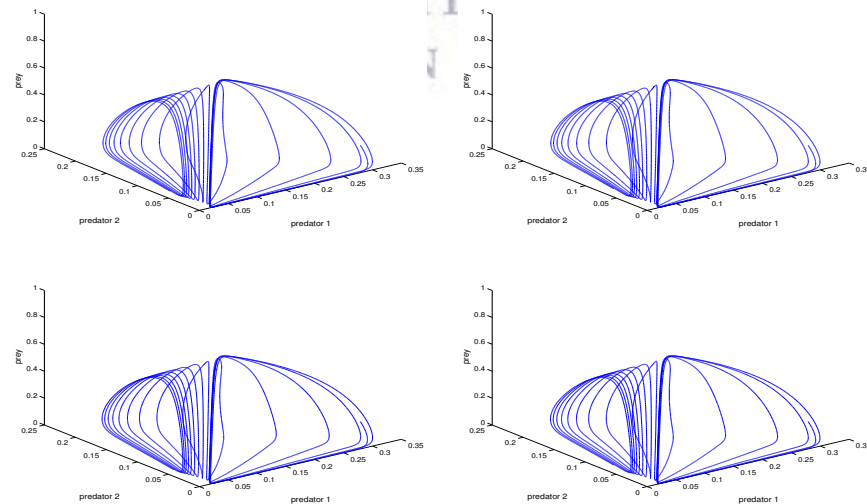


Figure 2.5.4: Simulation results showing trajectories in the phase space (predators over the prey) using extrapolated implicit Euler method with single-rate ($m = 1$) (upper figures) and implicit Euler method with multirate ($m = 4$) (lower figures) applied to the system (2.2.3). The amplitude decreases towards a limit cycle.

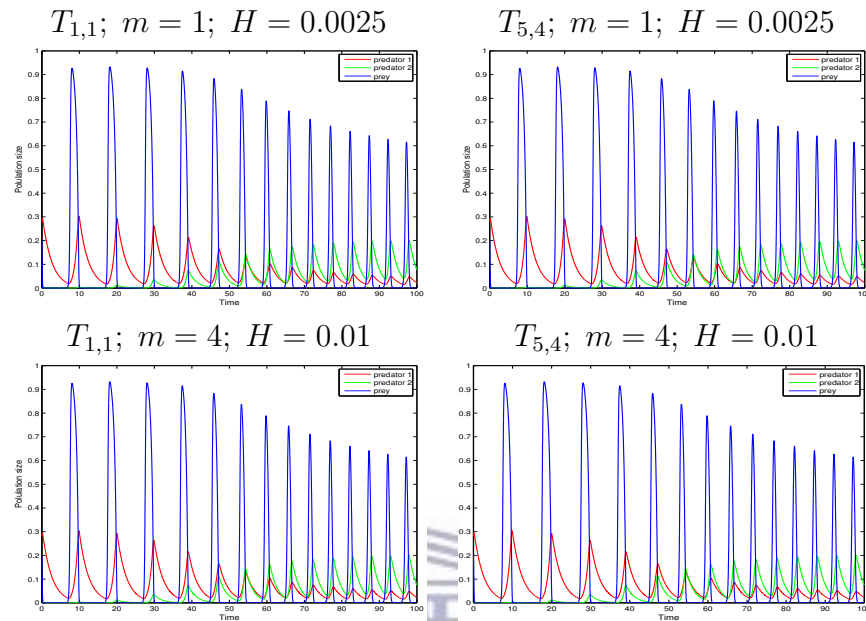


Figure 2.5.5: Simulation results displaying predators and prey over time using extrapolated single-rate ($m = 1$) Crank-Nicholson method (upper figures) and Crank-Nicholson method with multirate ($m = 4$) (lower figures) applied to the system (2.2.3).

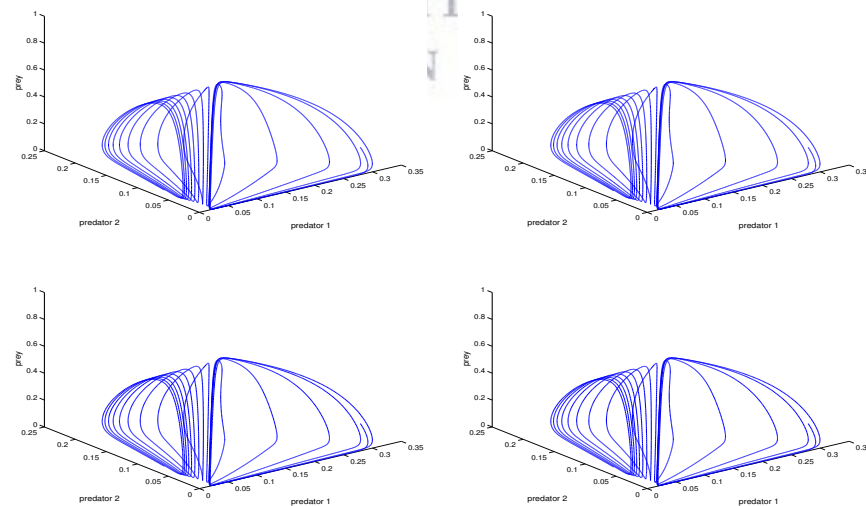


Figure 2.5.6: Simulation results showing the trajectories in the phase space (predators over the prey) using extrapolated Crank-Nicholson method with single-rate ($m = 1$) (upper figures) and Crank-Nicholson method with multirate ($m = 4$) (lower figures) applied to the system (2.2.3). The amplitude decreases towards a limit cycle.

2.6 Summary and discussion

We have presented multirate ($m > 1$) methods for solving a mathematical model of slow-fast dynamical system, described as a nonlinear system of ordinary differential equations. Efficiency is ensured by treating the slow and the fast components in such away that the slower (more or less inactive) component with larger (macro) step-size, while a fraction of the macro step-size (or micro) is allocated for the fast (more active) component in a single framework. With reference to some theoretical results, a thorough numerical experiments confirmed that these multirate schemes outperform the corresponding single-rate schemes substantially both in terms of computational work and CPU times. It is also demonstrated that these methods render solutions which have qualitatively similar behaviour as that of the continuous problem, thus ensuring dynamical consistency.

Note that, although the multirate schemes presented in this chapter capture the dynamics of the multiscale model efficiently, they are only limited to first-order since they are based on the linear Taylor series approximation. In the next chapter, we adapt the idea of multirate method to high-order (second-order) fractional-step methods applied to the same problem. For the nonlinearly-implicit cases, a couple of nonlinear solvers will be assessed for efficiency and robustness.

Chapter 3

Fractional-step θ -methods for singularly perturbed problems in ecology



In this chapter, we deal with the numerical simulation of the nonlinear predator-prey model that was considered in Chapter 2. In there, a class of multirate methods aimed at representing essential solution profiles of the model, such as relaxation oscillations, have been presented. While these methods performed well in replicating such qualitative features of the continuous problem, their accuracy is only limited to first-order, since the derivation is based on the Taylor's linear approximation about the current state in the time-stepping. Thus, the need to develop high-order methods to efficiently solve such models is self-evident. In this chapter, we develop a class of high-order algorithms based on the fractional-step (operator-splitting) θ -methods. In conjunction with the implicit schemes, nonlinearities are treated with two different iterative methods, namely Jacobian-Free Newton Krylov (JFNK) and Anderson's Acceleration (AA) fixed point algorithms. The main advantage of using fractional-step or operator-splitting based algorithms is its flexibility in applying different convenient methods for different part of the problem in a single computational framework, depending on

their respective dynamics. We also analyze these methods for stability and convergence. Several numerical experiments are performed to demonstrate the efficiency of the proposed methods and confirm results obtained from a theoretical investigation.

3.1 Introduction

Deterministic mathematical models are continuing to be indispensable tools for analyzing and understanding biological and ecological systems (in epidemiology, see, for example, [119] and the references therein). However, such models are typically nonlinear and highly complex systems of ordinary differential equations (ODEs) for which analytical study is limited to describing the underlying dynamics only qualitatively. The topic of interest in this chapter is the formulation of efficient, high-order numerical methods for solving problems in ecology that describe complex slow-fast dynamical systems, such as the one considered in the previous chapter. Slow-fast models are also referred to as singularly perturbed problems [88] due to a difference in time scales, characterized by the presence of a small parameter ε , that exists between the components of the system. For example, in a predator-prey model which exhibits slow-fast dynamics, differences in time scale arises as a result of different time scales of the species at different trophic levels. Qualitative properties such as the existence of invariant manifolds of slow-fast dynamical system of predator-prey models have been studied extensively using geometric singular perturbation theory [29, 56, 66, 88, 93, 98].

In this chapter, we deal with the numerical simulation of the slow-fast system that was considered in Chapter 2. The model which was studied in [98] consist of two predator populations compete for a prey population, and the dynamics of the prey population is fast relative to that of the predators. The model is nonlinear and so complex that their solutions are difficult (usually impossible) to obtain analytically, and hence the use of approximation numerical methods becomes significantly important. To this end, it is worth mentioning here that various numerical schemes have been proposed in the literature thus far for solving multiple-time scale models. For example,

Constantinescu and Sandu [27], developed multirate time integration schemes using extrapolation methods for efficient simulation of multiscale ODE and PDE problems. They applied the lower-order implicit and explicit Euler methods to each component of the problem in a sequential manner. But the time-steps were chosen according to the activity level of each component such that larger (macro) and smaller (micro) time-steps were used for the slow and fast components, respectively.

In [107], we extended the idea of extrapolation multirate algorithm [27] to solve a three-dimensional predator-prey model (the same as the one considered in this chapter) describing slow-fast dynamics. In our paper, we applied the same schemes to all the sub-systems but with different time-steps depending on the activity levels of the dynamics where the slow dynamics is integrated with a bigger time-step and the fast dynamics are integrated with relatively smaller time-steps. The accuracy and efficiency of multirate methods are found to be better than the corresponding single-rate methods where all components in the system are advanced simultaneously in time by the same time-stepping schemes. The qualitative properties of the dynamical system are also well preserved by the multirate methods presented in the paper.

The origin of multirate time integration algorithms trace back to 1960 [128], where the split explicit Runge-Kutta methods were analyzed. Multirate approaches were applied in [51] whereas their stability analysis can be found in [5]. In [69], multirate θ -method is used to study stiff ordinary differential equations with one level of temporal local refinement. They used different time-steps for different solution components and also analyzed local accuracy, propagation of interpolation error and linear stability.

In [26], extrapolation implicit-explicit time-stepping methods based on Euler method were used. They applied their method to solve ODEs, DAEs and PDEs having both stiff and non-stiff parts and categorized it informally as fast and slow components. In their work, implicit and explicit schemes are used for stiff and non-stiff components, respectively, to get advantage by gaining the desired accuracy and stability. Linear stability of the method was also analyzed.

Our aim in this chapter is to design efficient and high-order accurate numerical

method to solve the three-dimensional predator-prey models ([107]) which have different time scales. The proposed method, known as fractional-step θ -method, involves decoupling the system into slow and fast components, and at each time-step suitable numerical sub-algorithms (θ -method) are chosen to discretize each component independently using different time-steps. Then, the time-stepping algorithm for the full problem is obtained by utilizing a high-order product formula for merging the sub-algorithms at each time-step. Note that the multirate schemes developed in Chapter 2 have a little less desirable property than the fractional-step algorithms proposed in the current work. The reason is that, although those multirate methods, like the fractional-step algorithms, capture multiple time scale dynamics efficiently, they are only limited to first-order, since the underlying derivation is based on linear Taylor series approximation. The fractional-step methods overcome these weaknesses. They combine same or different integration schemes, using different time-steps within a time-stepping algorithm for the subproblems into an efficient high-order product scheme for the overall problem.

In using the θ -method, we use Jacobian-free Newton-Krylov (JFNK) method and Anderson's acceleration technique to solve the nonlinear system resulting from the implicit schemes. The JFNK method uses a combination of Newton-like methods for superlinear convergent solution of nonlinear equations, and Krylov subspace method for solving the Newton correction equation [83, 106]. The method requires only matrix-vector multiplication instead of direct computation of the Jacobian. In doing so, it reduces the computational cost associated with the construction and storage of the Jacobian resulting in an efficient solution algorithm. The latter is a fixed point iteration method which is used to increase the convergence of the fixed point method. The algorithm stores prior evaluation to the current step and computes the new iteration using a linear combination of them. Regarding the Anderson's acceleration technique, readers may note that it is also being applied in different areas, see, e.g., [30, 38, 63, 97, 163].

As far as the fractional-step methods are concerned, we note that these are very

powerful techniques for the numerical solution of complicated and coupled time-dependant real-life problems. These methods are used for solving ODEs [105], DAEs [159] and PDE's, see for example [22, 79, 123]. The idea behind the method is based on splitting the original system into sub-systems, apply appropriate numerical schemes for each sub-system and piecing these schemes together by fractional-step procedure. Note that the first splitting methods, based on the fundamental results of finite difference methods, were developed in the 1960s and 1970s. The Lie-Trotter splitting and the Strang splitting [150] were the most classical splitting methods. Splitting methods have been applied (sometimes with different names) in many different fields, ranging from parabolic and reaction-diffusion PDEs to quantum statistical mechanics, biology, dynamical system, chemical physics and Hamiltonian dynamical systems [105]. These techniques can also be applied for autonomous and non-autonomous ordinary differential equation.

The rest of the chapter is organized as follows. In Section 3.2, we specify the model problem that we are studying and give a brief discussion on qualitative properties of the model. In Section 3.3, the numerical methods are formulated in detail for the two time scale model problem described in Section 3.2. Treatment of nonlinearities using JFNK and Anderson's acceleration method are given in Section 3.4. In Section 3.5, stability analysis of the full discrete scheme is discussed. Numerical results and simulations are presented in Section 3.6. Finally, we present some concluding remarks and scope for further research in Section 3.7.

3.2 The mathematical model

To keep the exposition self-contained and brief, we summarize the scaled form of the model considered in Chapter 2. We also briefly analyze the global behaviour of its dynamics using geometric singular perturbation approach.

$$\left. \begin{aligned} \dot{x} &= x \left(\frac{m_1 z}{\beta_1 + z} - d_1 \right) =: f(x, y, z), \\ \dot{y} &= y \left(\frac{m_2 z}{\beta_2 + z} - d_2 \right) =: g(x, y, z), \\ \varepsilon \dot{z} &= w^*(x, y, z) =: w(x, y, z), \end{aligned} \right\} \quad (3.2.1)$$

where

$$w^*(x, y, z) = z \left(1 - z - \frac{m_1 x}{\beta_1 + z} - \frac{m_2 y}{\beta_2 + z} \right), \quad (3.2.2)$$

with appropriate initial conditions. The variables x, y , and z are time-dependant unknown functions; $f(x, y, z)$, $g(x, y, z)$, and $w(x, y, z)$ are smooth functions describing the dynamics of the system and ε is a small positive number ($0 < \varepsilon \ll 1$), which represents the separation of time scales between the fast and slow dynamics. This model problem is a form of standard singular perturbation problem.

This model problem have four equilibrium points $A(0, 0, 0)$, $B(0, 0, 1)$,

$$C \left(-\frac{\beta_1 ((\beta_1 + 1) d_1 - m_1)}{(\hat{d}_1)^2}, 0, -\frac{\beta_1 d_1}{\hat{d}_1} \right) \text{ and } D \left(0, -\frac{\beta_2 ((\beta_2 + 1) d_2 - m_2)}{(\hat{d}_2)^2}, -\frac{\beta_2 d_2}{\hat{d}_2} \right),$$

where $\hat{d}_i = d_i - m_i$, $i = 1, 2$. It is assumed that, \hat{d}_i are negative as the growth rate of the predators are greater than the death rate of them for the co-existence of all species involved in the dynamics.

3.2.1 Analysis via geometric singular perturbation theory

One can use geometric singular perturbation theory to study the global structure of the orbits. To do so, we proceed as follows: We first observe that the derivative in (3.2.1) is given with respect to slow time scale t . By transforming to the fast variable

$\tau = t/\varepsilon$, we obtain

$$\left. \begin{aligned} x' &= \varepsilon f(x, y, z), \\ y' &= \varepsilon g(x, y, z), \\ z' &= w^*(x, y, z), \end{aligned} \right\} \quad (3.2.3)$$

where $' = \frac{d}{d\tau}$. The two systems (3.2.1) and (3.2.3) are equivalent as long as $\varepsilon \neq 0$. As $\varepsilon \rightarrow 0$, the above defines two limiting systems. The first one is

$$\left. \begin{aligned} \dot{x} &= f(x, y, z), \\ \dot{y} &= g(x, y, z), \\ 0 &= w^*(x, y, z), \end{aligned} \right\} \quad (3.2.4)$$

which is the *reduced system*. It is a differential algebraic equation obtained from (3.2.1) where the algebraic constraint $w^*(x, y, z) = 0$, defines the critical manifold.

The second system, the *layer problem*, obtained from (3.2.3) is defined as

$$\left. \begin{aligned} x' &= 0, \\ y' &= 0, \\ z' &= w^*(x, y, z). \end{aligned} \right\} \quad (3.2.5)$$

The reduced problem (3.2.4) captures the slow dynamics while the layer problem (3.2.5) represents the fast dynamics.

The orbits of system (3.2.5) are parallel to the z -axis and their directions are characterized by the signs of $w^*(x, y, z)$. We refer to these orbits as fast orbits of system (3.2.1).

The critical set (manifold), which is the equilibria of the layer problem, is defined as

$$S_0 = \left\{ (x, y, z) : z \left(1 - z - \frac{m_1 x}{\beta_1 + z} - \frac{m_2 y}{\beta_2 + z} \right) = 0; x \geq 0, y \geq 0, z \geq 0 \right\}. \quad (3.2.6)$$

This defines two critical manifolds

$$S_1 = \{(x, y, z) \in S_0 : z = 0\}, \quad (3.2.7)$$

and

$$S_2 = \left\{ (x, y, z) \in S_0 : 1 - z - \frac{m_1 x}{\beta_1 + z} - \frac{m_2 y}{\beta_2 + z} = 0 \right\}. \quad (3.2.8)$$

The reduced system (3.2.4) is defined on the critical manifold S_0 , and the layer problem (3.2.5) is a one dimensional system in the variable z parameterized by the slow variables x, y with equilibria on S_0 .

The flow of the limiting fast system on S_1 is determined by the signs of

$$w_z^*(x, y, 0) = 1 - \frac{m_1 x}{\beta_1} - \frac{m_2 y}{\beta_2}. \quad (3.2.9)$$

The limiting fast dynamics, governed by system (3.2.5), has S_1 as a set of equilibria. Furthermore, $S_1^- = \{(x, y, 0) \in S_0 : w_z^*(x, y, 0) < 0\}$ is normally stable with vertical stable fibers and $S_1^+ = \{(x, y, 0) \in S_0 : w_z^*(x, y, 0) > 0\}$ is normally unstable with vertical unstable fibers. That is, all solutions of (3.2.5) in the vicinity of S_1^- move vertically toward S_1^- and all solutions of (3.2.5) in the vicinity of S_1^+ move vertically away from S_1^+ .

The slow dynamics on S_1 reduces to

$$\left. \begin{aligned} \dot{x} &= -xd_1, \\ \dot{y} &= -yd_2, \\ z &= 0. \end{aligned} \right\} \quad (3.2.10)$$

The origin $A(0, 0, 0)$ is the global attractor of system (3.2.10) with a vector field $(-xd_1, -yd_2)$.

For the equilibrium point $A(0, 0, 0)$ on S_1 , the fast flow is determined by the signs of

$$w_z^*(x, y, 0) = 1 - \frac{m_1 x}{\beta_1} - \frac{m_2 y}{\beta_2} > 0, \quad (3.2.11)$$

and therefore the equilibrium point $A(0, 0, 0)$ is normally hyperbolically unstable, that is, the point $A(0, 0, 0)$ is attracting point in the invariant xy -plane and repelling in the invariant

z -axis.

The flow of the limiting fast system on S_2 is determined by the signs of

$$w_z^*(x, y, z) = 1 - 2z - \frac{m_1\beta_1x}{(\beta_1 + z)^2} - \frac{m_2\beta_2y}{(\beta_2 + z)^2}. \quad (3.2.12)$$

For the limiting fast dynamic, it is clear that all solutions of system (3.2.5) in the vicinity of $S_2^- = ((x, y, z) \in S_0 : w_z^*(x, y, z) < 0)$ will move vertically toward S_2^- and those in the vicinity of $S_2^+ = ((x, y, z) \in S_0 : w_z^*(x, y, z) > 0)$ will move vertically away from S_2^- .

For the equilibrium point $B(0, 0, 1)$ on S_2 , we have

$$w_z^*(x, y, z) = 1 - 2z - \frac{m_1\beta_1x}{(\beta_1 + z)^2} - \frac{m_2\beta_2y}{(\beta_2 + z)^2} < 0. \quad (3.2.13)$$

Hence, the equilibrium point $B(0, 0, 1)$ is normally hyperbolic stable and is attracting along the invariant z -axis.

The slow dynamics on S_2 reduces to

$$\left. \begin{aligned} \dot{x} &= x \left(\frac{m_1 p(x, y)}{\beta_1 + p(x, y)} - d_1 \right), \\ \dot{y} &= y \left(\frac{m_2 p(x, y)}{\beta_2 + p(x, y)} - d_2 \right), \\ z &= p(x, y). \end{aligned} \right\} \quad (3.2.14)$$

The point $B(0, 0, 1)$ is repelling in the invariant xy -plane of (3.2.14). For the equilibrium points $C(0.1187, 0, 0.05)$ and $D(0, 0.1435, 0.0778)$, we can see from (3.2.12) that $w_z^*(x, y, z) > 0$ on S_2 which implies that these points are normally hyperbolic with repelling in the invariant z -axis. The point, $C(0.1187, 0, 0.05)$ is attracting along the invariant x -axis and repelling along the y -axis of xy -plane, whereas $D(0, 0.1435, 0.0778)$ is repelling along xy -plane.

In the next section, we will discuss the construction and formulation of a general fractional-step θ -method which enables us to solve the multiscale model problem (3.2.1) discussed in this section.

3.3 Numerical methods

The model problem (3.2.1) exhibits multiple time scales and is highly nonlinear thus difficult to be solved analytically. To solve such complicated systems of differential equations numerically, we use a time-stepping algorithm based on monolithic θ -method (MTS), fractional-step θ -method (FSTS) and fractional-step mixed implicit-explicit method (FSMIMEX). Below, we discuss the details of the construction of these methods.

3.3.1 Monolithic θ -method

Consider a general evolutionary system of the form

$$\dot{\mathbf{u}} = \mathbf{F}(t, \mathbf{u}), \quad \mathbf{u}(0) = \mathbf{u}_0, \quad (3.3.1)$$

where $\mathbf{u} : [0, T] \rightarrow \mathbb{R}^n$ and \mathbf{F} is a vector-valued function of t and \mathbf{u} .

We first consider a partition of the time interval $[0, T]$ of interest into N sub-intervals $[t_n, t_{n+1}]$ of length H , hence $t_n = nH$. Here we ignore the difference in time scale that could appear in the dynamics, and a single time step-size is considered in the numerical formulation. The finite difference θ -method for the system (3.3.1), in a monolithic approach, is formally defined as

$$\mathbf{u}_{n+1} = \mathbf{u}_n + H[(1 - \theta)\mathbf{F}(t_n, \mathbf{u}_n) + \theta\mathbf{F}(t_{n+1}, \mathbf{u}_{n+1})], \quad (3.3.2)$$

with $\mathbf{u}_0 = \mathbf{u}(0)$ for all $n = 1, \dots, N$, where $\theta \in [0, 1]$ is the discretization parameter, and \mathbf{u}_n and \mathbf{u}_{n+1} denote the numerical values of \mathbf{u} at the time-steps t_n and t_{n+1} , respectively.

Although, in monolithic θ -method, each component is treated with a single time-step length H , it can be applied for general problems including the multiscale problem considered in this study. The monolithic θ -method applied to the problem (3.2.1) gives the scheme

$$\begin{bmatrix} x_{n+1} \\ y_{n+1} \\ z_{n+1} \end{bmatrix} = \begin{bmatrix} x_n \\ y_n \\ z_n \end{bmatrix} + H(1 - \theta) \begin{bmatrix} f_n \\ g_n \\ w_n \end{bmatrix} + H\theta \begin{bmatrix} f_{n+1} \\ g_{n+1} \\ w_{n+1} \end{bmatrix}, \quad (3.3.3)$$

with initial condition

$$\begin{bmatrix} x_0 \\ y_0 \\ z_0 \end{bmatrix} = \begin{bmatrix} x(0) \\ y(0) \\ z(0) \end{bmatrix}, \quad (3.3.4)$$

where f_k , g_k , and w_k denotes the values of f , g , and w , at the k^{th} time-step t_k , respectively.

For $\theta \in [0, 1]$, the implicit recurrence relation (3.3.3) requires to solve the nonlinear algebraic system of equation

$$\mathbf{G}(\mathbf{u}) = \mathbf{0}, \quad (3.3.5)$$

at each time-step with the initial condition $\mathbf{u}_0 = \mathbf{u}(0)$, and the solution is the $n + 1^{\text{st}}$ time-step numerical value \mathbf{u}_{n+1} , where

$$\mathbf{G}(\mathbf{u}_{n+1}) := \mathbf{u}_{n+1} - \mathbf{u}_n - H[(1 - \theta)\mathbf{F}(t_n, \mathbf{u}_n) - \theta\mathbf{F}(t_{n+1}, \mathbf{u}_{n+1})], \quad (3.3.6)$$

where \mathbf{G} refers to the residual corresponding to the monolithic scheme (3.3.3).

Note that the θ -method, as it is generally formulated in (3.3.2), includes a class of known finite difference schemes. For example, $\theta = 0, 1, 1/2$, leads to explicit forward Euler (EE), implicit backward Euler (IE) and Crank-Nicholson (CN) schemes, respectively.

Despite the fact that the scheme (3.3.2) assumes a single-time scale, it can be applied for problems exhibiting multiple-time scales. However, the accuracy of the monolithic scheme is usually limited by the fastest changing dynamics. In other words, for such problems the monolithic scheme does not take advantage of the multiscale nature of the problem. To this end, we aim to use fractional-step θ -method as discussed below.

3.3.2 Fractional-step θ -method

Fractional-step θ -method is suitable for problems exhibiting multiple time scales. The idea behind this method is to decouple the original system into simpler sub-systems in terms of their time scale. Then each sub-system is treated using different time-step length according to the time scale of the dynamics in each partition of the full problem.

First, recall that the singularly perturbed system of differential equations (3.2.1), with $0 < \varepsilon \ll 1$ represents an intrinsic time scale of the fastest component, z . The other components,

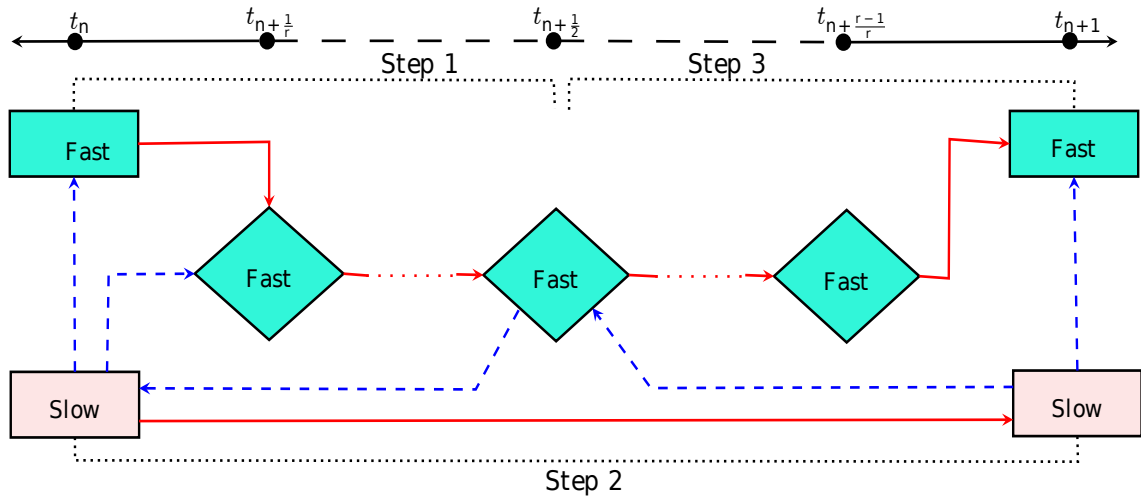


Figure 3.3.1: Schematic of fractional-step r -rate algorithm. The broken arrows show the input flow, where as, the solid arrow lines represent stepping from one compartment to the other. The algorithmic flow reads from left to right.

x and y are assumed to have a time scale of the same order but greater than that of z . Due to this difference in time scales, an accurate monolithic solution scheme would require a small time-step, dictated by ε . However, an efficient and accurate time integration scheme can be constructed by allocating different time-step length according to the time scale of each of the components involved. To achieve such multiscale scheme, we first need to split the system (3.2.1) into two sub-systems, each exhibiting a single time-step:

$$\left. \begin{array}{l} \dot{x} = 0 \\ \dot{y} = 0 \\ \dot{z} = w(t, x, y, z) \end{array} \right\} \text{(Fast phase)}, \quad \left. \begin{array}{l} \dot{x} = f(t, x, y, z) \\ \dot{y} = g(t, x, y, z) \\ \dot{z} = 0 \end{array} \right\} \text{(Slow phase)}. \quad (3.3.7)$$

In this split, note that in the fast phase the slow components (x and y) are fixed and in the slow phase the fast component is kept fixed.

Having the time partition as in the monolithic θ -method characterized by the step-size H , we now further subdivide each sub-interval $[t_n, t_{n+1}]$ into r ($= 2m, m \in \mathbb{N}$) divisions of length h :

$$t_n < t_{n+1/r} < \dots < t_{n+1/2} < \dots < t_{n+(r-1)/r} < t_{n+1}. \quad (3.3.8)$$

Since $H = t_{n+1} - t_n$ and $h = t_{n+(i+1)/r} - t_{n+i/r}; i = 1, \dots, r$, hence $H = rh$. We refer the

time-step $[t_n, t_{n+1}]$ as macro-step, and $[t_{n+i/r}, t_{n+(i-1)/r}]$ as the micro- step.

Next, we construct a discrete algorithm for system (3.3.7) in three steps. In the first step, the fast phase is solved over the time-steps $t_n, t_{n+1/r}, \dots$, and $t_{n+1/2}$, while the slow components are fixed at n^{th} -time-step, that is, $x_\ell = x_n$, and $y_\ell = y_n$, for each $\ell = n, n + 1/r, \dots, n + 1/2$. Overall, in the first step, only the fast sub-system is stepped up over a time interval of length $H/2$ in m -steps. The intermediate step involves solving the slow phase once over the time macro time-step. On the other hand, the fast component is fixed at $t_{n+1/2}$, that is, $z_n = z_{n+1} = z_{n+1/2}$, during the intermediate step. Finally, in the last step, the fast system is discretized using the θ -method to step up the fast component z from the time level $t_{n+1/2}$ to t_{n+1} , while the slow components are now fixed at the values x_{n+1}, y_{n+1} (the outputs from the middle slow sub-algorithm). The fractional-step algorithm is concisely summarized in a flow chart, see Figure 3.3.1.

Suppose that the current (n th time-step) solutions x_n, y_n , and z_n are known then the full description of the 3-step fractional-step θ -method (FSTS) for computing the next ($(n + 1)$ th time-step) solutions is presented as follows:

1. **The inner step.** During this phase only the fast component will be updated. Thus, the output of this step are x_n, y_n , and $z_{n+1/2}$.

We apply the θ -method for the problem in the fast phase (3.3.7)₁ as follows: for each $j = n, n + 1/r, \dots, n + 1/2 - 1/r$; we evaluate

$$z_{j+1/r} = z_j + h[(1 - \theta)w(t_j, z_j) + \theta w(t_{j+1/r}, z_{j+1/r})]. \quad (3.3.9)$$

For notational simplicity, in this step, the explicit dependence of w on x_n and y_n is omitted.

2. **The intermediate step.** Now, the input for this step is the output from the first step, that is, x_n, y_n , and $z_{n+1/2}$. The fast variable during this step is kept fixed at $z_{n+1/2}$. The θ -method applied to the problem in the slow phase (3.3.7)₂, gives

$$\begin{bmatrix} x_{n+1} \\ y_{n+1} \end{bmatrix} = \begin{bmatrix} x_n \\ y_n \end{bmatrix} + H(1 - \theta) \begin{bmatrix} f(t_n, x_n, y_n) \\ g(t_n, x_n, y_n) \end{bmatrix} + H\theta \begin{bmatrix} f(t_{n+1}, x_{n+1}, y_{n+1}) \\ g(t_{n+1}, x_{n+1}, y_{n+1}) \end{bmatrix}. \quad (3.3.10)$$

Since the fast variable is fixed in this step, we omit the explicit dependence of f and g on $z_{n+1/2}$. Solving the nonlinear implicit algebraic system (3.3.10) for x_{n+1} and y_{n+1} , we obtain the complete output from the intermediate step, that is, x_{n+1} , y_{n+1} , and $z_{n+1/2}$.

3. **The outer step.** Here only the fast phase problem is treated using the θ -method, as we did in the inner step. The input, in this step, is x_{n+1} , y_{n+1} , and $z_{n+1/2}$ – the output from the intermediate step. Keeping the slow variables at x_{n+1} and y_{n+1} , the fast variable is computed using the scheme

$$z_{j+1/r} = z_j + h[(1 - \theta)w(t_j, z_j) + \theta w(t_{j+1/r}, z_{j+1/r})], \quad (3.3.11)$$

for each $j = (n + 1/2), (n + 1/2) + 1/r, (n + 1/2) + 2/r, \dots, (n + 1/2) + (m - 1)/r$. Here the output x_{n+1} , y_{n+1} , and z_{n+1} is the overall solution of the coupled problem (3.2.1).

In summary, the fractional-step θ -method developed in this section can be compactly written as

$$\mathbf{u}_{n+1} = [\mathbb{A}_{\Delta t/r}^{\text{out}}]^{r/2} \circ \mathbb{A}_{\Delta t}^{\text{im}} \circ [\mathbb{A}_{\Delta t/r}^{\text{in}}]^{r/2} \mathbf{u}_n, \quad (3.3.12)$$

where $\mathbf{u}_k = (x_k, y_k, z_k)^T$ for $k = n$ or $n + 1$, the discrete operators $\mathbb{A}_{\Delta t/r}^{\text{out}}$, $\mathbb{A}_{\Delta t}^{\text{im}}$, and $\mathbb{A}_{\Delta t/r}^{\text{in}}$, represent the time-stepping algorithms constituting the outer, intermediate, and inner steps with time-step length $\Delta t/r$, Δt , and $\Delta t/r$, respectively.

3.3.3 Fractional-step mixed implicit-explicit method

The fractional-step θ -method uses the same $\theta \in [0, 1]$ for both the slow and the fast phases. Since the fast phase is solved in smaller time-step (micro-step) than slow phase, the use of implicit scheme for the fast phase is unnecessary. However, the slow phase using the larger time-step length H (macro-step) requires an implicit scheme to retain the accuracy of the corresponding fully implicit fractional-step θ -method for the full system. Motivated by this argument, we construct a time-stepping algorithm based on the fractional-step technique, which employs two θ values, one for each phase, that is, $\theta_f \in [0, 1/2)$ and $\theta_s \in [1/2, 1]$ for

the fast and the slow phases, respectively. Thus, the global algorithm of FSMIMEX, written in a compact form reads as

$$\mathbf{u}_{n+1} = [\mathbb{A}_{\Delta t/r}^{\theta_f}]^{\frac{r}{2}} \circ [\mathbb{A}_{\Delta t}^{\theta_s}] \circ [\mathbb{A}_{\Delta t/r}^{\theta_f}]^{\frac{r}{2}} \mathbf{u}_n, \quad (3.3.13)$$

where $\mathbb{A}_{\Delta t/r}^{\theta_f}$ denotes the discrete operator for both the outer and inner steps of the fractional-steps with $\theta = \theta_f$ and $\mathbb{A}_{\Delta t}^{\theta_s}$ denotes the discrete operator for the intermediate step with $\theta = \theta_s$. Note that in the FSMIMEX scheme, we particularly use $\theta_f = 0$ which corresponds to the forward Euler scheme.

Remark 3.3.1. The fractional-step algorithms used in this chapter are stable as long as each of the constituent method is stable. In the present case, the constituent methods used in the fractional-step algorithms are the basic θ -methods whose linear stability properties are well-known. These methods are unconditionally stable for θ in the interval $[1/2, 1]$ which is what one would normally be encouraged to use. Furthermore, the fractional-step methods used in this chapter have rate of convergence as 2 for $r \geq 2$ (in eq. (3.3.13)) if each of the constituent method is also convergent of order 2 or more (and the accuracy increases with increasing r beyond 2). Such convergence rate of fractional-step algorithms are reduced to first-order if at least one of the constituent method is first-order.

Remark 3.3.2. The advantages of the fractional-step algorithms (3.3.12) and (3.3.13) include ease of implementation as each component is treated individually in a decoupled manner, capability in accommodating different class of suitable solvers for different components of the problem in a single framework and ability in capturing the time scale differences in the discrete sense. On the other hand, their disadvantages are that they are only second-order accurate even if the components are solved using methods whose order is higher than two, and their performance is restricted by the strength of coupling that exists among various components.

3.4 Iterative treatment of nonlinearities

The schemes proposed above, result in fully-implicit nonlinear system of algebraic equations, which are required to be solved at each micro/macro time-step. The traditional nonlinear

solver is Newton's method. Under normal conditions, the Newton method is known for its fast (second-order) convergence, when the Jacobian of the residual function is computed exactly. However, forming and storing the Jacobian matrix is expensive from memory point of view. A combination of Newton-type method for superlinear convergent solution of nonlinear algebraic system of equations and Krylov subspace methods for solving the linearized system of equations for the Newton update has been the Jacobian-free Newton-Krylov (JFNK) method. In JFNK method, forming the Jacobian is substituted by a Jacobian-vector product which results in low computational cost relative to the cost of computing the full Jacobian matrix explicitly, and will be achieved by a finite difference approximation. In view of this, in what follows, we present a brief discussion on how we will implement JFNK method for the problems under consideration.

3.4.1 Jacobian-Free Newton-Krylov method

The Newton's method for approximating the roots of an algebraic nonlinear multi-valued function of $\mathbf{G}(\mathbf{u})$ involves solving for an update $\delta\mathbf{u}^k$, that is,

$$\mathbf{J}(\mathbf{u}^k)\delta\mathbf{u}^k = -\mathbf{G}(\mathbf{u}^k), \quad (3.4.1)$$

where $\mathbf{J}(\mathbf{u}^k) = \frac{\partial\mathbf{G}(\mathbf{u}^k)}{\partial\mathbf{u}^k}$. The current updated solution is obtained by

$$\mathbf{u}^{k+1} = \mathbf{u}^k + \delta\mathbf{u}^k. \quad (3.4.2)$$

Initialization from a suitable guess, (3.4.1) is solved iteratively in conjunction with the updating (3.4.2) until a desired level of convergence in terms of the norm of $\mathbf{G}(\mathbf{u}^k)$ and/or \mathbf{u}^k .

For problems with complicated nonlinearities, forming the exact Jacobian can be tedious and error prone [83]. In JFNK method, it is only required to obtain an approximation of matrix-vector product of $\mathbf{J}\mathbf{v}$ for some vector \mathbf{v} . Such matrix-vector product can be carried out by numerical differentiation by using forward difference [76]:

$$\mathbf{J}\mathbf{v} \approx \frac{\mathbf{G}(\mathbf{u} + \epsilon\mathbf{v}) - \mathbf{G}(\mathbf{u})}{\epsilon}, \quad (3.4.3)$$

where ϵ is a suitably chosen small perturbation parameter. Various options for choosing the parameter ϵ have been reported in [83]. In this chapter, we use ϵ to be of the order of the square root of the machine epsilon ($\epsilon_{machine}$).

The linear system $\mathbf{Ax} = \mathbf{b}$ obtained from (3.4.1), where $\mathbf{A} = \mathbf{J}(\mathbf{u}^k)$, $\mathbf{x} = \delta\mathbf{u}^k$, and $\mathbf{b} = \mathbf{G}(\mathbf{u}^k)$, are solved using Krylov subspace methods as a Galerkin projection over the (Krylov) subspace \mathbf{K}_j spanned (generated) by the vectors

$$\{\mathbf{r}_0, \mathbf{Ar}_0, \mathbf{A}^2\mathbf{r}_0, \dots, \mathbf{A}^{j-1}\mathbf{r}_0\}, \quad \text{or} \quad \mathbf{K}_j = \text{span} \{\mathbf{r}_0, \mathbf{Ar}_0, \mathbf{A}^2\mathbf{r}_0, \dots, \mathbf{A}^{j-1}\mathbf{r}_0\}, \quad (3.4.4)$$

where $\mathbf{r}_0 = \mathbf{Ax}_0 - \mathbf{b}$, and \mathbf{x}_0 is an initial estimation (typically \mathbf{x}_0 is chosen to be the zero vector [83]). There are different types of Krylov subspace methods available in the literature [83]. In this work, we employ the widely used Arnoldi-based method known as the Generalized Minimal RESidual (GMRES) method to solve the linear systems at each step of Newton's method. The j^{th} GMRES projection \mathbf{x}_j is approximated as an optimization problem for finding $\alpha_1, \dots, \alpha_j$ that minimizes the norm $\|\mathbf{Ax}_j - \mathbf{b}\|_2$ subject to \mathbf{x}_j in \mathbf{K}_j , where the j^{th} approximation \mathbf{x}_j is given by $\mathbf{x}_j = \mathbf{x}_0 + \sum_{i=1}^j \alpha_i \mathbf{A}^i \mathbf{x}_0$. The GMRES algorithm terminates when the Krylov subspace \mathbf{K}_j is large enough so that the residual norm, $\|\mathbf{Ax}_j - \mathbf{b}\|_2$, falls below a prescribed tolerance. Note that JFNK involves setting two tolerances, one for the outer iteration of the Newton's method and the other for the inner GMRES projections. Both tolerances can be set at the same value.

Another approach for solving (3.3.5) is to make use of Anderson's acceleration technique briefly described as follows.

3.4.2 Anderson's acceleration method

Consider solving the nonlinear system of equations (3.3.5):

$$\mathbf{G}(\mathbf{u}) = \mathbf{0}, \quad (3.4.5)$$

by an iterative process, which is equivalent to solving the fixed point iteration

$$\mathbf{u} = \mathbf{G}(\mathbf{u}) + \mathbf{u}. \quad (3.4.6)$$

We denote the most recent $p + 1$ iterates by $\mathbf{u}^{k-p}, \dots, \mathbf{u}^k$ and the corresponding output by $\mathbf{G}^{k-p}, \dots, \mathbf{G}^k$. Anderson's method determines the next iterate \mathbf{u}^{k+1} by

$$\bar{\mathbf{u}}^k = \mathbf{u}^k - \sum_{i=k-p}^{k-1} \gamma_i^{(k)} \Delta \mathbf{u}^i = \mathbf{u}^k - \Delta \mathcal{U}^k \gamma_k, \quad (3.4.7)$$

$$\bar{\mathbf{G}}^k = \mathbf{G}^k - \sum_{i=k-p}^{k-1} \gamma_i^{(k)} \Delta \mathbf{G}^i = \mathbf{G}^k - \Delta \mathcal{G}^k \gamma_k, \quad (3.4.8)$$

where

$$\Delta \mathbf{u}^i = \mathbf{u}^{i+1} - \mathbf{u}^i, \quad \Delta \mathbf{G}^i = \mathbf{G}^{i+1} - \mathbf{G}^i, \quad \gamma_k = [\gamma_{k-p}^{(k)}, \dots, \gamma_{k-1}^{(k)}], \quad (3.4.9)$$

and

$$\begin{aligned} \Delta \mathcal{U}^k &= [\Delta \mathbf{u}^{k-p}, \dots, \Delta \mathbf{u}^{k-1}], \\ \Delta \mathcal{G}^k &= [\Delta \mathbf{G}^{k-p}, \dots, \Delta \mathbf{G}^{k-1}]. \end{aligned} \quad (3.4.10)$$

Some rearrangements of the above gives

$$\bar{\mathbf{u}}^k = \sum_{j=k-p}^k \delta_j \mathbf{u}^j, \quad \bar{\mathbf{G}}^k = \sum_{j=k-p}^k \delta_j \mathbf{G}^j, \quad (3.4.11)$$

with

$$\sum_{j=k-p}^k \delta_j = 1. \quad (3.4.12)$$

The quantities $\bar{\mathbf{u}}^k$ and $\bar{\mathbf{G}}^k$ are weighted averages of \mathbf{u}^j 's and \mathbf{G}^j 's.

The γ_i 's are determined from the minimization problem,

$$\min_{\gamma^{(k)}} E(\gamma^{(k)}) = \min_{\gamma^{(k)}} \langle \bar{\mathbf{G}}^k, \bar{\mathbf{G}}^k \rangle = \min_{\gamma^{(k)}} \| \mathbf{G}^k - \Delta \mathcal{G}^k \gamma^{(k)} \|_2^2. \quad (3.4.13)$$

The corresponding normal equation is

$$((\Delta \mathcal{G}^k)^T \Delta \mathcal{G}^k) \gamma^{(k)} = (\Delta \mathcal{G}^k)^T \mathbf{G}^k. \quad (3.4.14)$$

Hence we obtain the updates from the above procedure as

$$\begin{aligned}
 \mathbf{u}^{k+1} &= \bar{\mathbf{u}}^k + \beta \bar{\mathbf{G}}^k, \\
 &= \mathbf{u}^k + \beta \mathbf{G}^k - (\Delta \mathcal{U}^k + \beta \Delta \mathcal{G}^k) \gamma^{(k)}, \\
 &= \mathbf{u}^k + \beta \mathbf{G}^k - (\Delta \mathcal{U}^k + \beta \Delta \mathcal{G}^k) ((\Delta \mathcal{G}_k)^T \Delta \mathcal{G}^k)^{-1} (\Delta \mathcal{G}_k)^T \mathbf{G}^k,
 \end{aligned} \tag{3.4.15}$$

where β is a positive number, known as the parameter of the Anderson's acceleration method. In our case, we take $\beta = 1$.

3.5 Stability analysis of the discrete schemes

In this section, we will analyze the stability of the discrete schemes to see whether the fixed points of methods correspond to the equilibria of the continuous model, and the discrete models have similar qualitative features near these equilibria as that of the continuous model. To proceed, let (x^*, y^*, z^*) be fixed points of the discrete scheme (3.3.12) which we obtain by solving

$$\left. \begin{aligned}
 F(x^*, y^*, z^*) &= x^*, \\
 G(x^*, y^*, z^*) &= y^*, \\
 W(x^*, y^*, z^*) &= z^*,
 \end{aligned} \right\} \tag{3.5.1}$$

where F, G , and W are the right-hand side functions of r -rate fractional-step θ -method obtained from the linearized equation (3.3.12).

Stability analysis of fixed points for a single scheme using explicit and implicit Euler method and Crank-Nicholson method is done in Chapter 2 and the results show same qualitative behaviour with the stability of the equilibrium points of the continuous model. In this chapter, we consider the discussion for $r = 2$ for fractional-step θ -method.

For $r = 2$, using implicit scheme for fast dynamics and explicit scheme for slow dynamics, the right-hand side function is defined as

$$\left. \begin{aligned} F(x^*, y^*, z^*) &= x^* + Hf(x^*, y^*, z_1), \\ G(x^*, y^*, z^*) &= y^* + Hg(x^*, y^*, z_1), \\ W(x^*, y^*, z^*) &= \underbrace{z^* + h(1 - hw_z(0))^{-1}w(x^*, y^*, z^*)}_{z_1} + \hat{w}_1, \end{aligned} \right\} \quad (3.5.2)$$

where, $\hat{w}_1 = h(1 - hw_z(0))^{-1}w(F(x^*, y^*, z^*), G(x^*, y^*, z^*), z_1)$, and $w_z(0)$ is the derivative of $w(x^*, y^*, z^*)$ with respect to z evaluated at the beginning of the current time-step (x_0^*, y_0^*, z_0^*) .

After some algebraic manipulations, we obtain the following fixed points

$$A(0, 0, 0), B(0, 0, 1), C(0.11875, 0, 0.05), D(0, 0.14345, 0, 0.0778), \quad (3.5.3)$$

$$E\left(\frac{(66.875 - 3.125H^*)H - 135H^2 + 0.625H^* - 7.5}{100H^2}, 0, \frac{-0.025H^* + \tilde{H}}{H}\right), \quad (3.5.4)$$

$$F\left(\frac{(66.875 + 3.125H^*)H - 135H^2 - 0.625H^* - 7.5}{100H^2}, 0, \frac{0.025H^* + \tilde{H}}{H}\right), \quad (3.5.5)$$

$$G\left(0, \frac{(109.3 - 0.5\hat{H})H - 257.32H^2 + 0.11\hat{H} - 11}{100H^2}, \frac{\bar{H}}{100H}\right), \quad (3.5.6)$$

$$I\left(0, \frac{(109.3 + 0.5\hat{H})H - 257.32H^2 - 0.11\hat{H} - 11}{100H^2}, \frac{\bar{H}}{100H}\right), \quad (3.5.7)$$

and

$$K\left(0, 0, \frac{0.1H \pm 0.1\sqrt{H^2(10H - 1)}}{H^2}\right), \quad (3.5.8)$$

where

$$\left. \begin{aligned} H^* &= \sqrt{1865H^2 - 1048H + 144}, \\ \hat{H} &= \sqrt{2142H^2 - 9178H + 9801}, \\ \bar{H} &= 5.6(\hat{H} - 475H + 99), \\ \tilde{H} &= -1.125H + 0.3. \end{aligned} \right\} \quad (3.5.9)$$

The first four fixed points expressed in (3.5.3) are the same as the equilibria of the continuous model (3.2.1). The other fixed points are the numerical artifact which comes as a trade off more accuracy in higher rate numerical schemes.

For $r = 2$: The right-hand side functions using the fractional-step explicit Euler scheme

for both slow and fast dynamics are defined as

$$\left. \begin{aligned} F(x^*, y^*, z^*) &= x^* + Hf(x^*, y^*, z_1), \\ G(x^*, y^*, z^*) &= y^* + Hg(x^*, y^*, z_1), \\ W(x^*, y^*, z^*) &= \underbrace{z^* + hw(x^*, y^*, z^*)}_{z_1} + hw(x^*, y^*, z_1), \end{aligned} \right\} \quad (3.5.10)$$

whereas the right-hand side functions corresponding to the fractional-step implicit Euler scheme for both dynamics are defined as

$$\left. \begin{aligned} F(x^*, y^*, z^*) &= x^* + H(1 - Hf_x(0))^{-1}f(x^*, y^*, z_1), \\ G(x^*, y^*, z^*) &= y^* + H(1 - Hg_y(0))^{-1}g(x^*, y^*, z_1), \\ W(x^*, y^*, z^*) &= \underbrace{z^* + h(1 - hw_z(0))^{-1}w(x^*, y^*, z^*)}_{z_1} + \hat{w}_1, \end{aligned} \right\} \quad (3.5.11)$$

where, $\hat{w}_1 = h(1 - hw_z(0))^{-1}w(F(x^*, y^*, z^*), G(x^*, y^*, z^*), z_1)$, $f_x(0)$ and $g_y(0)$ are the derivatives of $f(x^*, y^*, z^*)$ and $g(x^*, y^*, z^*)$ with respect to x and y respectively, evaluated at the beginning of the current time-step (x_0^*, y_0^*, z_0^*) .

On the other hand, the right-hand side functions corresponding to the fractional-step Crank-Nicholson method (for $r = 2$) for both slow and fast dynamics are defined as

$$\left. \begin{aligned} F(x^*, y^*, z^*) &= x^* + \frac{H}{2}(1 + (1 - Hf_x(0))^{-1})f(x^*, y^*, z_1), \\ G(x^*, y^*, z^*) &= y^* + \frac{H}{2}(1 + (1 - Hg_y(0))^{-1})g(x^*, y^*, z_1), \\ W(x^*, y^*, z^*) &= \underbrace{z^* + \frac{h}{2}(1 + (1 - hw_z(0))^{-1})w(x^*, y^*, z^*)}_{z_1} + \hat{w}_1, \end{aligned} \right\} \quad (3.5.12)$$

where, $\hat{w}_1 = \frac{h}{2}(1 + (1 - hw_z(0))^{-1})w(F(x^*, y^*, z^*), G(x^*, y^*, z^*), z_1)$.

In general, we see that the fractional-step θ -method satisfies

$$\left. \begin{aligned} F(x^*, y^*, z^*) &= x^* + H((1 - \theta) + \theta J_x)f(x^*, y^*, z_{r/2}), \\ G(x^*, y^*, z^*) &= y^* + H((1 - \theta) + \theta J_y)g(x^*, y^*, z_{r/2}), \\ W(x^*, y^*, z^*) &= \underbrace{\tilde{w}_0}_{z_1} + \tilde{w}_1 + \cdots + \tilde{w}_{(r/2)-1} + \hat{w}_{(r/2)} + \cdots + \hat{w}_{r-1}, \end{aligned} \right\} \quad (3.5.13)$$

$\underbrace{\hspace{10em}}_{z_2}$
 $\underbrace{\hspace{15em}}_{z_{r/2}}$
 $\underbrace{\hspace{20em}}_{z_{(r/2)+1}}$
 $\underbrace{\hspace{25em}}_{z_{r-1}}$

where

$$\begin{aligned} J_x &= (1 - Hf_x(0))^{-1}, \\ J_y &= (1 - Hg_y(0))^{-1}, \end{aligned} \quad (3.5.14)$$

$$\begin{aligned} J_z &= (1 - hw_z(0))^{-1}, \\ \tilde{w}_0 &= z^* + h((1 - \theta) + \theta J_z)w(x^*, y^*, z^*), \\ \tilde{w}_k &= h((1 - \theta) + \theta J_z)w(x^*, y^*, z_k), \end{aligned} \quad (3.5.15)$$

$k = 1, 2, \dots, r/2 - 1,$

$$\begin{aligned} \hat{w}_t &= h((1 - \theta) + \theta J_z)w(F(x^*, y^*, z^*), G(x^*, y^*, z^*), z_t), \\ t &= r/2, \dots, r - 1. \end{aligned} \quad (3.5.16)$$

By computing eigenvalues for the discrete schemes (3.5.10), (3.5.11), and (3.5.12), we find that the eigenvalues obtained from the fixed points, which are also equilibrium states, are all greater than unity in magnitude for $H > 0$, which implies that these fixed points are not asymptotically stable.

In summary, we have the following result:

Lemma 3.5.1. *The set of all equilibrium points of the continuous model (3.2.1) is contained in the set of fixed points of the discrete algorithm with $r = 2$, and solutions of the discrete and the continuous problems behave qualitatively in similar manner near these equilibrium points.*

3.6 Numerical results

In this section, we present numerical results demonstrating the performance of the numerical schemes proposed in this chapter by solving the singularly perturbed problem (3.2.1). The parameters used in the simulations are $m_1 = 2$, $d_1 = 0.4$, $\beta_1 = 0.2$; $m_2 = 5$, $d_2 = 0.5$, $\beta_2 = 0.7$; and $\varepsilon = 0.1$. In [98, 107], it was shown, using analytical and numerical techniques, that these set of parameter values in combination with the initial condition $(x_0, y_0, z_0) = (0.28, 0.001, 0.2)$ result in a long time behaviour known as a stable relaxation oscillation or coexistence of the predators and prey species.

In what follows, firstly, we analyze the convergence of the numerical schemes. In the analysis, for the implicit schemes, both JFNK and Anderson's acceleration methods were employed with tolerance 10^{-6} . Since there is no analytic solution available for the problem under consideration, we studied relative errors corresponding to a decreasing sequence of step-sizes. The effect of the parameter θ on convergence was analyzed for both MTS and FSTS methods. We also compared the convergence of MTS, FSTS and FSMIMEX methods.

Next, we compare the efficiency of the monolithic scheme MTS and the fractional-step scheme FSTS. Each of these schemes were implemented on MATLAB 2013a and the simulations were done in a serial computation on a single core of a machine with 2.4GHz x 8, IntelCore i7-4700MQ processor and 8GB RAM. We observed that roughly the comparable order of accuracy is obtained when the MTS and the fast component of the FSTS use the same time-step length. Furthermore, the number of iterations, at each time-step, taken by JFNK and Anderson's acceleration methods for each nonlinear implicit schemes of MTS and FSTS were also compared.

Finally, the stability of the numerical schemes were investigated. Long time ($T = 200$) runs were considered for the set of parameters and initial condition given above. The long time behaviour of solutions was examined in relation to the relaxation oscillation behaviour exhibited by the continuous problem. The relevant observations are indicated along with the discussions in each case.

Now we present results on convergence analysis of the proposed numerical schemes for different values of θ . To solve the implicitly nonlinear schemes at each time-step, JFNK or Anderson's acceleration iterations were used until the normalized residual is less than a

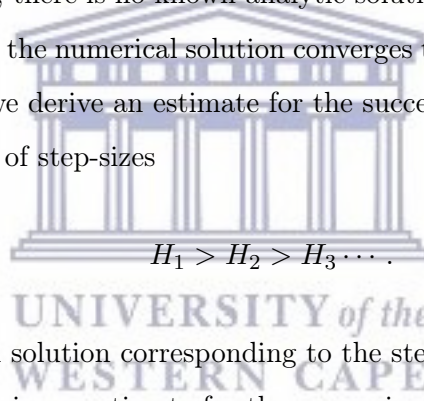
prescribed tolerance Tol, that is,

$$\frac{\|\mathbf{G}^k\|}{\|\mathbf{G}^0\|} < \text{Tol}.$$

For the convergence analysis, we prescribed the tolerance as Tol = 10^{-6} . It is well-known that if the nonlinear implicit schemes are solved sufficiently accurately, then the theoretical error estimate for the discrete schemes, as a function of the step-size H , has the form

$$\|\mathbf{u}(T) - \mathbf{u}^N\| \leq CH^q, \quad (3.6.1)$$

where $\mathbf{u}(T)$ is the exact solution at the final time T and \mathbf{u}^N the numerical solution at $T = NH$. The constant C (known as stability coefficient) is independent of H , and $q > 0$ is the order of convergence. However, there is no known analytic solution for the ODE system considered and as a result, assuming the numerical solution converges to the true solution as the step-size is getting close to zero, we derive an estimate for the successive relative errors corresponding to a decreasing sequence of step-sizes



$$H_1 > H_2 > H_3 \dots$$

We denote the numerical solution corresponding to the step-size H_i by \mathbf{u}_N^i .

Using (3.6.1), we obtain an estimate for the successive relative errors as follows:

$$\begin{aligned} \|\mathbf{u}_N^{i+1} - \mathbf{u}_N^i\| &= \|\mathbf{u}(T) - \mathbf{u}_N^{i+1} - (\mathbf{u}(T) - \mathbf{u}_N^i)\|, \\ &\leq \|\mathbf{u}(T) - \mathbf{u}_N^{i+1}\| + \|\mathbf{u}(T) - \mathbf{u}_N^i\|, \\ &\leq C(H_{i+1})^q + C(H_i)^q, \\ &\leq 2C\max\{(H_{i+1})^q, (H_i)^q\}, \\ &= 2C(H_i)^q. \end{aligned}$$

Denoting the relative error $\|\mathbf{u}_N^{i+1} - \mathbf{u}_N^i\|$ by $E_H(i)$, we see that the above implies

$$E_H(i) \leq \bar{C}(H_i)^q, \quad (3.6.2)$$

where $\bar{C} = 2C$. The estimate (3.6.2) becomes sharper for sufficiently small H_i 's. Hence, in

this analysis we take the final time to be $T = 1$, and consider sequence of step-sizes such that $H_i < 0.1$ (thus the corresponding N 's are greater than 10).

Figure 3.6.1 and 3.6.2 display the rate of convergence of MTS and FSTS for various values of the parameter θ when the nonlinear solvers JFNK and Anderson's acceleration are used. The results demonstrate that the rate of convergence of the schemes with $\theta = 1/2$ is twice faster, that is, the slope of the convergence curve corresponding to $\theta = 1/2$ is two whereas the same corresponding to $\theta = 1$ and $\theta = 0$ is only one. In addition, this scheme is more accurate than the schemes with $\theta = 0$ and $\theta = 1$. However, the effects of the nonlinear solvers are indistinguishable on the output of the solutions. To this end, first and second-order convergence, agreeing with theory, is obtained for the schemes used for these simulations.

Figure 3.6.3 displays the effect of convergence profile of the MTS, FSTS, and FSMIMEX by fixing $\theta = 1/2$ and it is shown that FSTS is more accurate than the other two.



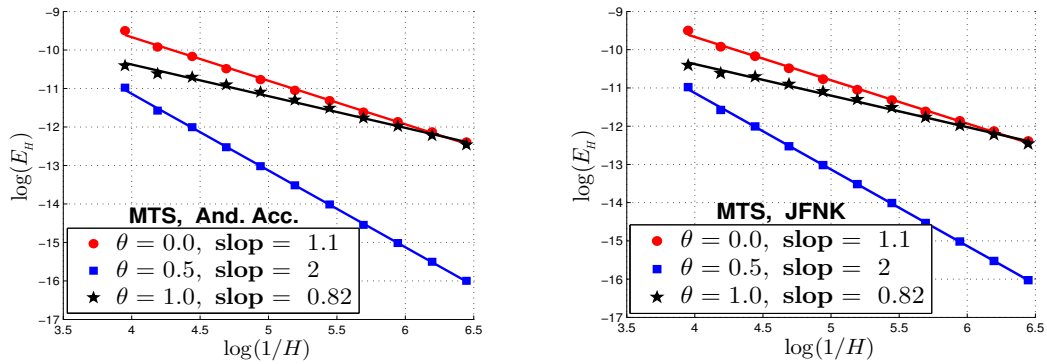


Figure 3.6.1: Rates of convergence of the monolithic θ -methods with Anderson's acceleration method (left) and with JFNK method (right).

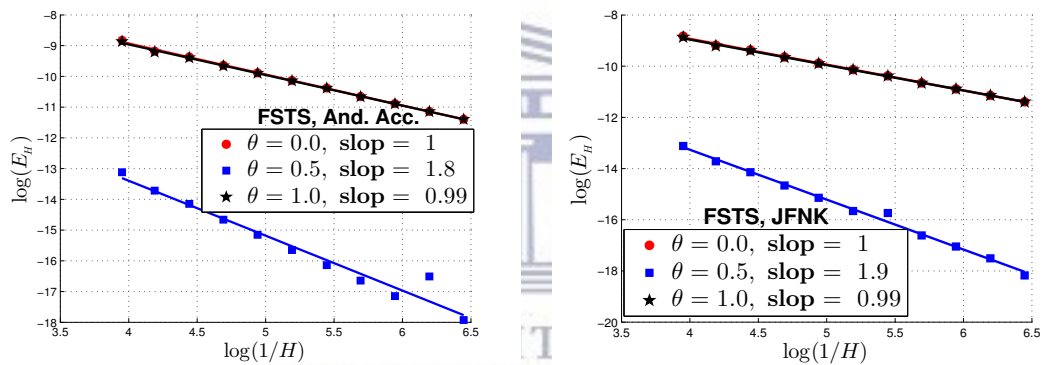


Figure 3.6.2: Rates of convergence of the fractional-step θ -methods with Anderson's acceleration method (left) and with JFNK method (right).

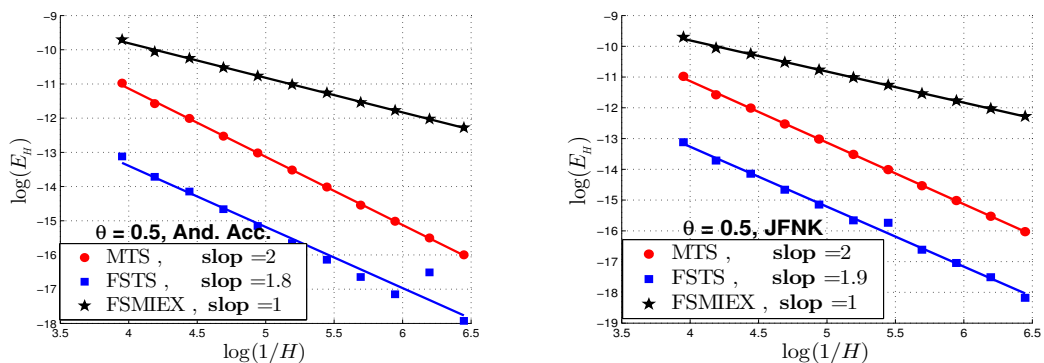


Figure 3.6.3: Rates of convergence of schemes with $\theta = 0.5$ using Anderson's acceleration method (left) and JFNK method (right).

Now the efficiency of the time-stepping algorithm is determined by several factors including the number of steps it takes to achieve a given level of accuracy, and the type of nonlinear solver it uses. We particularly focused on the comparison of the efficiencies of the MTS and FSTS methods for some values of the parameter θ , and demonstrated the effectiveness of the multiscale FSTS method as compared to the MTS method.

We further note that the FSMIMEX method is generally first-order accurate because of the use of explicit method for the fast dynamics. However, the simulation results corresponding to FSMIMEX scheme are used as reference solution when $\theta = 0.5$. As one would expect, the FSMIMEX method compared favourably against both the MTS and FSTS when $\theta = 1.0$. We observe the same order of magnitude of errors when the same step-size is used for the MTS method and the micro-step for the FSTS method.

Figure 3.6.4 and 3.6.5, display the efficiency result of the MTS, FSTS, and FSMIEX for $\theta = 0.5$ whereas Figure 3.6.6 and 3.6.7 display the efficiency result of these schemes for $\theta = 1.0$. The left plots display the level of accuracy of the schemes. All these results consistently demonstrate comparatively same level of accuracy, though FSTS method outperforms the MTS method.

The efficiencies of the nonlinear solvers JFNK and Anderson's acceleration were separately analyzed through Figure 3.6.8, 3.6.9 and 3.6.10 by comparing the number of iterations taken by each solvers using the three schemes for $\theta = 1.0$ and $\theta = 0.5$. As shown in all these plots, JFNK method generally took more number of iteration than Anderson's acceleration method.

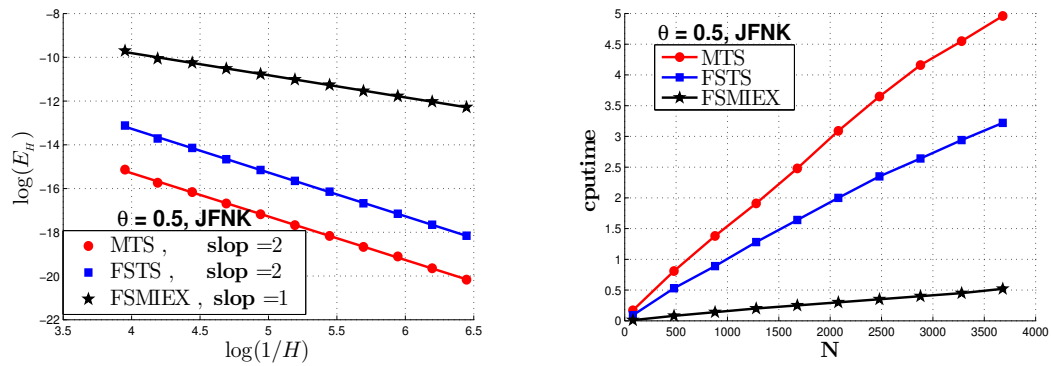


Figure 3.6.4: Comparison of efficiency results of the schemes with $\theta = 0.5$ using JFNK method: accuracy level of the schemes (left) and CPU time (right).

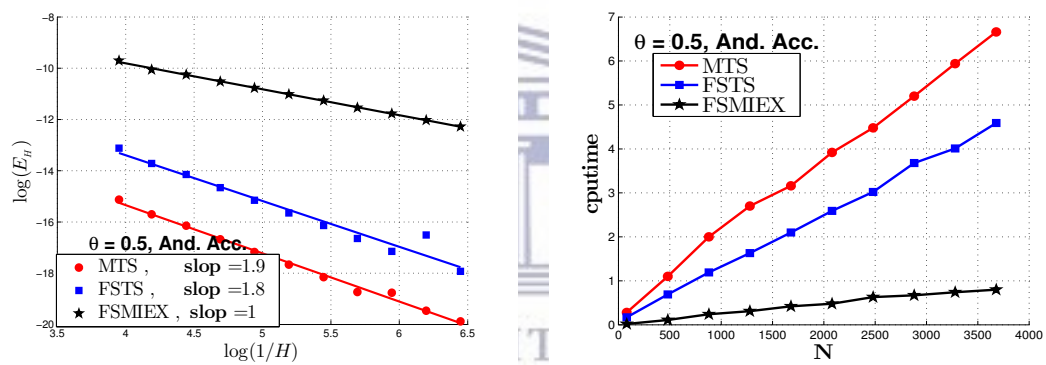


Figure 3.6.5: Comparison of efficiency results of the schemes with $\theta = 0.5$ using Anderson's acceleration method: accuracy level of the schemes (left) and CPU time (right).

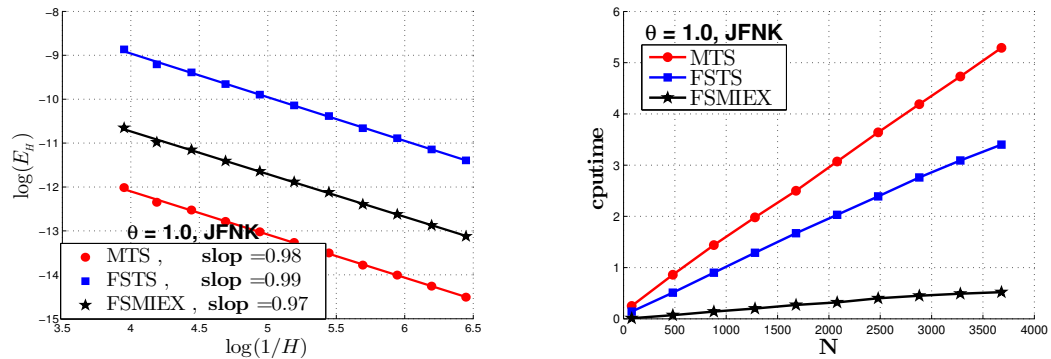


Figure 3.6.6: Comparison of efficiency results of the schemes with $\theta = 1$ using JFNK method: accuracy level of the schemes (left) and CPU time (right).

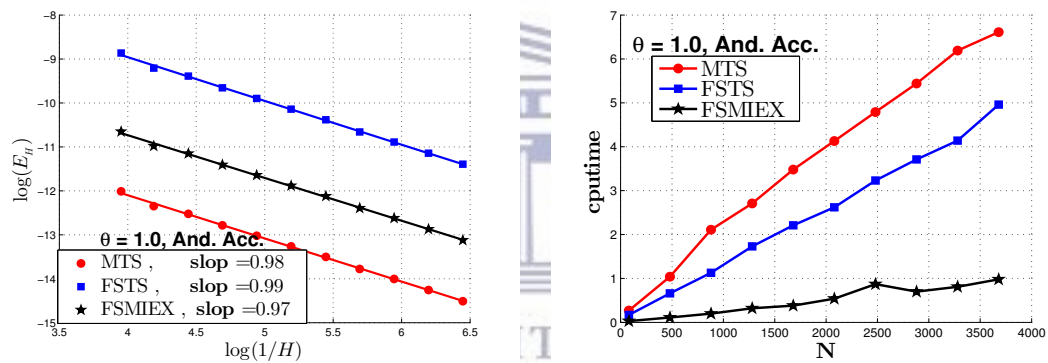


Figure 3.6.7: Comparison of efficiency results of the schemes with $\theta = 1$ using Anderson's acceleration method: accuracy level of the schemes (left) and CPU time (right).

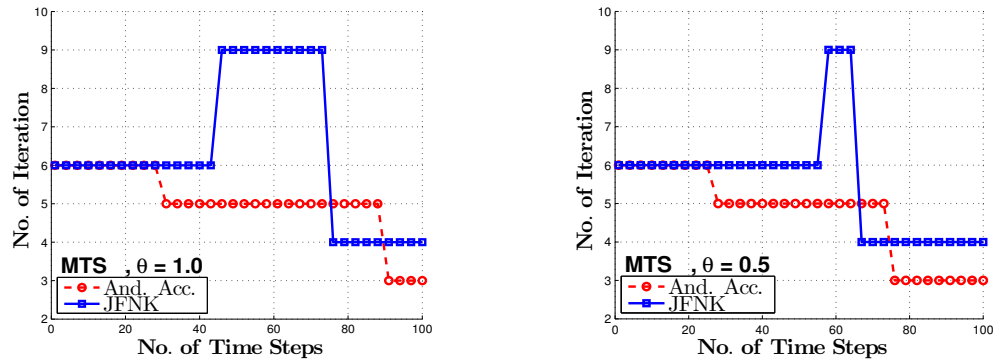


Figure 3.6.8: Comparison results of number of iterations taken by the monolithic θ -schemes with $\theta = 1.0$ (left) and $\theta = 0.5$ (right), using JFNK and Anderson's acceleration methods.

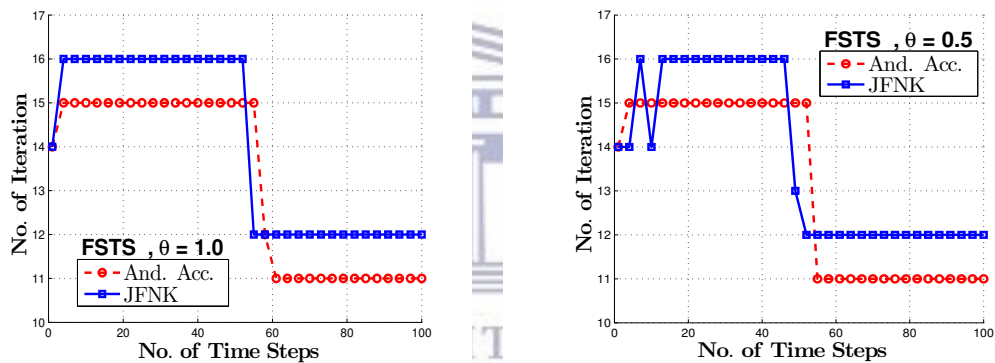


Figure 3.6.9: Comparison results of number of iterations taken by the fractional θ -schemes with $\theta = 1.0$ (left) and $\theta = 0.5$ (right), using JFNK and Anderson's acceleration methods.

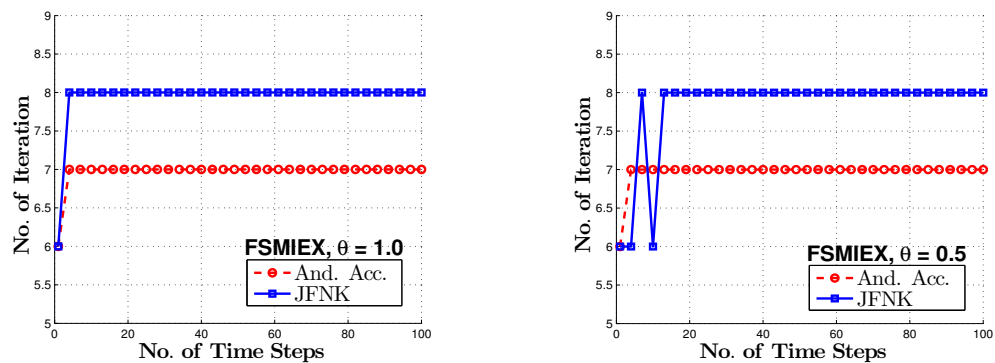


Figure 3.6.10: Comparison results of number of iterations taken by the mixed fractional implicit-explicit θ -schemes with $\theta = 1.0$ (left) and $\theta = 0.5$ (right), using JFNK and Anderson's acceleration methods.

Next, we discuss some stability results. In Table 3.6.1, we display comparative results regarding stability of the numerical solution of MTS, FSTS and FSMIMEX for the rate $r = 2$. The simulation is done using final time as $T = 200$. Different time-steps are considered for the simulation. As shown in this table, the FSTS scheme has better stability properties than the other two schemes. In addition, when the rate is $r = 4$, the FSTS converges to the limit cycle with a bigger time-step as shown in Table 3.6.2. Readers may note that the Anderson's acceleration nonlinear solvers are used for results presented in both of these tables.

Through Figure 3.6.11 and 3.6.12, we present additional results to show how the method FSTS appropriately captures the qualitative behaviour of the multiscale model describing the coexistence of the three species under stable relaxation oscillation. For all these plots, we use $H = 0.05$, $T = 200$ and rate factor as $r = 4$. Different initial conditions are used in each case. These plot display simulation results for interaction of the three population over time (Left) and trajectories in phase space (right). Starting with an initial condition $(x_0, y_0, z_0) = (0.28, 0.001, 0.2)$ close to the unstable equilibrium point $C(0.1187, 0, 0.05)$, the orbit in the Figure 3.6.11 converged to a stable limit cycle over long time interval. Again starting with another initial condition $(x_0, y_0, z_0) = (0.001, 0.2, 0.2)$ the periodic orbit converged to another stable limit cycle emerging from the unstable equilibrium point $D(0, 0.1435, 0.0778)$ as shown in Figure 3.6.12.

Table 3.6.1: Comparison of stability profiles of MTS, FSTS and FSMIMEX methods with rates $r = 2$.

H	MTS			FSTS			FSMIEX	
	$\theta = 0.0$	$\theta = 0.5$	$\theta = 1.0$	$\theta = 0.0$	$\theta = 0.5$	$\theta = 1.0$	$\theta = 0.5$	$\theta = 1.0$
0.40	–	–	–	–	–	–	–	–
0.20	–	–	–	–	CLC	CLC	CLC	CLC
0.10	–	CLC	CLC	CLC	CLC	CLC	CLC	CLC
0.05	CLC	CLC	CLC	CLC	CLC	CLC	CLC	CLC

*CLC: Convergence to Limit Cycle

Table 3.6.2: Comparison of stability profiles of MTS, FSTS and FSMIMEX methods with rates $r = 4$.

H	MTS			FSTS			FSMIEX	
	$\theta = 0.0$	$\theta = 0.5$	$\theta = 1.0$	$\theta = 0.0$	$\theta = 0.5$	$\theta = 1.0$	$\theta = 0.5$	$\theta = 1.0$
0.40	–	–	–	–	CLC	CLC	–	–
0.20	–	–	–	CLC	CLC	CLC	CLC	CLC
0.10	–	CLC	CLC	CLC	CLC	CLC	CLC	CLC
0.05	CLC	CLC	CLC	CLC	CLC	CLC	CLC	CLC

*CLC: Convergence to Limit Cycle

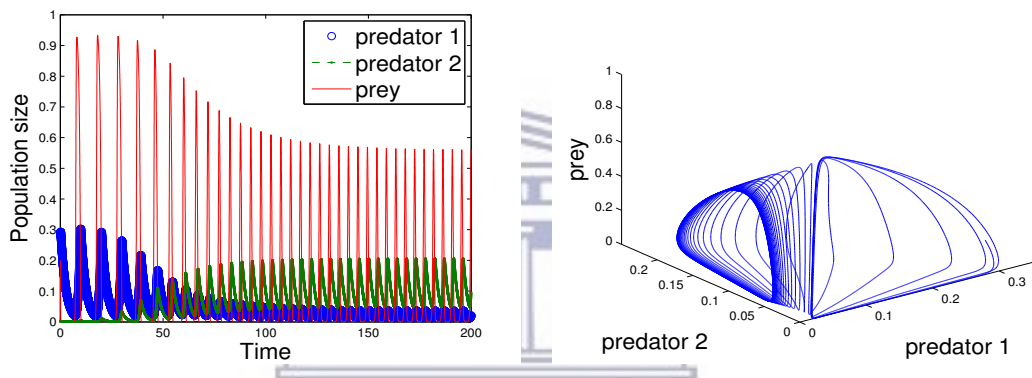


Figure 3.6.11: Simulation results displaying predators and prey over time (left) and trajectories in the phase space (right), using $r = 4$; $H = 0.05$; $T = 200$ and $(x_0, y_0, z_0) = (0.28, 0.001, 0.2)$.

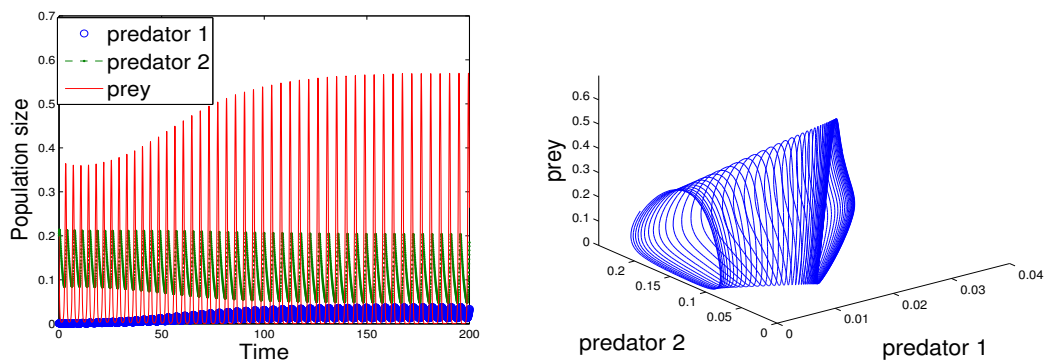


Figure 3.6.12: Simulation results displaying predators and prey over time (left) and trajectories in the phase space (right), using $r = 4$; $H = 0.05$; $T = 200$ and $(x_0, y_0, z_0) = (0.001, 0.2, 0.2)$.

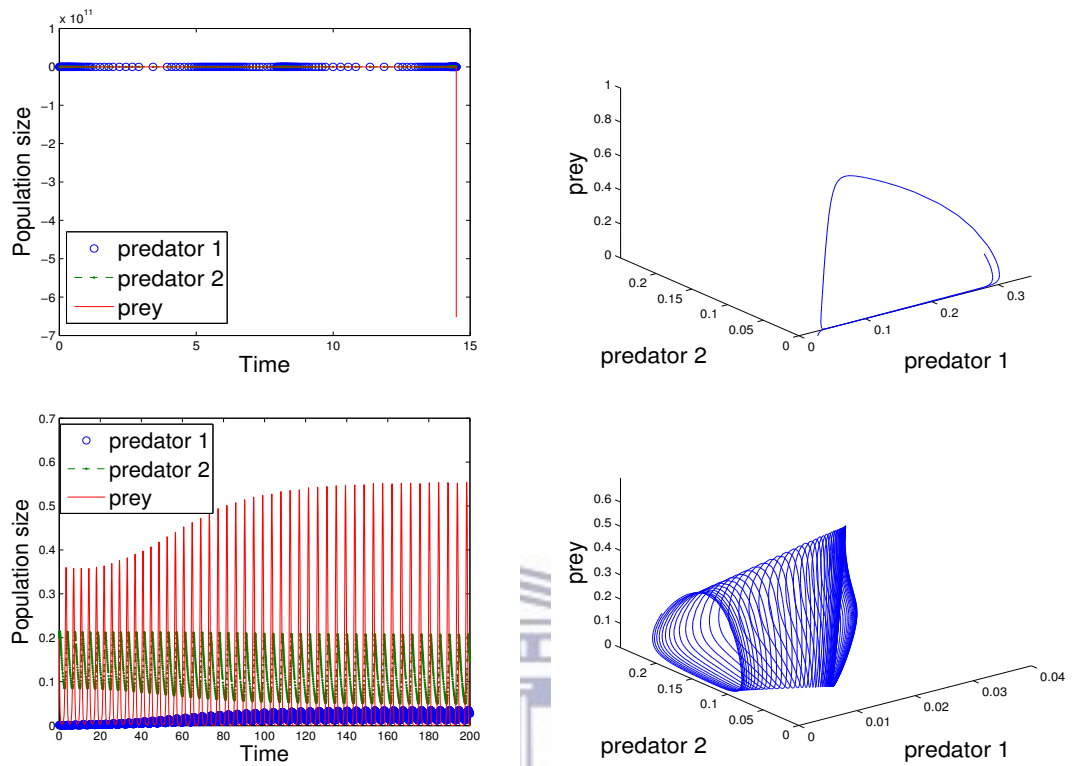


Figure 3.6.13: Simulation results displaying predators and prey over time (left) and trajectories in the phase space (right), using MATLAB ode15s, for $T = 200$ and $(x_0, y_0, z_0) = (0.28, 0.001, 0.2)$ (upper), $(x_0, y_0, z_0) = (0.01, 0.2, 0.2)$ (lower).

UNIVERSITY of the
 WESTERN CAPE

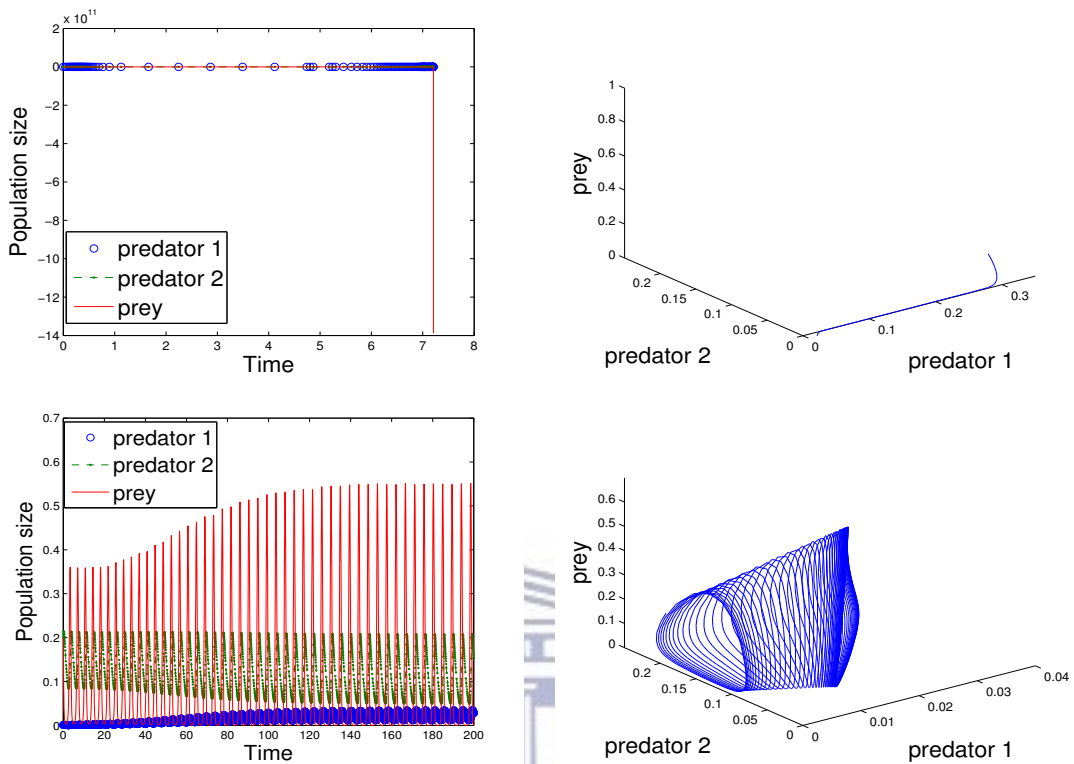


Figure 3.6.14: Simulation results displaying predators and prey over time (left) and trajectories in the phase space (right), using MATLAB `ode23s`, for $T = 200$ and $(x_0, y_0, z_0) = (0.28, 0.001, 0.2)$ (upper), $(x_0, y_0, z_0) = (0.01, 0.2, 0.2)$ (lower).

We also illustrate results obtained by using MATLAB ODE solvers that are often used for solving stiff problems. Figure 3.6.13 and 3.6.14 display the simulation results that we obtained by using MATLAB solvers `ode15s` and `ode23s`, respectively, to illustrate the long time behaviour of the model at $T = 200$ using different initial conditions. As shown in these figures, the two MATLAB solvers failed to converge to the limit cycle for the initial condition $(x_0, y_0, z_0) = (0.28, 0.001, 0.2)$ and converge to the limit cycle for the initial condition $(x_0, y_0, z_0) = (0.01, 0.2, 0.2)$. This indicates that these solvers are sensitive to different initial conditions given in this chapter whereas the fractional-step θ -schemes converge to the limit cycle as shown in the Figure 3.6.11 and 3.6.12.

3.7 Summary and discussion

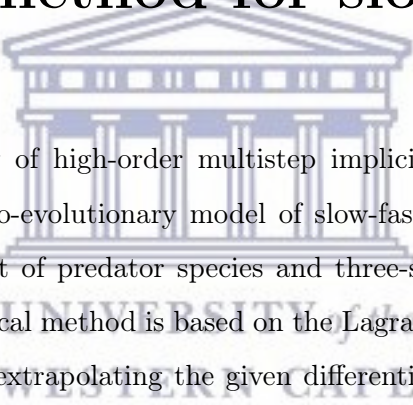
In this chapter, we have analyzed a predator-prey model that describes a slow-fast dynamical system. The design of the numerical methods have been done in such a way that, firstly, the original system is decoupled into slow and fast subproblems, and then suitable sub-algorithms based on the class of θ -methods are constructed for each subproblem. Finally the sub-algorithms are pieced together in some fashion to obtain an algorithm for the full problem. The nonlinear system resulting from the use of implicit schemes have been solved by appropriate nonlinear solvers such as JFNK and AA fixed point algorithms. We further analyzed these methods for stability and convergence. Several numerical experiments have confirmed our theoretical investigations.

Often, in slow-fast dynamics, the use of fractional-step algorithms that consist of implicit method for the slow component with macro time-step and explicit scheme for the fast with micro time-step can be highly efficient. However, such type of fractional-step methods, also referred to as FSMIMEX methods, are only conditionally stable at best. Hence, analysis to determine the largest possible time-step (macro or micro) such that such schemes are stable is of great importance. Such analysis is a highly challenging undertaking when the ODE system is as complex as the one considered in this chapter. As a result, we did not consider such analysis in this work. However, in the future work, we would like to consider this issues in depth.

While the schemes considered in this chapter have shown demonstrable performance in terms of efficiency, accuracy and the capability of capturing the dynamics of the problem, they are at most second-order accurate. In the next chapter, we formulate a class of high-order (stable upto fourth-order) linear multistep methods based on the Lagrange interpolation for a four-dimensional eco-evolutionary with multi-time-scale.

Chapter 4

A class of high-order IMEX linear multistep method for slow-fast model



In this chapter, a family of high-order multistep implicit-explicit method for a strongly-nonlinear and coupled eco-evolutionary model of slow-fast-type is presented. It consist of one-fast evolutionary trait of predator species and three-slow predator-prey interactions in ecology. Proposed numerical method is based on the Lagrange interpolation procedure which involves interpolating or extrapolating the given differential equation at a point designated by a parameter $\theta \in [0, 1]$. It is shown that the new method generalizes some of the classical multistep methods such as (Backward Differentiation Formulas) BDF schemes and (Crank-Nicholson-Leapfrog) CNLF schemes. The convergence and linear stability of the new family of methods corresponding to $\theta = 0.5$ are analyzed. An order-consistent start up scheme based on collocation method that uses the same Lagrangian polynomials as basis functions is proposed to approximate the starting solution for the underlying multistep method. The singularly perturbed ecological problem is solved by using the proposed scheme in conjunction with Anderson's acceleration fixed point iteration procedure for the nonlinear-implicit part of the scheme. Various numerical results are presented to confirm the theoretical convergence and stability results. We notice that the new method corresponding to $\theta = 0.5$ generally performs better than the classical BDF and CNLF methods in terms of accuracy, robustness and replicating the qualitative features of the continuous model.

4.1 Introduction

Ecological and evolutionary changes may occur simultaneously and interact with each other. On one hand, ecological changes resulting in natural selection produce change in some ecological traits, on the other hand, the evolved changes in these traits cause changes in the ecological dynamics. The evolutionary changes in the traits may occur at a rate comparable to or faster than the interaction of the species in ecology and vice-versa. Such eco-evolutionary interactions are typically modelled and studied using systems of ordinary differential equation with different time-scales. For example, in [29], a three dimensional eco-evolutionary model representing the predator-prey model with fast evolutionary trait of the predator was studied using geometric singular perturbation theory. Their work has laid clear insight as to how slow-fast dynamical systems theory offers a clear viewpoint through which the effects of evolution on ecological dynamics can be studied. The reduction in dimension and the resulting analytical tractability of this methodology makes it a powerful tool for understanding the interplay between ecological and evolutionary processes. In another work, Piltz et al. [125] developed a one-fast and three-slow dynamical system to study the influence of evolution on ecological systems. They considered adaptive change of diet of the predator population that switches between the two prey population. The change of diet is continuous but it is fast compared to the time-scale of population dynamics. It was assumed that the prey growth is unlimited and the functional response between the predator and the prey is due to the Lotka-Volterra model. Most importantly, by using geometric singular perturbation technique, they showed a family of periodic orbits.

The qualitative and quantitative behaviour of interaction of ecological dynamics with a rapid evolution has been studied by other researchers for some specific systems, see for example [2, 166]. In [166], it was made clear that theoretical predictions of how rapid evolution can affect ecological dynamics are inconclusive and often depend on untested model assumptions.

In this chapter we consider, a coupling of evolutionary and ecological models describing a slow-fast dynamical system of one-fast evolution of predator trait and three-slow predator-prey interaction in ecology [125]. This dynamics is described by a coupled system of nonlinear ordinary differential equation with different time-scales. Due to the fast evolution of the predator-trait, the model exhibit an interesting periodic patterns between a predator and the

two prey population.

Multi-time-scaled systems are often nonlinear and complex for which it is challenging to obtain explicit analytical solutions, hence one must resort to numerical approximations for their solutions. For the systems that exhibit regular oscillations, standard time integrators often reproduce the required qualitative feature of the solutions in long time simulations without much difficulty [70]. However, it is well understood that some standard explicit schemes such as forward Euler and Runge-Kutta generate some unwanted numerical artefacts such as oscillations, bifurcations, chaos and false steady states, despite using adaptive step-size [111, 130].

Various combinations of explicit and implicit multistep methods were first introduced in [9, 156], and further developed in [31, 44]. Hundsdorfer and Ruuth [68] employed IMEX multistep methods with monotonicity preserving and boundedness properties for hyperbolic systems with stiff sources or relaxation terms. Very often, IMEX methods have been developed for the numerical simulations of singular perturbed problems. Schütz and Kaiser [139] successfully applied multistep IMEX method for singularly perturbed systems of ordinary differential equations. They developed a new splitting method to partition the system into stiff and non-stiff parts. Constantinescu and Sandu [26] constructed different extrapolated IMEX time-stepping methods based on Euler steps to solve multiscale and multiphysics problems having both stiff and non-stiff parts and they have achieved high-order of consistency through extrapolation. They also presented the linear stability analysis of the schemes using a suitably crafted linear test problem having two time-scales. Durran and Blossey [31] proposed two new families of IMEX multistep methods for slow-fast wave problems. They developed the schemes based on Adams methods and backward differencing schemes and made some comparisons with linear multistep IMEX schemes.

Unlike those IMEX schemes that combine different methods with single step-size, multirate methods that employ implicit and explicit schemes of same family have been successfully applied for a wide range of multiscale problems, see for example [27, 42, 51, 107]. Such multirate methods use smaller step-size for the fastest changing components and larger one for the slowly varying components. In such cases, the computational complexity is mainly influenced by the fastest changing components. In the literature, some non-standard time integrators have been successfully applied to predator-prey models and other biological models

of slow-fast type, see for example [59, 70, 111, 167] among others.

While the standard explicit numerical schemes often require very restrictive step-size due to stringent stability criteria when the stiffness is high, the use of high-order implicit schemes require a large number of internal nonlinear iterations within a time-step. In order to utilize both the lower cost of explicit schemes and the good stability properties of implicit schemes, in this chapter, we formulate a family of high-order implicit-explicit (IMEX) multirate schemes for the slow-fast problem considered. The mechanism allows us to combine explicit and implicit schemes in one computational framework through partitioning the full problem into slow sub-system (which is non-stiff) and fast sub-system (which is stiff). The method is based on Lagrange interpolation and extrapolation procedure. It also generalizes other classes of multistep methods such as Backward differentiation formula, Crank-Nicholson-Leapfrog method, Adams Bashforth methods and other multistep methods. The Proposed method is more stable and accurate.

In the next step, we employ Anderson's acceleration fixed point iterative solver to treat the nonlinearity that arises as a result of the implicit part of the schemes. Readers may note that Anderson's acceleration method is a modified Picard's fixed point iterative method for robust and fast convergent solutions [97, 162]. The typical nonlinear solver is Newton's method. Under normal conditions, the Newton method is known for its fast (second-order) convergence, when the Jacobian of the residual is computed exactly. Forming and storing the Jacobian matrix is expensive from storage point of view. Instead, Jacobian-free Newton-Krylov (JFNK) method is an alternative tool since forming the Jacobian is substituted by a numerical approximate Jacobian-vector product which results in low computational cost than computing the full Jacobian. However, the JFNK method also requires one residual evaluation per linear iteration, which makes it to be viewed as not that much competitive to other methods such as the Anderson's acceleration method, in the absence of exploiting potentially problem specific features [12].

The rest of the chapter is organized as follows: In Section 4.2, we consider the model problem and give a brief discussion on qualitative properties of the model. In Section 4.3, the numerical methods are formulated and analyzed in details for a typical four-dimensional model with two time-scales. Treatment of nonlinearities using Anderson's acceleration method is discussed in Section 4.5. Numerical results are presented in Section 4.6. Finally, we present

some concluding remarks and scope for further research in Section 4.7.

4.2 The mathematical model and its qualitative analysis

In this section, we present an eco-evolutionary slow-fast system modelling the interaction of one-predator and two-prey species with a fast predator evolutionary trait treated as one system variables [125]. We also give an overview into the global structure of the periodic orbits of the dynamics that is determined using geometric singular perturbation theory. More details on the model and its theoretical analysis can be found in [125].

4.2.1 Coupled ecological and evolutionary dynamics

Consider the four-dimensional eco-evolutionary slow-fast model [125] that describes the interaction of one-predator and two-prey species with the a fast predator evolutionary trait,

$$\left. \begin{aligned} \dot{p}_1 &= p_1(r_1 - qz), \\ \dot{p}_2 &= p_2(r_2 - (1 - q)z), \\ \dot{z} &= z(eqp_1 + e(1 - q)\kappa p_2 - m), \\ \varepsilon \dot{q} &= q(1 - q)V e(p_1 - \kappa p_2), \end{aligned} \right\} \quad (4.2.1)$$

where, $i = 1, 2$; p_i represents the time varying population density of the i th prey, z represents the time varying population density of the predator, and q represents predator-trait. The constants r_1 and r_2 are the per capita growth rates of the prey p_i , e is the proportion of predation that goes into predator growth. Also $\kappa \in [0, 1]$ is the non-dimensional parameter that represents the extent of preference towards prey p_2 , m is the predators per capita death rate and V is a non-dimensional constant. In this model, all the parameters are strictly positive.

To proceed with the qualitative analysis, we non-dimensionalize (4.2.1) so that the scaled

system contains a minimum number of parameters. Using the scaling given in [125]:

$$t \rightarrow \frac{t}{r_1}, p_1 \rightarrow \frac{mr_1}{e}p_1, p_2 \rightarrow \frac{mr_1}{e\kappa}p_2, z \rightarrow r_1z, m \rightarrow r_1m, r_2 \rightarrow rr_1, \varepsilon \rightarrow \varepsilon mV,$$

we obtain

$$\left. \begin{aligned} \dot{p}_1 &= p_1(1 - qz) =: f_1(p_1, p_2, z, q), \\ \dot{p}_2 &= p_2(r - (1 - q)z) =: f_2(p_1, p_2, z, q), \\ \dot{z} &= z(qp_1 + (1 - q)p_2 - 1)m =: g(p_1, p_2, z, q), \\ \varepsilon \dot{q} &= q(1 - q)(p_1 - p_2) =: w(p_1, p_2, z, q), \end{aligned} \right\} \quad (4.2.2)$$

where $f_1(p_1, p_2, z, q)$, $f_2(p_1, p_2, z, q)$, $g(p_1, p_2, z, q)$, and $w(p_1, p_2, z, q)$ are smooth continuous functions describing the dynamics of the system and ε is a small positive number ($0 < \varepsilon \ll 1$), which represents the separation of time-scales. This model problem is a singularly perturbation problem due to the small parameter ε [66]. In this model, q corresponds to the fast predator evolution trait, while (p_1, p_2, z) represent the slow dynamics of the predator-prey interaction. The equilibria of system (4.2.2) are found to be $A(0, 0, 0, 0)$, $B(0, 0, 0, 1)$, $C(0, 1, r, 0)$, $D(1, 0, 1, 1)$ and $E(1, 1, 1 + r, \frac{1}{1+r})$, and corresponding Jacobian matrix is given by

$$J = \begin{pmatrix} 1 - qz & 0 & -qp_1 & -zp_1 \\ 0 & r - z(1 - q) & p_2(q - 1) & zp_2 \\ mqz & m(1 - q)z & m(qp_1 + p_2 - qp_2 - 1) & m(p_1 - p_2)z \\ \frac{1}{\varepsilon}(q - q^2) & -\frac{1}{\varepsilon}(q - q^2) & 0 & \frac{1}{\varepsilon}(1 - 2q)(p_1 - p_2) \end{pmatrix}. \quad (4.2.3)$$

We then study the local stability of each equilibrium points of the dynamic system by examining the eigenvalues of the Jacobian matrix J given by the equation (4.2.3) evaluated at the equilibrium points. Since the eigenvalues corresponding to both equilibrium points $A(0, 0, 0, 0)$ and $B(0, 0, 0, 1)$ are $\{0, 1, -m, r\}$, they are unstable saddle points, representing the total extinction of all the three species. The eigenvalues corresponding to C are $\{\frac{-1}{\varepsilon}, 1, -i\sqrt{mr}, i\sqrt{mr}\}$, and to D are $\{\frac{-1}{\varepsilon}, -i\sqrt{m}, i\sqrt{m}, r\}$. The non-trivial equilibrium point E that could possibly lead to co-existence of the populations has four purely imaginary eigen-

values which we obtain numerically by varying the parameters. This eigenvalue describes neutrally stable center, where the periodic solutions bifurcate off from the equilibrium point when the eigenvalues cross the imaginary axis. A complex conjugate pair of purely imaginary eigenvalues of the Jacobian, at an equilibrium point in the phase plane, corresponds to periodic orbits around this point. However, such linear analysis is insufficient to determine the nature of the orbits for the original nonlinear system [70]. In all the cases, the resulting eigenvalues of the equilibrium points show that all the equilibrium points are not locally asymptotically stable.

4.2.2 Analysis of (4.2.2) using geometric singular perturbation theory

The eco-evolutionary slow-fast system is analyzed with the geometric singular perturbation theory. To get more insight about the dynamics of the model problem, we use the geometric singular perturbation theory. Here we briefly outline results concerning the global structure of the orbits using invariant manifold in phase space.

We first note that the derivative in (4.2.2) is given with respect to slow time-scale t . By transforming to the fast variable $\tau = t/\varepsilon$, we obtain

$$\left. \begin{aligned} p_1' &= \varepsilon p_1(1 - qz), \\ p_2' &= \varepsilon p_2(r - (1 - q)z), \\ z' &= \varepsilon z(qp_1 + (1 - q)p_2 - 1)m, \\ q' &= q(1 - q)(p_1 - p_2), \end{aligned} \right\} \quad (4.2.4)$$

where $' = \frac{d}{d\tau}$. Note that systems (4.2.2) and (4.2.4) are equivalent as long as $\varepsilon \neq 0$. As $\varepsilon \rightarrow 0$, the above defines two limiting systems. The first one is

$$\left. \begin{aligned} \dot{p}_1 &= p_1(1 - qz), \\ \dot{p}_2 &= p_2(r - (1 - q)z), \\ \dot{z} &= z(qp_1 + (1 - q)p_2 - 1)m, \\ 0 &= q(1 - q)(p_1 - p_2), \end{aligned} \right\} \quad (4.2.5)$$

which is obtained from (4.2.2), and is referred to as *reduced problem*. This captures the dynamics of the slow flow. It is a differential algebraic equation obtained from (4.2.2) where the algebraic constraint $q(1 - q)(p_1 - p_2) = 0$, defines the critical manifold.

The second one is the layer problem (obtained from (4.2.4))

$$\left. \begin{aligned} p_1' &= 0, \\ p_2' &= 0, \\ z' &= 0, \\ q' &= q(1 - q)(p_1 - p_2), \end{aligned} \right\}. \quad (4.2.6)$$

which captures the dynamics of the fast flow.

The two limits (4.2.5) and (4.2.6) are two different approximations of the full system when $\varepsilon > 0$. The phase space of (4.2.5) is the critical manifold M_0 defined by

$$M_0 = \{(p_1, p_2, z, q) : w(p_1, p_2, z, q) = 0, p_1 \geq 0, p_2 \geq 0, z \geq 0, q \geq 0\}. \quad (4.2.7)$$

It consists of three parts, $M_0^1 = \{(p_1, p_2, z, q) | q = 0\}$, $M_0^2 = \{(p_1, p_2, z, q) | q = 1\}$ and $M_0^3 = \{(p_1, p_2, z, q) | p_1 = p_2\}$.

The orbits of system (4.2.6) are parallel to the q -axis and their directions are characterized by the signs of $w(p_1, p_2, z, q)$. We refer to these orbits as *fast orbits* of system (4.2.2).

The reduced system (4.2.5) is defined on the critical manifold M_0 , and the layer problem (4.2.6) is a one-dimensional system in the variable q parametrized by the slow variables (p_1, p_2, z) with equilibria on M_0 .

The fast flow on the critical manifold M_0^1

:

The flow of the fast limiting system on M_0^1 is determined by

$$\frac{\partial w}{\partial q} \Big|_{M_0^1} = (p_1 - p_2), \quad (4.2.8)$$

in which the limiting fast dynamic is governed by system (4.2.6), and have M_0^1 as a set of equilibria. From equation (4.2.8), we observe that $M_0^{1-} = \{(p_1, p_2, z, 0) \in M_0^1 : p_1 < p_2\}$

is normally stable with vertical stable fibers and $M_0^{1+} = ((p_1, p_2, z, 0) \in M_0^1 : p_1 > p_2)$ is normally unstable with vertical unstable fibers. That is, all solutions of (4.2.6) in the vicinity of M_0^{1-} move vertically toward M_0^{1-} and all solutions of (4.2.6) in the vicinity of M_0^{1+} move vertically away from M_0^{1+} .

The slow flow on the critical manifold M_0^1

: The slow dynamics on the manifold M_0^1 is given by

$$\left. \begin{aligned} \dot{p}_1 &= p_1, \\ \dot{p}_2 &= p_2(r - z), \\ \dot{z} &= z(p_2 - 1)m. \end{aligned} \right\} \quad (4.2.9)$$

The equilibrium points are $\tilde{A}(0, 0, 0)$ and $\tilde{B}(0, 1, r)$. The origin $\tilde{A}(0, 0, 0)$ with eigenvalues $(1, -m, r)$ is unstable saddle node. The semi-trivial equilibrium point $\tilde{B}(0, 1, r)$ describe the interaction of the predator z and the prey p_2 in the absence of prey p_1 . The corresponding eigenvalues are $(-i\sqrt{mr}, i\sqrt{mr})$, and hence it is a center. As we vary the parameters, a Hopf-bifurcation emanates from the equilibrium point $\tilde{B}(0, 1, r)$.

The fast flow on the critical manifold M_0^2

: The flow of the fast limiting system on M_0^2 is determined by

$$\frac{\partial w}{\partial q} \Big|_{M_0^2} = (p_2 - p_1). \quad (4.2.10)$$

Hence, for the limiting fast dynamics, it is clear that all solutions of system (4.2.6) in the vicinity of $M_0^{2-} = ((p_1, p_2, z, 1) \in M_0^2 : p_2 < p_1)$ will move vertically toward M_0^{2-} and those in the vicinity of $M_0^{2+} = ((p_1, p_2, z, 1) \in M_0^2 : p_2 > p_1)$ will move vertically away from M_0^{2+} .

The slow flow on the critical manifold M_0^2

: The slow dynamics on M_0^2 , is defined by

$$\left. \begin{aligned} \dot{p}_1 &= p_1(1 - z), \\ \dot{p}_2 &= rp_2, \\ \dot{z} &= z(p_1 - 1)m. \end{aligned} \right\} \quad (4.2.11)$$

The equilibrium points are $\hat{A}(0, 0, 0)$ and $\hat{B}(1, 0, 1)$. The eigenvalues corresponding to the equilibrium point \hat{A} are $(1, -m, r)$, which implies that \hat{A} is an unstable saddle node. The semi-trivial equilibrium $\hat{B}(1, 0, 1)$ describes the interaction of p_1 and z in the absence of p_2 . Corresponding eigenvalues are $(-i\sqrt{m}, i\sqrt{m})$ leading to a periodic orbit.

By Fenichel theory [39], for ε sufficiently small, a normally hyperbolic subset of the critical manifold M_0 of (4.2.5) persists as a locally invariant manifold of (4.2.2) that is $O(\varepsilon)$ close to the critical manifold. In addition, the stable manifold $W^s(M_0)$ of M_0 corresponding to M_0^{1-} , M_0^{2-} and the unstable manifold $W^u(M_0)$ of M_0 corresponding to M_0^{1+} , M_0^{2+} persist as manifolds $W^s(M_\varepsilon)$ and $W^u(M_\varepsilon)$ of the full system, respectively.

Typically a point of non-hyperbolicity can be a fold point of the critical manifold (4.2.7). At a generic fold point $p_1 = p_2$, the reduced problem (4.2.5) is singular and the solutions reaches $p_1 = p_2$ in a finite forward or backward time. This case is known as *jump point* and is an ingredient necessary for the existence of a relaxation oscillator ([87]).

Remark 4.2.1. *As discussed above both manifolds $q = 0$, and $q = 1$ have the attracting and repelling pieces. If we let the trajectories to start from the repelling part $p_1 > p_2$ of $q = 0$, then the trajectory immediately leaves the manifold $q = 0$ and stays to the attracting part of the manifold $q = 1$, that is, $p_1 > p_2$ in which, the two manifolds are connected via hetroclinic connection. The slow trajectory then moves to $q = 1$ manifold for some time and the time it passes to the repelling part of the pieces, then it immediately go to the jumping point to leave the manifold $q = 1$ and stays to the attracting part of $q = 0$. By concatenating the fast and slow limiting orbit gives a singular periodic orbit which in turn persists the orbits when ε is non-zero but small.*

In the next section, we discuss the general construction of a high-order IMEX multistep

method which enables us to efficiently and accurately solve the multiscale model problem (4.2.2) discussed in this section.

4.3 High-order multistep IMEX methods for slow-fast problems

Standard explicit numerical schemes require very restrictive time-steps to approximate solutions of stiff (or singularly perturbed) problems due to stability reasons, whereas, the use of implicit numerical schemes require large number of iterations for the convergence within a prescribed time-step. In order to utilize both lower cost advantage of explicit schemes and a good stability properties of implicit schemes, it makes sense to combine implicit and explicit methods in one scheme, generally known as implicit-explicit (IMEX) methods. To this end, in this section, we present various high-order IMEX schemes for the singularly perturbed problem (4.2.2) written in a general evolutionary equation form as

$$\dot{\mathbf{u}} = \mathbf{f}_F(t, \mathbf{u}) + \mathbf{f}_S(t, \mathbf{u}), \quad \mathbf{u}(0) = \mathbf{u}_0, \quad (4.3.1)$$

where \mathbf{f}_F the fast component (stiff), \mathbf{f}_S the slow component (non-stiff), and \mathbf{u} the unknown vector. These are denoted by

$$\mathbf{u} = \begin{bmatrix} p_1 \\ p_2 \\ z \\ q \end{bmatrix}, \quad \mathbf{f}_F(\mathbf{u}, t) = \begin{bmatrix} 0 \\ 0 \\ 0 \\ \frac{1}{\varepsilon}q(1-q)(p_1 - p_2) \end{bmatrix}, \quad \text{and} \quad \mathbf{f}_S(t, \mathbf{u}) = \begin{bmatrix} p_1(1 - qz) \\ p_2(r - (1 - q)z) \\ z(qp_1 + (1 - q)p_2 - 1)m \\ 0 \end{bmatrix}. \quad (4.3.2)$$

In the remaining part of this chapter, we use the terminology that the sub-equations $\dot{\mathbf{u}} = \mathbf{f}_F(t, \mathbf{u})$ and $\dot{\mathbf{u}} = \mathbf{f}_S(t, \mathbf{u})$ are termed as the *fast* and *slow sub-system*, respectively. Below in sections 4.3.1 and 4.3.2, we present overview of two of the commonly used IMEX schemes in the literature, namely IMEX-BDF (based on the Backward Differentiation Formula) and CNLF (the Crank-Nicholson–Leap Frog method). Later in section 4.3.3, we discuss the formulation

and stability of the new linear multistep IMEX method based on the Lagrange interpolation and extrapolation, abbreviated as *IMEX-LG*.

4.3.1 The Crank-Nicholson–Leapfrog (CNLF)

Here the implicit Crank-Nicholson method that approximates the solution at the time-step t_n is used for the fast component, i.e.,

$$\frac{\mathbf{u}^{n+1} - \mathbf{u}^{n-1}}{2h} = \frac{1}{2}[\mathbf{f}_F^{n-1} + \mathbf{f}_F^{n+1}], \quad (4.3.3)$$

where to avoid the notational complexity, we use \mathbf{f}_F^n for $\mathbf{f}_F(t_n, \mathbf{u}^n)$. This notation is adopted in all similar circumstances throughout the rest of this chapter.

Next, the explicit Leapfrog scheme is used for approximation of the slow sub-system. Thus the corresponding discrete equation is

$$\frac{\mathbf{u}^{n+1} - \mathbf{u}^{n-1}}{2h} = \mathbf{f}_S^n. \quad (4.3.4)$$

Note that both the implicit (4.3.3) and explicit (4.3.4) schemes are second-order accurate. Combining the two schemes together based on the structure of the global problem (4.3.1) formally gives IMEX scheme:

$$\mathbf{u}^{n+1} = \mathbf{u}^{n-1} + h[\mathbf{f}_F^{n-1} + \mathbf{f}_F^{n+1}] + 2h\mathbf{f}_S^n, \quad (4.3.5)$$

which is order consistent, i.e., it is also second-order as the constituent methods.

Linear stability of CNLF scheme

The linear stability analysis of IMEX schemes, such as the CNLF scheme (4.3.5), for slow-fast dynamical system of ODE (4.3.1) is carried out by considering a linear scalar test problem of the form

$$\dot{u} = \lambda u + \mu u, \quad (4.3.6)$$

where λ and μ represent the eigenvalues of the fast and slow components, respectively. Applying the schemes (4.3.3) and (4.3.4) to the test equation (4.3.6) gives the following characteristic

polynomials:

$$\Pi_{\text{CN}}(\xi; z) = (1 - z)\xi^2 - z - 1, \quad (4.3.7)$$

$$\Pi_{\text{LF}}(\xi; z) = \xi^2 - 2z\xi - 1, \quad (4.3.8)$$

where $z = h(\lambda + \mu)$.

We recall (see, for example [92]) that the stability of multistep schemes such as (4.3.3) and (4.3.4) applied to the test problem (4.3.6) are characterized by the following two definitions:

Definition 4.3.1 (Root condition). *The characteristic polynomials $\Pi(\xi; z)$ of a given multistep time-stepping scheme is said to satisfy the root condition if all of its roots ξ_i satisfy $|\xi_i| < 1$ for all i .*

Definition 4.3.2 (Absolute stability). *A multistep method is said to be absolutely stable for some z in some region \mathcal{S} in the complex plane if its characteristic polynomial satisfies the root condition. The largest of such set \mathcal{S} is said to be the absolute stability region of the multistep method.*

For the IMEX-CNLF method (4.3.5), the characteristic polynomial involves two complex variables which reads

$$\Pi_{\text{IMEX}}(\xi; \omega, \nu) = (1 - \omega)\xi^2 - 2\nu\xi - \omega - 1, \quad (4.3.9)$$

where $\omega = h\lambda$ and $\nu = h\mu$. The representation of stability region on the complex plane is presented in Section 4.3.4.

Remark 4.3.3. *The combination of the implicit Crank-Nicholson scheme and the explicit Leapfrog schemes are formally second-order accurate IMEX-CNLF scheme [8, 158]. The absolute stability regions are as shown in Figure 4.3.1. It is shown that the Crank-Nicholson scheme is Linearly stable, while Leap-Frog scheme shows linear instability. This results in a linear instability of the IMEX-CNLF scheme. Meaning, the LF (and hence IMEX-CNLF) scheme is not typically useful for problems whose eigenvalue is real. However, they are of great interest in applications involving systems of ODEs, for example, semi-discretization of hyper-*

bolic problems leads to antisymmetric system of ODEs whose eigenvalues are pure imaginary [68, 94].

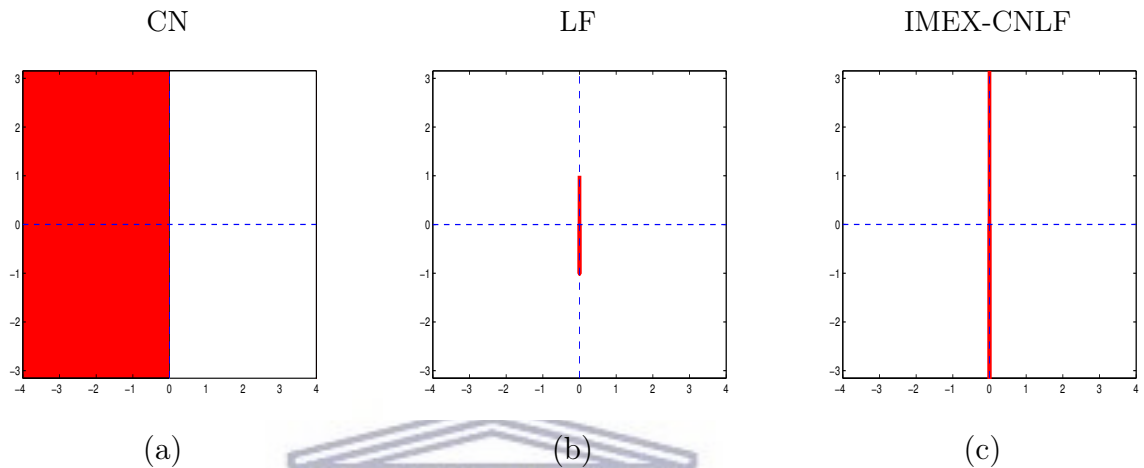


Figure 4.3.1: Stability region: (a) Crank-Nicholson scheme, (b) Leapfrog scheme and (c) and the IMEX-CNLF scheme.

4.3.2 The Backward Differentiation Formula (BDF)

We adopt the IMEX scheme based on the Backward differentiation formula (BDF), as discussed in [139], to solve the singularly perturbed problem (4.3.1). The linear r -step BDF scheme applied to the fast sub-system is given by

$$\frac{1}{h} \sum_{i=-1}^r \beta_i \mathbf{u}^{n-i} = \mathbf{f}_F^{n+1}. \quad (4.3.10)$$

The coefficients β_i , $i = -1, \dots, r$ are obtained by solving the $(r+2) \times (r+2)$ linear system

$$\mathbf{B}\boldsymbol{\beta} = \mathbf{e}_2, \quad (4.3.11)$$

where

$$\begin{aligned}\mathbf{B} &= [B_{ji}], \quad B_{ji} = -\frac{(i-1)^{j-1}}{(j-1)!}, \\ \boldsymbol{\beta} &= (\beta_{-1}, \dots, \beta_r)^\top, \\ \mathbf{e}_2 &= (0, 1, 0, \dots, 0)^\top.\end{aligned}$$

The implicit scheme (4.3.10) is of order $k = r + 1$, and is zero-stable for $r \leq 5$ (see [139]).

Next, for the slow sub-system, an explicit BDF scheme is obtained by replacing the right hand side of (4.3.10) by an $r + 1$ -degree polynomial extrapolation involving the values at the previous time-step solutions $\mathbf{u}^{n-r}, \dots, \mathbf{u}^n$. Hence, the explicit BDF scheme for the slow sub-system reads

$$\frac{1}{h} \sum_{i=-1}^r \beta_i \mathbf{u}^{n-i} = \sum_{i=0}^r \alpha_i \mathbf{f}_s^{n-i}. \quad (4.3.12)$$

The coefficients α_i are obtained by solving the $(r + 1) \times (r + 1)$ linear system

$$\mathbf{A}\boldsymbol{\alpha} = \mathbf{e}_1, \quad (4.3.13)$$

where

$$\begin{aligned}\mathbf{A} &= [A_{ji}], \quad A_{ji} = (-1)^{j-1} \frac{i^{j-1}}{(j-1)!}, \\ \boldsymbol{\alpha} &= (\alpha_0, \alpha_1, \dots, \alpha_r)^\top, \quad \text{and } \mathbf{e}_1 = (1, 0, \dots, 0)^\top.\end{aligned}$$

The IMEX-BDF scheme for the global problem is formally obtained by combining the schemes (4.3.10) and (4.3.12) and reads for problem (4.3.1) as

$$\sum_{i=-1}^r \beta_i \mathbf{u}^{n+1} = h \mathbf{f}_F^{n+1} + h \sum_{i=0}^r \alpha_i \mathbf{f}_S^{n-i}. \quad (4.3.14)$$

With regards to the linear stability of the IMEX-BDF scheme, we note that by applying the linear multistep IM-BDF (4.3.10), EX-BDF (4.3.12) and IMEX-BDF (4.3.14) schemes to the

test problem (4.3.6), we obtain the following characteristic polynomials:

$$\Pi_{\text{EX}}(\xi; z) = \sum_{i=-1}^r \beta_i \xi^{r-i} - z \xi^r, \quad (4.3.15)$$

$$\Pi_{\text{IM}}(\xi; z) = \sum_{i=-1}^r \beta_i \xi^{r-i} - z \sum_{i=0}^r \alpha_i \xi^{r-i}, \quad (4.3.16)$$

$$\Pi_{\text{IMEX}}(\xi; \omega; \nu) = \sum_{i=-1}^r \beta_i \xi^{r-i} - \omega \xi^r - \nu \sum_{i=0}^r \alpha_i \xi^{r-i}, \quad (4.3.17)$$

where $z = h(\lambda + \mu)$, $\omega = h\lambda$, $\nu = h\mu$.

Remark 4.3.4. *The IMEX scheme (4.3.14) (referred to as IMEX-BDF k) is also of order $k = r + 1$ as the constituent schemes [68], and combines the favourable stability property of the implicit scheme with the low cost of the explicit scheme.*

- *Some of the commonly used IMEX-BDF schemes are*

$$\text{IMEX-BDF1: } \mathbf{u}^{n+1} = \mathbf{u}^n + h[\mathbf{f}_F^{n+1} + \mathbf{f}_S^n],$$

$$\text{IMEX-BDF2: } \mathbf{u}^{n+1} = \frac{4}{3}\mathbf{u}^n - \frac{1}{3}\mathbf{u}^{n-1} + \frac{2}{3}h[\mathbf{f}_F^{n+1} + 2\mathbf{f}_S^n - \mathbf{f}_S^{n-1}],$$

$$\text{IMEX-BDF3: } \mathbf{u}^{n+1} = \frac{18}{11}\mathbf{u}^n - \frac{9}{11}\mathbf{u}^{n-1} + \frac{2}{11}\mathbf{u}^{n-2} + \frac{6}{11}h[\mathbf{f}_F^{n+1} + 3\mathbf{f}_S^n - 3\mathbf{f}_S^{n-1} + \mathbf{f}_S^{n-2}].$$

The stability regions of the various BDF schemes are shown in Figure 4.3.2. The improved stability of the IMEX schemes over the explicit ones is clearly evident from the plots in Figure 4.3.2 (a)-(c).

4.3.3 A Multistep Lagrange implicit-explicit (IMEX-LG) scheme

In this section we present a novel arbitrarily high-order IMEX method based on the Lagrange interpolation for singularly perturbed problems such as the one given in (4.3.1). The multistep method to be presented assumes that the r -element set $\{\mathbf{u}^{n-r}, \dots, \mathbf{u}^n\}$ of approximate solutions are known, and seeks to approximate the t_{n+1} time-step solution \mathbf{u}^{n+1} .

First, we interpolate $\mathbf{u}(t)$, $t \in [t_{n-r}, t_{n+1}]$, using the Lagrange polynomials P_{n-j}^k of degree $k = r + 1$ involving the known r -set of solution and including the unknown \mathbf{u}^{n+1} . Thus, the

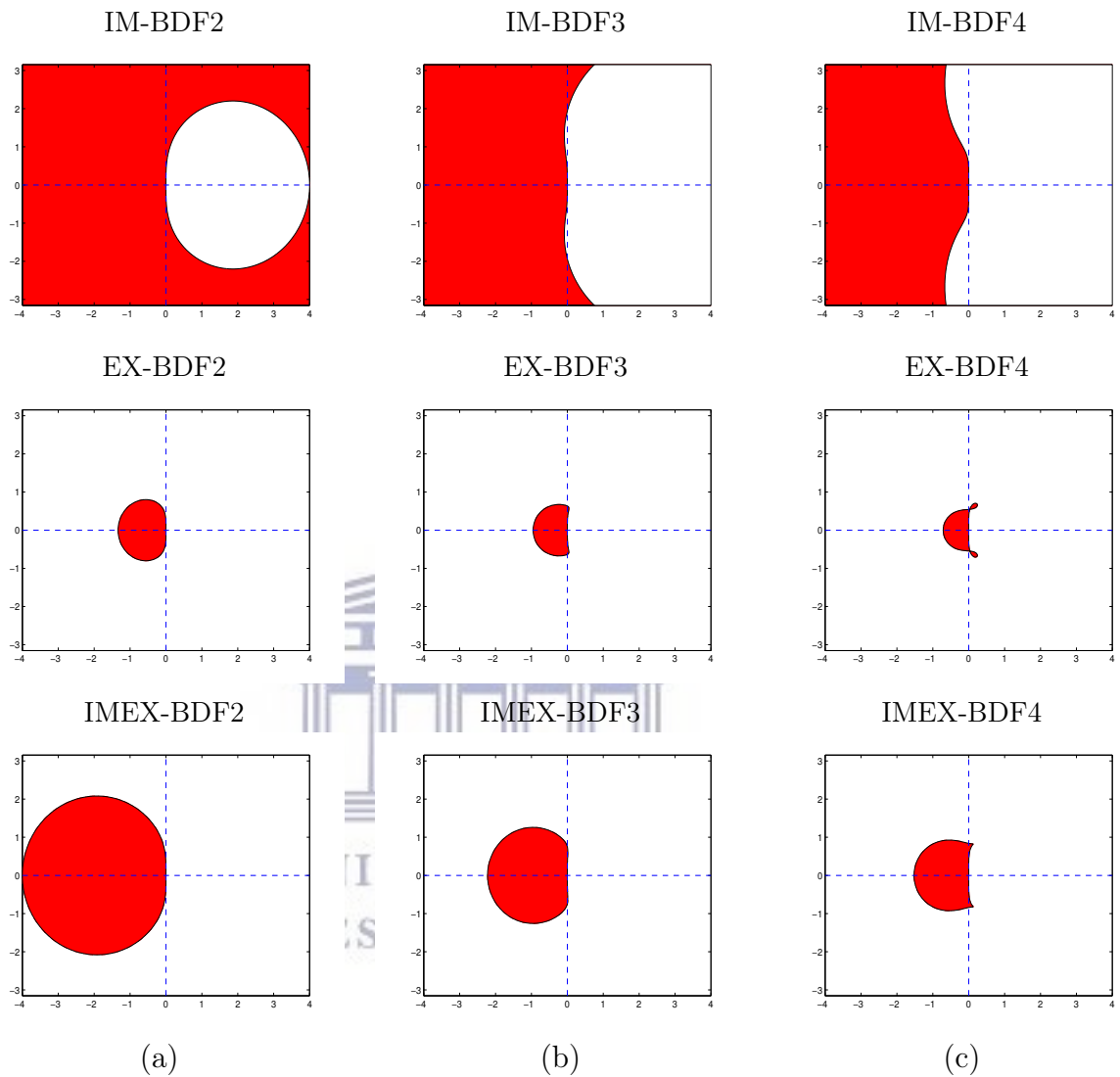


Figure 4.3.2: Stability region of the BDF schemes of order two (BDF2), three (BDF3) and four (BDF4): The shaded region in the first, second and third row indicates the stability regions of the implicit, explicit and IMEX schemes, respectively.

interpolation function reads

$$\mathbf{u}(t) = \sum_{j=-1}^r \mathbf{u}^{n-j} \mathbf{P}_{n-j}^k(t), \quad t \in [t_{n-r}, t_{n+1}]. \quad (4.3.18)$$

Then the derivative at $t_{n+\theta}$, $0 < \theta \leq 1$, of the interpolant becomes

$$\dot{\mathbf{u}}(t_{n+\theta}) = \mathbf{D}^T(t_{n+\theta})\mathbf{U}, \quad (4.3.19)$$

where

$$\mathbf{D}(t_{n+\theta}) = \left[\frac{d}{dt}P_{n-r}^k(t_{n+\theta}), \dots, \frac{d}{dt}P_{n+1}^k(t_{n+\theta}) \right]^T, \text{ and } \mathbf{U} = [\mathbf{u}^{n-r}, \dots, \mathbf{u}^{n+1}]^T,$$

and the Lagrange polynomials are defined by

$$P_{n-j}^k(t) = \prod_{\substack{i=-1 \\ i \neq j}}^{n+1} \frac{(t - t_{n-i})}{(t_{n-j} - t_{n-i})}, \quad j = -1, \dots, r. \quad (4.3.20)$$

An implicit scheme for the fast sub-system can be obtained by substituting the derivative of the interpolate (4.3.19) into the fast sub-system evaluated at $t_{n+\theta}$, that is,

$$\mathbf{D}^T(t_{n+\theta})\mathbf{U} = \mathbf{P}^T(t_{n+\theta})\mathbf{F}_F. \quad (4.3.21)$$

where

$$\mathbf{P} = [P_{n-r}^k(t_{n+\theta}), \dots, P_{n+1}^k(t_{n+\theta})]^T, \text{ and } \mathbf{F}_F = [\mathbf{f}_F^{n-r}, \dots, \mathbf{f}_F^{n+1}]^T. \quad (4.3.22)$$

Since the degree of interpolation is $k = r + 1$, the order of accuracy of the multistep scheme (4.3.21) is expected to be k . And this will be discussed in Section 4.3.4 in detail.

To find an explicit scheme for the slow sub-system based on the Lagrange scheme (4.3.21), we first interpolate the function $\mathbf{f}_S(t, \mathbf{u})$ using the r -degree Lagrange polynomials P_{n-j}^r involving only the values at the previous r time-steps, that is, $\mathbf{f}_S^{n-r}, \dots, \mathbf{f}_S^n$. Thus, the interpolation of \mathbf{f}_S is given by

$$\mathbf{f}_S(t, \mathbf{u}) = \sum_{j=0}^r \mathbf{f}_S^{n-j} P_{n-j}^r(t), \quad t \in [t_{n-r}, t_n]. \quad (4.3.23)$$

Next we extrapolate and evaluate (4.3.23) at $t_{n+\theta}$. This gives

$$\mathbf{f}_S(t_{n+\theta}, \mathbf{u}) = \tilde{\mathbf{P}}^T(t_{n+\theta})\mathbf{F}_S, \quad (4.3.24)$$

where

$$\tilde{\mathbf{P}}(t_{n+\theta}) = [\mathbf{P}_{n-r}^r(t_{n+\theta}), \dots, \mathbf{P}_n^r(t_{n+\theta})]^\top, \text{ and } \mathbf{F}_S = [\mathbf{f}_S^{n-r}, \dots, \mathbf{f}_S^n]^\top. \quad (4.3.25)$$

An explicit scheme for the slow sub-system is obtained by replacing the right hand side of (4.3.21) by the extrapolation (4.3.24), i.e,

$$\mathbf{D}^\top(t_{n+\theta})\mathbf{U} = \tilde{\mathbf{P}}^\top(t_{n+\theta})\mathbf{F}_S. \quad (4.3.26)$$

A k -order accurate IMEX scheme is thus obtained by combining the schemes (4.3.21) and (4.3.26) for the fast and slow sub-systems, respectively, and is given by

$$\mathbf{D}^\top(t_{n+\theta})\mathbf{U} = \mathbf{P}^\top(t_{n+\theta})\mathbf{F}_F + \tilde{\mathbf{P}}^\top(t_{n+\theta})\mathbf{F}_S. \quad (4.3.27)$$

It is to be noted that the schemes presented here are based on similar idea that the BDF schemes used in their derivation. The derivative $\dot{\mathbf{u}}$ in BDF schemes is replaced by a backward differencing interpolation formula involving previous step solutions. If $\theta = 1$, the BDF schemes are recovered and the coefficients are listed in table 4.3.2. The coefficients that define the LG (Lagrangian interpolation based) schemes with $\theta = 0.5$ are also listed in Table 4.3.1. In the following theorem an a priori error bound which estimates the one-step truncation error is of order h^{r+2} implying that the LG schemes converge with order $r + 1$.

Table 4.3.1: Coefficient vectors of the IMEX-LG schemes as given in (4.3.27) for $\theta = 0.5$.

LG ($\theta = 0.5$)														
r	\mathbf{D}^\top					IM (\mathbf{P}^\top)					EX ($\tilde{\mathbf{P}}^\top$)			
0	$\frac{1}{h}[-1 \quad 1]$					$[\frac{1}{2} \quad \frac{1}{2}]$					1			
1	$\frac{1}{2h}[0 \quad -2 \quad 2]$					$[-\frac{1}{8} \quad \frac{3}{4} \quad \frac{3}{8}]$					$[-\frac{1}{2} \quad \frac{3}{2}]$			
2	$\frac{1}{3h}[\frac{1}{8} \quad -\frac{3}{8} \quad -\frac{21}{8} \quad \frac{23}{8}]$					$[\frac{1}{16} \quad -\frac{5}{16} \quad \frac{15}{16} \quad \frac{5}{16}]$					$[\frac{3}{8} \quad -\frac{5}{4} \quad \frac{15}{8}]$			
3	$\frac{1}{4h}[-\frac{1}{6} \quad \frac{5}{6} \quad -\frac{3}{2} \quad -\frac{17}{6} \quad \frac{11}{3}]$					$[-\frac{5}{128} \quad \frac{7}{32} \quad -\frac{35}{64} \quad \frac{35}{32} \quad \frac{35}{128}]$					$[-\frac{5}{16} \quad \frac{21}{16} \quad -\frac{35}{16} \quad \frac{35}{16}]$			

Table 4.3.2: Coefficient vectors of the IMEX-BDF schemes as given in (4.3.27) for $\theta = 1$.

BDF (LG with $\theta = 1$)			
r	\mathbf{D}^T	IM (\mathbf{P}^T)	EX ($\tilde{\mathbf{P}}^T$)
0	$\frac{1}{h}[-1 \quad 1]$	$[0 \quad 1]$	1
1	$\frac{1}{2h}[1 \quad -4 \quad 3]$	$[0 \quad 0 \quad 1]$	$[-1 \quad 2]$
2	$\frac{1}{3h}[-1 \quad \frac{9}{2} \quad -9 \quad \frac{11}{2}]$	$[0 \quad 0 \quad 0 \quad 1]$	$[1 \quad -3 \quad 3]$
3	$\frac{1}{4h}[1 \quad -\frac{16}{3} \quad 12 \quad -16 \quad \frac{25}{3}]$	$[0 \quad 0 \quad 0 \quad 0 \quad 1]$	$[-1 \quad 4 \quad -6 \quad 4]$

4.3.4 Convergence and linear stability analysis of the LG schemes

Here, we present results on convergence and linear stability of the IM-, EX-, and IMEX-LG schemes. The necessary and sufficient condition for convergence is zero-stability and consistency. Zero-stability is the property of the scheme that involves only the left hand side of the multistep scheme of generic form

$$\sum_{j=0}^{r+1} \alpha_j \mathbf{u}^{n-r+j} = h \sum_j \beta_j \mathbf{f}^{n-r+j}. \quad (4.3.28)$$

For example, for the IM-LG scheme Eq. (4.3.21), the coefficients read

$$\left. \begin{aligned} \alpha_j &= h \frac{d}{dt} P_{n-r+j}^k(t_{n+\theta}), \\ \beta_j &= P_{n-r+j}^k(t_{n+\theta}), \end{aligned} \right\} j = 0, 1, \dots, r+1. \quad (4.3.29)$$

The multistep scheme (4.3.28) is said to be zero-stable if all roots of the (first-)characteristic polynomial are of modulus less than or equal to unity (provided that each root is of multiplicity one) [92]. In case of multiple roots, strict inequality should hold. Thus, the IM-, EX-, and IMEX-LG schemes have the same first-characteristic polynomial

$$\Pi(\xi) = \sum_{j=0}^{r+1} \alpha_j \xi^j, \quad (4.3.30)$$

where the coefficients are

$$\alpha_j = h \frac{d}{dt} P_{n-r+j}^k(t_{n+\theta}); \quad j = 0, 1, \dots, r + 1. \quad (4.3.31)$$

Note that the final expression of α_j does not involve h since $\frac{d}{dt} P_{n-r+j}^k(t_{n+\theta})$ has a factor $1/h$ which cancels out in the expression (4.3.30).

For order of approximation up to $r = 3$, it is noted that the LG schemes for $\theta = 0.5$ are zero-stable (see Table 4.3.3).

Now, we examine the consistency of the LG schemes. Note that a given multistep scheme (4.3.28) is said to be consistent if the discrete solution approaches to the exact problem in the limit as h tends to zero. Alternatively, consistency requires that the order of accuracy be at least one. The consistency of the LG schemes is given in the following theorem.

Table 4.3.3: Zero-stability of the LG methods for $\theta = 0.5$.

LG methods	$ \xi $	Zero-stability
$r = 1$ (order 2)	0 1	✓
$r = 2$ (order 3)	1 0.2564 0.1692	✓
$r = 3$ (order 4)	1 0.6302 0.2685 0.2685	✓
$r = 4$ (order 5)	1 0.2883 1.0539 0.3719 0.3719	×

In the following theorem an a priori, bound which estimates the one-step truncation error, is of order of h^{r+2} leading the LG schemes to converge with order $r + 1$.

Theorem 4.3.5. Assume that $\mathbf{u}^{n-r}, \dots, \mathbf{u}^n$ are the values of the exact solution \mathbf{u}_{ex} at the previous time-steps t_{n-r}, \dots, t_n . The IMEX-LG scheme (4.3.27) approximates $\mathbf{u}_{\text{ex}}(t_{n+1})$ within

an error of order $r + 1$, that is, the truncation error $\mathbf{E}(t_{n+1})$ is

$$\mathbf{E}(t_{n+1}) := \mathbf{u}_{\text{ex}}(t_{n+1}) - \mathbf{u}^{n+1} = \mathcal{O}(h^{r+2}), \quad (4.3.32)$$

where \mathbf{u}^{n+1} is the approximate solution at t_{n+1} .

Proof. The interpolation error, by construction, takes the form

$$\mathbf{E}(t) = \mathbf{u}_{\text{ex}}(t) - \mathbf{P}^T(t)\mathbf{U} = \frac{1}{(r+1)!} \prod_{i=0}^r (t - t_{n-i}) \frac{d^{(r+1)}}{dt^{(r+1)}} \mathbf{u}_{\text{ex}}(\xi), \quad (4.3.33)$$

for some $\xi \in (t_{n-r}, t_n)$. Since the maximum value of the product at the right hand side is of order h^{r+1} , this can also be written, in big-o notation, as

$$\mathbf{E}(t) = \mathcal{O}(h^{r+1}). \quad (4.3.34)$$

Similarly, since both of the right-hand side terms of (4.3.27) are interpolation polynomials that agree at each $r + 1$ previous solutions of the exact solutions, the interpolation error in approximating $\mathbf{f} := \mathbf{f}_F + \mathbf{f}_S$ is also of order $r + 1$, that is,

$$\mathbf{f}(t) - (\mathbf{P}^T(t)\mathbf{F}_F + \tilde{\mathbf{P}}^T(t)\mathbf{F}_S) = \mathcal{O}(h^{r+1}). \quad (4.3.35)$$

Noting that \mathbf{u}_{ex} satisfies the differential equation (4.3.1) exactly, hence in particular, at $t_{n+\theta}$ we have

$$\dot{\mathbf{u}}_{\text{ex}}(t_{n+\theta}) = \mathbf{f}(\mathbf{u}_{\text{ex}}(t_{n+\theta})). \quad (4.3.36)$$

Next, subtracting the discrete equation (4.3.27) from equation (4.3.36) gives an error estimate for the derivative of the local truncation at $t_{n+\theta}$, that is

$$\dot{\mathbf{E}}(t_{n+\theta}) = \mathcal{O}(h^{r+1}). \quad (4.3.37)$$

Now, we take the differential equation into consideration. To find the order of the truncation error at t_{n+1} , Taylor's theorem is employed to expand $\mathbf{E}(t_{n+\theta})$ about t_n (note that since the

$\mathbf{P}^\top(t_n)\mathbf{U} = \mathbf{u}^n$ is exact, then $\mathbf{E}(t_n) = 0$). This gives

$$0 = \mathbf{E}(t_n) = \mathbf{E}(t_{n+\theta}) - \underbrace{\theta h \dot{\mathbf{E}}(t_{n+\theta}) + \frac{\theta^2 h^2}{2} \ddot{\mathbf{E}}(t_{n+\theta}) + \dots}_{\mathcal{O}(h^{r+2})} \quad (4.3.38)$$

This immediately implies that

$$\mathbf{E}(t_{n+\theta}) = \mathcal{O}(h^{r+2}). \quad (4.3.39)$$

Applying Taylor's theorem again, and expanding $\mathbf{E}(t_{n+1})$ about $t_{n+\theta}$, we obtain

$$\mathbf{E}(t_{n+1}) = \underbrace{\mathbf{E}(t_{n+\theta}) + (1-\theta)h\dot{\mathbf{E}}(t_{n+\theta}) + \frac{(1-\theta)^2 h^2}{2} \ddot{\mathbf{E}}(t_{n+\theta}) + \dots}_{\mathcal{O}(h^{r+2})} \quad (4.3.40)$$

Hence, the truncation error $\mathbf{E}(t_{n+1})$ is of order $r+2$ as required. \square

The above theorem implies that the order of accuracy of an LG scheme involving $r+1$ previous solutions is of order $k=r+1$. Hence the LG scheme is consistent, since $r \geq 0$.

Now the linear stability analysis requires us to consider a linear scalar test problem of the form

$$\dot{u} = \lambda u + \mu u, \quad (4.3.41)$$

where λ and μ represent the eigenvalues of the fast and slow components, respectively. In what follows the readers may note that the following notations have been used consistently for extracting characteristic polynomial of the IM and EX multistep schemes discussed in this chapter:

α_j : coefficients corresponding to the left-hand-side of the IM or EX schemes,

β_j : coefficients corresponding to the right-hand-side of the IM schemes, and

γ_j : coefficients corresponding to the right-hand-side of the EX schemes.

We first apply, the implicit LG scheme (4.3.21) to the test problem (4.3.41) and obtain the characteristic polynomial

$$\Pi_{\text{IM}}(\xi; z) = \sum_{j=0}^{r+1} \alpha_j \xi^j - z \sum_{j=0}^{r+1} \beta_j \xi^j, \quad (4.3.42)$$

where $z = h(\lambda + \mu)$, and the coefficient of the last sum is

$$\beta_j = P_{n-r+j}^k(t_{n+\theta}). \quad (4.3.43)$$

For the IMEX scheme the resulting right-hand-side coefficient becomes $(\beta_j + \gamma_j)$.

In a similar manner, we obtain the characteristic polynomials corresponding to the explicit scheme (4.3.26) and the IMEX scheme (4.3.27) as

$$\Pi_{\text{EX}}(\xi, z) = \sum_{j=0}^{r+1} \alpha_j \xi^j - z \sum_{j=0}^r \gamma_j \xi^j, \quad (4.3.44)$$

$$\Pi_{\text{IMEX}}(\xi, \omega, \nu) = \sum_{j=0}^{r+1} \alpha_j \xi^j - \omega \sum_{j=0}^{r+1} \beta_j \xi^j - \nu \sum_{j=0}^r \gamma_j \xi^j, \quad (4.3.45)$$

where $\omega = h\lambda$, $\nu = h\mu$, and

$$\gamma_j = \tilde{P}_{n-r+j}^r(t_{n+\theta}). \quad (4.3.46)$$

Following the standard criteria (see [92]) for stability, we say that a given time-stepping scheme is absolutely stable if all roots of the corresponding characteristic polynomial are of modulus strictly less than unity.

It is possible to determine the stability region \mathcal{S} of a given multistep scheme with a characteristic polynomial $\Pi(r; z)$ without necessarily computing all of its roots. We know that the set of complex numbers r such that $|r| = 1$ can be represented by the formula

$$r = e^{i\vartheta}, \quad 0 \leq \vartheta \leq 2\pi; \quad i = \sqrt{-1}. \quad (4.3.47)$$

If the locus of points z satisfying the stability criteria is a bounded (or partially bounded) region of the complex plane, then the boundary of such region is given by the parametric curve in the complex plane

$$\Pi(e^{i\vartheta}; z) = 0, \quad 0 \leq \vartheta \leq 2\pi. \quad (4.3.48)$$

To determine the part of the complex plane bounded by the parametric curve that belongs to the stability region \mathcal{S} , we take a root r of the characteristic polynomial inside the unit disc for some z . Then the part of the complex plane, bounded by the parametric curve, that contains

the corresponding z value is the stability region.

Since the characteristic polynomials corresponding to the IMEX methods involve two parameters ω and ν , stability regions of such methods, such as IMEX-BDF, -LG, and -CNLF, are formed in the complex hyper-plane $\mathbb{C} \times \mathbb{C}$. However, it is possible to represent this region in the complex plane \mathbb{C} as follows; we first take both ω and ν equal to z . Then we determine the corresponding region from the characteristic polynomial involving only the variable z . For the interpretation of this region, we first define the following notion: The pair $(\omega, \nu) \in \mathbb{C} \times \mathbb{C}$ is said to be *stable pair* for the IMEX scheme under consideration if both ω and ν are in the region of stability such that $\omega/\lambda = \nu/\mu$. Hence the stability region of the IMEX methods in the complex hyper-plane $\mathbb{C} \times \mathbb{C}$ is defined as the set of all stable pairs, that is,

$$\left\{ (\omega, \nu) \in \mathbb{C} \times \mathbb{C} : \frac{\omega}{\lambda} = \frac{\nu}{\mu}, \text{ and } \omega, \nu \in \mathcal{S} \right\}. \quad (4.3.49)$$

The region of absolute stability of the various LG schemes are shown in Figure 4.3.3. We first note that in contrast to the stability regions of the implicit BDF and CN schemes, shown in Figure 4.3.3 and 4.3.1, the stability regions of that of the LG schemes are finite (bounded). However, it is clearly evident that the stability regions of the IMEX-BDF and -LG schemes are comparatively similar as can be seen from the shaded areas. It should also be noted that the less stability feature of the LG schemes is favourably compensated by its better accuracy than the respective BDF schemes, as evident in Figure 4.6.2 and 4.6.3. Moreover, numerical experiments (not displayed in here) have shown that it takes fewer iterations per time-step to achieve a prescribed tolerance of error with the LG scheme than that of the BDF counterparts.

4.4 An order consistent starting solution scheme

For multistep schemes that involve previous solutions at multiple time-steps, it is very crucial to emphasize how the starting solutions are obtained. This is due to the fact that the overall accuracy may not reflect the true accuracy of the multistep method used in the approximation if the order of the scheme for the starting solutions does not match. For example, if the order of the start up scheme is lower than that of the multistep method, then the order of the overall solution will be reduced.

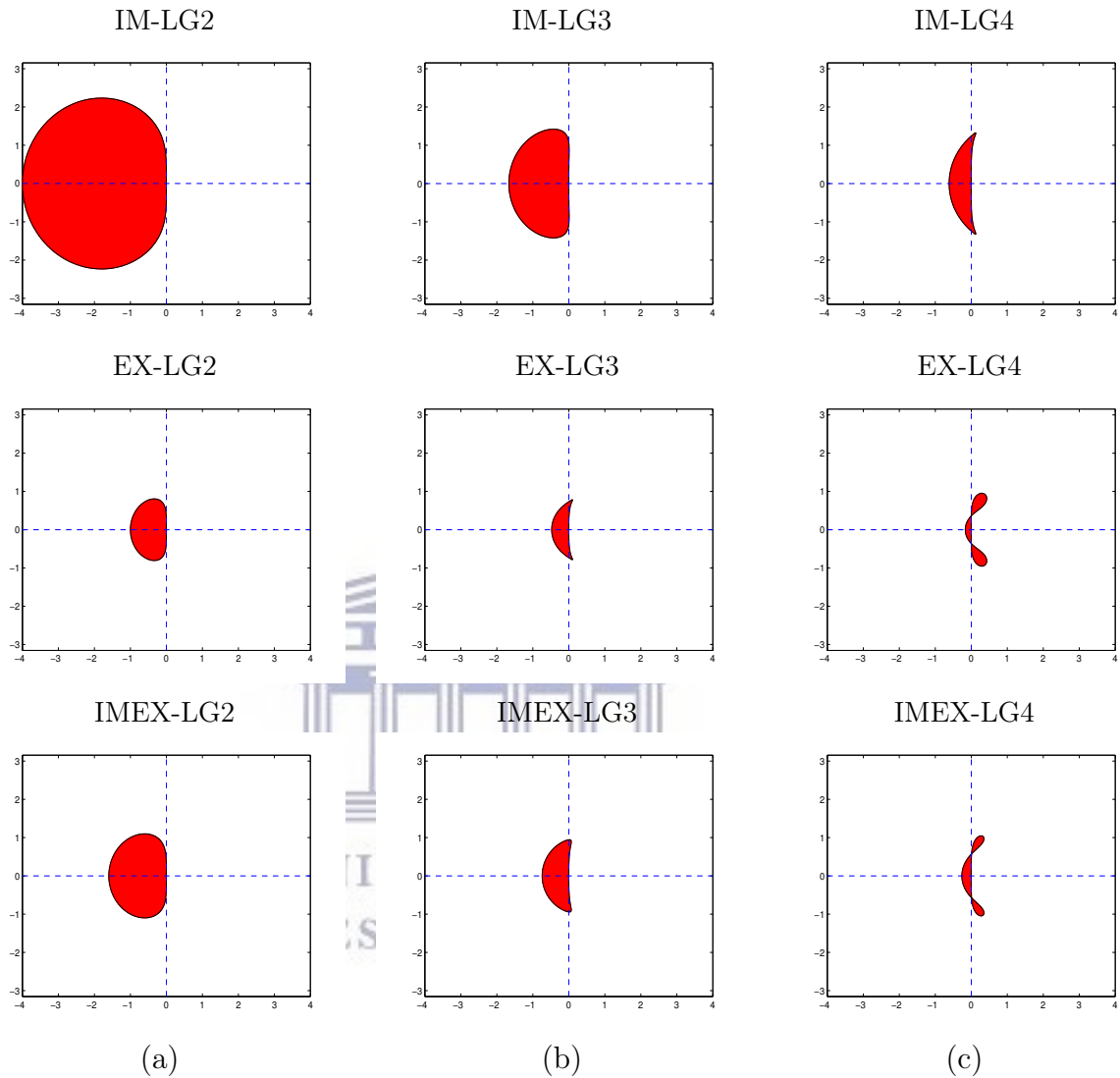


Figure 4.3.3: Stability region of the Lagrange based schemes of order two (LG2), three (LG3) and four (LG4): The shaded region in the first, second and third row indicates the stability regions of the implicit, explicit and IMEX schemes, respectively.

The standard practice in multistep methods is to use some adaptive single step method with a given tolerance. Unfortunately, such approach has two drawbacks: (i) it requires to take extremely small time-steps to meet the given tolerance which makes it unnecessarily costly in terms of computation time; (ii) when a high-order multistep method is used with small step-size, the accuracy of the starting solution may limit the accuracy of the overall solution even if a very small tolerance has been used for the starting scheme.

An implicit numerical scheme for simultaneously solving the starting solution can be constructed based on the same idea that the multistep Lagrangian used as discussed above. It is basically a spectral collocation method which uses the same Lagrangian interpolation functions as its basis. Consequently, the start up scheme will be consistent with the multistep Lagrangian scheme in that both schemes are same order of accuracy.

Consider the $r + 1$ -order Lagrangian scheme. Since it is an r -step method the initial solutions $\{\mathbf{u}^0, \dots, \mathbf{u}^r\}$ have to be solved. For this, first we interpolate \mathbf{u} over the interval $[t_0, t_r]$ using the Lagrange functions as

$$\mathbf{u}(t) = \sum_{j=0}^r \mathbf{u}^j P_j^k(t), \quad t \in [t_0, t_r]. \quad (4.4.1)$$

Consequently, its derivative at the collocation point $t_j, j = 1, \dots, r$, is

$$\dot{\mathbf{u}}(t_j) = \mathbf{D}_j^T \mathbf{U}_{\text{full}}, \quad (4.4.2)$$

where

$$\mathbf{D}_j = \left[\frac{d}{dt} P_0^k(t_j), \dots, \frac{d}{dt} P_r^k(t_j) \right]^T, \quad \text{and } \mathbf{U}_{\text{full}} = [\mathbf{u}^0, \dots, \mathbf{u}^r]^T. \quad (4.4.3)$$

The implicit scheme is obtained by posing the initial value problems at each of r collocation points t_1, \dots, t_r as

$$\begin{aligned} \mathbf{D}_1^T \mathbf{U}_{\text{full}} &= \mathbf{f}(\mathbf{u}^1), \\ &\vdots \\ \mathbf{D}_r^T \mathbf{U}_{\text{full}} &= \mathbf{f}(\mathbf{u}^r). \end{aligned} \quad (4.4.4)$$

Here \mathbf{f} refers to the full problem, i.e., $\mathbf{f} = \mathbf{f}_F + \mathbf{f}_S$. The matrix form of the above equation reads

$$\mathbb{D} \mathbf{U}_{\text{st}} = \mathbf{F}, \quad \text{where } \mathbf{U}_{\text{st}} = [\mathbf{u}^1, \dots, \mathbf{u}^r]^T, \quad (4.4.5)$$

in which the elements of the matrix \mathbb{D} are given by

$$\mathbb{D}_{ij} = \frac{d}{dt} P_j^k(t_i); \quad 1 \leq i, j \leq r, \quad (4.4.6)$$

and those of the right hand side vector \mathbf{F} are given by

$$\mathbf{F}_i = \mathbf{f}(\mathbf{u}^i) - \frac{d}{dt} P_0^k(t_i) \mathbf{u}^0. \quad (4.4.7)$$

For multivalued problem such as the one we are considering in this chapter, the matrix \mathbb{D} can be taken as a block diagonal matrix $\widehat{\mathbb{D}}$, that is,

$$\widehat{\mathbb{D}} = \begin{bmatrix} \mathbb{D}_{|1} & \mathbf{0} & \mathbf{0} & \mathbf{0} \\ \mathbf{0} & \mathbb{D}_{|2} & \mathbf{0} & \mathbf{0} \\ \mathbf{0} & \mathbf{0} & \mathbb{D}_{|3} & \mathbf{0} \\ \mathbf{0} & \mathbf{0} & \mathbf{0} & \mathbb{D}_{|4} \end{bmatrix}, \quad (4.4.8)$$

where $\mathbb{D}_{|1} = \mathbb{D}_{|2} = \mathbb{D}_{|3} = \mathbb{D}_{|4} = \mathbb{D}$ and the corresponding right hand side vector $\widehat{\mathbf{F}}$ is

$$\widehat{\mathbf{F}} = \begin{bmatrix} \left[\begin{array}{c} f_1(\mathbf{u}^1) - \frac{d}{dt} P_0^k(t_1) u_1^0 \\ \vdots \\ f_1(\mathbf{u}^r) - \frac{d}{dt} P_0^k(t_r) u_1^0 \\ \vdots \end{array} \right] \\ \left[\begin{array}{c} f_4(\mathbf{u}^1) - \frac{d}{dt} P_0^k(t_1) u_4^0 \\ \vdots \\ f_4(\mathbf{u}^r) - \frac{d}{dt} P_0^k(t_r) u_4^0 \end{array} \right] \end{bmatrix}. \quad (4.4.9)$$

The resulting system $\widehat{\mathbb{D}} U_{st} = \widehat{\mathbf{F}}$ is then solved to obtain the desired solution. In the next section, we discuss how we handle the nonlinearities.

4.5 Iterative treatment of nonlinearities using Anderson's acceleration method

In the IMEX framework, the slow components will be explicitly solved based on the previous time-step solutions to obtain the current step solution of the slow components. Then the fast discrete problem is updated based on the current values of the slow components. The

resulting implicitly-nonlinear algebraic system can then be recasted into a fixed point problem of the form

$$\mathbf{G}(\mathbf{u}) = \mathbf{u}. \quad (4.5.1)$$

For example, the implicit LG scheme (4.3.21) can be written as a fixed point problem (4.5.1) in which

$$\mathbf{G}(\mathbf{u}) = \mathbf{u} + \mathbf{D}^T \mathbf{U} - \mathbf{P}^T \mathbf{F}_F. \quad (4.5.2)$$

Here the current unknown solution \mathbf{u}^{n+1} in the vector \mathbf{U} is replaced by the variable of the fixed point problem \mathbf{u} . Therefore, a fixed point solution of (4.5.1) is the current solution \mathbf{u}^{n+1} .

The methodology adopted here to solve the nonlinear fixed point problems is a fixed point iterative method known as Anderson's acceleration [163]. This method is built up on the classical Picard iteration in order to accelerate the poor convergence by employing multiple previous iterations (upto some prescribed depth, usually < 10). At each iteration a constrained minimization problem involving some convex combination of the residuals on the previous iterates need to be solved. Compared to the complexity of evaluating the fixed point map \mathbf{G} , the cost of solving these minimization problems is negligible [154]. Anderson's acceleration has advantages over some of the most commonly used techniques to solve nonlinear problems. It is easy to implement and has low cost per iteration as it does not require Jacobian information. As all nonlinear solvers, its main drawback is the lack of globalization. However, for initial value problems such as ODEs, this is less of an issue as the previous time-step solution provides generally a good initial guess.

4.6 Numerical results

In this section, we present results demonstrating the performance of the numerical schemes proposed in this chapter by applying to the singularly perturbed problem (4.2.2). Particularly, the parameters $m = 0.5$, $r = 0.4$ and various epsilon (ε) values were used. It was shown, using analytical and numerical techniques, that these set of parameter values in combination with the initial condition $(p_1, p_2, z, q) = (1.18, 0.87, 1.50, 0.99)$ result in a two parametric family of periodic orbits [125].

In what follows, firstly the numerical schemes are analyzed for convergence. For the implicit schemes, Anderson’s acceleration was employed with tolerance 10^{-11} and 10^{-12} depending on the stiffness of the problems. Since there is no known analytic solution for the problem considered, maximum errors are computed using a double mesh principle as explained below. For this, the final time is set to $T = 1$, and an initial temporal mesh with a given step-size h is considered. The mesh is successively refined by halving the step-size of the previous courser mesh as shown in Figure 4.6.1. Maximum error between the solutions of the successive meshes is computed at the common nodes (marked with open dots). For example, the maximum error between meshes with $h/2$ and $h/4$ is denoted by $E_{h/2}$. Then order of convergence in going from a mesh with h through $h/2$ is calculated as

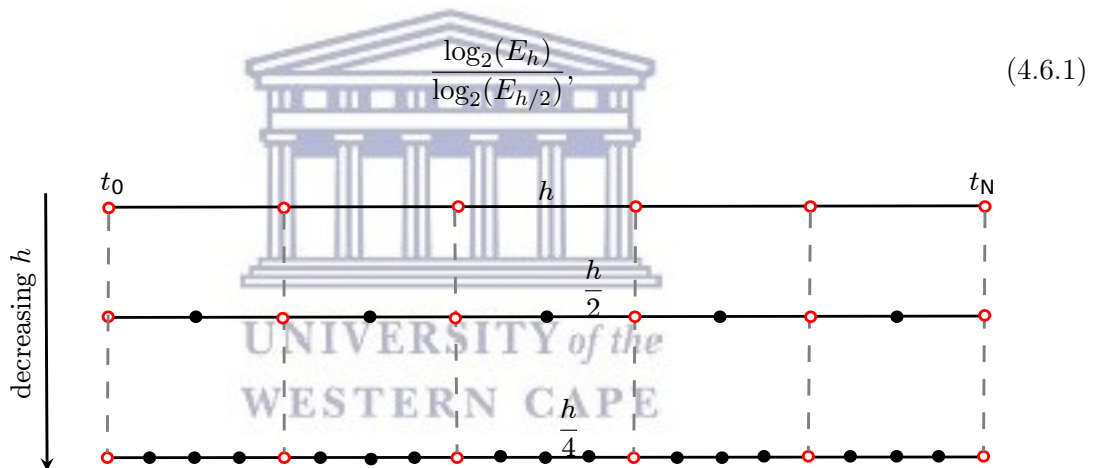


Figure 4.6.1: Successive mesh refinement. The open dots denote the common nodes at which maximum errors are computed.

Table, 4.6.1, 4.6.2, and 4.6.4 present maximum errors and order of convergence of the implicit (IM), explicit (EX), and implicit-explicit (IMEX) versions of the three methods, CNLF, BDF2, and LG2 methods, respectively. Table 4.6.3 and 4.6.5 present maximum errors and order of convergence of the implicit (IM), explicit (EX), and implicit-explicit (IMEX) versions of the methods: BDF4, and LG4, respectively. It is shown that IMEX schemes in each of the methods replicates the good convergence behaviour of the corresponding fully implicit method. It is also shown that the LG2 and CNLF exhibit better order of convergence than the BDF2 in each case. Between the fourth-order schemes, the LG4 schemes shows better accuracy than the corresponding BDF4.

Table 4.6.1: Maximum errors and order of convergence of the implicit (IM-CN), explicit (EX-LF) and the implicit-explicit (IMEX-CNLF) schemes. Here $\varepsilon = 0.1$, $\text{To1} = 10^{-12}$, and final time $T = 1$.

N	Maximum error			Order of convergence		
	IM-CN	EX-LF	IMEX-CNLF	IM-CN	EX-LF	IMEX-CNLF
10	0.0187611059	0.0044816528	0.0191058838	2.38	1.84	2.42
20	0.0036039265	0.0012545499	0.0035665635	2.10	2.02	2.10
40	0.0008431444	0.0003093285	0.0008306734	2.02	2.04	2.03
80	0.0002073687	0.0000750404	0.0002039910	2.01	2.03	2.01
160	0.0000516324	0.0000183553	0.0000507600	2.00	2.02	2.00
320	0.0000128832	0.0000045306	0.0000126739	2.01	2.01	2.00

Table 4.6.2: Maximum errors and order of convergence of the implicit (IM-BDF2), explicit (EX-BDF2) and the implicit-explicit (IMEX-BDF2) schemes. Here $\varepsilon = 0.1$, $\text{To1} = 10^{-12}$, and final time $T = 1$.

N	Maximum error			Order of convergence		
	IM-BDF2	EX-BDF2	IMEX-BDF2	IM-BDF2	EX-BDF2	IMEX-BDF2
10	0.0164955797	0.0038961442	0.0180150816	2.01	0.78	2.05
20	0.0040989510	0.0022695858	0.0043463790	1.93	1.38	1.93
40	0.0010779476	0.0008708676	0.0011376353	1.94	1.71	1.94
80	0.0002818532	0.0002660704	0.0002973353	1.96	1.86	1.96
160	0.0000725115	0.0000730664	0.0000764910	1.98	1.94	1.98
320	0.0000183745	0.0000191055	0.0000194331	2.00	1.97	1.99

Table 4.6.3: Maximum errors and order of convergence of the implicit (IM-BDF4), explicit (EX-BDF4) and the implicit-explicit (IMEX-BDF4) schemes. Here $\varepsilon = 0.1$, $\text{To1} = 10^{-12}$, and final time $T = 1$.

N	Maximum error			Order of convergence		
	IM-BDF4	EX-BDF4	IMEX-BDF4	IM-BDF4	EX-BDF4	IMEX-BDF4
10	0.0027867270	0.0028424109	0.0029678758	3.32	2.58	3.31
20	0.0002786170	0.0004769295	0.0002984421	3.65	3.40	3.64
40	0.0000221566	0.0000452193	0.0000239543	3.84	3.76	3.83
80	0.0000015448	0.0000033377	0.0000016816	3.93	3.90	3.92
160	0.0000001014	0.0000002235	0.0000001109	3.97	3.96	3.96
320	0.0000000065	0.0000000144	0.0000000071	4.00	3.97	4.00

The efficiencies of the IMEX and IM schemes are compared in terms of the CPU times that each algorithm spends in solving the same problem. These schemes were implemented on Matlab 2013a and the simulations were done in a serial computation on a single core of a machine with 2.4GHz x 8, IntelCore i7-4700MQ processor and 8GB RAM. The time-scale

Table 4.6.4: Maximum errors and order of convergence of the implicit (IM-LG2), explicit (EX-LG2) and the implicit-explicit (IMEX-LG2) schemes. Here $\varepsilon = 0.1$, $\text{To1} = 10^{-12}$, and final time $T = 1$.

N	Maximum error			Order of convergence		
	IM-LG2	EX-LG2	IMEX-LG2	IM-LG2	EX-LG2	IMEX-LG2
10	0.0030445566	0.0049272821	0.0033257199	2.17	1.24	2.14
20	0.0006756094	0.0020848616	0.0007539527	2.10	1.67	2.07
40	0.0001572329	0.0006554798	0.0001791964	2.05	1.86	2.04
80	0.0000378382	0.0001805156	0.0000437035	2.04	1.94	2.02
160	0.0000092321	0.0000470864	0.0000107972	2.02	1.97	2.01
320	0.0000022736	0.0000120042	0.0000026841	2.02	1.99	2.00

Table 4.6.5: Maximum errors and order of convergence of the implicit (IM-LG4), explicit (EX-LG4) and the implicit-explicit (IMEX-LG4) schemes. Here $\varepsilon = 0.1$, $\text{To1} = 10^{-12}$, and final time $T = 1$.

N	Maximum error			Order of convergence		
	IM-LG4	EX-LG4	IMEX-LG4	IM-LG4	EX-LG4	IMEX-LG4
10	0.0003336782	0.0020637481	0.0003873648	3.75	3.14	3.53
20	0.0000247892	0.0002345047	0.0000335620	3.66	3.68	3.58
40	0.0000019599	0.0000182928	0.0000027989	3.75	3.88	3.82
80	0.0000001460	0.0000012444	0.0000001978	3.85	3.95	3.92
160	0.0000000101	0.0000000804	0.0000000131	3.92	3.98	3.96
320	0.0000000007	0.0000000051	0.0000000008	4.04	3.98	3.94

parameter that was taken is $\varepsilon = 0.1$ and the simulations were done up to the final time $T = 10$. As shown in Table 4.6.6, while the second-order IMEX-BDF2, IMEX-LG2, and IMEX-CNLF have shown comparatively the same order of efficiencies (though LG schemes consistently display fairly better performance over the other schemes), it is seen that they show clear gain in efficiencies over their respective implicit schemes. Essentially the same scenario is exhibited for the high-order BDF and LG schemes as shown in tables 4.6.7 and 4.6.8. However, we note that increasing the order of the methods do not seem to have effect on the efficiency of the method, as can be seen from the results in tables 4.6.6-4.6.8.

In Figure 4.6.2, we present comparison of maximum errors obtained by second-order multistep IMEX schemes of the three methods. We notice that all the multistep IMEX schemes gave second-order convergence with the IMEX-LG2 demonstrating high-order of accuracy than the other two. The superior performance of the third- and fourth-order IMEX-LG schemes are seen through their comparison with the corresponding IMEX-BDF schemes as

Table 4.6.6: CPU comparison of the second-order of the IMEX-BDF2, IMEX-LG2 and IMEX-CNLF and their corresponding implicit IM-BDF2, IM-LG2 and IM-CNLF with parameters $\varepsilon = 0.1$, $\text{Tol} = 10^{-12}$ and final time $T = 10$.

h	CPU comparison of IMEX			CPU comparison of IM		
	IMEX-BDF2	IMEX-LG2	IMEX-CNLF	IM-BDF2	IM-LG2	IM-CNLF
1×10^{-3}	3.7100	3.4500	4.4300	11.7000	11.3000	8.1400
5×10^{-4}	9.0500	7.1700	9.8900	23.5000	21.3800	15.8600
2×10^{-4}	33.0600	23.8900	35.5100	55.5200	49.8700	50.7300

Table 4.6.7: CPU comparison of the third-order of the IMEX-BDF3 and IMEX-LG3 and their corresponding implicit IM-BDF3 and IM-LG3 with parameters $\varepsilon = 0.1$, $\text{Tol} = 10^{-11}$ and final time $T = 10$.

h	CPU comparison of IMEX		CPU comparison of IM	
	IMEX-BDF3	IMEX-LG3	IM-BDF3	IM-LG3
1×10^{-3}	3.8300	3.4600	11.8000	10.9200
5×10^{-4}	8.1800	7.4900	23.1600	20.4800
2×10^{-4}	33.2000	34.1800	54.8500	47.2200

Table 4.6.8: CPU comparison of the fourth-order of the IMEX-BDF4 and IMEX-LG4 and their corresponding implicit IM-BDF4 and IM-LG4 with parameters $\varepsilon = 0.1$, $\text{Tol} = 10^{-11}$ and final time $T = 10$.

h	CPU comparison of IMEX		CPU comparison of IM	
	IMEX-BDF4	IMEX-LG4	IM-BDF4	IM-LG4
1×10^{-3}	3.8100	3.4600	12.1300	11.0100
5×10^{-4}	7.8300	7.1900	24.1300	20.6300
2×10^{-4}	33.7000	32.8900	57.0900	46.9200

shown in Figure 4.6.3. The slight reduction in the order around the right end of IMEX-LG4 may be due to the higher tolerance prescribed for the nonlinear solver.

Figure 4.6.4 shows the influence of the separation time-scale, ε between the fast and slow components on the order and precession of the 2nd-order IMEX-CNLF, IMEX-BDF2 and IMEX-LG2 schemes. As expected, while the schemes for various values of ε converges to the correct order, it is clearly evident that the accuracy for fixed step-size h deteriorates as ε becomes smaller. However, in this situation the LG scheme shows less accuracy degradation than those by other schemes. Similar observation is shown for high-order LG and BDF implicit-explicit schemes, see, Figure 4.6.5 and 4.6.6. Notice that due to the prescribed tolerance ($\text{Tol} = 10^{-11}$) for the nonlinear Anderson's acceleration solver, we observe a small

deflection for the finest mesh corresponding to the fourth-order IMEX-LG and -BDF schemes for larger time-scale ($\varepsilon = 0.5$).

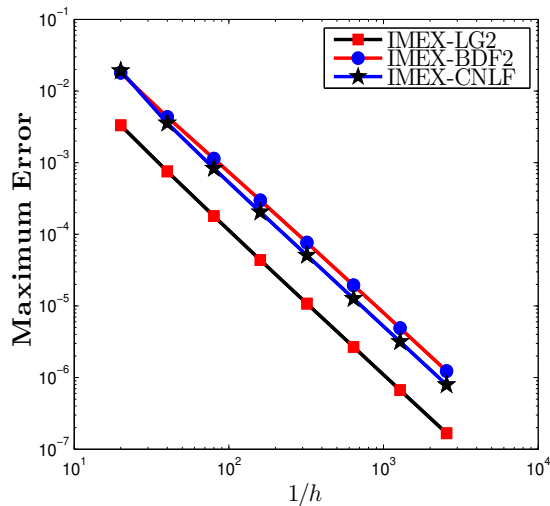
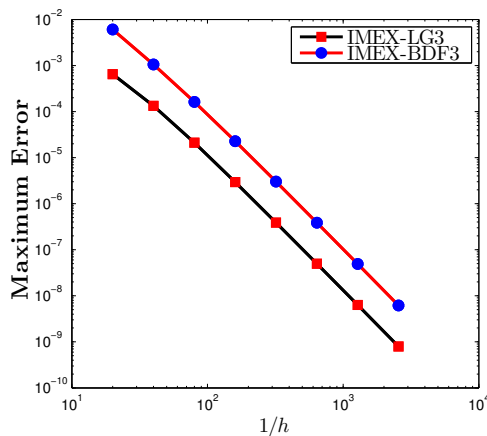
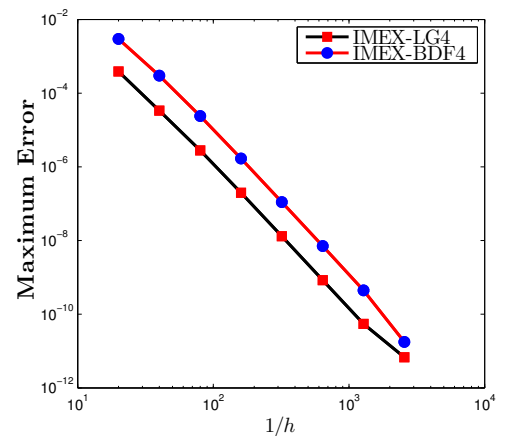


Figure 4.6.2: Comparison of the maximum error obtained by the second-order schemes IMEX-LG2, IMEX-BDF2 and IMEX-CNLF at various time-steps applied to (4.2.2). Here $\varepsilon = 0.1$, and $\text{To1} = 10^{-12}$.



(a)



(b)

Figure 4.6.3: Comparison of the maximum error obtained by the third-order schemes IMEX-LG3 and IMEX-BDF3 (a), and fourth-order schemes IMEX-BDF4 and IMEX-LG4 (b), at various time-steps applied to (4.2.2). Here $\varepsilon = 0.1$ and $\text{To1} = 10^{-12}$.

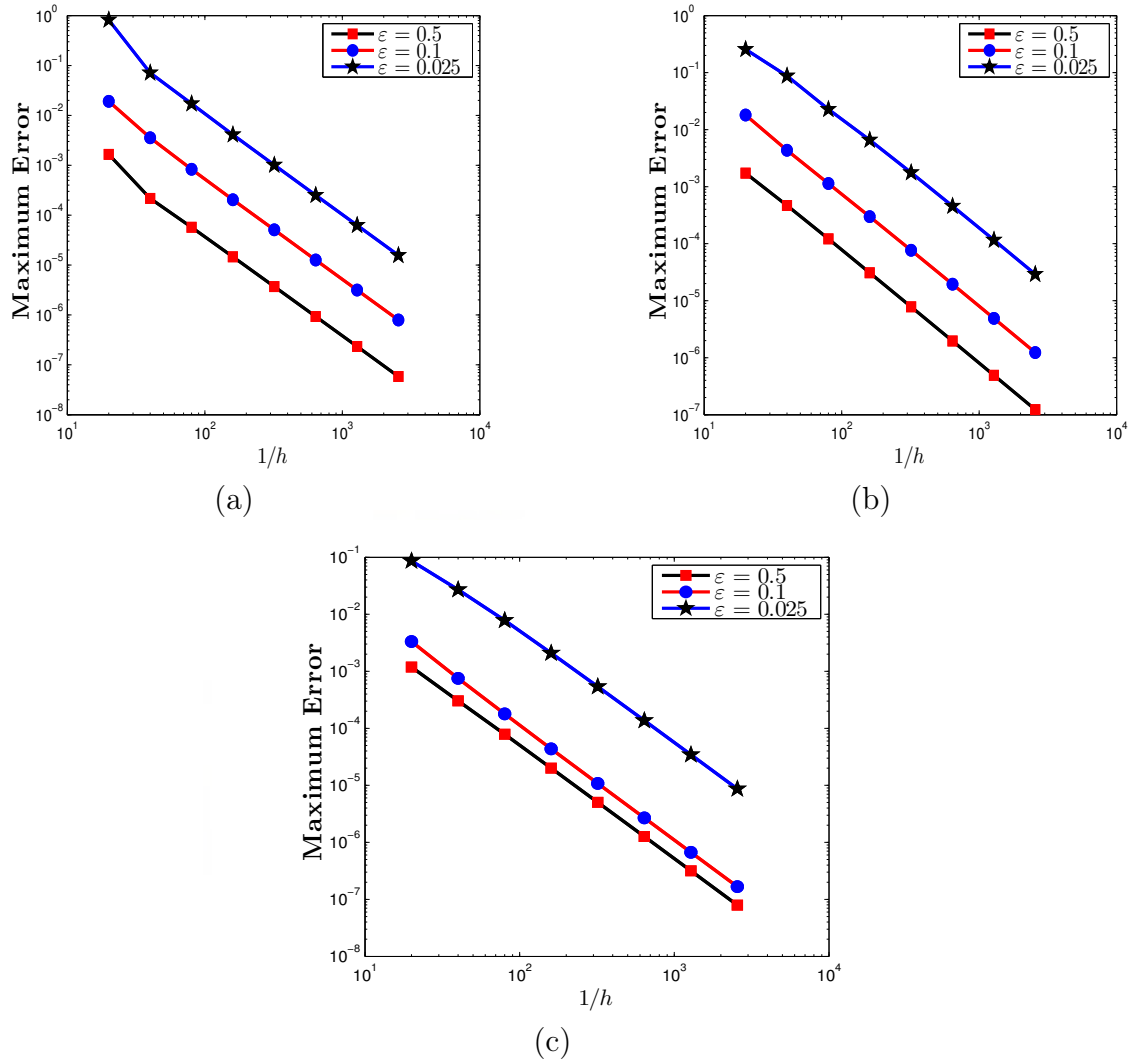


Figure 4.6.4: Comparison of the maximum error obtained by the second-order schemes IMEX-CNLF (a), IMEX-BDF2 (b), and IMEX-LG2 (c), at various time-steps applied to (4.2.2). Here $\varepsilon = 0.5, 0.1, 0.025$, and $Tol = 10^{-11}$.

In Figure 4.6.7, we display the qualitative behaviour of the model problem (4.2.2) for various values of separation of time-scale ε to show the structure of singular periodic orbit analyzed using geometric singular perturbation theory in section 4.2 when ε goes to zero. The final time, $T = 10$ is considered here. The small value of the separation of time-scale $\varepsilon = 0.001$ is detected by our numerical method which is $\mathcal{O}(\varepsilon)$ distance away from the singular orbit, where as, in [125] the smaller values which is $\mathcal{O}(\varepsilon)$ distance away from the singular

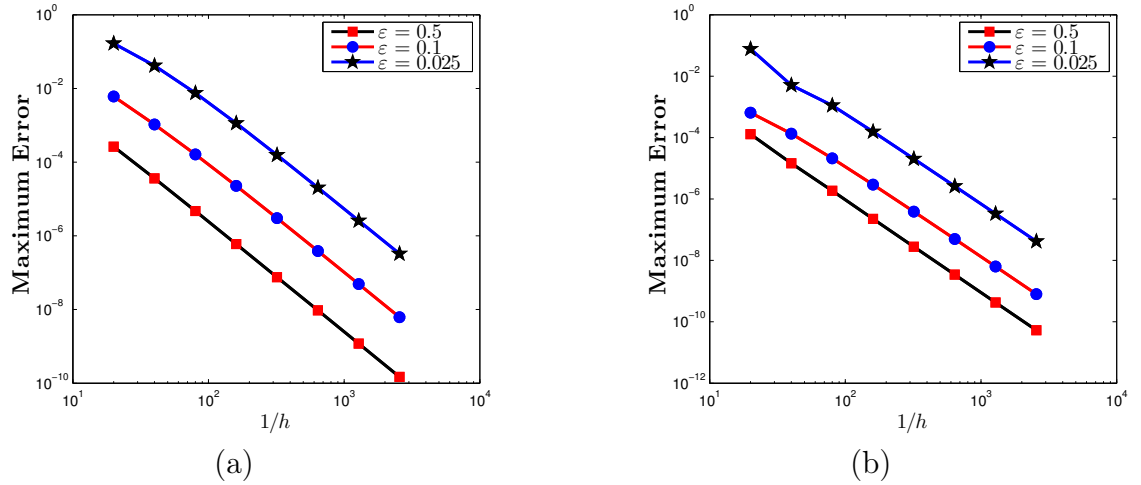


Figure 4.6.5: Comparison of the maximum error obtained by the third-order schemes IMEX-BDF3 (a), and IMEX-LG3 (b), at various time-steps applied to (4.2.2). Here $\varepsilon = 0.5, 0.1, 0.025$, and $T_{o1} = 10^{-11}$.

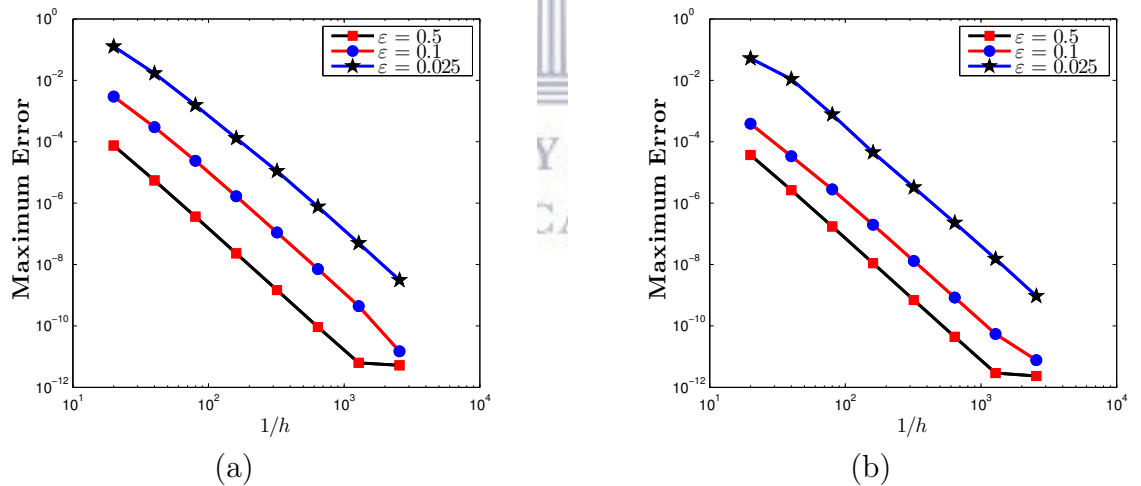


Figure 4.6.6: Comparison of the maximum error obtained by the fourth-order schemes IMEX-BDF4 (a), and IMEX-LG4 (b), at various time-steps applied to (4.2.2). Here $\varepsilon = 0.5, 0.1, 0.025$, and $T_{o1} = 10^{-11}$.

orbit is obtained with $\varepsilon = 0.025$. For a relatively larger values of time-scale, periodic orbit is also observed in Figure 4.6.7 (b), (c), (d). Other interesting behaviour of the dynamics observed in the figures are the anti-phase oscillation between the two prey populations, and the placement of the peaks of the predator between the peaks of the two preys. We can also

see that the phase space of the interaction of dynamics in a long time run, $T = 100$ forms a family of periodic orbit which is far from the equilibrium solution as shown in the Figure 4.6.8 for sufficiently small $\varepsilon = 0.001$. The constructed scheme preserves the periodicity of the model problem, which is one of the important properties of the model. The closed trajectories also shows the dependence of the species.

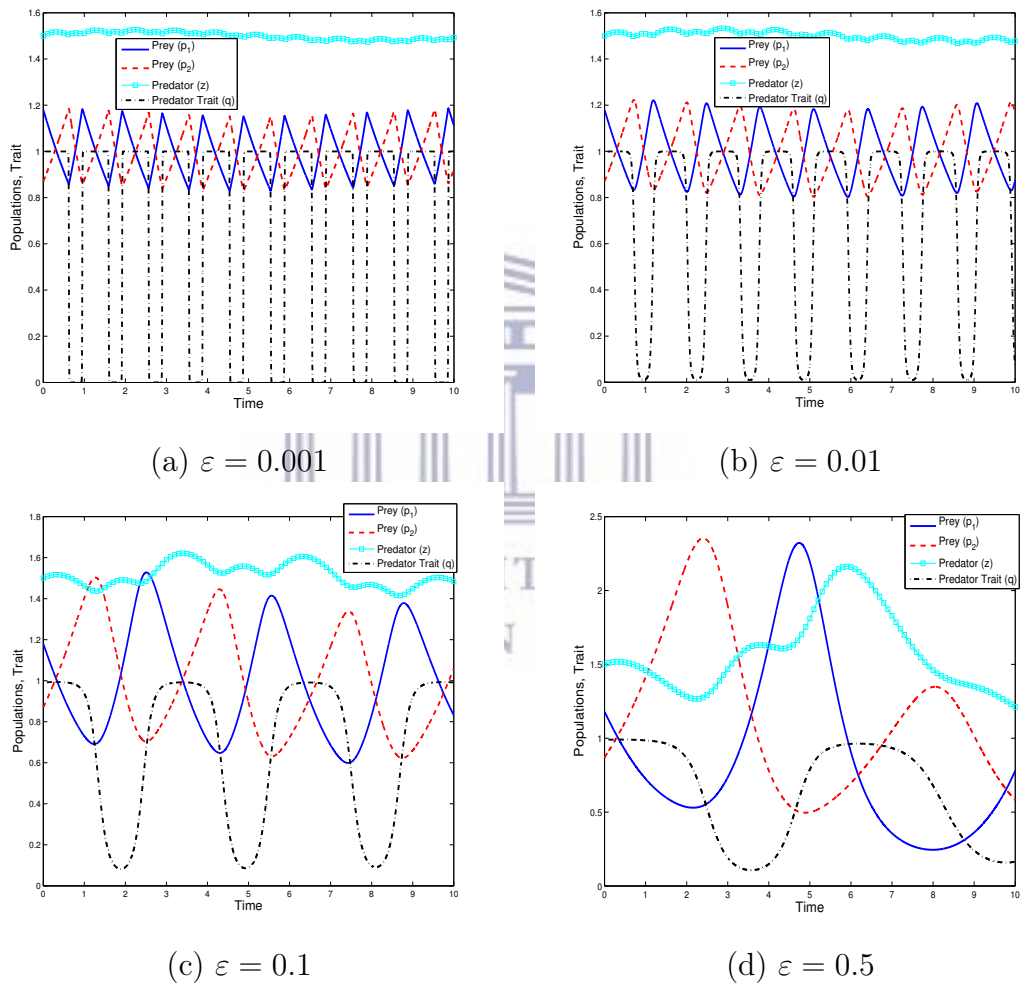


Figure 4.6.7: Eco-evolutionary dynamics of predator-trait and predator-prey interaction over time of the system (4.2.2) which is obtained at different value of separation of time-scale ε .

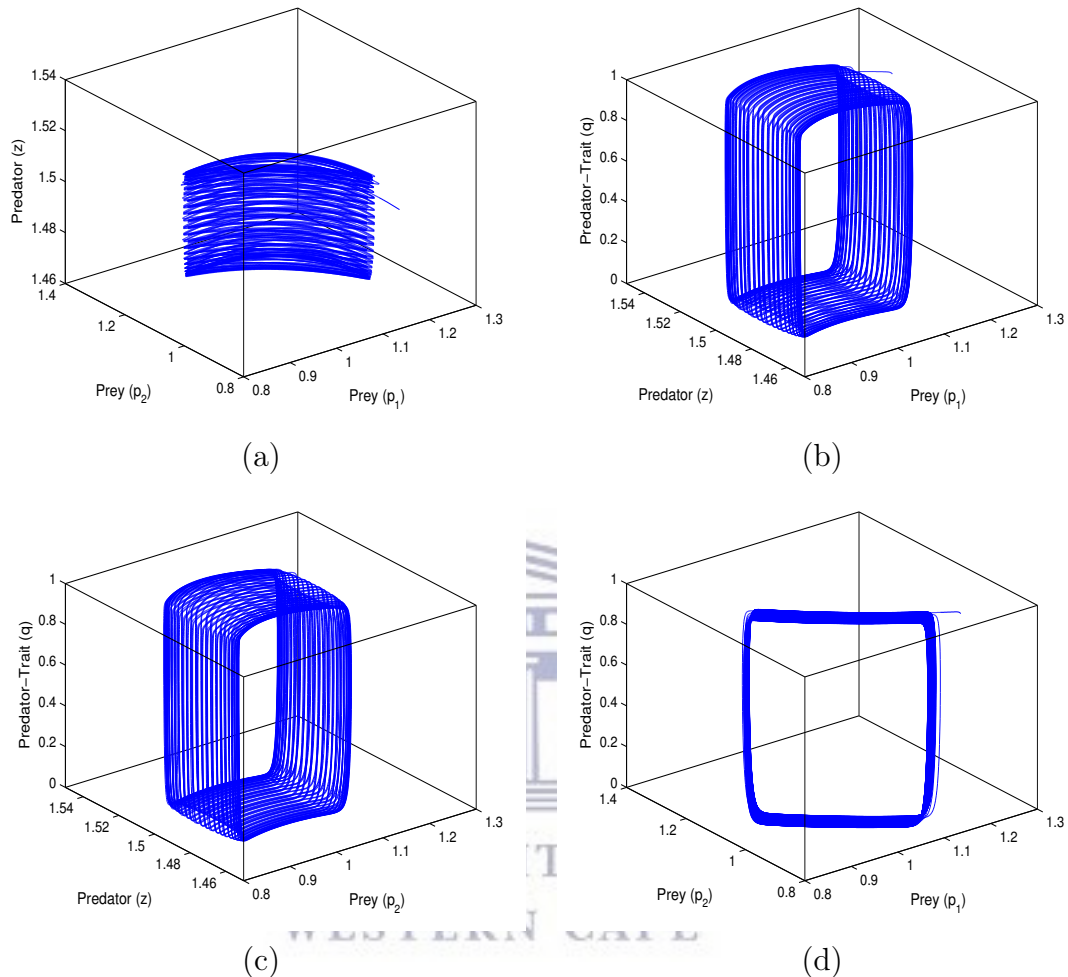


Figure 4.6.8: Phase space of the system (4.2.2) with the dynamics of predator and the two preys interaction (a); predator, predator-trait and prey (p_1) (b); predator, predator-trait and prey p_2 (c); and the interaction of the two preys with respect to the predator-trait (d). Here the value of separation of time-scale ε is taken as 0.001 and $T = 100$.

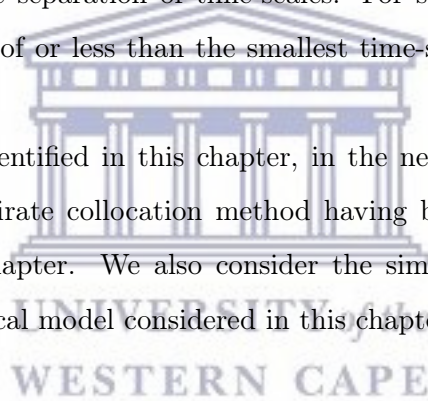
4.7 Summary and discussion

In this chapter, a novel high-order multistep implicit-explicit (IMEX) method for solving singularly perturbed slow-fast dynamical systems is presented. The method is based on the Lagrange interpolation and extrapolation procedure in which the discrete problem is posed at a specific point identified with a parameter $\theta \in [0, 1]$. It is shown that the new method generalizes other classes of multistep methods such as (Backward Differentiation formulas)

BDF and (Crank-Nicholson–Leapfrog) CNLF methods. We also established an a-priori error estimate for the convergence of the proposed LG schemes. Furthermore, a consistent start up scheme that uses the same Lagrange polynomials as its basis function is presented. Since the start up scheme is similar to the underlying multistep method in construction, it is found that the order of convergence of the overall scheme matches the theoretical error limit.

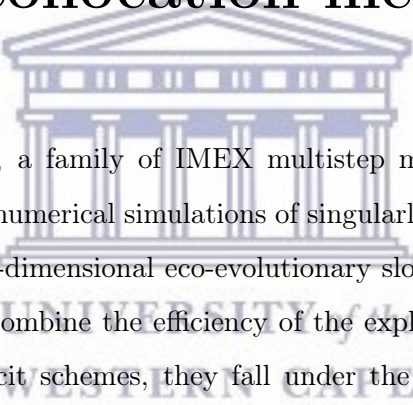
Various IMEX scheme including the new ones have been applied to solve the nonlinear and singularly perturbed problem proposed in [125]. Extensive results have been displayed in the form of tables and figures to demonstrate the performance and capabilities of the proposed method. It was determined that as with other IMEX schemes for multiscale problems commonly used in the literature, the current methods also exhibit some stability issues for problems with very wide separation of time-scales. For such problems, a very small time-step length of the order of or less than the smallest time-scale is required with the existing methods.

Due to such issue identified in this chapter, in the next one, we develop another novel high-order implicit multirate collocation method having better stability property than the one presented in this chapter. We also consider the simulation of the multiscale coupled evolutionary and ecological model considered in this chapter.



Chapter 5

A family of fully implicit, high-order, multirate collocation method



In the preceding chapter, a family of IMEX multistep methods based on the Lagrangian interpolation for efficient numerical simulations of singularly perturbed problems with particular attention to the four-dimensional eco-evolutionary slow-fast system has been discussed. Although, such schemes combine the efficiency of the explicit methods and the good stability property of the implicit schemes, they fall under the class of single-rate schemes (i.e., schemes that use a single step-size). Alternatively, one may be interested in achieving a high-order method with maximized stability property and better accuracy (especially for long time simulations) by treating the faster components with smaller (micro) step-size and the slower ones with larger (macro) step-size, in a single fully-implicit scheme. In this chapter, a novel high-order fully-implicit multirate collocation method for singularly perturbed systems is proposed. The Anderson's Acceleration (AA) fixed point iteration procedure is employed to treat nonlinearities which arise as a result of the implicit nature of the algorithm. The scheme is also analyzed for stability and convergence. Various numerical results are presented to demonstrate the performance of the new methods. The multirate schemes performs better than the corresponding single-rate schemes in terms of accuracy, efficiency, and replicating the qualitative features of the continuous model.

5.1 Introduction

It is often the case that theoretical studies, such as bifurcation analysis, of singularly perturbed problems are aided by numerical simulations in order to obtain a unified picture of the various solution structures of the system under consideration. Such simulations typically carried out over a time duration which is several magnitudes larger than the largest time scale appearing in the system. Thus, in such cases, the need for stable numerical schemes is paramount.

For numerical solutions of multiscale problems, three research directions have been suggested in the last few decades: multi-method, multi-order and multirate methods [153]. All of them are based on partitioning the full problem into two parts, namely slow subproblem and fast subproblem, in relation to their respective time scales. The difference in each case lies on how one treats the two subproblems numerically. For example, in multi-method schemes such as IMEX, the fast and the slow subproblems are separately treated with different methods with same step-size. Such schemes have been applied in different areas with some success [9, 25, 31, 44, 68, 110, 139, 156]. Multi-order schemes on the other hand use the same method and same step-size but the orders of the methods are different. For example, in [37], various multi-order schemes based on the extrapolation and Runge-Kutta methods have been proposed for differential equations with multiple time scales. However, Multi-order methods are suitable for problems with mild stiffness (or weak coupling of the slow and fast sub-systems).

Unlike both multi-method and multi-order schemes that use same step-size for each sub-system in the partition, a multirate method uses different step-sizes for different subproblems, according to the activity level of the dynamics of the involved sub-systems, while using same numerical method. Such multirate methods generally use smaller (micro) time-step to discretize the faster sub-system and larger (macro) time-step to the slower one. In this way, one can significantly reduce the complexity of the solution scheme by reducing the computational cost and memory relative to a corresponding single-rate scheme with a comparative level of accuracy. In order to handle the coupling between the slow and fast components at the micro time-steps, a multirate method uses interpolation or extrapolation algorithms, which lead to further sources of error. However, such errors do not cause degradation of accuracy, since such interpolations or extrapolation algorithms are typically of the same order as the underlying scheme. Generally multirate methods are typically well suited for stiff (multiscale) problems,

and can also be used for weakly coupled slow-fast problems.

Various multirate methods have been introduced in the literature over the last three decades. The first multirate method for slow-fast problems was due to Gear and Wells [51]. In the experimental code known as MARTE, they showed that their scheme performs better when the coupling between the slow and fast components is weak. In [10], a one-step multirate method, in which only one previous step solution is required, has been applied for problems in electrical networks. Other multirate versions of one-step (and lower-order methods) have also been studied in different fields of applications, see, e.g., [27, 37, 107, 109]. Applications of multirate method using backward Euler time-stepping scheme to circuit simulation have also been presented in [157]. In other works such as [133, 5, 49, 51, 90, 129, 145, 144], stability of various one-step multirate methods have been analyzed.

In this chapter a high-order fully-implicit multirate collocation time-stepping method (MCSm) is designed for singularly perturbed problems such as the eco-evolutionary model considered in Chapter 4. In this method, depending on the order, solutions of multiple number of steps can be simultaneously computed per each step. It uses piecewise Lagrange polynomial interpolation for the collocations of the fast subproblem at the micro-steps as well as the slow ones at the macro-steps. For the collocation of the fast subproblem at the interior micro-steps, coupling is enforced by an internal interpolation of the slow variables. The method is characterized by its enhanced stability property relative to similar one-step multirate schemes. Collocation methods were first introduced for initial value ordinary differential equation in the late 1960s, see [18] and the references therein. It was shown that collocation in continuous piecewise polynomial spaces lead to an important class of implicit (high-order) Runge-Kutta methods. Various collocation methods have also been successfully applied to different problems, see for example, [11, 18, 34, 43, 67].

For the nonlinearities that arises as a result of the implicit nature of the scheme, iterative techniques such as Anderson's Acceleration fixed point algorithm are applied. The Anderson's acceleration method is built upon the Picard's fixed point iterative method for a more robust and fast converging solution [97, 162]. Some advantages of the methods over the other nonlinear solvers such as Newton's method include its ease of implementation and low cost per iteration as it does not require Jacobian information.

The rest of the chapter is as follows: In Section 5.2, we present the model problem

considered in this chapter and give a brief discussion on theoretical results regarding the qualitative properties of its solutions. In Section 5.3, the numerical method is formulated and analyzed for stability and convergence in details for a typical two time-scale problem. An overview of the Anderson's acceleration method is presented in Section 5.4. Numerical results and simulations are presented in Section 5.5. Finally, we present some concluding remarks in Section 5.6.

5.2 The mathematical model and its qualitative analysis

In this section, an overview of the eco-evolutionary singularly perturbed problem describing the interaction of one-predator and two-prey species with fast evolution of predator-trait [125] is revisited. Furthermore, results on the linear stability analysis of the model are also presented.

5.2.1 The eco-evolutionary model

Consider the coupled multiscale eco-evolutionary system in a non-dimensional form,

$$\left. \begin{aligned} \dot{p}_1 &= p_1(1 - qz) =: f_1(p_1, p_2, z, q), \\ \dot{p}_2 &= p_2(r - (1 - q)z) =: f_2(p_1, p_2, z, q), \\ \dot{z} &= z(qp_1 + (1 - q)p_2 - 1)d =: g_1(p_1, p_2, z, q), \\ \varepsilon \dot{q} &= q(1 - q)(p_1 - p_2) =: w(p_1, p_2, z, q), \end{aligned} \right\} \quad (5.2.1)$$

where, for $i = 1, 2$; p_i represents the time varying population density of the i th prey, z the time varying population density of the predator, and q represents the predator-trait which is assumed to vary between 0 and 1. When $q = 0$, the predator feeds only prey p_1 and when $q = 1$, the predator feeds only p_2 . Furthermore, the constant r is the per capita growth rates of the prey p_2 , and d is the predators per capita death rate. In this model all the parameters are strictly positive.

The parameter ε is a small positive number ($0 < \varepsilon \ll 1$), which represents the separation

of time-scale between the slow and fast components. In this model, q characterizes the fast dynamics of predator evolution and (p_1, p_2, z) represents the slow ecological dynamics of the predator-prey interaction.

5.2.2 Linear stability analysis of the model

The model has five equilibrium points $A(0, 0, 0, 0)$, $B(0, 0, 0, 1)$, $C(0, 1, r, 0)$, $D(1, 0, 1, 1)$ and $E(1, 1, 1 + r, \frac{1}{1+r})$. The trivial steady states $A(0, 0, 0, 0)$ and $B(0, 0, 0, 1)$ describe total extinction of the three species. The steady state C corresponds to a biological relevant situation in which only the prey p_2 and predator survive. The steady state solution D represents a situation in which prey p_1 and the predator survive.

We analyze the linear stability of these five equilibria by calculating the eigenvalues of the following Jacobian matrix of the system in (5.2.1) evaluated at these points:

$$J = \begin{pmatrix} \frac{\partial f_1}{\partial p_1} & \frac{\partial f_1}{\partial p_2} & \frac{\partial f_1}{\partial z} & \frac{\partial f_1}{\partial q} \\ \frac{\partial f_2}{\partial p_1} & \frac{\partial f_2}{\partial p_2} & \frac{\partial f_2}{\partial z} & \frac{\partial f_2}{\partial q} \\ \frac{\partial g}{\partial p_1} & \frac{\partial g}{\partial p_2} & \frac{\partial g}{\partial z} & \frac{\partial g}{\partial q} \\ \frac{\partial w}{\partial p_1} & \frac{\partial w}{\partial p_2} & \frac{\partial w}{\partial z} & \frac{\partial w}{\partial q} \end{pmatrix} = \begin{pmatrix} 1 - qz & 0 & -qp_1 & -zp_1 \\ 0 & r - z(1 - q) & p_2(q - 1) & zp_2 \\ dqz & d(1 - q)z & d(qp_1 + p_2 - qp_2 - 1) & d(p_1 - p_2)z \\ \frac{1}{\varepsilon}(q - q^2) & -\frac{1}{\varepsilon}(q - q^2) & 0 & \frac{1}{\varepsilon}(1 - 2q)(p_1 - p_2) \end{pmatrix}. \quad (5.2.2)$$

The eigenvalues corresponding to each of the equilibrium points are summarized in Ta-

ble 5.2.1.

Table 5.2.1: Summary of the linear stability analysis for the system (5.2.1) (here, v_i , $i = 1, 2$ satisfies (5.2.4)).

	Description	λ_1	λ_2	λ_3	λ_4
A	trivial	0	1	$-d$	r
B	p_1, p_2, p_3 extinct	0	1	$-d$	r
C	p_1 extinct	$\frac{-1}{\varepsilon}$	1	$-i\sqrt{dr}$	$i\sqrt{dr}$
D	p_2 extinct	$\frac{-1}{\varepsilon}$	$-i\sqrt{d}$	$i\sqrt{d}$	r
E	coexistence	$i\sqrt{ v_1 }$	$-i\sqrt{ v_1 }$	$i\sqrt{ v_2 }$	$-i\sqrt{ v_2 }$

Equation (5.2.1) has a non-hyperbolic equilibrium at the two steady states C and D having positive, negative and a pair of pure imaginary eigenvalues.

Steady state E is the most interesting biological state because it represents coexistence of the three population. However, the eigenvalues at E are all pure imaginary. With the aid of geometric singular perturbation theory, it has been determined that the non-hyperbolic equilibrium point E is a center and the solution near E is periodic and bifurcates off from it when the eigenvalues cross the imaginary axis. For more detail analysis of the model using geometric singular perturbation analysis, the readers are referred to [125].

The eigenvalues of the steady state E satisfy the characteristic equation:

$$\lambda^4 + \frac{m + 2r + mr^2}{1 + r}\lambda^2 + mr = 0. \quad (5.2.3)$$

For the sake of simplification, let $v = \lambda^2$, then it follows from equation (5.2.3) that

$$v^2 + \frac{m + 2r + mr^2}{1 + r}v + mr = 0. \quad (5.2.4)$$

This is a quadratic equation that has two real (negative) solutions denoted by v_1 and v_2 . Hence the eigenvalues corresponding to the steady state E are given by $\lambda_{1,2} = \pm i\sqrt{|v_1|}$ and $\lambda_{3,4} = \pm i\sqrt{|v_2|}$.

In the next section, we discuss the formulation of the multirate high-order implicit col-

location method for accurate and stable solutions of slow-fast problems such as the model (5.2.1) presented in this section.

5.3 A fully-implicit multirate collocation methods for the slow-fast system (5.2.1)

In this section, we present a fully-implicit multirate collocation schemes for the singularly perturbed problems. The idea is to approximate the solution components as linear combination of Lagrangian interpolation polynomial used as basis functions. Then the discrete problem is collocated at certain designated points based on the relative scale of the subproblems.

Consider the general evolutionary equation of slow-fast-type,

$$\left. \begin{aligned} \dot{\mathbf{u}} &= \mathbf{f}(t, \mathbf{u}, \mathbf{v}), \\ \dot{\mathbf{v}} &= \frac{1}{\varepsilon} \mathbf{g}(t, \mathbf{u}, \mathbf{v}), \end{aligned} \right\} \quad (5.3.1)$$

where \mathbf{u} the slow components (non-stiff), \mathbf{v} the fast component (stiff), ε is a small positive parameter ($0 < \varepsilon \ll 1$) representing the time-scale difference between the fast and slow components. The functions \mathbf{f} , and \mathbf{g} are sufficiently smooth functions of t , \mathbf{u} , and \mathbf{v} . For the particular slow-fast system (5.2.1), the various parts of general equation (5.3.1) are,

$$\mathbf{u} = \begin{bmatrix} p_1 \\ p_2 \\ z \end{bmatrix}, \mathbf{v} = [q], \mathbf{f}(t, \mathbf{u}, \mathbf{v}) = \begin{bmatrix} p_1(1 - qz) \\ p_2(r - (1 - q)z) \\ z(qp_1 + (1 - q)p_2 - 1)d \end{bmatrix}, \text{ and} \quad (5.3.2)$$

$$\mathbf{g}(t, \mathbf{u}, \mathbf{v}) = [q(1 - q)(p_1 - p_2)]. \quad (5.3.3)$$

Consider a sub-division of the time interval $I = [0, T]$ into intervals $I_n = [t_n, t_{n+1}]$, where $0 = t_0 < \dots < t_N = T$. The subinterval I_n is referred to as *macro-step*. Furthermore, each macro-step I_n , $0 \leq n < N$, is uniformly sub-divided into m intervals $I_n^j = [t_n^j, t_n^{j+1}]$ (termed as *micro-steps*), where $t_n = t_n^0 < \dots < t_n^m = t_{n+1}$. The situation is depicted as shown in Figure 5.3.1. Define the mesh parameters H and h with respect to the sub-divisions of I into

macro- and micro-steps, respectively, by

$$H = \max_{0 \leq n < N} H_n, \quad \text{and} \quad h = \max_{0 \leq n < N} h_n, \quad (5.3.4)$$

where $H_n = |t_{n+1} - t_n|$ and $h_n = |t_n^{j+1} - t_n^j|$ for any j such that $0 \leq j < m$.

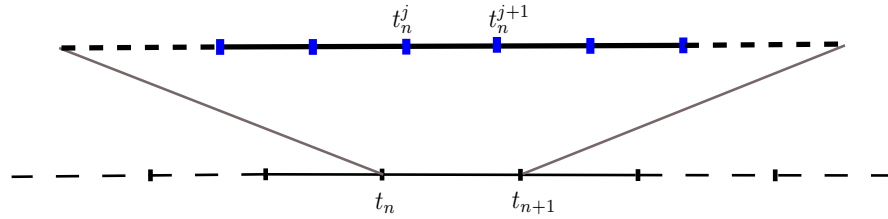


Figure 5.3.1: Sub-division of the time domain into macro- and micro-steps.

5.3.1 Collocation of the slow and fast components

For simplicity of exposition of the method, we assume that both the fast and the slow variables are scalars, i.e., we replace the pair (\mathbf{u}, \mathbf{v}) by (u, v) . First, we consider a set containing $r + 1$ equally spaced nodes $\{\tau_0, \dots, \tau_r\}$ in the macro-step I_n , where $t_n = \tau_0 < \dots < \tau_r = t_{n+1}$. We refer to such nodes as *slow nodes*. Consider also the set of r -degree Lagrange polynomials $\{N_0, \dots, N_r\}$ defined on the interval and corresponding to the slow nodes. These polynomials are defined by

$$N_i(t) = \prod_{\substack{k=0 \\ k \neq i}}^r \frac{(t - \tau_k)}{(\tau_i - \tau_k)}, \quad (t \in I_n). \quad (5.3.5)$$

The slow variable u is thus replaced by its interpolation u_H using the Lagrange polynomials as

$$u_H(t) = \sum_{k=0}^r u_n^k N_k(t), \quad (t \in I_n), \quad (5.3.6)$$

where u_n^k is the nodal value at the slow node τ_k with $u_n^0 = u_{n-1}^r$ (i.e., for continuity, the last nodal value u_{n-1}^r of the previous interval I_{n-1} equals the first nodal value u_n^0 of the current subinterval I_{n-1}).

Next, in each micro-step I_n^j , we also consider $r + 1$ equally spaced nodes, termed as *fast nodes*. Hence, the total number of fast nodes over each macro-step I_n is $rm + 1$, and these

nodes are denoted by $t_n = \hat{\tau}_0, \dots, \hat{\tau}_{rm} = t_{n+1}$. Note that $\hat{\tau}_{jr} = t_n^j$ for $j = 0, \dots, m$ (implying that the end points of each micro-step are also fast nodes).

To define piecewise polynomial interpolatory functions corresponding to the set of fast nodes, we first group the fast nodes as follows. The set of all fast nodes which are also end points of micro-steps, that is, $\{\hat{\tau}_0, \hat{\tau}_r, \hat{\tau}_{2r}, \dots, \hat{\tau}_{mr}\}$ is referred to as set of *adjacent* fast nodes. Whereas, those fast nodes which are not adjacent are termed as *interior* fast nodes.

Denote the α^{th} local Lagrange $(r + 1)$ -degree polynomial N_α^j with respect to the fast nodes in I_n^j . (Illustrations of various distribution of nodes in a micro-step are depicted in Figure 5.3.2). The piecewise polynomial interpolatory function \hat{N}_k corresponding to the fast node $\hat{\tau}_k$ is defined as follows:

- if $\hat{\tau}_k$ is an interior node in some micro-step I_n^j and there is $\alpha = 1, \dots, r - 1$ such that N_α^j is the local Lagrangian function corresponding to the node $\hat{\tau}_k \in I_n^j$, then (see Figure 5.3.3 (a))

$$\hat{N}_k(t) = \begin{cases} N_\alpha^j(t) & \text{if } t \in I_n^j, \\ 0 & \text{if } t \in I_n \setminus I_n^j, \end{cases} \quad (5.3.7)$$

- if $\hat{\tau}_k$ is an adjacent node and $k = rj$ for some $j = 0, \dots, m$, then (see Figure 5.3.3 (b))

$$\hat{N}_k(t) = \begin{cases} N_r^j(t) & \text{if } t \in I_n^j, \\ N_0^{j+1}(t) & \text{if } t \in I_n^{j+1}, \\ 0 & \text{if } t \in I_n \setminus (I_n^j \cup I_n^{j+1}). \end{cases} \quad (5.3.8)$$

Note that the function \hat{N}_k is continuous over the macro-step I_n and satisfies the interpolatory condition

$$\hat{N}_k(\hat{\tau}_j) = \delta_{kj}, \quad (0 \leq k, j \leq rm), \quad (5.3.9)$$

where δ_{kj} is the Kronecker delta function. Thus, the fast variable v is replaced by an interpolation v_h and defined as

$$v_h(t) = \sum_{k=0}^{rm} v_n^k \hat{N}_k(t), \quad (t \in I_n), \quad (5.3.10)$$

where $v_n^k = v(\hat{\tau}_k)$ is the exact value of v at the fast node $\hat{\tau}_k$. Note that the error of interpolation

of v by equation (5.3.10) is of order h^{r+1} and the difference in the interpolation error of the fast and slow interpolations are of the same order $r + 1$.

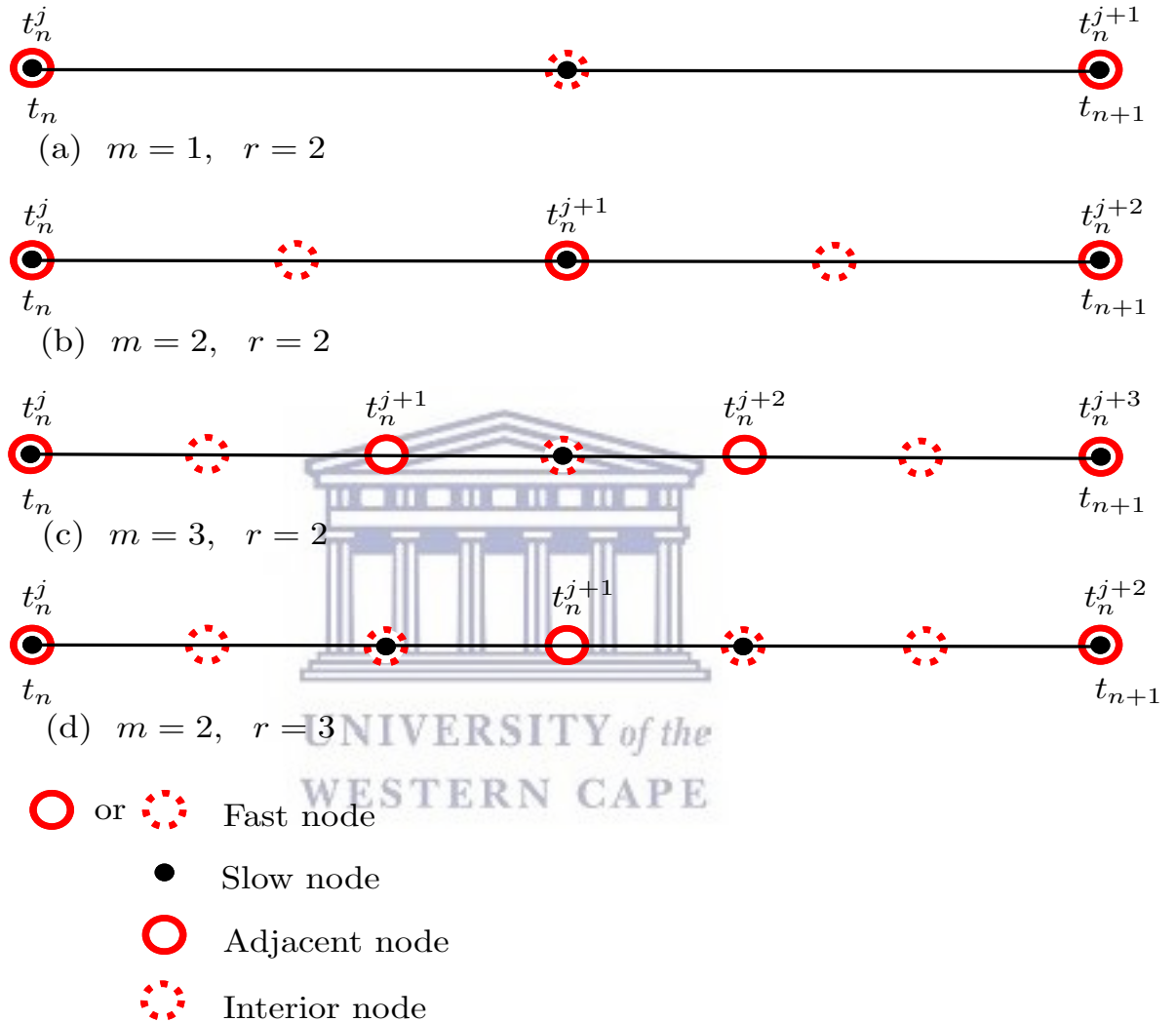
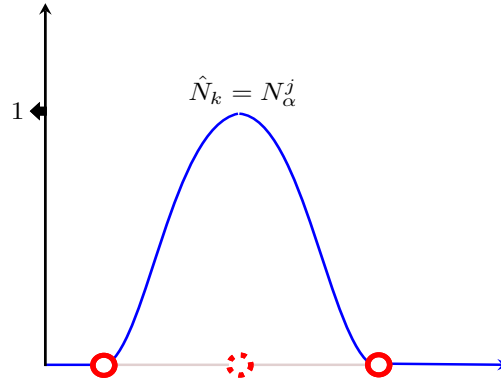


Figure 5.3.2: Configurations and types of nodes distributed in the macro-step $[t_n, t_{n+1}]$.

To define the problem of approximating the unknowns u and v at the slow and fast nodes respectively, we define the collocation points as follows: the slow component of the ODE is collocated at the slow nodes τ_1, \dots, τ_r , and the fast component at the fast nodes $\hat{\tau}_1, \dots, \hat{\tau}_{rm}$. Note that the set of slow nodes is contained in the set of fast nodes, more precisely, for each $j = 0, \dots, r$ we have that $\tau_j = \hat{\tau}_{jm}$. Thus the slow component of the ODE is enforced at the

(a) Piecewise polynomial corresponding to an interior node



(b) Piecewise polynomial corresponding to an adjacent node

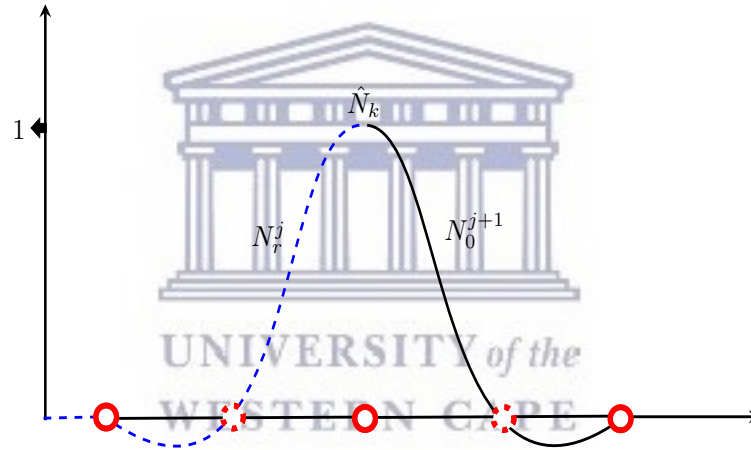


Figure 5.3.3: Piecewise polynomial interpolatory functions corresponding to interior and adjacent fast nodes.

slow node τ_j as

$$\dot{u}_H(\tau_j) = f(u_n^j, v_n^{jm}); \quad j = 1, \dots, r. \quad (5.3.11)$$

The matrix form of this equation is given by

$$\mathbf{D}\mathbf{u}_n = \mathbf{f}, \quad (5.3.12)$$

where the matrix $\mathbf{D} = [D_{ij}]$ and the right-hand-side $\mathbf{f} = \{f_i\}$ are defined by

$$D_{ij} = H_n \frac{d}{dt} N_j(\tau_i), \quad f_i = H_n \left[f(u_n^i, v_n^{im}) - u_n^0 \frac{d}{dt} N_0(\tau_i) \right], \quad (5.3.13)$$

for $i, j = 1, \dots, r$. Here the vector of unknowns \mathbf{u}_n is defined as

$$\mathbf{u}_n = \begin{bmatrix} u_n^1 \\ \vdots \\ u_n^r \end{bmatrix}. \quad (5.3.14)$$

The derivative matrix \mathbf{D} is independent of H_n , and hence equivalent to that of the matrix obtained when the interval I_n is replaced by the unit interval $[0, 1]$.

Next, we define the discrete problem for the fast component of the ODE. Before we proceed, we need to consider a couple of issues. The first is, as indicated from the outset, the fast component is enforced at each of the fast nodes, and this requires to evaluate an approximation of $g(u, v)$ at each $\hat{\tau}_k$, $k = 1, \dots, rm$. However, since the slow variables u_n^j are involved as unknown only at the slow nodes, one needs to obtain an approximation of u at each fast nodes that are not slow. Such approximation, with the correct order, is obtained by evaluating u_H at the fast node $\hat{\tau}_k$ using the equation (5.3.10). The other point that needs to be considered is that since the interpolation function v_h of the fast variable v is piecewise polynomial, its derivatives at some of the fast nodes may not exist, precisely, the two sided derivatives of v_h at each adjacent fast nodes except $\hat{\tau}_0$ may not be equal, hence derivatives may not exist at such nodes. For this reason only the one sided derivatives at such fast nodes are considered. In fact, one can understand derivatives concerning the fast interpolation v_h as being one sided. In this study, we choose derivatives from the left side of a node. Therefore, the fast component of the ODE is enforced at the fast node $\hat{\tau}_k$ as (the derivatives are understood as left-sided)

$$\dot{v}_h(\hat{\tau}_k) = g(u_H(\hat{\tau}_k), v_n^k); \quad k = 1, \dots, rm. \quad (5.3.15)$$

Understanding derivatives of v_h as one-sided (left-sided) facilitates the construction of the matrix form of (5.3.15) in an element-by-element basis as it is customarily done in the finite

element method. Hence, the contribution of the e -th micro-step I_n^e , in a matrix form, is

$$\mathbf{D}\mathbf{v}_n^e = \mathbf{g}^e, \quad (5.3.16)$$

where the local unknown vector \mathbf{v}_n^e and the right-hand-side \mathbf{g}^e are defined by

$$\mathbf{v}_n^e = \begin{bmatrix} v_n^{(e-1)r+1} \\ v_n^{(e-1)r+2} \\ \vdots \\ v_n^{er} \end{bmatrix}, \quad (5.3.17)$$

$$\mathbf{g}^e = h_n \begin{bmatrix} g(u_H(\hat{\tau}_{(e-1)r+1}), v_n^{(e-1)r+1}) - v_n^{(e-1)r} \frac{d}{dt} N_0^e(\hat{\tau}_{(e-1)r+1}) \\ g(u_H(\hat{\tau}_{(e-1)r+2}), v_n^{(e-1)r+2}) - v_n^{(e-1)r} \frac{d}{dt} N_0^e(\hat{\tau}_{(e-1)r+2}) \\ \vdots \\ g(u_H(\hat{\tau}_{er}), v_n^{er}) - v_n^{(e-1)r} \frac{d}{dt} N_0^e(\hat{\tau}_{er}) \end{bmatrix}. \quad (5.3.18)$$

Therefore, the matrix form of (5.3.15) becomes

$$\begin{bmatrix} \mathbf{D} & & \\ & \ddots & \\ & & \mathbf{D} \end{bmatrix} \begin{bmatrix} \mathbf{v}_n^1 \\ \vdots \\ \mathbf{v}_n^m \end{bmatrix} = \begin{bmatrix} \mathbf{g}^1 \\ \vdots \\ \mathbf{g}^m \end{bmatrix}. \quad (5.3.19)$$

At a glance, the block structure of the derivative matrix of equation (5.3.19) may suggest that the set of unknowns in one micro-step are decoupled from that of the other micro-step. However, the necessary coupling between unknowns of adjacent micro-steps is established from the definition of the right-hand-side (5.3.18).

By combining the matrix forms of the slow component (5.3.12) and the fast component

(5.3.19) of the ODE, we obtain the matrix form of the global discrete problem given as

$$\underbrace{\begin{bmatrix} \mathbf{D} & & & \\ \text{---} & \mathbf{D} & & \\ \text{---} & \text{---} & \ddots & \\ \text{---} & & & \mathbf{D} \end{bmatrix}}_{\widehat{\mathbf{D}}} \underbrace{\begin{bmatrix} \mathbf{u}_n \\ \mathbf{v}_n^1 \\ \vdots \\ \mathbf{v}_n^m \end{bmatrix}}_{\mathbf{U}} = \underbrace{\begin{bmatrix} \mathbf{f} \\ \text{---} \\ \mathbf{g}^1 \\ \text{---} \\ \vdots \\ \text{---} \\ \mathbf{g}^m \end{bmatrix}}_{\mathbf{F}(\mathbf{U})}. \tag{5.3.20}$$

Compactly, (5.3.20) can be written as

$$\widehat{\mathbf{D}}\mathbf{U} = \mathbf{F}(\mathbf{U}). \tag{5.3.21}$$

To preserve the full convergence of the method (which is of $r + 1$ as stated in the Theorem 5.3.1), the fully-implicit system (5.3.21) has to be solved by using an efficient nonlinear solver which will be discussed in Section 5.4.

5.3.2 Convergence and stability analysis of the scheme

Noting that $H = mh$ and the convergence and stability property of the multirate implicit scheme (5.3.21) depend on the underlying single-rate method, hence here we focus on the analysis of the single-rate schemes applied to the scalar ODE problem of the form

$$\dot{\varphi} = f(\varphi, t), \text{ with } \varphi(t_0) = \varphi_0. \tag{5.3.22}$$

For the sake of simplicity of notations, we ignore the explicit dependence of f on t , and simply write $f(\varphi, t)$. Hence, the single-rate scheme with order of interpolation r for the scalar problem (5.3.22) is given by

$$\frac{d}{dt}\varphi_h(t_{n+k}) = f(\varphi_h(t_{n+k})), \text{ for } k = 1, \dots, r \tag{5.3.23}$$

where

$$\varphi_h(t) = \sum_{k=0}^r N_k(t) \varphi_n^k, \quad t \in I_n = [t_{n-1}, t_n].$$

Since equation (5.3.23) is satisfied at r points on the interval I_n , from the interpolation theory we obtain

$$\frac{d}{dt} \varphi_h(t) = f(\varphi_h(t)) + \mathcal{O}(h^{r+1}), \quad \forall t \in I_n. \quad (5.3.24)$$

The following result gives an estimation of the truncation error, denoted by $e = \varphi - \varphi_h$, that is committed at the n -th step assuming that there is no error from the previous step, i.e., $\varphi_n^0 = \varphi(t_n)$.

Theorem 5.3.1. *Suppose that $\varphi_n^0 = \varphi(t_n)$, and both the exact solution φ and f are sufficiently smooth. Then the truncation error for (5.3.23) is*

$$e(t) = \mathcal{O}(h^{r+1}). \quad (5.3.25)$$

Proof. From the smoothness hypothesis, subtracting (5.3.24) from (5.3.22), we obtain that

$$\frac{d}{dt} e(t) = f(\varphi(t)) - f(\varphi_h(t)) + \mathcal{O}(h^{r+1}). \quad (5.3.26)$$

By the mean value theorem, equation (5.3.26) becomes

$$\frac{d}{dt} e(t) = G(t)e(t) + \mathcal{O}(h^{r+1}), \quad (5.3.27)$$

where

$$G(t) = \frac{\partial}{\partial \varphi} f(\eta(t)), \quad (5.3.28)$$

for some $\eta(t)$ in the interval whose end points are $\varphi(t)$ and $\varphi_h(t)$. Note that equation (5.3.27) is a homogeneous linear differential equation (for the error function) upto an error of order $\mathcal{O}(h^{r+1})$. Then from (5.3.27) it follows that

$$e(t) = e(t_n) \exp\left(t \int_{t_n}^t G(\tau) d\tau\right) + \mathcal{O}(h^{r+1}). \quad (5.3.29)$$

Now, by assumption, $e(t_n) = 0$; hence equation (5.3.29) leads to the required result. \square

Next, we analyze the stability of the single-rate scheme. For this, we consider the scalar, linear test problem such that $f(\varphi) = \lambda\varphi$. Note that, for $\lambda < 0$, the continuous problem has stable equilibrium point at $\varphi = 0$.

The corresponding single-rate scheme for the linear test problem thus reads

$$h \frac{d}{dt} \varphi_h(t_{n+k}) = h\lambda\varphi_n^k, \quad k = 1, \dots, r. \quad (5.3.30)$$

This can be written in a block matrix equation form as

$$\begin{bmatrix} \mathbf{d} & \mathbf{D} \end{bmatrix} \begin{bmatrix} \varphi_{n-1}^r \\ \varphi_n \end{bmatrix} = z\mathbf{I}\varphi_n, \quad (5.3.31)$$

where \mathbf{d} is a column vector of size r , and \mathbf{D} is a square matrix of size $r \times r$, whose components are given by

$$D_{ij} = h \frac{d}{dt} N_j(t_{n+i}), \quad d_j = h \frac{d}{dt} N_0(t_{n+j}), \quad i = 0, \dots, r, \quad \text{and } j = 1, \dots, r; \quad (5.3.32)$$

\mathbf{I} is the $r \times r$ unit matrix, and $z = h\lambda$.

Equation (5.3.31) can also be written as

$$\underbrace{\begin{bmatrix} \mathbf{O} & \mathbf{d} \end{bmatrix}}_{\mathbf{M}} \varphi_{n-1} + \mathbf{D}\varphi_n = z\mathbf{I}\varphi_n, \quad (5.3.33)$$

where \mathbf{O} is the r -by- $(r - 1)$ matrix of zeros. It follows from equation (5.3.33) that

$$\varphi_n = \underbrace{-(\mathbf{D} - z\mathbf{I})^{-1}\mathbf{M}}_{\text{magnifying matrix}} \varphi_{n-1}. \quad (5.3.34)$$

Here the magnifying matrix relates the current nodal values to the previous ones. Thus for the scheme to be stable, it requires that the spectral radius (i.e., the maximum of the modulus of the eigenvalues) must be less than or equal to one. Regarding the stability analysis, we note that the expressions for the calculations of the eigenvalues for the general case are very complicated and therefore we use a numerical approach, with the aid of software for symbolic

calculation. The results for the first few cases (i.e., $r = 1, 2, 3, 4, 5, 6$) are shown in the Figure 5.3.4. As shown all the corresponding schemes are linearly stable, and similar results (not shown here) for orders as high as $r = 25$ also gave the same linear stability behaviour.

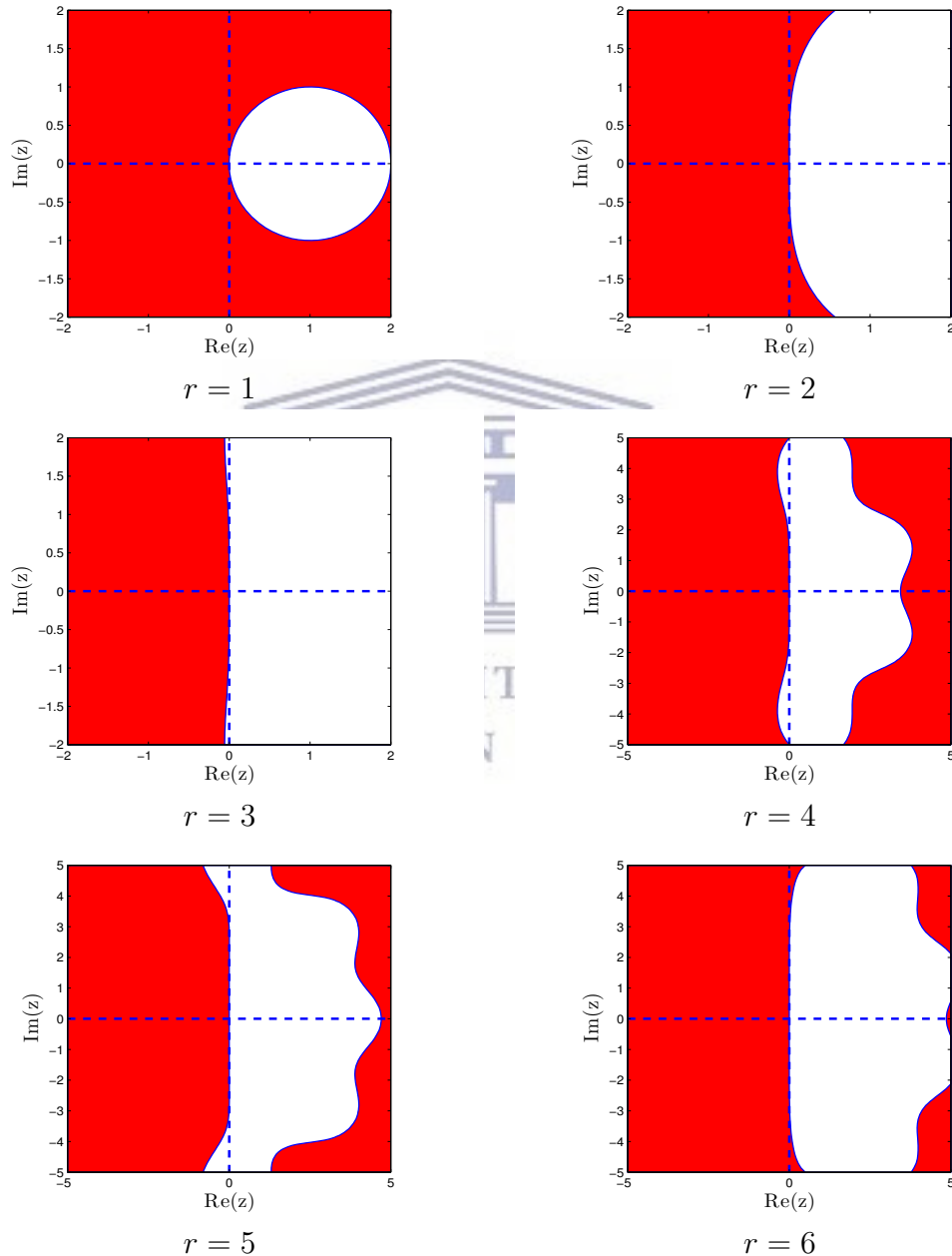


Figure 5.3.4: Stability regions of the single-rate collocation scheme.

5.4 Iterative treatment of nonlinearities: Anderson's Acceleration method

The proposed multirate collocation scheme results in fully-implicit nonlinear algebraic system of equations which requires to be solved at each time-step using some nonlinear solver. The resulting implicit-nonlinear algebraic system can then be recasted into a fixed point problem of the form

$$\mathbf{G}(\mathbf{U}) = \mathbf{U}. \quad (5.4.1)$$

In the present case, the implicit multirate collocation scheme (5.3.21) can be written as a fixed point problem (5.4.1) in which

$$\mathbf{G}(\mathbf{U}) = [\mathbf{I} + \hat{\mathbf{D}}]\mathbf{U} - \mathbf{F}(\mathbf{U}). \quad (5.4.2)$$

The methodology adopted here to solve the nonlinear fixed point problems (5.4.1) and (5.4.2) for \mathbf{U} is the Anderson's acceleration fixed point method which is known for its superlinear convergence [163]. The Anderson's acceleration method is built upon the classical Picard's iteration for an accelerated convergence by employing multiple of previous iterations (upto some prescribed depth, usually < 10). At each iteration a constrained minimization problem involving some convex combination of the residuals on the previous iterates need to be solved. Compared to the complexity of evaluating the fixed point map \mathbf{G} , the cost of solving these minimization problems is negligible [154].

5.5 Numerical results

In this section, we present numerical simulations of the coupled singularly perturbed eco-evolutionary model (5.2.1) solved by using the multirate collocation schemes (MCS m) proposed in Section 5.3, with the m referring to the rate of the scheme, and the corresponding single-rate collocation scheme is denoted by SCS1 or, simply SCS. For the numerical simulations, the non-dimensional parameters are chosen as $d = 0.5$, $r = 0.4$ with various choices of the time-scale parameter ε . Such set of parameter values, in combination with the initial

condition $(p_1, p_2, z, q) = (1.18, 0.87, 1.50, 0.99)$, result in a two parametric family of periodic orbits [110, 125]. We, therefore, present results demonstrating the performance of the numerical schemes proposed in this chapter.

Firstly, we analyze the convergence of the numerical schemes. The Anderson's acceleration fixed point iterative method was employed with tolerance 10^{-10} . Since there is no known analytic solution for the problem considered, maximum errors are computed using a double mesh principle (by successively doubling the time mesh, see Figure 4.6.1) in Chapter 4. The order of convergence of the successive refinements is computed with the formula (4.6.1). For the convergence tests, the final time is set to $T = 1$, and an initial temporal mesh with a given step-size H is considered.

Table 5.5.1: Maximum error of the single-rate (SCS) and multirate (MCS4) collocation scheme of second-order. Here $\varepsilon = 0.025$; $T = 1$; $\text{To1} = 10^{-10}$.

SCS			MCS4		
H	Error	Order	H	Error	Order
1/80	8.474E-4	2.16	1/20	1.088E-3	2.05
1/160	1.899E-4	2.08	1/40	2.629E-4	2.03
1/320	4.48E-5	2.04	1/80	6.4272E-5	2.00
1/640	1.09E-5	2.02	1/160	1.6089E-5	2.00

Table 5.5.2: Maximum error of the single-rate (SCS) and multirate (MCS4) collocation scheme of third-order. Here $\varepsilon = 0.025$; $T = 1$; $\text{To1} = 10^{-10}$.

SCS			MCS4		
H	Error	Order	H	Error	Order
1/80	2.556E-5	3.02	1/20	4.062E-5	3.03
1/160	3.1414E-6	3.02	1/40	4.969E-6	3.01
1/320	3.884E-7	3.00	1/80	6.171E-7	3.00
1/640	4.87E-8	2.98	1/160	7.69E-8	3.00

Tables 5.5.1, 5.5.2 and 5.5.3 present the maximum errors of the single-rate collocation scheme (SCS) and multirate collocation scheme (MCS4) at the final time $T = 1$ for second-, third and fourth-order schemes. The results are given for SCS with time-steps of $H = T/N$ and for MCS4 with time-steps given by $h = T/N$, which in other words, the time-step considered for SCS is to be equal to the micro time-step of the MCS. With such analysis, it is demonstrated that, with the multirate schemes, one can obtain a comparable accuracy

Table 5.5.3: Maximum error of the single-rate (SCS) and multirate (MCS4) collocation scheme of fourth-order. Here $\varepsilon = 0.025$; $T = 1$; $\text{To1} = 10^{-10}$.

Tol	SCS			MCS4		
	H	Error	Order	H, h	Error	Order
	1/80	1.7873E-7	4.04	1/20	3.2597E-6	4.05
	1/160	1.0832E-8	3.54	1/40	1.971E-7	4.03
	1/320	9.3274E-10	2.31	1/80	1.210E-8	3.99
	1/640	1.8835E-10	0.3	1/160	8.00E-10	3.21

relative to the corresponding SCS with less computational cost as larger time-steps H is used for the slowly varying components.

Figure 5.5.1 displays comparison of the maximum error of SCS, the multirates MCS2 and MCS4 of the first- (a), second- (b), third- (c) and fourth-order (d). The comparison is done by considering the macro-step of the multirate schemes and the time-step of SCS to be the same i.e., $H = T/N$. As can be seen from these figures, the multirate schemes have better accuracy compared to the corresponding single-rate schemes.

Efficiency of the schemes are compared in terms of the CPU times that each algorithm spends in solving the same problem in a serial computation on a machine with 2.4GHz x 8, IntelCore i7-4700MQ processor and 8GB RAM. Simulations were carried for $T = 1$ and $\varepsilon = 0.1$. The codes were implemented on Matlab 2013a. As shown in Figure 5.5.2, while the second-order SCS, MCS2 and MCS4 have shown comparatively the same order of accuracy, it is seen that the multirate schemes show clear gain in efficiencies over the corresponding single-rate scheme. Same scenario is exhibited for the high-order SCS and MCS as shown in Figure 5.5.3 and 5.5.4.

Finally, we discuss how the schemes capture the qualitative behaviour of the model. For the chosen parameter values and initial conditions, periodic behaviour of interactions of the predator and the two prey species with rapid evolution of the predator-trait are captured with the proposed method. As shown in Figure 5.5.5 and 5.5.6, the SCS and the MCS2 are compared in terms of their performance in capturing the periodic oscillation behaviour of the solution for different values of ε . Here, $H = 0.005$, $\text{To1} = 10^{-11}$. It is shown that such dynamics of the solutions are in fact captured by both schemes, however, for smaller value of $\varepsilon = 0.001$, as shown in the Figure 5.5.5 (a), the SCS is unable to capture the strongly oscillating dynamics as compared to the solution displayed in Figure 5.5.6 for MCS2.

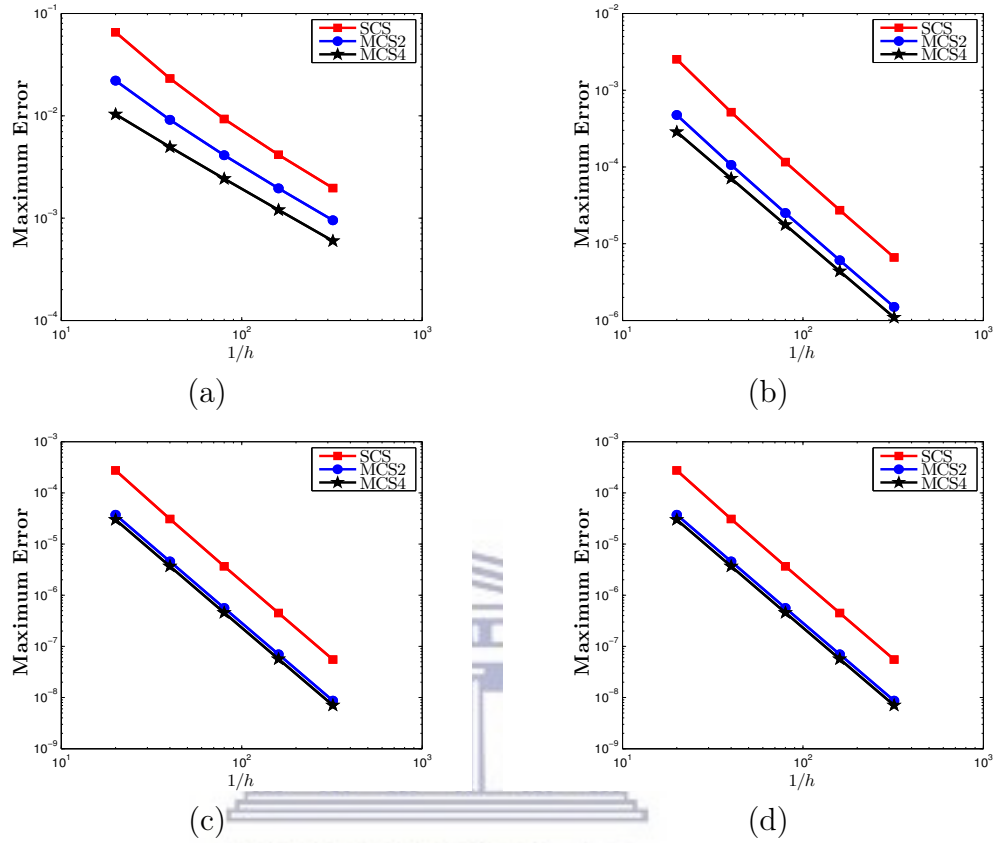


Figure 5.5.1: Comparison of maximum error results of the SCS and MCS of first-order (a), second-order (b), third-order (c) and fourth-order (d). Here $T = 1$; $To1 = 10^{-10}$; $\varepsilon = 0.1$.

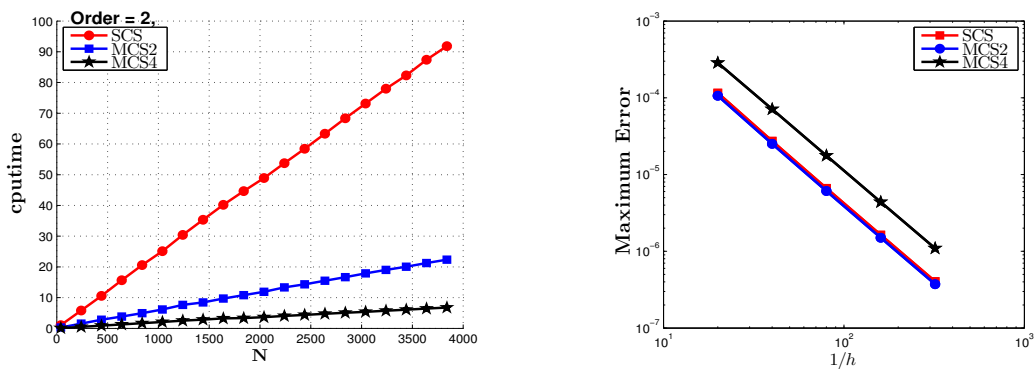


Figure 5.5.2: Comparison of efficiency results (CPUtime) of the SCS and MCS of second-order (right) and accuracy level of the schemes (left). Here $T = 1$; $To1 = 10^{-10}$; $\varepsilon = 0.1$.

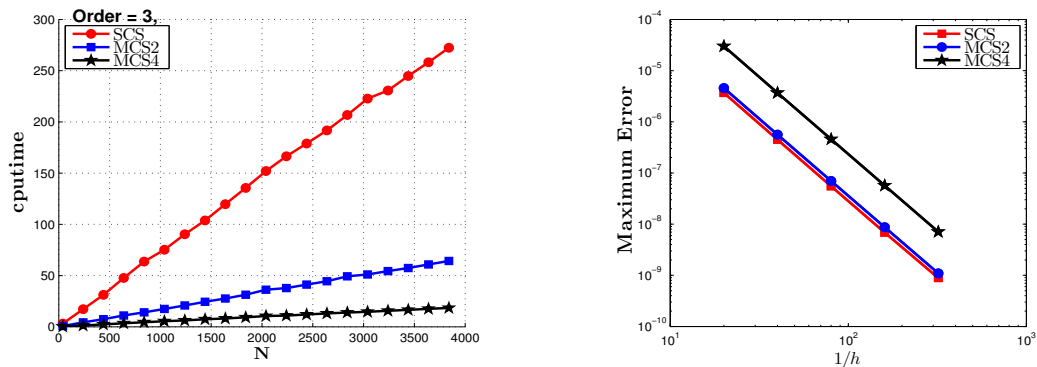


Figure 5.5.3: Comparison of efficiency results (CPUtime) of the SCS and MCS of third-order (right) and accuracy level of the schemes (left). Here $T = 1$; $To1 = 10^{-10}$; $\varepsilon = 0.1$.

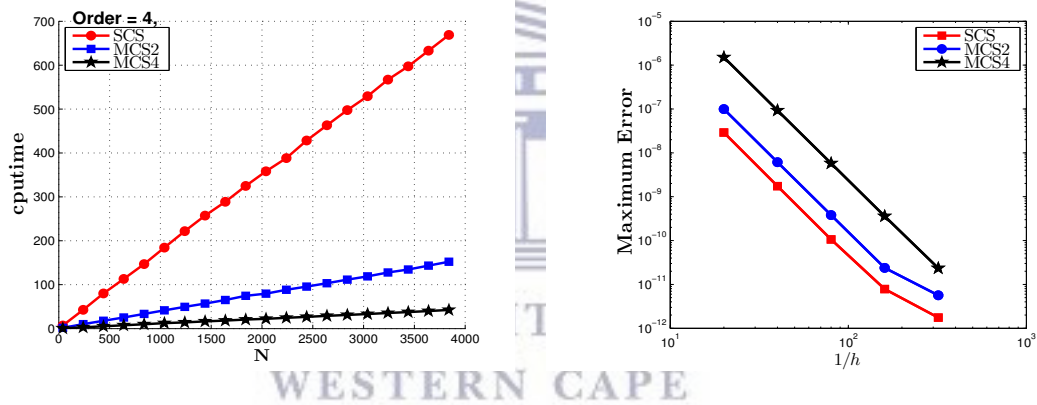


Figure 5.5.4: Comparison of efficiency results (CPUtime) of the SCS and MCS of fourth-order (right) and accuracy level of the schemes (left). Here $T = 1$; $To1 = 10^{-11}$; $\varepsilon = 0.1$.

5.6 Summary and discussion

In this chapter, we have developed a new highly stable multirate collocation method for a system of singularly perturbed eco-evolutionary model. The method is based on the piecewise interpolation of the unknowns using the Lagrange polynomials. We proved that convergence of the scheme and showed that it is of the same order as the underlying Lagrangian interpolation of the variables. Through the linear stability analysis we showed that the stability property of the proposed method and as can be seen from this analysis, this method is more stable as compared to any conventional one-step or multistep methods and their multirate counterparts.

Extensive results have been displayed in the form of tables and figures to demonstrate the

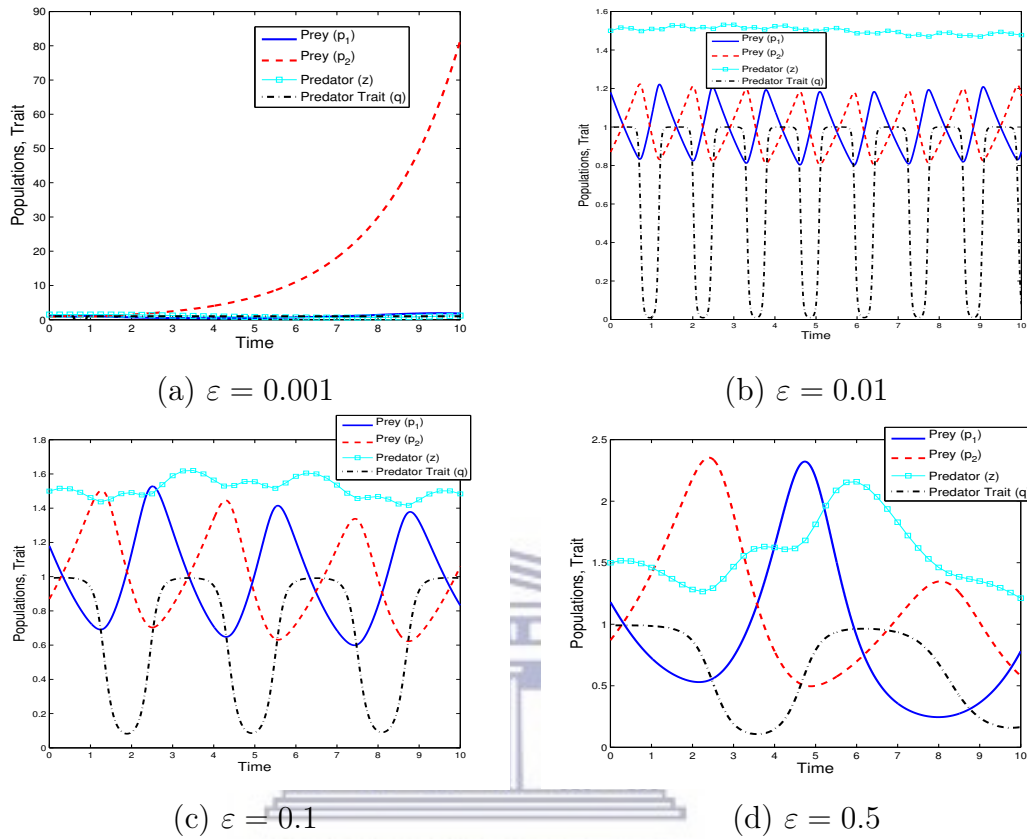


Figure 5.5.5: Simulation results displaying eco-evolutionary dynamics of predator-trait and predator-prey interaction over time of the system (5.2.1) which is obtained using second-order SCS at different value of time-scale ε . Here $T = 10$; $H = 0.005$; $T_{ol} = 10^{-11}$.

performance of the proposed method. It has been obtained that the multirate scheme outperforms the corresponding single-rate scheme in approximating problems of multiscale nature. The method has also been applied to the eco-evolutionary slow-fast model, to demonstrate the superior performance in efficiently capturing the oscillatory behaviour of the solution for a very small time-scale parameter.

The implementation of the method, however, can be highly complex for a rather high-order of convergence scheme. However, the implementation can be facilitated by constructing the appropriate derivative matrix a priori.

The focus of the next two chapters are slightly different from what have been dealt in all the previous chapters; in those chapters we deal with time-dependant partial differential

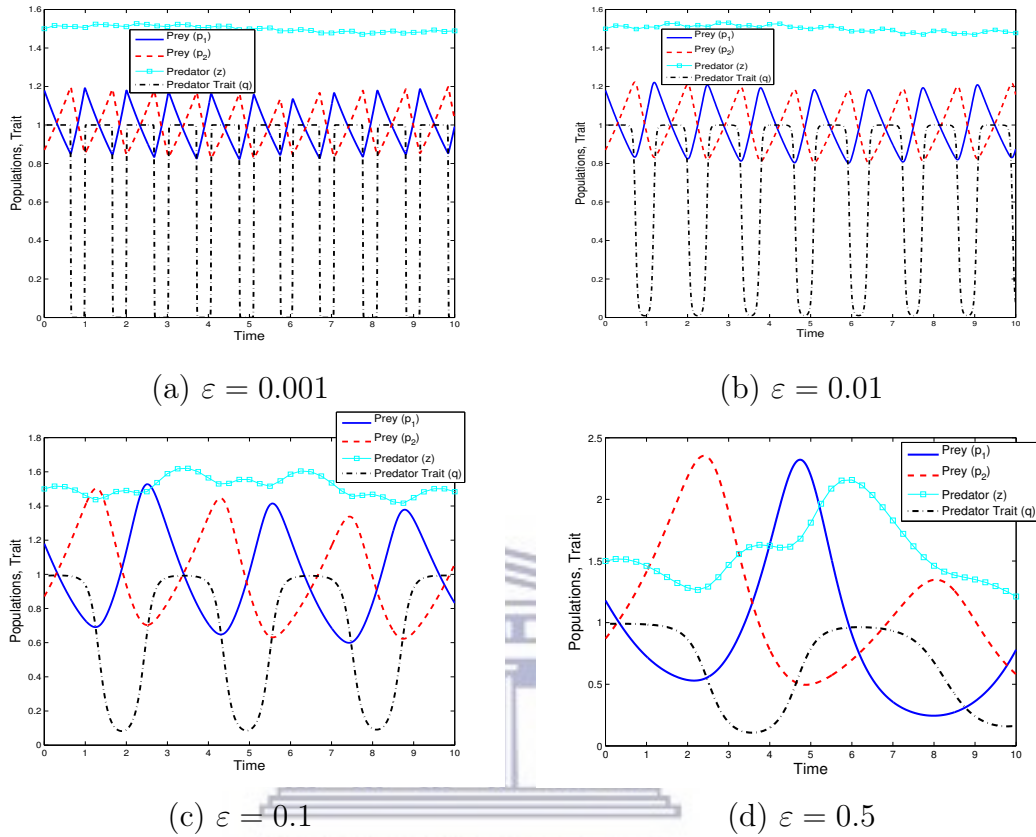
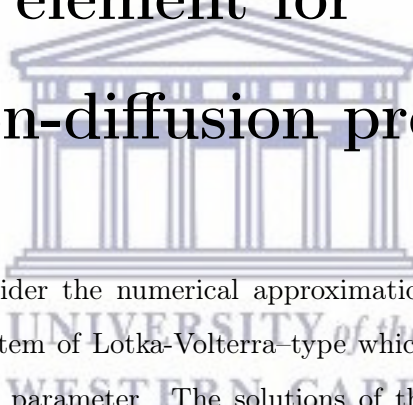


Figure 5.5.6: Simulation results displaying eco-evolutionary dynamics of predator-trait and predator-prey interaction over time of the system (5.2.1) which is obtained using second-order MCS2 scheme at different value of separation of time-scale ε . Here $T = 10$; $H = 0.005$; $To1 = 10^{-11}$.

equations which arises in ecology. The ecological phenomena they describe is competition-diffusion of singularly perturbed-type, in which the rate of diffusion of species occurs in quite small order of magnitude compared to the competition/interaction of the species. The numerical simulation of such problems will be the focus of the next two chapters.

Chapter 6

A semi-implicit multistep methods with finite element for competition-diffusion problems



In this chapter, we consider the numerical approximation of a three-species fully-coupled competition-diffusion system of Lotka-Volterra-type which is characterized by the presence of a very small diffusion parameter. The solutions of the model problem exhibit internal layers with various spatial segregation patterns. For such problems, it is a challenging task to develop an efficient numerical method that is also capable of capturing the various transient regimes and fine spatial structures of the solutions. In this chapter, we develop a high-order semi-implicit multistep scheme based on the Lagrange temporal interpolation coupled with the conforming finite element methods for the nonlinear competition-diffusion problem in two spatial dimensions. A major advantage of the proposed method is that it is essentially linear in terms of the current time-step values (no need for nonlinear iterative treatment), while, its order of convergence is higher. Moreover, the couplings of current step values of the unknowns are one sided, which is a very desirable property in terms of algorithmic efficiency since each unknown is solved sequentially, thus avoiding solving for all unknowns simultaneously. We also discussed stability and convergence of the proposed schemes are discussed. Furthermore, various simulations are carried out to demonstrate the performance

of our schemes in simulating different type of interaction patterns such as the onset of spiral-like coexistence pattern, complex spatio-temporal patterns and competitive exclusion of the species.

6.1 Introduction

Understanding of the formation of spatio-temporal patterns in ecologically interacting species is a central problem in biodiversity studies. Various competitive-diffusion models have been used in the mathematical biology community to theoretically investigate the problem of coexistence and exclusion in competition of interacting species. The case of two competing species have been extensively studied by many researchers. In [80, 82], it has been theoretically shown that two strongly competing species can never coexist in any convex habitat. However, coexistence can be achieved when a third exotic competing species is introduced into a habitat that holds two native and strongly competing species [28]. Such mechanism of coexistence of competing species is referred to as *competitive-mediated coexistence*. Over the years quite few works have been devoted to the study of coexistence of three or more interacting species using competition-diffusion models [28, 35, 74, 75, 112, 113].

More and more sophisticated competition-diffusion models have been introduced in recent years [23, 35, 72, 75, 121, 140]. The well-known Lotka-Volterra competition-diffusion model has been extensively studied in mathematical biology community. This model has been used to investigate various transient regimes and complex spatio-temporal coexistence patterns using different combinations of analytical and numerical approaches, see, for example [74, 75, 113]. Through a singularly perturbation problem and a numerical approach based on an explicit finite difference method, Mimura and Fife [113] showed coexistence with segregated patterns in a three-component competition-diffusion system of Lotka-Volterra-type when the mobility rates of the two competing species are sufficiently smaller than that of the third species. A transient regime in the form of spiral-like motion and spatial segregation coexistence pattern with a triple junctions have been demonstrated numerically in [35, 115] when all the three competing species were sufficiently small and had equal mobility rate.

However, a fundamental understanding of possible type of dynamical regimes and coexistence patterns in well-known competition-diffusion models such as the Lotka-Volterra system

is still lacking [20]. Numerical simulations have been playing a vital role in the research community to aid a more complete understanding of the formation of spatio-temporal patterns and dynamical regimes. In the numerical approximation of time-dependant PDEs such as the Lotka-Volterra system using a method-of-lines approach [136, 137], the availability of higher-order spatial discretization schemes motivates the development of sophisticated higher-order time integration methods. Higher-order methods usually yield more accuracy and better efficiency than lower-order methods. Many modern PDE solvers are able to employ higher-order spatial discretizations, for example, by using high degree polynomials in a Galerkin finite element approach. There is a need to develop higher-order time-stepping formulas to be used in conjunction with higher-order spatial discretizations [168].

Semi-implicit methods have been applied with some success in different fields involving the study of reaction-diffusion systems type or related problems, see for example, in [14, 40, 54, 55, 64, 147, 169]. In [15], higher-order semi-implicit RK methods have been developed for time-dependant partial differential equations such as reaction-diffusion, convection-diffusion and nonlinear diffusion systems. However, it is shown that solving the resulting nonlinear-implicit equations by simple fixed point iteration requires a relatively small time-step to guarantee convergence, thus defeating the purpose of the semi-implicit method.

Recently, Cangiani et al. [20] developed an interesting computational framework to investigate various types of wave propagation and pattern formation in a cyclic competition with spatial diffusion. To resolve moving internal boundary layers separating different patches of relative homogeneity in which a single species dominates, they employed an *adaptive* finite element method with an *a posteriori* error estimate in conjunction with a second-order IMEX method for the temporal integration.

While adaptive schemes are typically efficient when the solution consists of large patches or involves fine structures in a significantly small areas, sometimes they can be as good as a non-adaptive scheme with global refinement if such fine structures occur over a large area. It is observed that, in some cases, transient regimes of the competition-diffusion model involve very small patches that are multiplying and expanding over the entire spatial domain [20]. Moreover, for problems whose nonlinear reaction terms dominating the diffusion terms such as the one considered in this chapter, an explicit treatment for the reaction terms leads to weak stability behaviour of the IMEX scheme. Motivated by these observations, in this chapter, we

develop a numerical method based on the conforming finite element method in combination with a novel semi-implicit and multistep high-order temporal integration technique to study various spatio-temporal patterns in two spatial domain. In this method the nonlinear reaction terms are treated using a semi-implicit scheme resulting in an increased stability behaviour as compared to the IMEX method. The performance of the method is demonstrated in replicating dynamical regimes complex spatio-temporal coexistence patterns that have been found in the literature. The numerical scheme is also analyzed for stability and convergence in space, time, and both.

The rest of this chapter is organized as follows. In Section 6.2, we give a brief description of the model problem under consideration. The details of the proposed space and time discretization are given in Section 6.3. Discussions of stability and convergence of the method also presented in this section. In Section 6.4, numerical experiments and results are presented and discussed. Finally, conclusion remarks and an outline of future research are presented in Section 6.5.

6.2 The Lotka-Volterra competition-diffusion model

Let Ω be a bounded domain, with piecewise smooth boundary $\partial\Omega$, representing the spatial habitat of an ecosystem in which two competing species, denoted U and V , live in and interact with each other. One possible scenario in a biodiversity is the so-called *competitor-mediated coexistence*. It refers to a phenomenon in which, in the absence of any other competing species, these two species may never coexist. However, if an exotic species, denoted by W invades the ecosystem and compete with them, all the three species coexist.

In this chapter, we consider the following competition-diffusion model of Lotka-Volterra-type in which the three competing species are assumed to disperse in the ecosystem randomly [35, 112]:

$$\left. \begin{aligned} \dot{u} &= D_1 \Delta u + u f_1(u, v, w), \\ \dot{v} &= D_2 \Delta v + v f_2(u, v, w), \\ \dot{w} &= D_3 \Delta w + w f_3(u, v, w), \end{aligned} \right\} \text{in } \Omega \times \mathbb{R}^+, \quad (6.2.1)$$

where the superposed dot denotes time derivative and Δ is the Laplacian operator. The population densities of U , V , and W are denoted by u , v , and w , respectively. The constant $D_i = \varepsilon^2 d_i > 0$ ($i = 1, 2, 3$) denotes the diffusivity of the corresponding species, where ε is a small positive constant that represents the characteristic thickness of boundary layers that may appear as the system stabilizes. The linear factors of the growth terms are given by

$$\left. \begin{aligned} f_1(u, v, w) &= r_1 - a_{11}u - a_{12}v - a_{13}w, \\ f_2(u, v, w) &= r_2 - a_{21}u - a_{22}v - a_{23}w, \\ f_3(u, v, w) &= r_3 - a_{31}u - a_{32}v - a_{33}w, \end{aligned} \right\} \quad (6.2.2)$$

where the parameters r_i and a_{ij} ($i, j = 1, 2, 3$) are the intrinsic growth rates and the inter-specific when $i \neq j$, or intra-specific competition rates, and it is assumed that all are positive. The system (6.2.1) together with (6.2.2) are supplemented with the homogeneous Neumann boundary conditions

$$\frac{\partial u}{\partial \mathbf{n}} = 0, \quad \frac{\partial v}{\partial \mathbf{n}} = 0, \quad \text{and} \quad \frac{\partial w}{\partial \mathbf{n}} = 0, \quad \text{on } \partial\Omega \times \mathbb{R}^+, \quad (6.2.3)$$

and initial conditions of the form

$$u(\mathbf{x}, 0) = u_0(\mathbf{x}), \quad v(\mathbf{x}, 0) = v_0(\mathbf{x}), \quad \text{and} \quad w(\mathbf{x}, 0) = w_0(\mathbf{x}). \quad (6.2.4)$$

Here \mathbf{x} represents the coordinate of a point in Ω , \mathbf{n} is a unit vector normal to the boundary $\partial\Omega$, and u_0, v_0, w_0 are some prescribed positive functions defined over the spatial domain Ω .

The system (6.2.1) together with the growth terms (6.2.2), in the absence of diffusion, have eight equilibrium points of which $A(r_1/a_{11}, 0, 0)$, $B(0, r_2/a_{22}, 0)$ and $C(0, 0, r_3/a_{33})$ are stable, whereas all the remaining equilibrium points are unstable. Any positive initial solution converges to either A , B , or C . That means, if diffusion is ignored, competitive exclusion occurs among the three species. However, in the presence of diffusion, if the diffusivity coefficient is sufficiently small enough, a spatially segregated pattern with very thin internal layers will occur. Detailed study on the qualitative nature of the solutions of the competitive-diffusion system (6.2.1) can be found in the articles [35, 112].

Due to the presence of very fine spatial features as internal layers and the strongly-

nonlinear coupling in the growth terms, numerical approximation of such competitive-diffusion systems is very challenging. Hence, in what follows, we present a numerical method in which finite element is employed to discretize in space resulting in a large system of ODEs, which then will be integrated temporally using a high-order semi-implicit method based on the Lagrange scheme.

6.3 The numerical method

In this section, we present a high-order, semi-implicit method for the competition-diffusion system of partial differential equations (6.2.1)-(6.2.4). In the first step, we employ a Galerkin finite element for spatial discretization. This results in a large system of nonlinear ODEs. We then use a specially tailored high-order semi-implicit scheme based on the multistep Lagrange methods to integrate this nonlinear system of ODEs in a sequential manner.

6.3.1 Spatial discretization: Galerkin finite element method

Considering a test function ϕ , we integrate (6.2.1) over the domain Ω , use integration by parts and employ Neumann boundary conditions (6.2.3). This yields

$$\left. \begin{aligned} \int_{\Omega} \dot{u}\phi \, d\mathbf{x} &= -D_1 \int_{\Omega} \nabla u \cdot \nabla \phi \, d\mathbf{x} + \int_{\Omega} u f_1(u, v, w)\phi \, d\mathbf{x}, \\ \int_{\Omega} \dot{v}\phi \, d\mathbf{x} &= -D_2 \int_{\Omega} \nabla v \cdot \nabla \phi \, d\mathbf{x} + \int_{\Omega} v f_2(u, v, w)\phi \, d\mathbf{x}, \\ \int_{\Omega} \dot{w}\phi \, d\mathbf{x} &= -D_3 \int_{\Omega} \nabla w \cdot \nabla \phi \, d\mathbf{x} + \int_{\Omega} w f_3(u, v, w)\phi \, d\mathbf{x}, \end{aligned} \right\} \quad (6.3.1)$$

where ∇ is the spatial gradient operator. The strong form (6.2.1) and the weak form (6.3.1) are equivalent in the sense that any sufficiently smooth solution of one also satisfies the other.

Now let $\mathcal{T} = \{\Omega^e\}_{e=1}^{ne}$ be a triangulation of the spatial domain Ω into non-overlapping simplexes covering Ω , i.e.,

$$\Omega = \bigcup_e \Omega^e, \quad (6.3.2)$$

where ne is the total number of elements. Let $\{\varphi_k\}_{k=1}^{nd}$ be a set of basis (shape) functions on the mesh \mathcal{T} , where nd is the total number of nodes in the mesh. Each shape function

φ_k has a local support over elements that share the k -th node, and is piecewise polynomial (usually Lagrange polynomials) whose degree is determined by the local number of nodes that a typical element Ω^e has. Moreover, they also satisfy the interpolatory condition, such that

$$\varphi_k(\mathbf{x}_j) = \delta_{kj}, \quad k, j = 1, 2, \dots, nd; \quad (6.3.3)$$

where δ_{kl} is the Kronecker delta function and \mathbf{x}_j is the coordinate of the j -th node.

Now, we replace the population density functions u , v , and w by the finite element interpolations u^h , v^h , and w^h , respectively, i.e.,

$$\left. \begin{aligned} u^h(\mathbf{x}, t) &= \sum_{k=1}^{nd} \varphi_k(\mathbf{x}) u_k(t), \\ v^h(\mathbf{x}, t) &= \sum_{k=1}^{nd} \varphi_k(\mathbf{x}) v_k(t), \\ w^h(\mathbf{x}, t) &= \sum_{k=1}^{nd} \varphi_k(\mathbf{x}) w_k(t), \end{aligned} \right\} \quad (6.3.4)$$

where $u_k(t)$, $v_k(t)$, and $w_k(t)$ are the k -th nodal value of u , v , and w , respectively, at time t . We also replace the test function ϕ by the analogues shape functions φ_j and then the discrete form of (6.3.1) becomes

$$\left. \begin{aligned} \mathbf{M}\dot{\mathbf{u}} &= D_1 \mathbf{K}\mathbf{u} + \mathbf{M}\mathbf{u} \odot \mathbf{f}_1(\mathbf{u}, \mathbf{v}, \mathbf{w}), \\ \mathbf{M}\dot{\mathbf{v}} &= D_2 \mathbf{K}\mathbf{v} + \mathbf{M}\mathbf{v} \odot \mathbf{f}_2(\mathbf{u}, \mathbf{v}, \mathbf{w}), \\ \mathbf{M}\dot{\mathbf{w}} &= D_3 \mathbf{K}\mathbf{w} + \mathbf{M}\mathbf{w} \odot \mathbf{f}_3(\mathbf{u}, \mathbf{v}, \mathbf{w}), \end{aligned} \right\} \quad (6.3.5)$$

where \odot denotes component-wise product of vectors. The entries of the mass and stiffness matrices are respectively given by

$$\mathbf{M}_{jk} = \int_{\Omega} \varphi_j \varphi_k \, d\mathbf{x}, \quad \text{and} \quad \mathbf{K}_{jk} = \int_{\Omega} \nabla \varphi_j \cdot \nabla \varphi_k \, d\mathbf{x}, \quad (6.3.6)$$

and the vector of nodal values \mathbf{u} , \mathbf{v} , and \mathbf{w} and vector valued growth functions \mathbf{f}_1 , \mathbf{f}_2 , and

\mathbf{f}_3 are given by

$$\left. \begin{aligned} \mathbf{u} &= [u_1, u_2, \dots, u_{nd}]^T, \quad \mathbf{v} = [v_1, v_2, \dots, v_{nd}]^T \\ \mathbf{w} &= [w_1, w_2, \dots, w_{nd}]^T, \quad \mathbf{f}_i = [f_i^1, f_i^2, \dots, f_i^{nd}]^T, \quad i = 1, 2, 3 \end{aligned} \right\}. \quad (6.3.7)$$

Here $f_i^k = f_i(u_k, v_k, w_k)$. Hence, by lumping or by multiplying each of the semi-discrete equations in (6.3.5) by \mathbf{M}^{-1} we obtain a more simplified form

$$\left. \begin{aligned} \dot{\mathbf{u}} &= D_1 \widehat{\mathbf{K}} \mathbf{u} + \mathbf{u} \odot \mathbf{f}_1(\mathbf{u}, \mathbf{v}, \mathbf{w}), \\ \dot{\mathbf{v}} &= D_2 \widehat{\mathbf{K}} \mathbf{v} + \mathbf{v} \odot \mathbf{f}_2(\mathbf{u}, \mathbf{v}, \mathbf{w}), \\ \dot{\mathbf{w}} &= D_3 \widehat{\mathbf{K}} \mathbf{w} + \mathbf{w} \odot \mathbf{f}_3(\mathbf{u}, \mathbf{v}, \mathbf{w}). \end{aligned} \right\} \quad (6.3.8)$$

The semi-discrete system (6.3.8) together with the initial conditions (6.2.4) define the system of nonlinear ODEs which will be integrated temporally using a semi-implicit linear multistep Lagrange based method presented below.

6.3.2 Temporal integration: a high-order semi-implicit method

Let $I = [0, T]$ be the interval of interest, and $\{I_n\}_{n=1}^N$ be its uniform partition of non-overlapping subintervals of the form $I_m = [t_{m-1}, t_m]$, $m = 2, 3, \dots, N$ with step-size $\Delta t = t_m - t_{m-1}$. Our aim is to present a semi-implicit multistep method of order r , for $r = 1, 2, 3, \dots$, based on the Lagrange temporal interpolations.

To proceed with let θ be a scalar function defined over the space-time domain in which the vector of its values over the spatial grid \mathcal{T} at the time-step t_m is denoted as $\boldsymbol{\theta}^m$, i.e.,

$$\boldsymbol{\theta}^m = [\theta_1^m, \dots, \theta_{nd}^m]^T. \quad (6.3.9)$$

Hence we have a matrix of values,

- matrix of values of $\boldsymbol{\theta}$

$$\boldsymbol{\theta}^{[r+1]} = \begin{bmatrix} \theta_1^{n-r} & \dots & \theta_1^n \\ \vdots & & \vdots \\ \theta_{nd}^{n-r} & \dots & \theta_{nd}^n \end{bmatrix}, \quad \boldsymbol{\theta}^{[r]} = \begin{bmatrix} \theta_1^{n-r} & \dots & \theta_1^{n-1} \\ \vdots & & \vdots \\ \theta_{nd}^{n-r} & \dots & \theta_{nd}^{n-1} \end{bmatrix}. \quad (6.3.10)$$

We denote the derivatives and extrapolation vectors

- derivative and extrapolation vectors as

$$\mathbf{D}^{r+1} = \begin{bmatrix} d^1 \\ \vdots \\ d^{r+1} \end{bmatrix}, \quad \mathbf{P}^r = \begin{bmatrix} p^1 \\ \vdots \\ p^r \end{bmatrix}, \quad (6.3.11)$$

where \mathbf{D}^{r+1} and \mathbf{P}^r are derived from the Lagrange temporal interpolations (see Chapter 4) and presented in Table 6.3.1.

Table 6.3.1: Derivative and extrapolation coefficient vectors.

r	\mathbf{D}^{r+1}	\mathbf{P}^r
1	$\frac{1}{h}[-1 \quad 1]^T$	1
2	$\frac{1}{2h}[1 \quad -4 \quad 3]^T$	$[-1 \quad 2]^T$
3	$\frac{1}{3h}[-1 \quad \frac{9}{2} \quad -9 \quad \frac{11}{2}]^T$	$[1 \quad -3 \quad 3]^T$
4	$\frac{1}{4h}[1 \quad -\frac{16}{3} \quad 12 \quad -16 \quad \frac{25}{3}]^T$	$[-1 \quad 4 \quad -6 \quad 4]^T$

Now, assume that the approximate values of \mathbf{u} , \mathbf{v} , and \mathbf{w} over the spatial grid at the time-steps t_{n-r}, \dots, t_{n-1} are known, then the semi-implicit multistep scheme for finding the approximate solutions at the current time-step t_n is defined as

$$\left. \begin{aligned} \mathbf{u}^{[r+1]}\mathbf{D}^{r+1} &= D_1\widehat{\mathbf{K}}\mathbf{u}^n + \mathbf{u}^n \odot \mathbf{f}_1(\mathbf{u}^{[r]}\mathbf{P}^r, \mathbf{v}^{[r]}\mathbf{P}^r, \mathbf{w}^{[r]}\mathbf{P}^r), \\ \mathbf{v}^{[r+1]}\mathbf{D}^{r+1} &= D_2\widehat{\mathbf{K}}\mathbf{v}^n + \mathbf{v}^n \odot \mathbf{f}_2(\mathbf{u}^n, \mathbf{v}^{[r]}\mathbf{P}^r, \mathbf{w}^{[r]}\mathbf{P}^r), \\ \mathbf{w}^{[r+1]}\mathbf{D}^{r+1} &= D_3\widehat{\mathbf{K}}\mathbf{w}^n + \mathbf{w}^n \odot \mathbf{f}_3(\mathbf{u}^n, \mathbf{v}^n, \mathbf{w}^{[r]}\mathbf{P}^r). \end{aligned} \right\} \quad (6.3.12)$$

The scheme (6.3.12) is linearly-implicit and r -order convergent in time. The solution procedure is to solve first for \mathbf{u}^n from (6.3.12)₁ and use it to solve (6.3.12)₂ for \mathbf{v}^n , then finally use both \mathbf{u}^n and \mathbf{v}^n to solve (6.3.12)₃ for \mathbf{w}^n . For such multistep schemes a bunch of initial solutions are required to start the algorithm. For these we use the standard RK4 to find the first $r - 1$ time-step solutions after the initial step.

6.3.3 Convergence and stability analysis

The Semi-implicit Lagrangian method based finite element discretization (SILM-FE) (6.3.12) is comparable to an implicit-explicit finite element discretization (IMEX-FE) of multistep type in which, as in (6.3.12), the diffusion term is discretized implicitly while the nonlinear reaction term is treated explicitly. It is well-known that such IMEX schemes are high-order accurate for $r > 1$, where r is the number of previous time-steps used in the scheme. This is also true for the SILM-FE discretization as demonstrated in the Figs. 6.3.2 & 6.3.3. The results in Figure 6.3.2 represent the temporal convergence of the SILM- and IMEX-FE discretization schemes in solving the system of ODEs obtained from the finite element semi-discretization using a fixed and uniform spatial mesh of size $h = 1/8$. Figure 6.3.3 shows convergence results of the two schemes as the space-time domain is refined uniformly. The parameters used in all convergence experiments (i.e., to produce Figs. 6.3.1, 6.3.2, and 6.3.3) are

$$\left. \begin{aligned} a_{ii} = r_i = d_i = \varepsilon = 1, \quad (i = 1, 2, 3), \\ a_{ij} = 3, \quad (i, j = 1, 2, 3 \text{ and } i \neq j). \end{aligned} \right\} \quad (6.3.13)$$

Moreover, the computational space and time domain are $\Omega = [-1, 1] \times [-1, 1]$ and $I = [0, 1]$, respectively. For the temporal and spatial errors, we use the L^2 -norm of the relative error at the terminal time $T = 1$. For Figure 6.3.3, the true error is computed from an exact solution obtained as follows: a pseudo-source term is added to each equation in (6.2.1) which corresponds to the analytic solutions

$$u = v = w = \sin(t) \sin(\pi x/2) \sin(\pi x). \quad (6.3.14)$$

The source terms are then computed analytically as the residual when these exact solutions are substituted in Eq. (6.2.1). The boundary and initial conditions are then computed from the exact solutions (6.3.14).

The space discretization that is used in this study is the standard conforming Galerkin finite element which is optimal in the sense that, if the exact solution is sufficiently smooth, the finite element approximation is $\mathcal{O}(h^{2k})$ in the L^2 -norm, where k is the order of the local polynomial interpolation, for example, $k = 1$ and 2 for the bilinear ($Q1$) and biquadratic ($Q2$)

elements, respectively. These estimations are remarkably demonstrated in the spatial convergence experimental results as shown in Figure 6.3.1. In these experiments, the convergence of the finite element semi-discretization is determined based on the following view point on the discretization process. The standard way of approximating solutions for time-dependant PDEs is the method-of-lines, that is, spatial discretization is typically employed using finite element method leading to a large system of ODEs which is often then discretized temporally using finite difference. But this is equivalent to viewing the approach the other way around, that is, temporal discretization leading to a semi-discrete boundary value problem (BVP) at each time-step which is then treated using finite element in space. Assuming that, for some fixed temporal discretization with time-step length Δt , the BVPs at each time-steps are well posed, we denote their exact solutions by $\mathbf{u}_{\Delta t}$, and the finite element approximations corresponding to mesh size h by $\mathbf{u}_{\Delta t}^h$. Hence the relative error **Rel. Error** between the approximations with mesh size h and $h/2$ is given by

$$\begin{aligned} \mathbf{Rel. Error} &= \|\mathbf{u}_{\Delta t}^{h/2} - \mathbf{u}_{\Delta t}^h\| \leq \|\mathbf{u}_{\Delta t} - \mathbf{u}_{\Delta t}^{h/2}\| + \|\mathbf{u}_{\Delta t} - \mathbf{u}_{\Delta t}^h\|, \\ &= C(h/2)^{2k} + C(h)^{2k}, \\ &= C_1(h)^{2k}, \end{aligned} \tag{6.3.15}$$

where C is a positive constant independent of h (but it may possibly be dependant on Δt and other parameters in the problem), and $C_1 = C(1/2^{2k} + 1)$. Therefore, (6.3.15) implies that **Rel. Error** is of $\mathcal{O}(h^{2k})$. As shown in the Figure 6.3.1, the differences between the curves corresponding to each temporal discretization schemes ($r = 1, 2, 3, 4$) are very small demonstrating that C_1 is independent of the type of temporal discretization. Generally, a fully-linear implicit scheme for a nonlinear problem cannot be high-order convergent. On the other hand, a partially-linear implicit scheme arising from an implicit-explicit method for problems composed of linear and nonlinear parts can be high-order if one chooses high-order implicit discretization for the linear part while treating the nonlinear part explicitly. However, this procedure will only result in a scheme that often has poor stability property, particularly, when the nonlinear part is more dominant. In this work, our aim is to develop a semi-implicit method which results in a fully-linear implicit scheme that is high-order convergent and has better stability property than implicit-explicit methods.

Spatial convergence

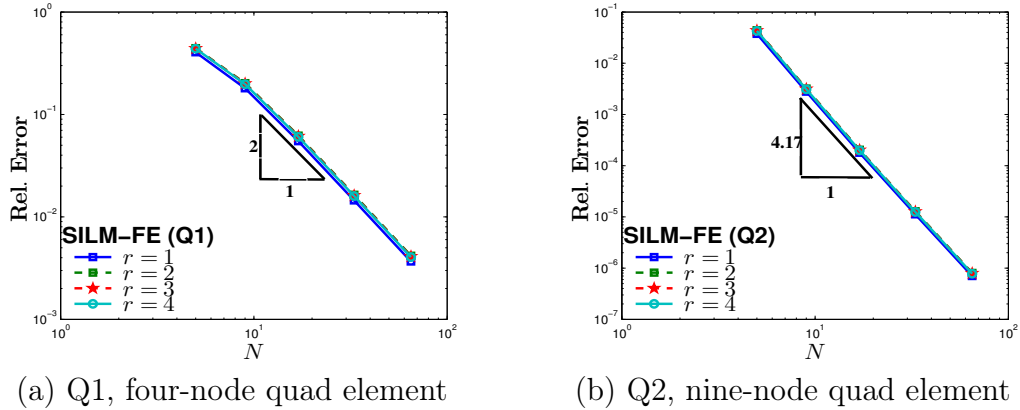


Figure 6.3.1: Spatial convergence of SILM-FE schemes for the model problem (6.2.1) with parameters in (6.3.13). The horizontal axis label ‘ N ’ refers to the number of elements along each side of the square spatial domain.

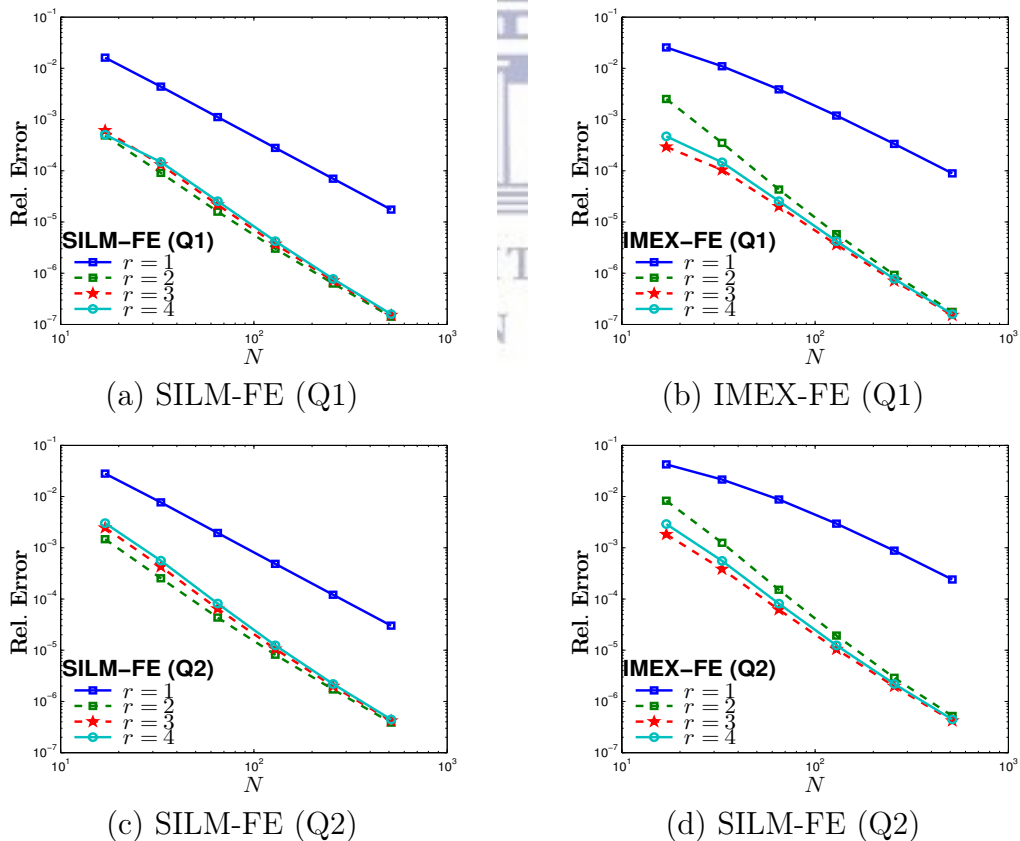


Figure 6.3.2: Temporal convergence of the SILM-FE and IMEX-FE schemes applied to the model problem (6.2.1) with same parameters in Figure 6.3.1. Here the horizontal axis label ‘ N ’ refers to the number of time-steps.

Convergence in both space and time

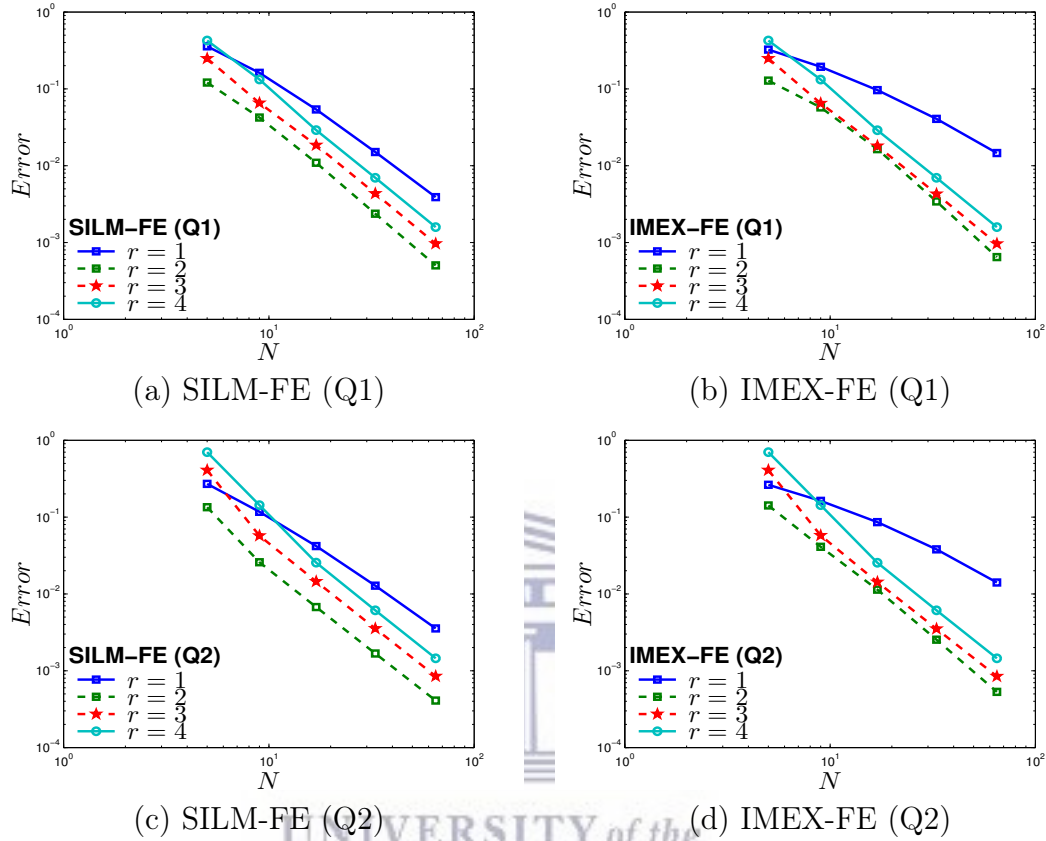


Figure 6.3.3: Convergence in both space and time of SILM-FE and IMEX-FE schemes applied to the model problem (6.2.1) with parameters same as in Figure 6.3.1. Here the space and time meshes are simultaneously refined so that $\Delta t = 2h_x = 2h_y$ and the horizontal axis N refers to the number of elements either of the sides of the spatial square domain (or twice of the number of time-steps).

However, from 6.3.2, it appears that the second-order method is most accurate, while the slope of the curves corresponding to the third and fourth-order approximation looks slightly steeper than the second-methods while the others semi-implicit schemes are only conditionally stable. This means that one has to respect the CFL conditions for such conditionally stable methods in order to get the theoretical convergence property. However, in our analysis shown in 6.3.2, we only refine the temporal discretization keeping the spatial mesh constant. This may result in violation of the CFL conditions for those schemes up to some temporal refinement levels, which in turn degrades their accuracy.

It is computationally challenging to approximate singularly perturbed reaction-diffusion problems with the diffusion coefficients that are significantly smaller than that of the nonlinear reaction terms. This is the case in ecological application of competition-diffusion models where spatial mobility is small compared to the rate of interactions between the species. In such cases, one of the most critical issues in the numerical approximation of such problems is the stability. To avoid the nonlinearity as a result of the reaction term and obtain high-order approximation, the commonly used scheme such as IMEX-finite element discretizations treat the diffusion term implicitly and the reaction term explicitly. However, such methods may lead to a weakened stability behavior as the dominant term is explicit. In addition to treating the diffusion term implicitly, the proposed SILM-FE discretization described by (6.3.12) enhances the stability property by using a semi-linearized but high-order scheme for the reaction term. Since it is essential to analyze how the reaction term impacts the stability of the proposed numerical scheme, we assume the following reduced problem by ignoring the v, w and the diffusion terms,

$$\dot{u} = \lambda u(1 - u). \quad (6.3.16)$$

Here we assume that $r_1 = a_{11} = -\lambda > 0$. The ODE (6.3.16) has $u = 0$ and $u = 1$ as equilibrium solution where only the former is stable. Applying the multistep semi-linearized scheme (6.3.12) to the simplified model (6.3.16) leads to

$$\Delta t u^{[r+1]} \mathbf{D}^{r+1} = \Delta t \lambda u^n \odot (\mathbf{1} - u^{[r]}), \quad (6.3.17)$$

where

$$u^{[r+1]} = [u^{n-r}, \dots, u^{n-1}, u^n]^T, \text{ and } u^{[r]} = [u^{n-r}, \dots, u^{n-1}]^T. \quad (6.3.18)$$

Following the standard procedure of stability analysis of finite difference schemes, we replace ξ^r for u^{n-r} to obtain the characteristic polynomial corresponding to the scheme (6.3.17) of the form

$$\Pi(\xi; z) = \sum_{j=0}^r \Delta t d^{j+1} \xi^{r-j} - z \xi^r \sum_{j=0}^{r-1} (1 - p^{j+1} \xi^{r-j}), \quad (6.3.19)$$

where $z = \Delta t \lambda$, and d^j and p^k are as in equation (6.3.11). Thus, the stability of the schemes correspond to the region in the complex z -plane for which the roots of the characteristic

equation are less than or equal to one. These regions are shown in Figure 6.3.4.

In addition to the use of semi-linearization of the reaction term, the solution is updated successively based on the current time-step solutions. This process makes the method more stable.

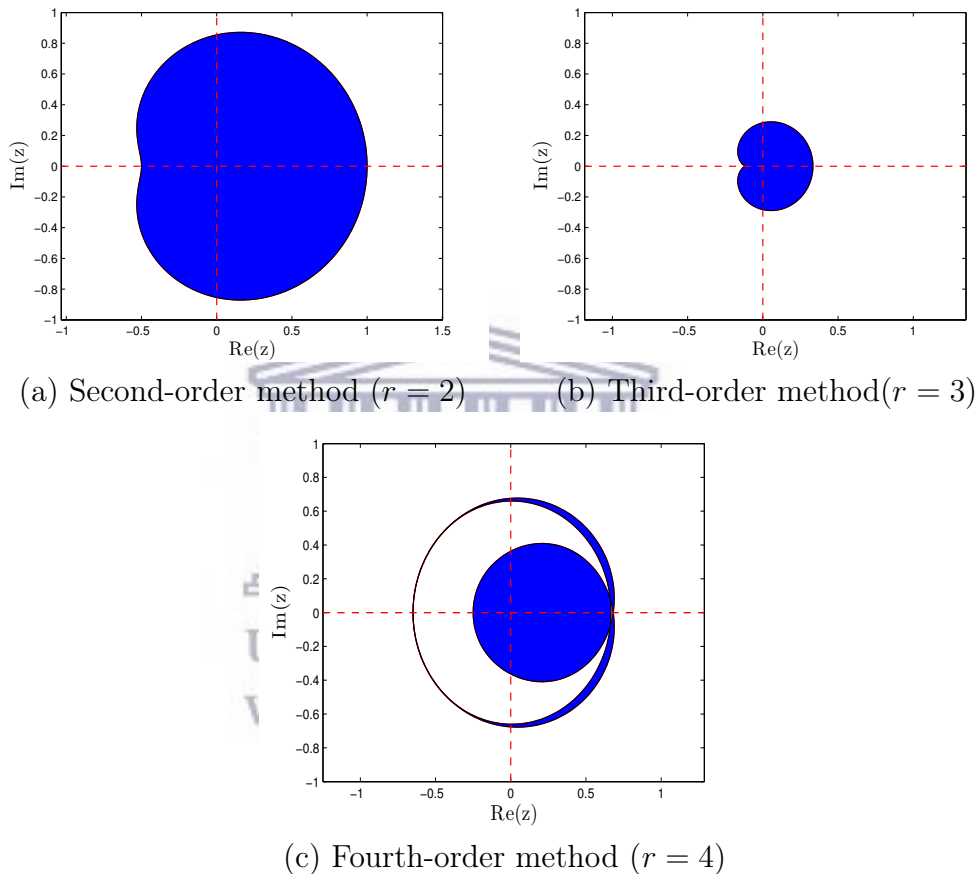


Figure 6.3.4: Stability regions of the semi-linear multistep methods applied to the reduced nonlinear problem (6.3.16).

6.4 Numerical results

In this section, we present various numerical experiments to demonstrate the performance of our proposed schemes for simulating a number of interaction patterns such as the onset of spiral-like shape, spatial segregation and other spatio-temporal patterns. We have examined the capability of the schemes in representing different modes of interaction for different sets

of parameters. In all the simulations, the spatial domain Ω is subdivided into 251×251 grid of four-node quadrilateral (Q1 or bilinear) elements. We first consider the completely symmetrical case. Initially, uniform pseudo-random distribution of the species were assumed. Then a segregation pattern of three regions each occupied by only one species is emerged as shown in Figure 6.4.1. The regions are separated by very thin internal layers due to the small diffusion coefficient compared to the competition (reaction) parameters. Eventually, the internal layers separating the segregated regions stretches to almost straight lines, from which the dynamics is shown to change more slowly.

Next, we consider a non-symmetrical case in which one species eventually dominates and excludes the other two as shown in Figure 6.4.2 which is called competitive exclusion. Simulation results of Figure 6.4.3, 6.4.4, and 6.4.5 each correspond to a semi-symmetric case but due to the initial distributions and transposing, the reaction parameters different form of spiral-like spatio-temporal coexistence patterns were observed. Such coexistence is expected because of the cyclic competition of the species U, V and W in space as is dictated by the reaction parameters. Finally, Figure 6.4.6 displays the complex spatio-temporal coexistence pattern of the three species with many clustering spirals where each one is rotating in their vicinity of triple junction.

UNIVERSITY of the
WESTERN CAPE

6.5 Summary and discussion

In this chapter, we developed high-order semi-implicit linear multistep schemes based on Lagrange interpolation for the temporal discretization in conjunction with conforming finite element method for a nonlinear time-dependant three species competition-diffusion model in two-dimensional spatial domain. The optimal convergence of the finite element spatial discretization has been verified using numerical experiments. To maintain the full accuracy and order of the multistep schemes, the classical fourth-order Runge-Kutta (RK4) has been used to obtain the required starting solutions. It is also observed that the semi-linearized implicit schemes are high-order in both space and time for $r = 2, 3, 4$. The comparison between the temporal convergence results have revealed that the second-order SILM performs comparatively in the same way as the other high-order schemes (i.e., for $r = 3$ and 4), but outperforms them when convergence is considered in both space and time. Moreover, the

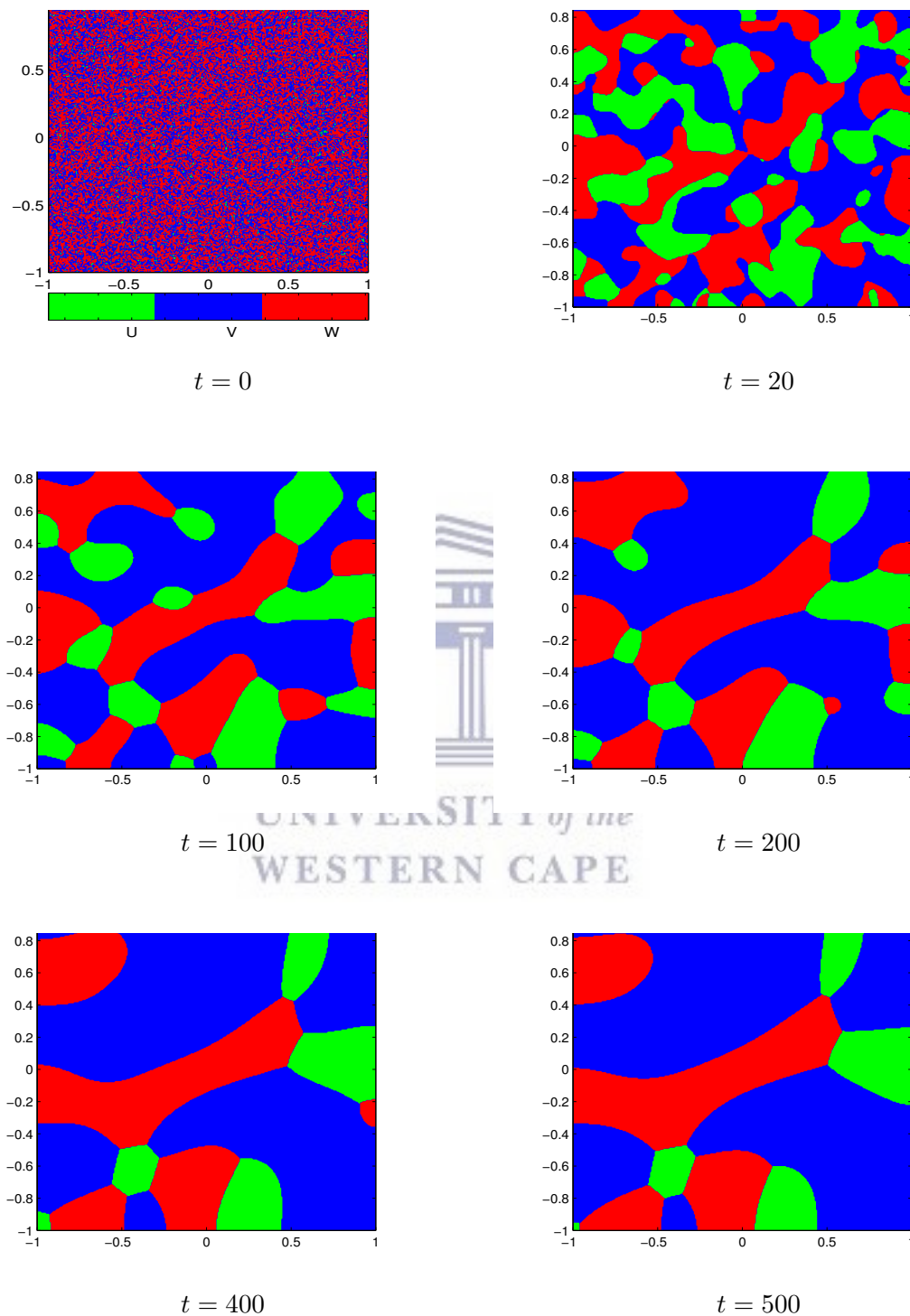


Figure 6.4.1: Simulation of occurrence of segregation pattern of the three species U, V and W with triple junction at different times. Parameters used for the simulation are $a_{ii} = r_i = d_i = 1$, $(i = 1, 2, 3)$, $a_{12} = a_{23} = a_{31} = a_{13} = a_{21} = a_{32} = 3$, $\varepsilon = 0.1$, and $\Delta t = 1$.

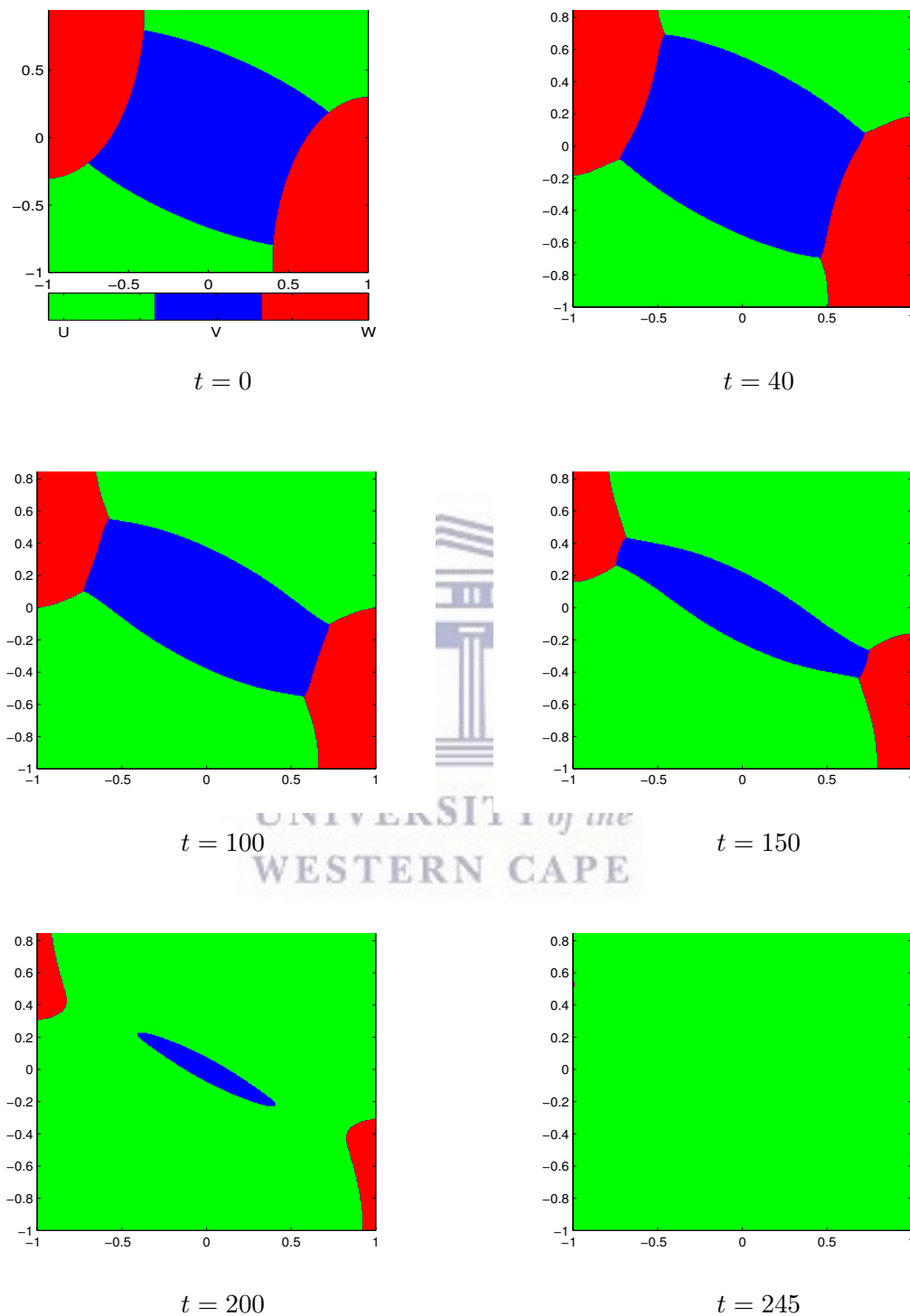


Figure 6.4.2: Competitive exclusion patterns of the three species U, V and W at different times. Parameters used for the simulation are $a_{ii} = r_i = d_i = 1$, ($i = 1, 2, 3$), $a_{12} = 2$, $a_{31} = 5$, $a_{13} = a_{21} = a_{23} = 3$, $a_{32} = 4$, $\varepsilon = 0.1$, and $\Delta t = 1$.

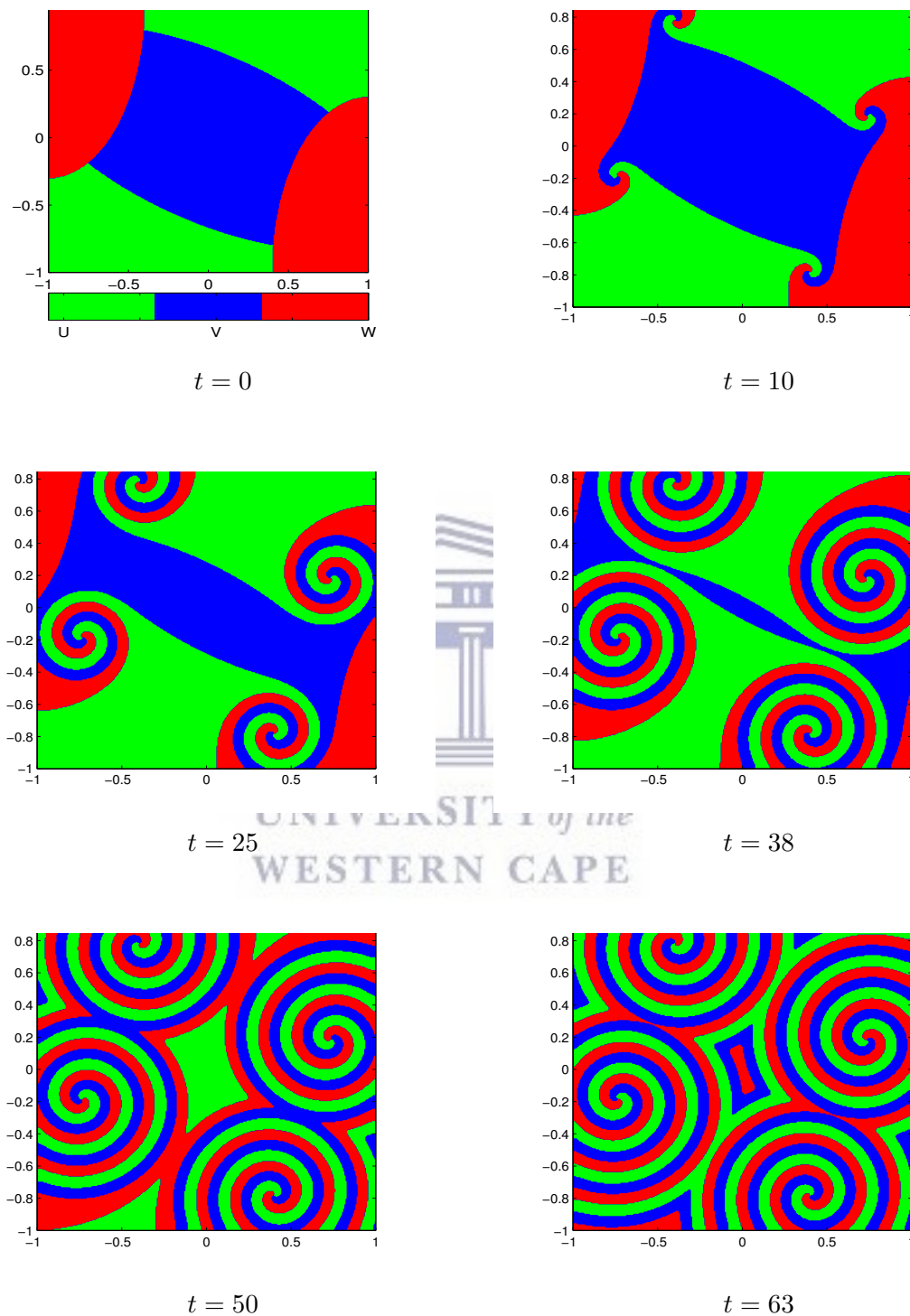


Figure 6.4.3: Coexistence pattern ('inward' spiral-like) in the dynamics of the three species U, V and W at different times. Parameters used for the simulation are the transpose of $a_{ii} = r_i = d_i = 1$, $a_{12} = a_{23} = a_{31} = 2$, $a_{13} = a_{21} = a_{32} = 7$, $\varepsilon = 0.1$, and $\Delta t = 0.25$.

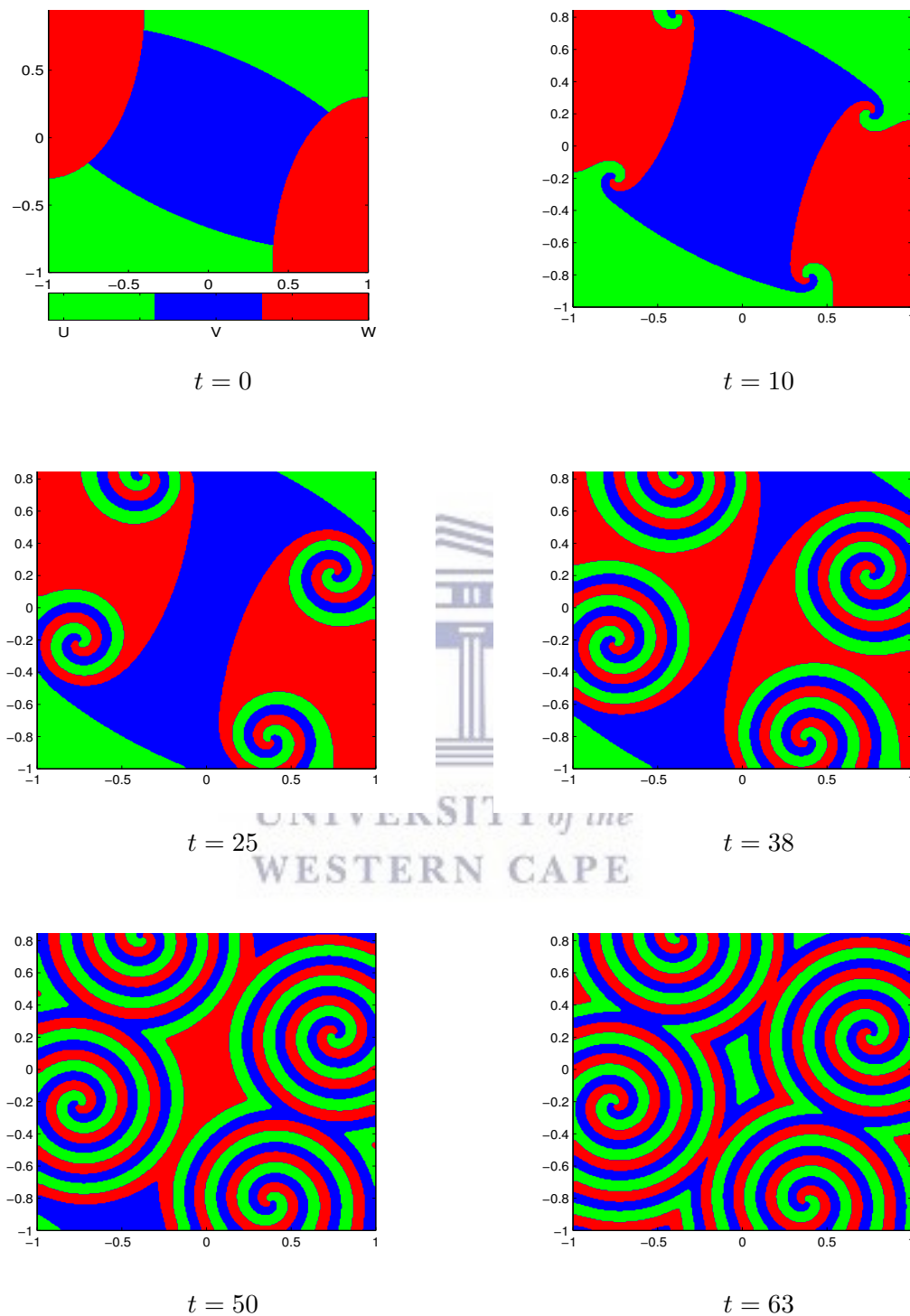


Figure 6.4.4: Coexistence pattern ('outward' spiral-like) in the dynamics of the three species U, V and W at different times. Parameters used for the simulation are $a_{ii} = r_i = d_i = 1$, ($i = 1, 2, 3$), $a_{12} = a_{23} = a_{31} = 2$, $a_{13} = a_{21} = a_{32} = 7$, $\varepsilon = 0.1$, and $\Delta t = 0.25$.

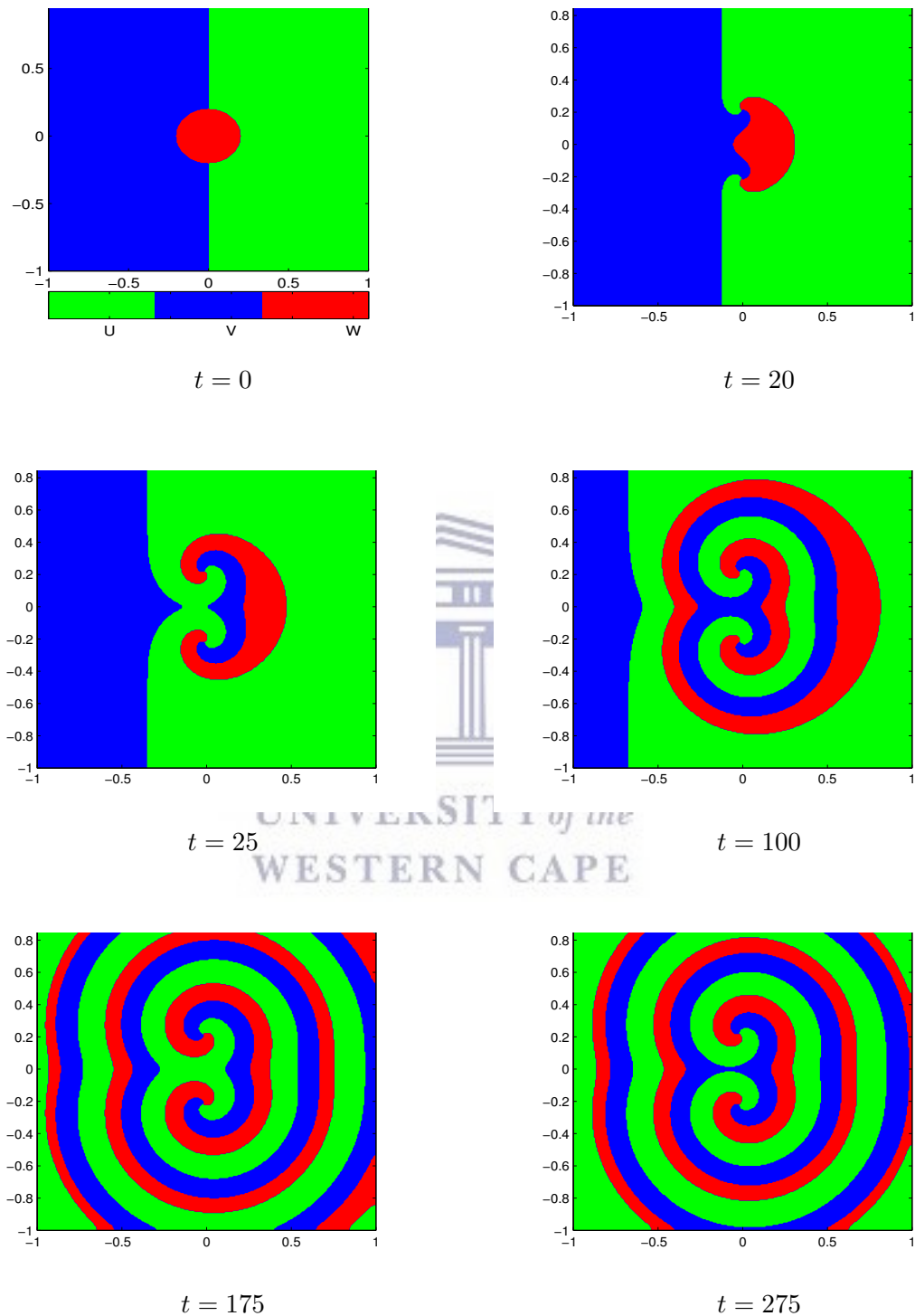
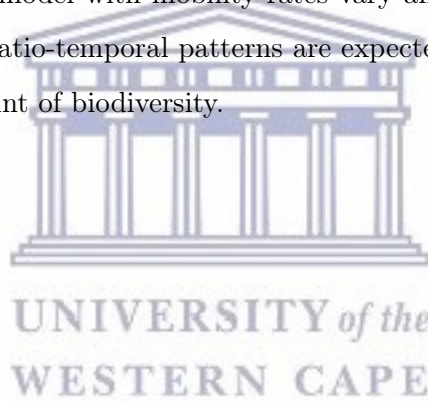


Figure 6.4.5: Coexistence pattern in the dynamics of the three species U, V and W at different times. Parameters used for the simulation are $a_{ii} = r_i = d_i = 1$, $a_{12} = a_{23} = a_{31} = 2$, $a_{13} = a_{21} = a_{32} = 7$, $\varepsilon = 0.1$, and $\Delta t = 0.25$.

second-order scheme displays better stability behaviour than the other high-order schemes. We have also compared the convergence of our methods (SILM) with the corresponding IMEX method. We notice that SILM has better stability property than the IMEX methods when the linear diffusion behaviour is significantly less than the reaction term. Several types of two-dimensional spatio-temporal patterns are simulated. Our method captures very well the dynamics of the appearance of the internal layer and other behaviour of the dynamics such as competitive-mediated-coexistence (with spiral-like patterns) and complex spatio-temporal coexistence patterns of the model by considering all the diffusion coefficients small.

In the next chapter, we deal with the numerical simulations, using a second-order multi-implicit scheme based on the Crank-Nicholson and Adams-Bashforth methods, of the competition-diffusion Lotka-Volterra model with mobility rates vary among the involved species. In this case, some interesting spatio-temporal patterns are expected which may have useful application from the view of point of biodiversity.



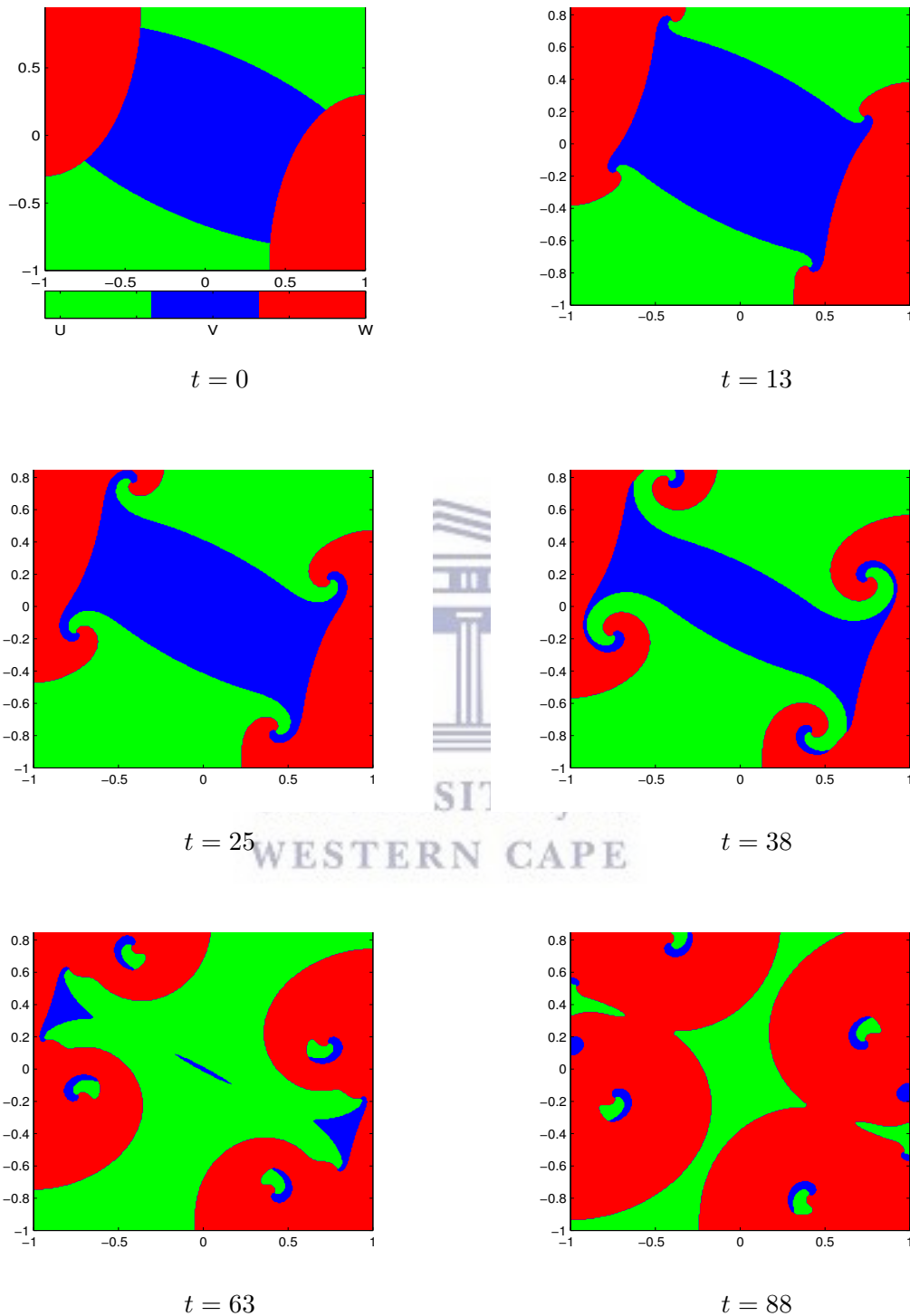
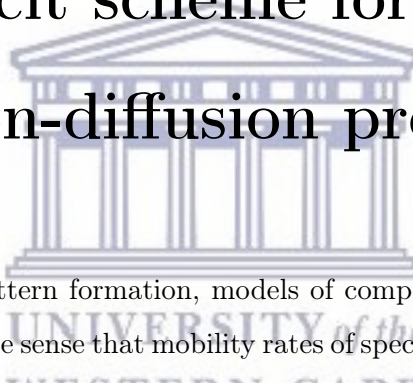


Figure 6.4.6: A spatio-temporal dynamic coexistence pattern ('cluster' shape) of the three species U, V and W at different times. Parameters used for the simulation are $a_{ii} = r_i = d_i = 1$, ($i = 1, 2, 3$), $a_{12} = 3$, $a_{13} = 6$, $a_{21} = 6.5$, $a_{23} = 3.5$, $a_{31} = 2.9$, $a_{32} = 6.1$, $\varepsilon = 0.1$, and $\Delta t = 0.5$.

Chapter 7

An asymptotically consistent semi-implicit scheme for competition-diffusion problems

The logo of the University of the Western Cape, featuring a classical building facade with columns and a pediment, with the text 'UNIVERSITY of the WESTERN CAPE' overlaid in a light blue color.

In ecological study of pattern formation, models of competitive-diffusion-type are generally singularly perturbed in the sense that mobility rates of species are significantly small compared to the rate of intra- and inter-specific interaction between the involved species. This leads to the presence of a wide range of spatial scales from regions each of which are completely dominated by one species to thin moving internal layers separating such regions. As a result of this, numerical approximation of such models is challenging. In this chapter, we propose a semi-implicit nonlinear multistep scheme based on the Crank-Nicholson and Adams-Bashforth methods, in conjunction with a C^0 -conforming finite element method to solve a competitive-diffusion model involving three interacting species with different mobility rates. Stability of the discrete scheme that is analogous to the asymptotic stability of the continuous problem is examined, and it is shown that the scheme strictly inherits the asymptotic stability behaviour of the continuous model without restrictions on the time step-size. A number of simulations for various mobility rates are also carried out to demonstrate the capability of the method in replicating different type of complex spatio-temporal patterns obtained in the literature.

7.1 Introduction

The study of spatio-temporal pattern formation in ecologically interacting species has been an intense research area since last few decades. Some similar works in this field is accounted to the famous ecologists and mathematicians such as Fisher [41], Kolomogrov et al, [85] and Volterra [160]. It is still continuously attracting enormous research interest, see, e.g., [118, 120, 141].

The availability of mathematical modelling and modern computing facilities play an important role in the field of mathematical ecology. One way of mathematically describing interaction of two or more species, such as competing for resources like food and territory, is through competition-diffusion models. Such models have been investigated intensively by many researchers. For example in [28, 35, 112], a three species Lotka-Volterra competition-diffusion model with the involved species having equal and very small mobility rates compared to the magnitude of the growth terms has been used to demonstrate some new types of spatio-temporal patterns which have important applications in biodiversity. However, in nature it is evident that majority of such interactions of the competing species disperse at different rates. Furthermore, previous studies have shown that differences in the dispersal distributions of competing species can fundamentally alter the outcome of competition [124]. In this chapter, we consider the numerical simulation of the Lotka-Volterra cyclic competition-diffusion model with different mobility rates [124]. This system is described by a system of time-dependant partial differential equation of reaction-diffusion-type. The model problem exhibits new dynamical behavior with cyclic competition and are different from the existing patterns formed from reaction-diffusion systems used previously [20, 124].

For problems which can be additively split into a linear and nonlinear parts, implicit-explicit (IMEX) methods, in which the linear part is treated implicitly while the nonlinear part explicitly, have been among the most popular choices in the research community. Various IMEX schemes have been developed to deal with reaction-diffusion problem in different fields of study. Boscarino *et. al* [15] developed higher-order semi-implicit IMEX schemes based on Runge-Kutta (RK) methods for a general class of problems with stiff and non-stiff additive parts, including reaction-diffusion problems. Cai and Cen [23] proposed a slightly different second-order convergent scheme based stretched variable for the singularly perturbed two

species predator-prey model in two space dimensions. In [20], an IMEX-type scheme with automatic spatial adaptive capability has been developed to study various types of interaction patterns in cyclic competition-diffusion systems of three species that have different mobility rates. They applied the explicit Adams-Bashforth method for the nonlinear reaction term and the implicit Crank-Nicholson's for the diffusion term. In Chapter 6, we developed a class of high-order semi-implicit schemes based on Lagrange collocation methods for competition-diffusion system of three interacting species in ecology. But, the mobility rates were assumed to be the same for all species.

The numerical method presented in this chapter takes into account a C^0 -conforming finite element method for the discretization in space, which leads to a large nonlinear system of ODEs. Then it is temporally discretized using a high-order stable finite difference method. Due to the relative dominance of the reaction rates over the diffusion rates, the commonly used temporal integration schemes IMEX methods lead to schemes with a very weakened stability behaviour. This is because of the fact that, in such IMEX methods, the diffusion (the less dominant part) is treated implicitly, whereas the reaction terms (the dominant part) is treated explicitly, thus leading to a higher tendency of the global scheme to behave as an explicit scheme. To overcome such restrictive nature of IMEX methods, in addition to treating the diffusion term implicitly, we use a semi-implicit method based on the Crank-Nicholson and Adams-Bashforth methods for the reaction term while the diffusion terms are treated implicitly using the Crank-Nicholson method. Therefore, the resulting scheme is multistep and nonlinear with respect to the previous time-steps. This leads to one of the desirable property in time-stepping algorithms, referred to as *asymptotic consistency*, that the discrete problem replicates the asymptotic stability behavior of the continuous problem. Interestingly, it should be noted that the scheme is implicitly linear with respect to the current unknown step; hence no iterative nonlinear solver is required. In addition, we demonstrate the existence of several new complex regular spatio-temporal patterns in two dimensions which may have important biological applications and are not available in most literature. Note that, the cyclic competition of the three species without diffusion leads to the extinction of one or more species and it is shown in [53, 101] however, the same model of cyclic competition with diffusion term allow for the existence of all the three species [32, 124, 126].

The organization of rest of this chapter is as follows. In Section 7.2, we gave an overview

of the governing mathematical model and its analysis. In Section 7.3, the proposed numerical methods is formulated, and its asymptotic consistency is proved. Extensive numerical simulations demonstrating the performance of the numerical scheme presented in Section 7.4. Finally, we present some concluding remarks in Section 7.5.

7.2 A three-species competitive-diffusion model

Let Ω be an open and bounded subset of \mathbb{R}^2 , with piecewise smooth boundary $\partial\Omega$, representing the habitat of an ecosystem in which three competing species, whose population densities denoted by u_i ($i = 1, 2, 3$), live in and interact with each other. We consider the three species Lotka-Volterra competition-diffusion model describing the spatial interaction of the species [101, 124],

$$\dot{u}_i = \nabla \cdot (D_i \nabla u_i) + u_i f_i(u_1, u_2, u_3); \quad i = 1, 2, 3, \quad (7.2.1)$$

where the superposed dot denotes time derivative and ∇ is the gradient operator. D_i ($i = 1, 2, 3$), which may possibly depend on position and time, is the (mobility) diffusivity of species i . The linear factor of the growth term is given by

$$f_i(u_1, u_2, u_3) = r_i - \sum_{j=1}^3 a_{ij} u_j, \quad (i = 1, 2, 3), \quad (7.2.2)$$

where the parameters r_i are the intrinsic growth rates, and a_{ij} is the inter-specific (when $i \neq j$), or intra-specific competition (self-limitation) rates. It is assumed that these parameters are also positive. The system (7.2.1) together with (7.2.2) are supplemented with the homogeneous Neumann boundary conditions, for each

$$\frac{\partial u_i}{\partial \mathbf{n}} = 0, \quad \text{for } \partial\Omega \times \mathbb{R}^+; \quad i = 1, 2, 3, \quad (7.2.3)$$

and initial conditions

$$u_1(\mathbf{x}, 0) = u_0(\mathbf{x}), \quad u_2(\mathbf{x}, 0) = v_0(\mathbf{x}), \quad \text{and } u_3(\mathbf{x}, 0) = w_0(\mathbf{x}). \quad (7.2.4)$$

Here \mathbf{x} represents the coordinate of a point in Ω , \mathbf{n} is a unit vector normal to the boundary $\partial\Omega$, and u_0, v_0, w_0 are some prescribed positive functions defined over the spatial domain Ω .

Eq. (7.2.1) has 15 parameters that could make the analysis complicated, hence it is instructive to scale densities of each species density according to their carrying capacities and then rescale the time and space coordinates. This gives

$$\left. \begin{aligned} a_{11} = a_{22} = a_{33} = 1, \quad \varepsilon_1 = 1, \\ \varepsilon_2 = \frac{D_2}{D_1}, \quad \varepsilon_3 = \frac{D_3}{D_1}, \quad \tilde{x} = \sqrt{\frac{1}{D_1}}x, \\ a_{12} = a_{23} = a_{31} = a, \quad a_{13} = a_{21} = a_{32} = b. \end{aligned} \right\} \quad (7.2.5)$$

Doing so, we obtain the following simplified competition-diffusion system

$$\left. \begin{aligned} \dot{u}_1 &= \Delta u_1 + u_1(1 - u_1 - au_2 - bu_3), \\ \dot{u}_2 &= \varepsilon_2 \Delta u_2 + u_2(1 - bu_1 - u_2 - au_3), \\ \dot{u}_3 &= \varepsilon_3 \Delta u_3 + u_3(1 - \alpha u_1 - bu_2 - u_3), \end{aligned} \right\} \quad (7.2.6)$$

where, $\alpha = a_{31}$, unless stated otherwise $\alpha = a$. To make the dynamics richer we sometimes consider $\alpha \neq a$; hence the total number of parameters become five. We also assume that $0 < \varepsilon_1, \varepsilon_2 \leq 1$.

Now let us first consider the local behaviour of the model problem (7.2.6) without diffusion. In this case Eq. (7.2.6), gives

$$\left. \begin{aligned} \frac{du_1}{dt} &= u_1(1 - u_1 - au_2 - bu_3) := g_1(u_1, u_2, u_3), \\ \frac{du_2}{dt} &= u_2(1 - bu_1 - u_2 - au_3) := g_2(u_1, u_2, u_3), \\ \frac{du_3}{dt} &= u_3(1 - \alpha u_1 - bu_2 - u_3) := g_3(u_1, u_2, u_3). \end{aligned} \right\} \quad (7.2.7)$$

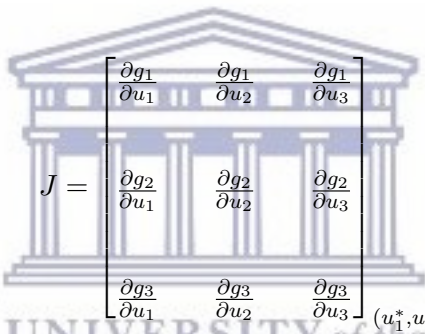
We now analyze the local stability of the spatial homogeneous system (7.2.7) because the dynamics of (7.2.6) is to a large extent controlled by it. In addition, the analysis provides us a necessary information on the choice of the parameters for simulation. We obtain the equilibrium points of (7.2.7) by equating the right hand side to zero. This results in eight

equilibria. However, the number of equilibrium points in the positive octant can be different for a different values of the parameters. Furthermore, we assume that

$$a + b > 2, \quad a > 1 > b. \tag{7.2.8}$$

Thus, under the condition stipulated in (7.2.8), the system consists of exactly five equilibrium points in the positive quadrants, $A(0, 0, 0)$, $B(0, 0, 1)$, $C(0, 1, 0)$, $D(1, 0, 0)$ and $E\left(\frac{1}{1+a+b}, \frac{1}{1+a+b}, \frac{1}{1+a+b}\right)$.

Following the standard procedure, we analyze the linear stability of these five equilibria by calculating the eigenvalues of the Jacobian matrix of the system in (7.2.7) evaluated at the equilibria (u_1^*, u_2^*, u_3^*) :



$$J = \begin{bmatrix} \frac{\partial g_1}{\partial u_1} & \frac{\partial g_1}{\partial u_2} & \frac{\partial g_1}{\partial u_3} \\ \frac{\partial g_2}{\partial u_1} & \frac{\partial g_2}{\partial u_2} & \frac{\partial g_2}{\partial u_3} \\ \frac{\partial g_3}{\partial u_1} & \frac{\partial g_3}{\partial u_2} & \frac{\partial g_3}{\partial u_3} \end{bmatrix}_{(u_1^*, u_2^*, u_3^*)}. \tag{7.2.9}$$

The trivial equilibrium state $A(0, 0, 0)$, having the eigenvalues $\lambda_1 = \lambda_2 = \lambda_3 = 1$, is unstable node describing the total extinction of the three species. The one-species equilibrium states $B(0, 0, 1)$, $C(0, 1, 0)$ and $D(1, 0, 0)$ have eigenvalues $\lambda_1 = -1$, $\lambda_2 = 1-b$ and $\lambda_3 = 1-a$; which implies that all of them are saddle points. These equilibrium points are biologically important in that they represent coexistence when all of them appear at the same time in different regions of the spatial habitat.

Steady state E is the most interesting biological state because at E , all the three population densities coexist. At E the corresponding Jacobian matrix becomes

$$J(E) = -\frac{1}{1+a+b} \begin{bmatrix} 1 & a & b \\ b & 1 & a \\ a & b & 1 \end{bmatrix}, \tag{7.2.10}$$

and the associated eigenvalues are

$$\left. \begin{aligned} \lambda_1 &= -(1 + a + b), \\ \lambda_{2,3} &= -(1 - (a + b)/2) \pm i(\frac{\sqrt{3}}{2})(a - b). \end{aligned} \right\} \quad (7.2.11)$$

Hence, this equilibrium point is asymptotically stable if $a + b < 2$, neutrally stable if $a + b = 2$ and unstable if $a + b > 2$.

Under the restriction (7.2.8) the only coexistence pattern is always a saddle point and the only attractor in the phase space is a hetroclinic cycle consisting of the three one-species equilibrium points.

Dynamical behavior of complex patterns arising in the competition-diffusion model (7.2.1) has been extensively studied, see, e.g., [3, 21, 28, 81, 108, 112, 113, 124]. Coexistence in the form of cyclic competition patterns is one of the interesting aspect of such models in the ecological and related applications. A cyclic competition pattern corresponds to a scenario, in relation to a family of parameters, in which one species dominates the other in a cyclical way, as depicted in the Figure 7.2.1. In the case where each of these species has the same mobility rate, under cyclic competition, spiral waves occur at each triple junction (a point where the three distinct regions, each dominated by a single species, meet) as in the case of Chapter 6. However, when the species have different rates of mobility, the scenario is much more complex. One of the aims of this chapter is to illustrate the capabilities of numerical method, which will be discussed in Section 7.3, in generating some interesting complex spatio-temporal patterns that have been studied in [3, 20, 124].

Due to the presence of strong nonlinear coupling in the growth terms and the fact that the solutions of such competitive-diffusion system may involve very fine moving spatial features as internal layers, numerical approximation of such competitive-diffusion systems is very challenging. In Chapter 6, we have employed semi-linear multistep methods, coupled with C^0 -conforming Galerkin finite element method (SILM-FE) to successfully approximate their solutions. In what follows, we will be presenting following semi-implicit nonlinear multistep method based on Method-of-Lines framework in which C^0 -conforming finite element method is employed for spatial discretization.

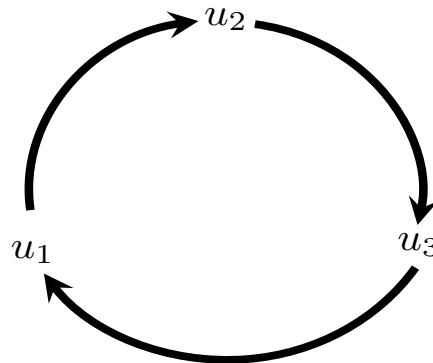


Figure 7.2.1: Schematic representation of cyclic competition. The arrows indicate the direction of domination.

7.3 The numerical method

In this section, we present a high-order, semi-implicit method for the competition-diffusion system of partial differential equations (7.2.1)-(7.2.4). Firstly, employ the Galerkin finite element method to discretize the problem in space resulting in a large system of nonlinear ODEs. We then use a novel high-order semi-implicit scheme based on a multistep Lagrange method [108] to integrate the system of ODEs in a staggered way.

7.3.1 Spatial discretization: Galerkin finite element method

The first step in Galerkin finite element method for partial differential equations is to convert the strong form into a suitable equivalent integral equation, known as a weak form. To this end, let v be any test function in the space $H^1(\Omega)$ (the set of functions on Ω whose derivatives are square integrable). We then multiply (7.2.1) by v and integrate it over the spatial domain Ω . Then after employing integration by parts together with the boundary conditions (7.2.3), one obtains the weak form which reads as: find $u_i \in H^1(\Omega)$, $i = 1, 2, 3$ such that

$$\langle \dot{u}_i, v \rangle = -\langle D_i \nabla u_i, \nabla v \rangle + \langle u_i f_i(u_1, u_2, u_3), v \rangle, \text{ for every } v \in H^1(\Omega) \quad (7.3.1)$$

where $\langle \cdot, \cdot \rangle$ denotes integral-inner product between two functions. The strong form (7.2.1) and the weak form (7.3.1) are equivalent in the sense that any sufficiently smooth solution of one is also a solution to the other.

Let $\mathcal{T} = \{\Omega^e\}_{e=1}^{ne}$ be a triangulation of the spatial domain Ω into total ne non-overlapping quadrilaterals that approximately covers Ω . Let $\{\varphi_k\}_{k=1}^{nd}$ be a set of basis (shape) functions on the mesh \mathcal{T} , where nd is the total number of nodes in the mesh. Each shape function φ_k has a local support over the elements that share the k -th node, and is piecewise polynomial (usually Lagrange polynomials) whose degree is determined by the local number of nodes that a typical element Ω^e possesses. Moreover, they also satisfies the interpolatory condition

$$\varphi_k(\mathbf{x}_j) = \delta_{kj}; \quad k, j = 1, 2, \dots, nd, \quad (7.3.2)$$

where δ_{kj} is the Kronecker delta function and \mathbf{x}_j is the coordinate of the j -th node.

Now, we replace the population density function u_i by the finite element interpolations u_i^h which is defined by

$$u_i^h(\mathbf{x}, t) = \sum_{k=1}^{nd} \varphi_k(\mathbf{x}) u_{i[k]}(t), \quad (7.3.3)$$

where $u_{i[k]}(t)$ is the k -th nodal value of u_i at time t . We also replace the test function v by the shape functions φ_j . Then the discrete form of (7.3.1) becomes

$$\langle \dot{u}_i^h, \varphi_j \rangle = -\langle D_i \nabla u_i^h, \nabla \varphi_j \rangle + \langle \pi_h [u_i f_i(u_1, u_2, u_3)], \varphi_j \rangle, \quad \text{for all } j = 1, \dots, nd, \quad (7.3.4)$$

$i = 1, 2, 3$, and π_h is the L^2 -projection operator from $L^2(\Omega)$ onto the finite element space, which, for $v \in L^2(\Omega)$, is defined by

$$\langle \pi_h v, \varphi_j \rangle = \langle v, \varphi_j \rangle, \quad \text{for all } j = 1, \dots, nd. \quad (7.3.5)$$

In matrix form, (7.3.4) can be written as

$$\mathbf{M} \dot{\mathbf{u}}_i(t) = D_i \mathbf{K} \mathbf{u}_i(t) + \mathbf{M} \mathbf{u}_i(t) \odot \mathbf{f}_i(\mathbf{u}_1(t), \mathbf{u}_2(t), \mathbf{u}_3(t)), \quad (7.3.6)$$

where $\mathbf{u}_i(t)$ is the vector of nodal values u_i^h at time t , and \odot denotes component-wise product

of vectors. The entries of the mass and the stiffness matrices are respectively given by

$$\mathbf{M}_{jk} = \langle \varphi_j, \varphi_k \rangle, \text{ and } \mathbf{K}_{jk} = \langle \nabla \varphi_j, \nabla \varphi_k \rangle, \quad (j, k = 1, \dots, nd). \quad (7.3.7)$$

By lumping (or multiplying the semi-discrete equations in (7.3.4) by \mathbf{M}^{-1}), and dropping the time dependence, we obtain

$$\dot{\mathbf{u}}_i = D_i \widehat{\mathbf{K}} \mathbf{u}_i + \mathbf{u}_i \odot \mathbf{f}_i(\mathbf{u}_1, \mathbf{u}_2, \mathbf{u}_3), \text{ where } \widehat{\mathbf{K}} = \mathbf{M}^{-1} \mathbf{K}. \quad (7.3.8)$$

Remark 7.3.1.

1. *The advantage of taking $\pi_h[u_i f_i(u_1, u_2, u_3)]$ instead of $u_i^h f_i(u_1^h, u_2^h, u_3^h)$, in the semi-discrete form (7.3.4), is that its coefficient matrix is just the mass matrix \mathbf{M} . Otherwise, the matrix would have been different and its computation would be more complex (as it involves high-order quadrature rules than what is normally needed for the computation of the mass matrix). Nevertheless, this choice does not affect the over all convergence of the finite element approximation.*
2. *The standard C^0 -conforming Galerkin finite element for space discretization is optimal in the sense that if the exact solution is sufficiently smooth, the finite element approximation is $\mathcal{O}(h^{2k})$ in the L^2 -norm, where k is the order of the local polynomial interpolation, for example, $k = 1$ and 2 for the bilinear (Q1) and biquadratic (Q2) elements, respectively.*

The semi-discrete system (7.3.8) together with the initial conditions (7.2.4) define the system of nonlinear ODEs. Temporal integration will be performed using a semi-implicit multistep scheme based on the Crank-Nicholson and Adams-Bashforth methods. In Chapter 4, we have derived these methods as a special case of the Lagrangian based methods (for $\vartheta = 1/2$) for singularly perturbed ODE problems.

7.3.2 Temporal integration

Let $I = [0, T]$ be the interval of interest, and $\{I_n\}_{n=1}^N$ be its uniform partition of non-overlapping subintervals of the form $I_m = [t_{m-1}, t_m]$, $m = 2, 3, \dots, N$ with step-size $\Delta t =$

$t_m - t_{m-1}$.

In this section, we discuss the temporal discretization of (7.3.8) using a second-order semi-implicit technique involving the Crank-Nicholson and Adams-Bashforth methods. From an efficiency requirement point of view, we set up the semi-implicit scheme in stage-by-stage (in staggered) algorithm as follows:

Suppose we have the approximate solutions at t_n and all previous steps, in particular, we have $\{\mathbf{u}_j^{n-1}\}_{j=1}^3$ and $\{\mathbf{u}_j^n\}_{j=1}^3$. Then the Crank-Nicholson and Adam-Bashforth methods read,

$$\left. \begin{aligned} \hat{\mathbf{u}}_i^{n+1/2} &= \frac{1}{2}\mathbf{u}_i^n + \frac{1}{2}\mathbf{u}_i^{n+1}, \\ \tilde{\mathbf{u}}_i^{n+1/2} &= -\frac{1}{2}\mathbf{u}_i^{n-1} + \frac{3}{2}\mathbf{u}_i^n, \end{aligned} \right\} (i = 1, 2, 3). \quad (7.3.9)$$

We want to obtain the solution $\{\mathbf{u}_j^{n+1}\}_{j=1}^3$ at t_{n+1} . To do so, we proceed as follows:

Stage 1: Solve for \mathbf{u}_1^{n+1} from

$$\frac{\mathbf{u}_1^{n+1} - \mathbf{u}_1^n}{\Delta t} = D_1 \widehat{\mathbf{K}} \hat{\mathbf{u}}_1^{n+1/2} + \hat{\mathbf{u}}_1^{n+1/2} \odot \mathbf{f}_1(\hat{\mathbf{u}}_1^{n+1/2}, \tilde{\mathbf{u}}_2^{n+1/2}, \tilde{\mathbf{u}}_3^{n+1/2}). \quad (7.3.10)$$

Having obtained \mathbf{u}_1^{n+1} , we now compute $\hat{\mathbf{u}}_1^{n+1/2}$.

Stage 2: Now, since we have \mathbf{u}_1^{n+1} , we compute $\hat{\mathbf{u}}_1^{n+1/2}$. Then solve for \mathbf{u}_2^{n+1} from

$$\frac{\mathbf{u}_2^{n+1} - \mathbf{u}_2^n}{\Delta t} = D_2 \widehat{\mathbf{K}} \hat{\mathbf{u}}_2^{n+1/2} + \hat{\mathbf{u}}_2^{n+1/2} \odot \mathbf{f}_2(\hat{\mathbf{u}}_1^{n+1/2}, \hat{\mathbf{u}}_2^{n+1/2}, \tilde{\mathbf{u}}_3^{n+1/2}). \quad (7.3.11)$$

Stage 3: We now compute $\hat{\mathbf{u}}_2^{n+1/2}$ and then solve for \mathbf{u}_3^{n+1} from

$$\frac{\mathbf{u}_3^{n+1} - \mathbf{u}_3^n}{\Delta t} = D_3 \widehat{\mathbf{K}} \hat{\mathbf{u}}_3^{n+1/2} + \hat{\mathbf{u}}_3^{n+1/2} \odot \mathbf{f}_3(\hat{\mathbf{u}}_1^{n+1/2}, \hat{\mathbf{u}}_2^{n+1/2}, \hat{\mathbf{u}}_3^{n+1/2}). \quad (7.3.12)$$

Finally, from each of the above stages we obtain a complete solution $\{\mathbf{u}_j^{n+1}\}_{j=1}^3$ at the current time t_{n+1} . The stage-by-stage algorithm mentioned above is linearly-implicit and formally second-order convergent in time. Moreover, updating the linear factor \mathbf{f}_i at stages 2 and 3 based on the already known solutions from stage 1 and 2 may enhance the stability property without additional computational cost.

7.3.3 Stability analysis

Numerical approximation of competitive-diffusion problems is challenging. This is particularly the case in ecological application of competition-diffusion models where spatial mobility (diffusion) is typically very small compared to the rate of interactions between the species. Such problems are characterized by the presence of very small spatial scale as internal layers. In such cases, one of the most critical issues in the numerical approximation of their solutions is the stability of the associated scheme(s).

The implicit-explicit (IMEX) schemes use a high-order explicit scheme for reaction terms and an implicit scheme of same order for the linear diffusion terms, it usually lead to a weakened stability behavior as the dominant term (reaction) is explicit. Hence, in addition to treating the diffusion terms implicitly, the stage-by-stage method outlined in Section 7.3.2 enhances the stability property by using a semi-linearized but high-order scheme based on the Crank-Nicholson and Adams-Bashforth methods for the reaction term.

It is then essential to analyze how the discretization of the reaction term impacts the stability of the proposed numerical scheme. In particular, we analyze how the discrete scheme based on the Crank-Nicholson and Adams-Bashforth methods imitates the behavior of the continuous problem. To this end, we consider the following reduced scalar problem, obtained by ignoring the u_2, u_3 and other diffusion terms, i.e.,

$$\dot{u} = \lambda u(1 - u). \quad (7.3.13)$$

Here, for simplicity, we also assume that $r_1 = a_{11} = -\lambda > 0$, and dropped the subscript 1. The scalar problem (7.3.13) has $u = 0$ and $u = 1$ as equilibrium solutions from which only the former is asymptotically stable. Applying the Crank-Nicholson and Adams-Bashforth semi-linearized scheme to the reduced model (7.3.13) leads to

$$u^{n+1} = G(u^{n-1}, u^n; z), \quad (7.3.14)$$

where

$$G(u^{n-1}, u^n; z) = \frac{1 + \frac{1}{2}z(1 + \frac{1}{2}u^{n-1} - \frac{3}{2}u^n)}{1 - \frac{1}{2}z(1 + \frac{1}{2}u^{n-1} - \frac{3}{2}u^n)} u^n, \quad z = \Delta t \lambda. \quad (7.3.15)$$

A discrete analogy of the equilibrium points of the continuous model (7.3.13) is a fixed point

of its discrete version (7.3.14), that is, find u^* satisfying

$$u^* = G(u^*, u^*; z). \quad (7.3.16)$$

Hence, one of the consistency implications of the discrete scheme is that any equilibrium point is also a fixed point. Remarkably, this is verified since $u^* = 0$ and $u^* = 1$ are also fixed points of the discrete problem.

What remains now is to show that in the discrete sense, these fixed points have similar local stability property as the equilibrium points have in the continuous case. To do this we proceed as follows, since equation (7.3.14) involves nonlinear terms in u^{n-1} and u^n , we take the partial derivatives of the right-hand-side of (7.3.15) and evaluate them at the fixed points. This gives us a and obtain the locally linearized discrete system

$$u^{n+1} = \frac{\partial G}{\partial u^{n-1}} \Big|_{u^{n-1}=u^n=u^*} u^{n-1} + \frac{\partial G}{\partial u^n} \Big|_{u^{n-1}=u^n=u^*} u^n. \quad (7.3.17)$$

For $u^* = 0$, (7.3.17) becomes

$$u^{n+1} = \frac{2+z}{2-z} u^n, \quad (7.3.18)$$

while for $u^* = 1$, it becomes

$$u^{n+1} = \frac{1}{2} z u^{n-1} + \left(1 - \frac{3}{2} z\right) u^n. \quad (7.3.19)$$

Following the standard procedure, we replace ξ^{k+1} for u^{n+k} , for $k = -1, 0, 1$; to obtain the following characteristic polynomials corresponding to the linearized schemes (7.3.18) and (7.3.19):

$$\Pi_0(\xi; z) = \xi^2 - \frac{2+z}{2-z} \xi, \text{ and } \Pi_1(\xi; z) = \xi^2 - \left(1 - \frac{3}{2} z\right) \xi - \frac{1}{2} z. \quad (7.3.20)$$

The stability requirement is that the roots of the characteristic polynomials should lie inside the unit ball centred at the origin of the complex ξ -plane. Hence, as shown in the Figure 7.3.1, the fixed point $u^* = 0$ is unconditionally stable whereas $u^* = 1$ is unconditionally unstable as required.

In addition to the use of semi-linearization of the reaction term, updating each equation successively based on the current time-step solutions of the already solved ones at the same

time further increases the stability even more.

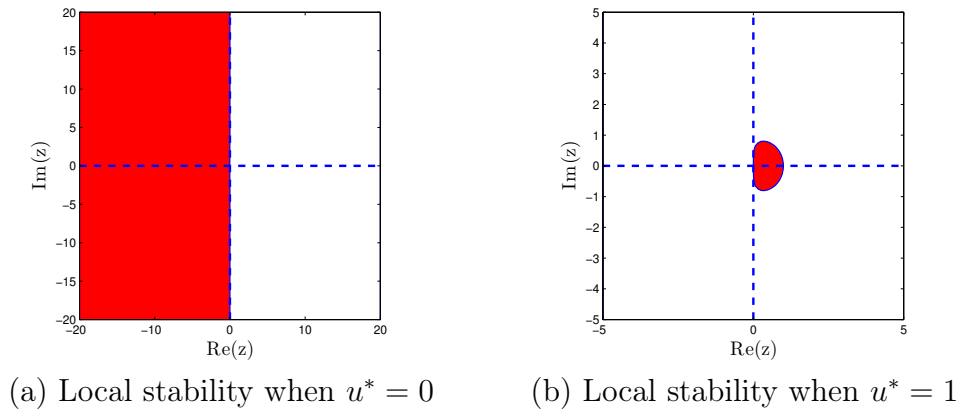


Figure 7.3.1: Stability regions of the semi-linearized scheme applied to the reduced nonlinear problem (7.3.13).



7.4 Numerical results

In this section, we present various numerical results to demonstrate the performance of our proposed schemes in simulating a number of cyclic competition patterns. The nonlinear complex spatio-temporal structures which were recently explored in [20] are presented. These spatio-temporal patterns include droplet-like, band-like, glider-like and regular spiral-like structures each of which corresponds to a parameter set for which $a = 1$, $b = 2$ according to the rescaled system (7.2.5), and with different mobility rates. In all simulations the spatial domain is combined as $\Omega \in [-2, 2] \times [-2, 2]$ with mesh grid 251×251 of Q1 quadrilateral elements are considered, except in the case of strip-like banded patterns as shown in Figure 7.4.2 for which we consider $\Omega \in [-8, 8] \times [-8, 8]$ with mesh grid 291×291 . The time-step length used for all simulation is $\Delta t = 1$. The initial condition is a simple segregation configuration with a single triple-junction at the top-right quarter of the domain with separation angle for each species is $2\pi/3$. The following color code has been used throughout the simulations: green for u_1 , blue for u_2 , and red for u_3 .

We first consider the classical case of cyclic competition patterns as shown in Figure 7.4.1, 7.4.2, and 7.4.3. The shape of the patterns is different depending on the mobility rates of the species.

As shown in Figure 7.4.1, where $\varepsilon_2 = 0.1$ and $\varepsilon_3 = 0.6$ were used, an expanding triangular droplet-like structures with complex patterns inside it is formed. A highly structured coexistence pattern of the three species is emerged towards the left bottom of the sharp wedge. The other type of coexistence pattern as shown in Figure 7.4.2, where $\varepsilon_2 = 0.1$ and $\varepsilon_3 = 0.9$, is a strip-like structure. It starts in the same way as Figure 7.4.1 with the inside appearing irregular coexistence pattern, but as time goes on, the shape diverges from the droplet-like pattern with the inside becoming more regular that involves band-like structures at the left bottom of the envelope. The number of bands increases and the envelope expands as time increases. Figure 7.4.3 shows the simple spiral-like dynamical coexistence pattern with the spiral centring at the initial triple junction. The diffusion coefficients in this case are equal, i.e., $\varepsilon_2 = 1$ and $\varepsilon_3 = 1$. Finally, a conditional cyclic competition of the three species is displayed for the parameter $\alpha = 1.3$ and diffusion coefficients $\varepsilon_2 = 0.55$ and $\varepsilon_3 = 0.5$ in Figure 7.4.4. As shown in this figure, initially it forms a spiral tip from which a droplet shape detached later. The dynamics move in the left corner of the domain in which some of the structure persist for longer time and some disappear faster. At last only one species survive in a longer time as shown in the last sub-figure of Figure 7.4.4.

7.5 Summary and discussion

In this chapter, we developed a high-order semi-implicit multistep schemes based on the Crank-Nicholson and Adams-Bashforth methods for the temporal discretization in conjunction with C^0 -conforming finite element method for the nonlinear singularly perturbed three species competition-diffusion model in two-dimensional spatial domain. The semi-implicit scheme is second-order accurate in time and has a very good stability property. Moreover, the proposed scheme has better stability property than IMEX-based methods for singularly competitive-diffusion problems in which the diffusion is significantly less dominant than the reaction term. Several types of two-dimensional spatio-temporal patterns, arising from the fact that the species have different mobilities, are simulated to demonstrate the performance of the proposed scheme.

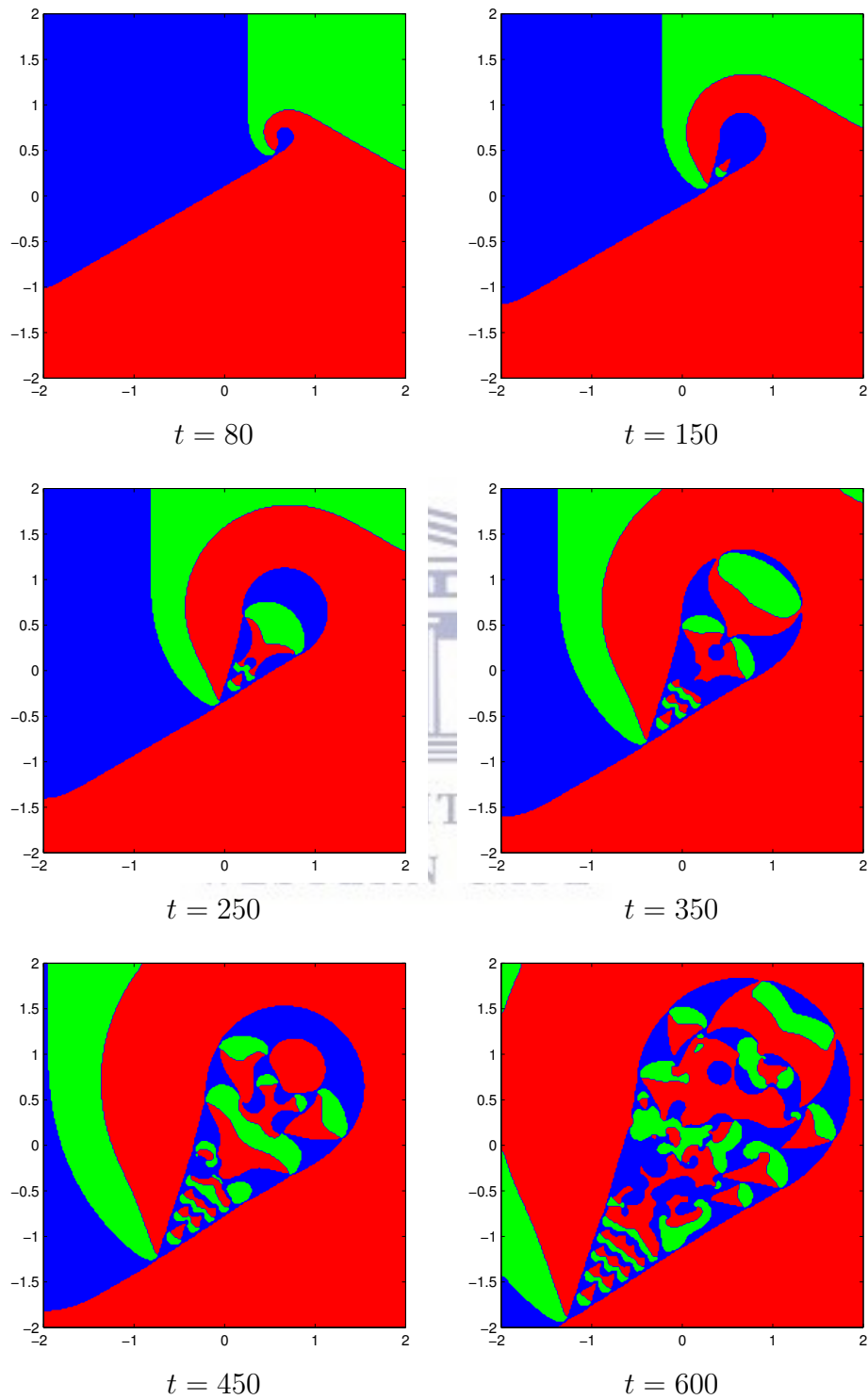


Figure 7.4.1: Droplet-like pattern of the three species at different times. Parameters used for the simulation are $a = 1$, $b = 2$, $\varepsilon_2 = 0.1$, $\varepsilon_3 = 0.6$, and $\Delta t = 1$.

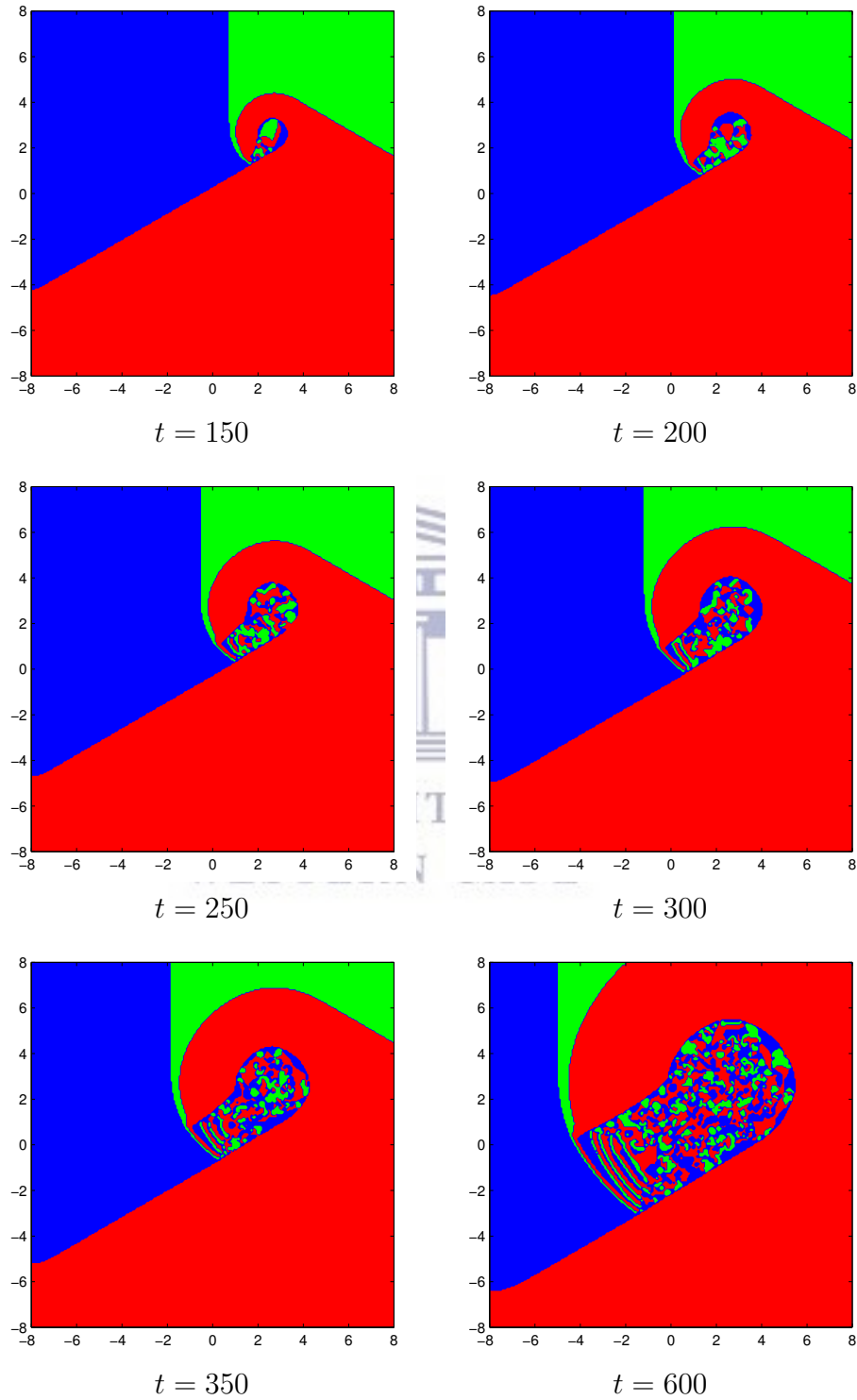


Figure 7.4.2: Strip-like pattern in the dynamics of the three species at different times. Parameters used for the simulation are $a = 1$, $b = 2$, $\varepsilon_2 = 0.1$, $\varepsilon_3 = 0.9$, and $\Delta t = 1$.

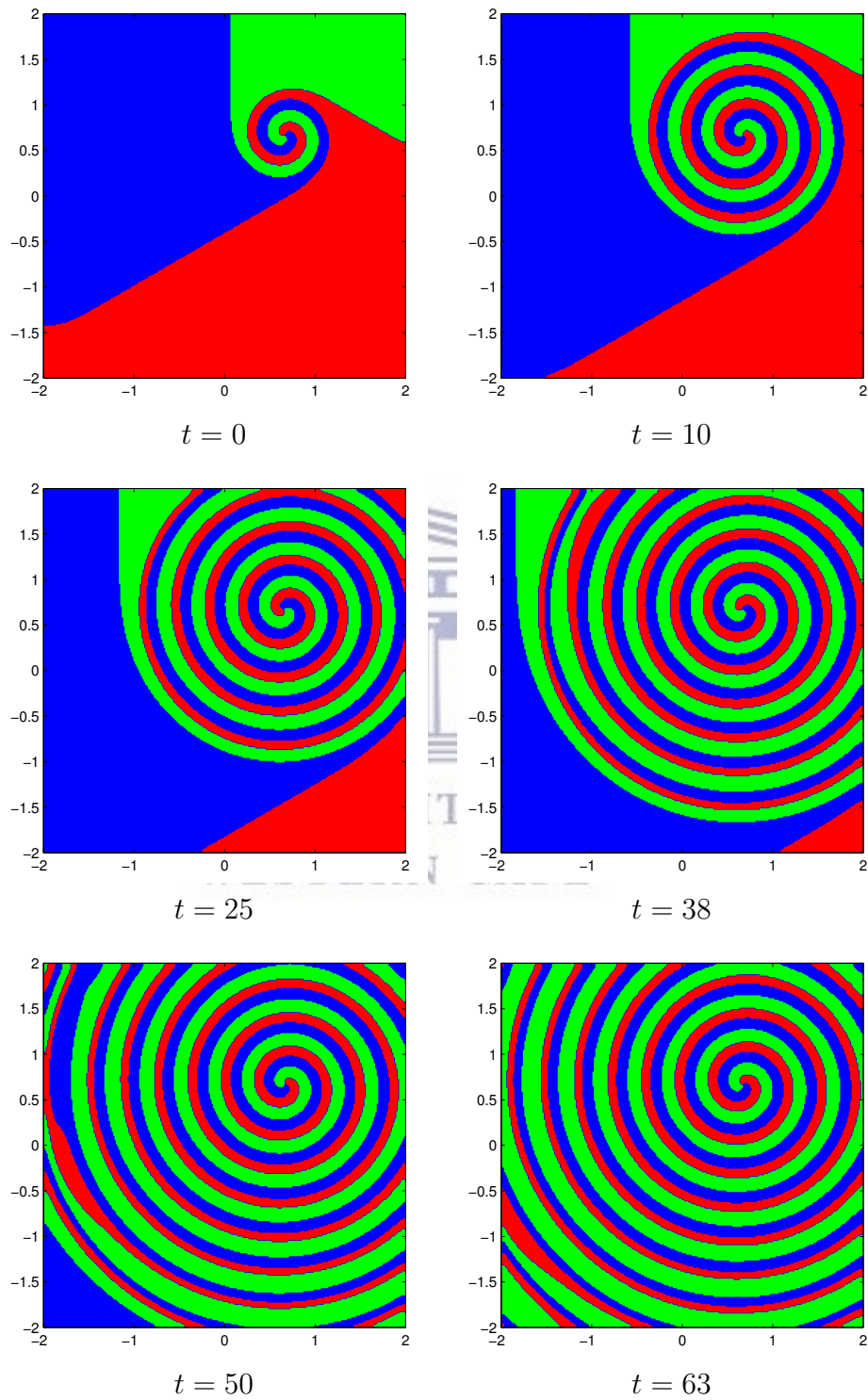


Figure 7.4.3: Spiral-like pattern in the dynamics of the three species at different times. Parameters used for the simulation are $a = 1$, $b = 2$, $\varepsilon_2 = 1.0$, $\varepsilon_3 = 1.0$, and $\Delta t = 1$.

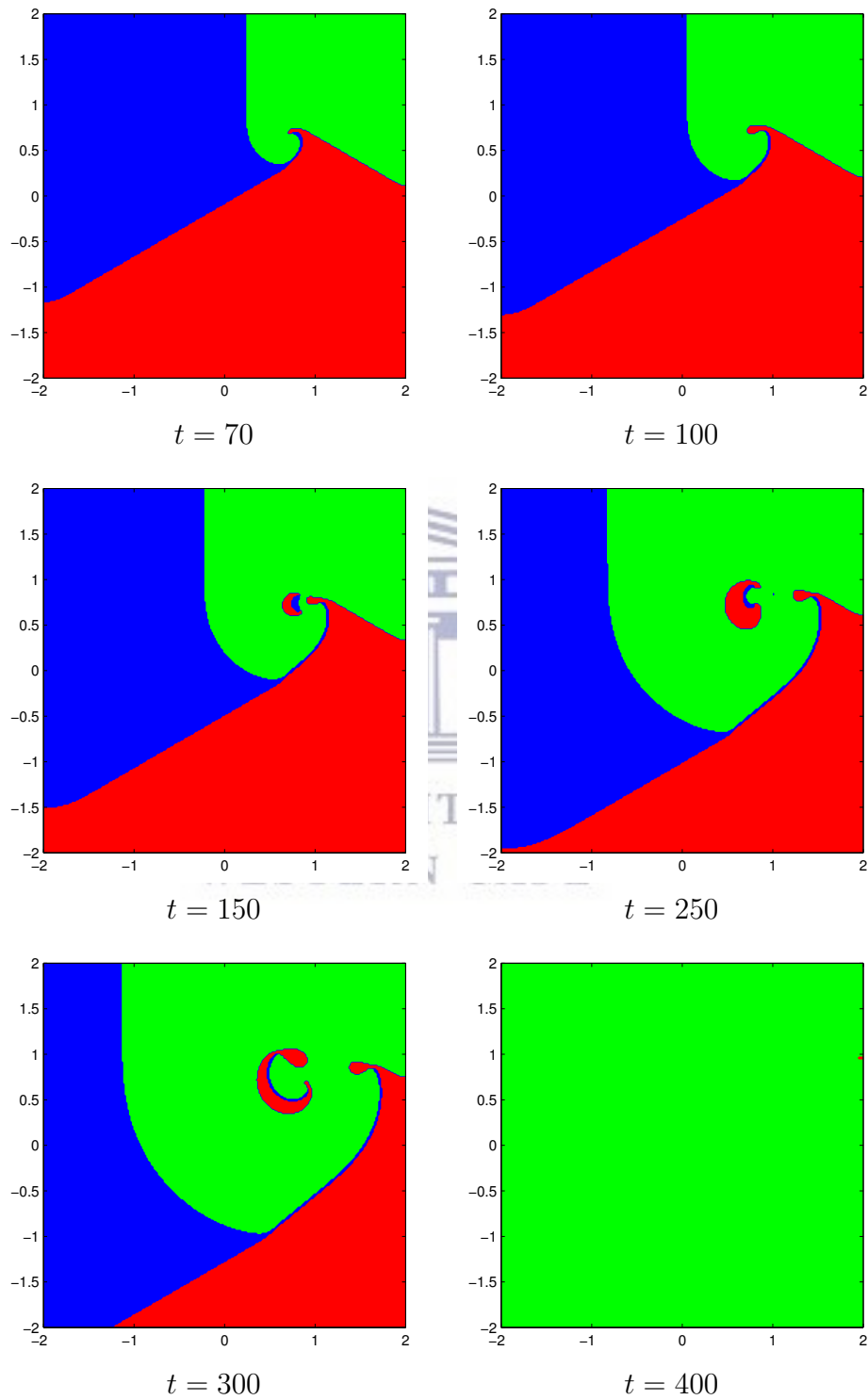
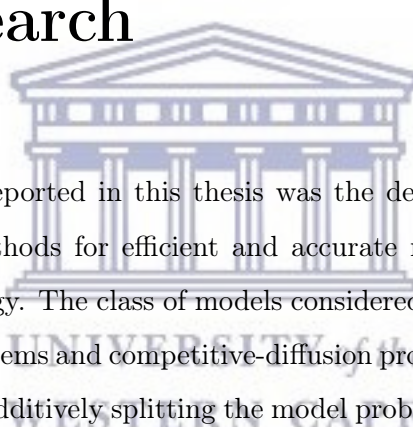


Figure 7.4.4: Glider-like patterns of the three species at various times. Parameters used for the simulation are $a = 1$, $b = 2$, $\alpha = 1.3$, $\varepsilon_2 = 0.55$, $\varepsilon_3 = 0.5$, and $\Delta t = 1$.

Chapter 8

Concluding remarks and scope for future research



The focus of the work reported in this thesis was the design, analysis and implementation of various numerical methods for efficient and accurate numerical simulation of multiscale problems arising in ecology. The class of models considered include (slow-fast) singularly perturbed predator-prey systems and competitive-diffusion problems. Various numerical methods based on the method of additively splitting the model problems according to their temporal or spatial scales and treating each partition differently have been explored. For comparison purpose, related monolithic methods that treat the full problem in a single framework have also been developed. A careful analysis of these solution algorithms, required for their numerical realization applied to complex and nonlinear problems of multiscale nature, were performed.

In Chapter 2, we considered a singularly perturbed ecological model describing a slow-fast system in which two slow predators compete for one fast prey species in a quite diversified time response. The system exhibits coexistence of all three species in stable limit cycles for some range of parameters. A detailed discussion on the formulation of a class of multirate schemes based on an extrapolation algorithm has been presented. A discrete counterpart of the local stability analysis of the fixed points of the discrete problems has also been investigated. Through the use of these numerical schemes, it was demonstrated that computation time was reduced by a large factor compared to the use of the corresponding single-rate schemes. It was also obtained that, through long time simulations of problems corresponding to parametric

values for which the solutions exhibit strong relaxation-oscillation character, the multirate schemes compared favourably against the corresponding single-rate schemes. Furthermore, extensive numerical experiments were carried out to demonstrate that the multirate schemes outperform the corresponding single-rate schemes in terms of both accuracy and efficiency.

In Chapter 3, we dealt with the numerical simulations of the nonlinear slow-fast model considered in Chapter 2. Although, the primary focus was on a multirate fractional-step θ -method (denoted FSTS), the derivation also included other related methods such as monolithic θ -method and fractional-step mixed implicit-explicit methods (denoted, respectively, as MTS and FSMIMEX). To treat the nonlinearities arising as the result of the implicit part of these schemes, two iterative algorithms, namely Jacobian-free Newton-Krylov (JFNK) methods and Anderson's Acceleration (AA) fixed point iterative algorithm were considered. While FSMIMEX compared favourably against FSTS and MTS in terms of efficiency, it is at best conditionally stable as it partly consist of explicit algorithms. Numerical experiments have shown that AA method almost outperformed the JFNK method in terms of efficiency and convergence. Long time simulation experiments, for initial values corresponding to solution orbits of relaxation-oscillations type in the phase space, have also revealed that the FSTS method replicated these solutions reliably well compared to the MTS and FSMIMEX, as well as the well-known MATLAB's built-in functions such as `ode15` and `ode23`.

An eco-evolutionary system of singularly perturbed-type that describes a dynamical system consisting of one fast predator evolutionary trait and a slow predator-prey system of one predator and two prey species was considered in Chapter 4. A theoretical analysis of the model using geometric singular perturbation theory has shown the existence of two-parametric family of periodic orbits between the ecological and evolutionary dynamics. For the numerical solutions of the model problem, a class of high-order linear multistep implicit-explicit methods based on the temporal Lagrange interpolation has been developed in an abstract manner. It was revealed that standard methods such as BDF and Crank-Nicholson, Leap-Frog and Adams-Bashforth methods and their IMEX combinations can be obtained as special cases by simply changing the values of a parameter used in the formulation. Zero- and absolute-stability of the methods were analyzed by applying the standard approach in which the methods are applied to a scalar test problem with its eigenvalue used as a stiffness parameter. Based on the observation made in Chapter 3, the AA fixed point iterative algorithm has been con-

joined with the IMEX methods to treat nonlinearities. Various numerical experiments have been conducted to test the convergence and stability behaviours of the methods as well as to demonstrate their capabilities in capturing the desirable solution features such as periodic orbits reliably well. However, experience has shown that these methods perform well when the separation of time-scales between the fast and the slow components is small to moderate.

For a highly stable numerical solutions of singularly perturbed and strongly nonlinear problems such as the one considered in Chapter 4, a multirate collocation method based on the piecewise Lagrangian interpolation of the unknowns corresponding to the fast and slow components has been developed in Chapter 5. Convergence of the scheme which is of the same order as the underlying Lagrange interpolation of the unknowns has been proved. Remarkably, linear stability analysis demonstrated the superior stability property of the method compared to most of the conventional one-step or multistep methods used in the literature or to those discussed in this work. Extensive numerical results have been presented in the form of tables and figures to demonstrate the performance of the multirate collocation method. It has been observed that the proposed scheme outperformed the corresponding single-rate schemes in accurately approximating singularly perturbed problems with very wide separation of time-scale difference. However, it should be noted that the implementation of the method can be highly complex for rather high-order of interpolation and high number of internal steps (micro-steps) needed for the piecewise interpolation of the fast unknown. Nevertheless, this can be facilitated by constructing the corresponding derivative matrix a priori.

In Chapter 6 and 7, we considered the numerical solutions of a three-species fully-coupled competitive-diffusion system, in two space dimensions, characterized by the presence of a spatial scale such that species diffusion (mobility) occur much more slowly than the rate of competition (interaction) of species. high-order semi-implicit multistep schemes have been developed for the large nonlinear system of ODEs which are resulted in the space discretization using a high-order conforming FEM. In Chapter 6 it was considered that the involved species have the same mobility rates, where as, in Chapter 7 they have different diffusion rates. In both cases, the solutions exhibit various interesting spatio-temporal coexistence patterns and transient regimes with complex internal boundary layers. The semi-implicit multistep temporal integrations used in Chapter 6 were based on the Lagrange interpolation of the unknowns, whereas, that of Chapter 7 was based the Crank-Nicholson and Adams-Bashforth

methods. In both cases, it was shown that these numerical schemes perform better than the corresponding IMEX schemes in terms of stability. This is the consequence of high-order linearization of the dominant and nonlinear competition part. In contrast, the competition part is typically treated explicitly in IMEX schemes resulting in a less stability property. Various numerical tests have been performed in both cases to replicate those spatio-temporal coexistence patterns. It was observed that these schemes numerically simulated the problems considered reliably well.

Finally, in the following we list a number of avenues which need further exploration and study.

- Even though, the multirate extrapolation methods discussed in Chapter 2 have very good accuracy and stability properties when applied to singularly perturbed problems, their derivations were only limited to first-order approximations. Therefore, extension of these methods to high-order convergent ones is one of the recommended extension.
- Since the IMEX methods developed in Chapter 3 are essentially single-rate as a single step-size is employed for both fast and slow components, they are less favourable for singularly perturbed problems with very small time-scale parameter ε . We are exploring including some multirate features into these IMEX methods in order to obtain asymptotically preserving behaviour (i.e., the numerical solutions behave in the same way as the exact ones as ε approaches zero including the limiting case).
- The multirate collocation methods formulated in Chapter 4 are fully implicit and involve determining a multiple number of unknowns simultaneously per macro-step. This is a challenge in terms of computational efficiency. For this, it is essential to use some preconditioning mechanisms such as multigrid methods.
- The conforming finite element methods used in Chapter 6 and 7 can be extended in order to add some adaptivity features in space. A Discontinuous Galerkin (DG) methods can also be another alternative extension.
- Extension of the schemes for competition-diffusion problems to three space dimension is an area which needs future investigation. Programming environment that will facilitate

the implementation of the above mentioned finite element extensions is a major requirement. Thus we are assessing the possibility of open-source programming environments.

- Proposed numerical methods in this thesis can also be extended to solve high-order fractional order differential equations.



UNIVERSITY *of the*
WESTERN CAPE

Bibliography

- [1] P.A. Abrams and H. Matsuda, Positive indirect effects between prey species that share predators, *Ecology* **77** (2) (1996), 610-616.
- [2] P.A. Abrams and H. Matsuda, Prey adaptation as a cause of predator-prey cycles, *Evolution* **51** (6) (1997), 1742-1750.
- [3] M.W. Adamson and A.Y. Morozov, Revising the role of species mobility in maintaining biodiversity in communities with cyclic competition, *Bulletin of Mathematical Biology* **74** (9) (2012), 2004-2031.
- [4] L.J.S. Allen, *An Introduction to Mathematical Biology*, Prentice Hall, NJ, 2007.
- [5] J.F. Andrus, Stability of a multi-rate method for numerical integration of ode's, *Computers & Mathematics with Application* **25** (2) (1993), 3-14.
- [6] J.F. Andrus, Numerical solution of systems of ordinary differential equations separated into subsystems, *SIAM Journal on Numerical Analysis* **16** (4) (1979), 605-611.
- [7] R.A. Armstrong and R. McGehee, Competitive exclusion, *The American Naturalist* **115** (2) (1980), 151-170.
- [8] U.M. Ascher, S.J. Ruuth and B.T. Wetton, *Implicit-explicit methods for time-dependent PDE's*, University of British Columbia, Department of Computer Science, 1993.
- [9] U.M. Ascher, S.J. Ruuth and B.T. Wetton, Implicit-explicit methods for time-dependent partial differential equations, *SIAM Journal on Numerical Analysis* **32** (3) (1995), 797-823.

- [10] A. Bartel and M. Günther, A multirate W-method for electrical networks in state-space formulation, *Journal of Computational and Applied Mathematics* **147** (2) (2002), 411-425.
- [11] A. Bellen, One-step collocation for delay differential equations, *Journal of Computational and Applied Mathematics* **10** (3) (1984), 275-283.
- [12] M.A. Berrill, K.T. Clarno, S.P. Hamilton and R.P. Pawlowski, Evaluation of Coupling Approaches, *Consortium for Advanced Simulation of LWRs, Oak Ridge National Laboratory*, CASL Milestone Report: CASL-U-2014-0081-000, 2014.
- [13] B.J.M. Bohannan and R.E. Lenski, Linking genetic change to community evolution: Insights from studies of bacteria and bacteriophage, *Ecology Letters* **3** (4) (2000), 362-377.
- [14] S. Boscarino, P.G. LeFloch, and G. Russo, High-order asymptotic-preserving methods for fully non linear relaxation problems, *SIAM Journal on Scientific Computing* **36** (2) (2014), A377-A395.
- [15] S. Boscarino, F. Filbet and G. Russo, High Order Semi-implicit Schemes for time dependent partial differential equations, *SIAM Journal on Scientific Computing* **68** (3) (2016), 975-1001.
- [16] F. Brauer, C. Castillo-Chavez and C. Castillo-Chavez, *Mathematical models in population biology and epidemiology*, New York: Springer, 2001.
- [17] F. Brauer and C. Castello-Chavez, *Mathematical Models in Population Biology and Epidemiology*, Springer, 2012.
- [18] H. Brunner, *Collocation Methods for Volterra Integral and Related Functional Differential Equations*, Cambridge University Press, Cambridge, 2004.
- [19] X. Cia and Z. Cen, Numerical Simulation Technique for Nonlinear Singularly Perturbed Predator-Prey Reaction Diffusion System in Biomathematics, *Natural Computation, ICNC*, **5** (2007), 44-48.

- [20] A. Cangiani, E.H. Georgoulis, A.Y. Morozov and O.J. Sutton, Revealing new dynamical patterns in a reaction-diffusion model with cyclic competition via a novel computational framework, *Proceedings of the Royal Society A*, **474** (**2213**) (2018), pp. 20170608.
- [21] C.-C. Chen, L.-C. Hung, M. Mimura and D. Ueyama, Exact travelling wave solutions of three-species competition-diffusion systems, *Discrete & Continuous Dynamical Systems-Series B* **17**(8) (2012), 2653-2669.
- [22] J.C. Chrispell, V.J. Ervin and E.W. Jenkins, A fractional step θ -method for convection-diffusion problems, *Journal of Mathematical Analysis and Applications* **333** (**1**) (2007), 204-218.
- [23] X. Cia and Z. Cen, Numerical Simulation Technique for Nonlinear Singularly Perturbed Predator-Prey Reaction Diffusion System in Biomathematics, *Natural Computation, 2007. ICNC 2007*. **5** IEEE (2007), 44-48.
- [24] E.M. Constantinescu and A. Sandu, Multirate timestepping methods for hyperbolic conservation laws, *Journal of Scientific Computing* **33** (**3**) (2007), 239-278.
- [25] E.M. Constantinescu and A. Sandu, On extrapolated multirate methods, *Progress in Industrial Mathematics at European Conference on Mathematics for Industry (ECMI) 2008*, Springer-Verlag, Berlin, (2010), 341-347.
- [26] E.M. Constantinescu and A. Sandu, Extrapolated implicit-explicit time stepping, *SIAM Journal on Scientific Computing* **31** (**6**) (2010), 4452-4477.
- [27] E.M. Constantinescu and A. Sandu, Extrapolated multirate methods for differential equations with multiple time scales, *Journal of Scientific Computing* **56** (**1**) (2013), 28-44.
- [28] L. Contento, M. Mimura and M. Tohma, Two-dimensional travelling waves arising from planar front interaction in a three-species competition-diffusion system, *Japan Journal of Industrial and Applied Mathematics* **32** (**3**) (2015), 707-747.
- [29] M.H. Cortez and S.P. Ellner, Understanding rapid evolution in predator-prey interactions using the theory of fast-slow dynamical systems, *The American Naturalist* **176** (**5**) (2010), E109-E127.

- [30] S. Duminil and H. Sadok, Reduced rank extrapolation applied to electronic structure computations, *Electronic Transactions on Numerical Analysis* **38** (2011), 347-362.
- [31] D.R. Durran and P.N. Blossey, Implicit-explicit multistep methods for fast-wave-slow-wave problems, *Monthly Weather Review* **140** (4) (2012), 1307-1325.
- [32] R. Durrett and S. Levin, Spatial aspects of interspecific competition, *Theoretical Population Biology* **53** (1) (1998), 30-43.
- [33] W. Eckhaus, Relaxation oscillations including a standard chase on French ducks, *Lecture Notes in Mathematics* **985** (1983), 449-494.
- [34] S.A. Edalatpanah and E. Abdolmaleki, A new collocation method for systems of nonlinear fredholm integral equations, *Applied Mathematics and Physics* **2** (1) (2014), 15-18.
- [35] S.I. Ei, R. Ikota and M. Mimura, Segregating partition problem in competition-diffusion systems, *Interfaces and Free Boundaries* **1** (1) (1999), 57-80.
- [36] S.P. Ellner, M.A. Geber and N.G. Hairston, Does rapid evolution matter? Measuring the rate of contemporary evolution and its impacts on ecological dynamics, *Ecology Letters* **14** (6) (2011), 603-614.
- [37] C. Engstler and C. Lubich, Multirate extrapolation methods for differential equations with different time scales, *Computing* **58** (2) (1997), 173-185.
- [38] H. Fang and Y. Saad, Two classes of multiseant methods for nonlinear acceleration, *Numerical Linear Algebra with Applications* **16** (3) (2009), 197-221.
- [39] N. Fenichel, Geometric singular perturbation theory for ordinary differential equations, *Journal of Differential Equations* **31** (1) (1979), 53-98.
- [40] F. Filbet, and S. Jin, A class of asymptotic-preserving schemes for kinetic equations and related problems with stiff sources, *Journal on Computational Physics* **229** (20) (2010), 7625-7648.
- [41] R.A. Fisher, The wave of advance of advantageous genes, *Annals of Human Genetics* **7** (4) (1937), 355-369.

- [42] A.D. Fitt, J. Norbury, H. Ockendon and E. Wilson, *Progress in Industrial Mathematics at ECMI 2008*, Springer Science & Business Media **15**, 2010.
- [43] J.E. Flaherty and W. Mathon, Collocation with polynomial and tension splines for singularly-perturbed boundary value problems, *SIAM Journal on Scientific and Statistical Computing* **1** (1980), 260-289.
- [44] J. Frank, W. Hundsdorfer and J.G. Verwer, On the stability of implicit-explicit linear multistep methods, *Applied Numerical Mathematics* **25** (2) (1997), 193-205.
- [45] M. Frean and R. Abraham, Rock-scissors-paper and the survival of the weakest, *Proceedings of the Royal Society of London B: Biological Sciences* **268** (1474) (2001), 1323-1327.
- [46] G.F. Fussmann, S.P. Ellner, K.W. Shertzer and N.G. Hairston, JR., Crossing the Hopf bifurcation in a live predator-prey system, *Science* **290** (5475) (2000), 1358-1360.
- [47] G.F. Fussmann, M. Loreau and P.A. Abrams, Eco-evolutionary dynamics of communities and ecosystems, *Functional Ecology* **21** (3) (2007), 465-477.
- [48] M. Gasca and T. Sauer, Polynomial interpolation in several variables, *Advances in Computational Mathematics* **12** (4) (2000), 377-410.
- [49] W.C. Gear, Multirate methods for ordinary differential equations, *Tech. Report Rept. No. UIUCDCS-F-74-880*, Univ. of Illinois, Urbana Champaign (USA). Department of Computer Science, 1974.
- [50] C.W. Gear, Numerical solution of ordinary differential equations: is there anything left to do?, *SIAM review* **23** (1) (1981), 10-24.
- [51] W.C. Gear and D.R. Wells, Multirate linear multistep methods, *BIT Numerical Mathematics* **24** (4) (1984), 484-502.
- [52] S.A.H. Geritz, E. Kisdi, G. Meszina and J.A.J. Metz, Evolutionarily singular strategies and the adaptive growth and branching of the evolutionary tree, *Evolutionary Ecology* **12** (1) (1998), 35-57.

- [53] M.E. Gilpin, Limit cycles in competition communities, *The American Naturalist* **109** (965) (1975), 51-60.
- [54] F.X. Giraldo, J.F. Kelly and E.M. Costantinescu, Implicit–explicit formulations of a three-dimensional nonhydrostatic unified model of the atmosphere (NUMA) *SIAM Journal on Scientific Computing* **35** (5) (2013), B1162-B1194.
- [55] F.X. Giraldo, M. Restelli, and M. Láuter, Semi-implicit formulations of the Navier–Stokes equations: application to nonhydrostatic atmospheric modeling, *SIAM Journal on Scientific Computing* **32** (6) (2010), 3394-3425.
- [56] J.-M. Ginoux, B. Rossetto and J.-L. Jamet, Chaos in a three dimensional Volterra–Gause model of predator–prey type, *International Journal of Bifurcation and Chaos* **15** (5) (2005), 1689-1708.
- [57] W. Gragg and H. Stetter, Generalized multistep predictor-corrector methods, *Journal of the Association for Computing Machinery* **11** (2) (1964), 188-209.
- [58] P.R. Grant and B.R. Grant, Unpredictable evolution in a 30-year study of Darwin’s finches, *Science* **296** (5568) (2002), 707-711.
- [59] A.B. Gumel, K.C. Patidar and R.J. Spiteri, Asymptotically consistent nonstandard finite difference methods for solving mathematical models arising in population biology, *Advances in the Applications of Nonstandard Finite Difference Schemes*, R.E. Mickens (ed.), World Scientific, Singapore, (2005), pp. 385-421.
- [60] M. Günther, P. Rentrop, Multirate row methods and latency of electric circuits, *Applied Numerical Mathematics* **13** (1-3) (1993), 83-102.
- [61] M. Günther, A. Kvaernø and P. Rentrop, Multirate partitioned Runge-Kutta methods, *BIT Numerical Mathematics* **41** (3) (2001), 504-514.
- [62] N.G. Hairston, JR., W. Lampert, C.E. Cáceres, C.L. Holtmeier, L.J. Weider, U. Gaedke, J. M. Fischer, J. A. Fox and D. M. Post, Lake ecosystems: rapid evolution revealed by dormant eggs, *Nature* **401** (6752) (1999), p. 446.

- [63] N.J. Higham and N. Strabić, Anderson acceleration of the alternating projections method for computing the nearest correlation matrix, *Numerical Algorithms* **72** (2016), 1021-1042.
- [64] I. Higuera, J.M. Mantas, and T. Roldán, Design and implementation of predictors for additive semi-implicit Runge–Kutta methods, *SIAM Journal on Scientific Computing* **31** (3) (2009), 2131-2150.
- [65] M.W. Hirsch, Differential equations and convergence almost everywhere of strongly monotone semiflows, *Contemp. Math* **17** (1983), 267-285.
- [66] G. Hek, Geometric singular perturbation theory in biological practice, *Journal of Mathematical Biology* **60** (3) (2010), 347-386.
- [67] E. Houstis, A collocation method for systems of nonlinear ordinary differential equations, *Journal of Mathematical Analysis and Applications* **62** (1) (1978), 24-37.
- [68] W. Hundsdorfer and S.J. Ruuth, IMEX extensions of linear multistep methods with general monotonicity and boundedness properties, *Journal of Computational Physics* **225** (2) (2007), 2016-2042.
- [69] W. Hundsdorfer and V. Savcenco, Analysis of a multirate theta-method for stiff ODEs, *Applied Numerical Mathematics* **59** (3) (2009), 693-706.
- [70] A. Hone, On non-standard numerical integration methods for biological oscillators, *In Workshop on Complex Systems Modelling and Simulation*, Luniver Press, (2009), pp. 45-66.
- [71] L.E. Jones, L. Becks, S.P. Ellner, N.G.J. Hairston, T. Yoshida and G.F. Fussmann, Rapid contemporary evolution and clonal food web dynamics, *Philosophical Transactions of the Royal Society of London B: Biological Sciences* **364** (1523) (2009), 1579-1591.
- [72] M. Jia-qi and H. Xiang-lin, Nonlinear predator-prey singularly perturbed Robin Problems for reaction diffusion systems, *Journal of Zhejiang University-Science A* **4** (5) (2003), 511-513.

- [73] F. Jopp, B. Breckling and H. Reuter, *Modelling Complex Ecological Dynamics*, Springer-Verlag, Berlin, 2011.
- [74] Y. Kan-On and M. Mimura, Predation-mediated coexistence and segregation structures, *Studies in Mathematics and its Applications* **18** (1986), 129-155.
- [75] Y. Kan-On and M. Mimura, Singular perturbation approach to a 3-component reaction-diffusion system arising in population dynamics, *SIAM Journal on Mathematical Analysis* **29** (6) (1998), 1519-1536.
- [76] C.T Kelley, *Solving Nonlinear Equations with Newton's Method*, SIAM, Philadelphia, 2003.
- [77] J.K. Kevorkian and J.D. Cole, *Multiple Scale and Singular Perturbation Methods*, Springer Science & Business Media, 2012.
- [78] A.I. Khibnik and A.S. Kondrashov, Three mechanisms of red queen dynamics, *Proceedings of the Royal Society of London B: Biological Sciences* **264** (1384) (1997), 1049-1056.
- [79] J. Kim and M. Parviz, Application of a fractional-step method to incompressible Navier-Stokes equations, *Journal of Computational Physics* **59** (2) (1985), 308-323.
- [80] K. Kishimoto, Instability of non-constant equilibrium solutions of a system of competition-diffusion equations, *Journal of Mathematical Biology* **13** (1) (1981), 105-114.
- [81] K. Kishimoto, The diffusive Lotka-Volterra system with three species can have a stable non constant equilibrium solution, *Journal of Mathematical Biology* **16** (1) (1982), 103-112.
- [82] K. Kishimoto and H.F. Weinberger, The spatial homogeneity of stable equilibria of some reaction-diffusion systems on convex domains, *Journal of Differential Equation* **58** (1) (1985), 15-21.
- [83] D.A. Knoll and D.E. Keyes, Jacobian-free Newton-Krylov methods: a survey of approaches and application, *Journal of Computational Physics* **193** (2) (2004), 357-397.

- [84] A.L. Koch, Competitive coexistence of two predators utilizing the same prey under constant environmental conditions, *Journal of Theoretical Biology* **44** (2) (1974), 387-395.
- [85] A.N. Kolmogorov, I. Petrovsky and N. Piskunov, Investigation of the equation of diffusion combined with increasing of the substance and its application to a biology problem, *Moscow University Mathematics Bulletin* **1** (6) (1937), 1-25.
- [86] A. Kopf, W. Paul and B. Dunweg, Multiple time step integrators and momentum conservation, *Computer Physics Communications* **101** (1-2) (1997), 1-8.
- [87] M. Krupa and P. Szmolyan, Relaxation oscillation and canard explosion, *Journal of Differential Equations* **174** (2) (2001), 312-368.
- [88] C. Kuehn, *Multiple Time Scale Dynamics*, Springer-Verlag, Berlin, 2015.
- [89] A. Kværnø and P. Rentrop, Low order multirate Runge-Kutta methods in electric circuit simulation, Technical report 2/1999, Norwegian University of Science and Technology, Trondheim, Norway, 1999.
- [90] A. Kværnø, Stability of multirate Runge-Kutta schemes, *International Journal of Differential Equations and Applications* (1) (2000), 97-105.
- [91] P.A. Lagerstrom, *Matched Asymptotic Expansions: Ideas and Techniques*, Springer Science & Business Media, 2013.
- [92] J.D. Lambert, *Computational Methods in Ordinary Differential Equations*, John Wiley and Sons, London, 1973.
- [93] Y. Lenbury, Singular perturbation analysis of a model for a predator-prey system invaded by a parasite, *Biosystems* **39** (3) (1996), 251-262.
- [94] R.J. LeVeque, *Finite Difference Methods for Ordinary and Partial Differential Equations: Steady State and Time-dependant Problems*, SIAM, Philadelphia, 2007.
- [95] A.J. Lotka, Undamped oscillations derived from the law of mass action, *Journal of the American Chemical Society* **42** (8) (1920), 1595-1599.

- [96] A.J. Lotka, Elements of Physical Biology, *Science Progress in the Twentieth Century (1919-1933)* **21** (82) (1926), 341-343.
- [97] P.A. Lott, H.F. Walker, C.S. Woodward and U.M. Yang, An accelerated Picard method for nonlinear systems related to variably saturated flow, *Advances in Water Resources* **38** (2012), 92-101.
- [98] W. Lue, D. Xiao and Y. Yi, Relaxation oscillations in a class of predator-prey systems, *Journal of Differential Equations* **188** (1) (2003), 306-331.
- [99] H. Matano and M. Mimura, Pattern formation in competition-diffusion systems in non-convex domains, *Publications of the Research Institute for Mathematical Sciences* **19** (3) (1983), 1049-1079.
- [100] R.M. May, Limit cycles in predator-prey communities, *Science* **177** (4052) (1972), 900-902.
- [101] R.M. May and W.J. Leonard, Nonlinear aspects of competition between three species, *SIAM Journal of Applied Mathematics* **29** (2) (1975), 243-253.
- [102] R.M. May, *Stability and complexity in model ecosystems*, Princeton university press, 2001.
- [103] R. McGehee and R.A. Armstrong, Some mathematical problems concerning the ecological principle of competitive exclusion, *Journal of Differential Equations* **23** (1) (1977), 30-52.
- [104] B.J. McGill, B.J. Enquist, E. Weiher and M. Westoby, Rebuilding community ecology from functional traits, *Trends in ecology & evolution* **21** (4) (2006), 178-185.
- [105] R.I. McLachlan and G.R.W. Quispel, Splitting methods, *Acta Numerica* **11** (2002), 341-434.
- [106] T.M. Merlis and S. Khatiwala, Fast dynamical spin-up of ocean general circulation models using Newton-Krylov methods, *Ocean Modelling* **21** (3) (2008), 97-105.

- [107] W.D. Mergia and K.C. Patidar, Efficient simulation of a slow-fast dynamical system using multirate finite difference schemes, *Quaestiones Mathematicae* **39** (5) (2016), 689-714.
- [108] W.D. Mergia, K.C. Patidar, Semi-implicit linear multistep methods for three species Lotka-Volterra-type competition-diffusion system in ecology, *Submitted for Publication*, 2019
- [109] W.D. Mergia and K.C. Patidar, Fractional-step θ -method for solving singularly perturbed problem in ecology, *Advances in Computational Mathematics* **44** (3) (2018), 645-671.
- [110] W.D. Mergia and K.C. Patidar, High-order linear multistep methods for strongly-nonlinear slow-fast eco-evolutionary model, *Submitted for publication*, 2019.
- [111] R.E. Mickens, *Advances in the Applications of Nonstandard Finite Difference Schemes*, World Scientific, Singapore, 2005.
- [112] M. Mimura, and M. Tohma, Dynamic coexistence in a three-species competition-diffusion system, *Ecological Complexity* **21** (2015), 215-232.
- [113] M. Mimura and P.C. Fife, A 3-component system of competition-diffusion system, *Hiroshima Mathematical Journal* **16** (1986), 189-207.
- [114] E. Mishchenko, *Differential equations with small parameters and relaxation oscillations*, Springer Science & Business Media, 2013.
- [115] J. Mo and R. Tang, Nonlinear singularly perturbed predator-prey reaction diffusion systems, *Applied Mathematics-A Journal of Chinese Universities* **19** (1) (2004), 57-66.
- [116] S. Muratori and S. Rinaldi, Remarks on competitive coexistence, *SIAM Journal on Applied Mathematics* **49** (5) (1989), 1462-1472.
- [117] D.J. Murray, *Mathematical Biology: I. An Introduction*, Springer-Verlag, Berlin, 2002.
- [118] J.D. Murray, *Mathematical Biology*, Springer-Verlag, Berlin, 1989.

- [119] H.A. Obaid, R. Ouifki and K.C. Patidar, An unconditionally stable non standard finite difference method applied to a mathematical model of HIV infection, *International Journal of Applied Mathematics and Computer Science* **23 (2)** (2013), 357-372.
- [120] A. Okubo, *Diffusion and Ecological Problems: Mathematical Models*, Springer-Verlag, Berlin, 1989.
- [121] M.R. Owen and M.A. Lewis, How predation can slow, stop or reverse a prey invasion, *Bulletin of Mathematical Biology* **63 (4)** (2001), 655-684.
- [122] F. Pelletier, T. Clutton-Brock, J. Pemberton, S. Tuljapurkar and T. Coulson, The evolutionary demography of ecological change: Linking trait variation and population growth, *Science* **315 (5818)** (2007), 1571-1574.
- [123] J.B. Perot, An analysis of the fractional step method, *Journal of Computational Physics* **108 (1)** (1993), 51-58.
- [124] S. Petrovskii, K. Kawasaki, F. Takasu and N. Shigesada, Diffusive waves, dynamical stabilization and spatiotemporal chaos in a community of three competitive species, *Japan Journal of Industrial and Applied Mathematics* **18 (2)** (2001), 459-481.
- [125] S.H. Piltz, F. Veerman, P.K. Maini and M.A. porter, A predator-2 prey fast-slow dynamical system for rapid predator evolution, *SIAM Journal on Applied Dynamical Systems* **16 (1)** (2017), 54-90.
- [126] T. Reichenbach, M. Mobilia and E. Frey, Mobility promotes and jeopardizes biodiversity in rock-paper-scissors games, *Nature* **448 (7157)** (2007), 1046-1049.
- [127] P. Rentrop, Partitioned runge-kutta methods with stiffness detection and step-size control, *Numerische Mathematik* **47 (4)** (1985), 545-564.
- [128] J.R. Rice, Split Runge-Kutta methods for simultaneous equations, *Journal of Research of the National Bureau of Standards-B. Mathematics and Mathematical Physics* **64B(3)** (1960), 151-170.

- [129] G. Rodríguez-Gómez, P. González-Casanova and J. Martínez-Carballido, Computing general companion matrices and stability regions of multirate methods, *International Journal for Numerical Methods in Engineering* **61** (2) (2004), 255-273.
- [130] L.I.W. Roeger, Local Stability of Euler's and Kahan's Methods, *Journal of Difference Equations and Applications* **10** (6) (2004), 601-614.
- [131] M.L. Rosenzweig and R.H. MacArthur, Graphical representation and stability conditions of predator-prey interactions, *The American Naturalist* **97** (895) (1963), 209-223.
- [132] A. Rückgauer and W. Schiehlen, Simulation of modular dynamic systems, *Mathematics and Computers in Simulation* **46** (5) (1998), 535-542.
- [133] J. Sand and S. Skelboe, Stability of backward Euler multirate methods and convergence of waveform relaxation, *BIT Numerical Mathematics* **32** (2) (1992), 350-366.
- [134] V. Savcenco, Comparison of the asymptotic stability properties for two multirate strategies, *Journal of Computational and Applied Mathematics* **220** (1-2) (2008), 508-524.
- [135] V. Savcenco, Construction of a multirate RODAS method for stiff ODEs, *Journal of Computational and Applied Mathematics* **225** (2) (2009), 323-337.
- [136] W.E. Schiesser and G.W. Griffiths, *A Compendium of Partial Differential Equation Models: Method of Lines Analysis with Matlab*, Cambridge University Press, Cambridge, 2009.
- [137] W.E. Schiesser, *Numerical Method of Lines: Integration of Partial Differential Equations*, Academic Press, Inc., San Diego, 1991.
- [138] T. W. Schoener, The newest synthesis: understanding the interplay of evolutionary and ecological dynamics, *Science* **331** (6016) (2011), 426-429.
- [139] J. Schütz and K. Kaiser, A new stable splitting for singularly perturbed ODEs, *Applied Numerical Mathematics* **107** (2016), 18-33.
- [140] L. Sewalt, A. Doelman, H.G.E. Meijer, V. Rottschäfer and A. Zagaris, Tracking pattern evolution through extended center manifold reduction and singular perturbations, *Physica D: Nonlinear Phenomena* **298** (2015), 48-67.

- [141] N. Shigesada and K. Kawasaki, *Biological Invasions: Theory and Practice*, Oxford University Press, Oxford, 1997.
- [142] Y. Shimazu, K. Sugiyama, T. Kojima and E. Tomida, Some problems in ecology oriented environmentology, Terrestrial environmentology II, *The Journal of Earth Sciences, Nagoya University* **20** (1972) (1972), 31-89.
- [143] S.S. Shome, E.J. Haug and L.O. Jay, Dual-rate integration using partitioned runge-kutta methods for mechanical systems with interacting subsystem, *Mechanics Based Design of Structures and Machines* **32** (3) (2004), 253-282.
- [144] S. Skelboe, The numerical solution of stiff systems of ordinary differential equations by multirate integration methods, *Report. No. ECR-150, ElektronikCentralen, Venlighedsvej* **24** (1984).
- [145] S. Skelboe and P.U. Andersen, Stability properties of backward Euler multirate formulas, *SIAM Journal on Scientific and Statistical Computing* **10** (5), (1984) 1000-1009.
- [146] S. Skelboe, Stability properties of backwards differentiation multirate formulas, *Applied Numerical Mathematics* **5** (1) (1989), 151-160.
- [147] P. Smereka, Semi-implicit level set methods for curvature and surface diffusion motion, *Journal on Scientific Computing* **19** (1) (2003), 439-456.
- [148] T. Solcia and P. Masarati, Multirate simulation of complex multibody systems, *In ECCOMAS Thematic Conference*, 2011.
- [149] D.W. Stephens and J.R. Krebs, *Foraging Theory*, Princeton University Press, Princeton, NJ, 1986.
- [150] G. Strang, On the construction and comparison of difference schemes, *SIAM Journal on Numerical Analysis* **5** (3) (1968), 506-517.
- [151] Y. Yasuhiro, Global dynamical properties of Lotka-Volterra systems, World Scientific (1996) p. 302.
- [152] E. Teramoto, K. Kawasaki and N. Shigesada, Switching effect of predation on competitive prey species, *Journal of Theoretical Biology* **79** (3) (1979), 303-315.

- [153] E.J.W. ter Maten and M. Günther, Minisymposium multirate time integration for multiscaled systems, *Progress in Industrial Mathematics at ECMI 2008*, Springer (2010), pp. 317-318.
- [154] A. Toth, C.T. Kelly, S. Slattery, S. Hamilton, K. Clarno and R. Pawlowski, Analysis of Anderson acceleration on a simplified neutronics/thermal hydraulics system, *ANS MC2015 - Joint International Conference on Mathematics and Computation (M&C), Supercomputing in Nuclear Applications (SNA) and Monte Carlo (MC) Method*, Nashville, Tennessee, 2015. 34 Pages.
- [155] M.E. Tuckerman and B.J. Berne, Molecular dynamics in systems with multiple time scales: Systems with stiff and soft degrees of freedom and with short and long range forces, *Journal of Chemical Physics* **95** (11) (1991), 8362-8364.
- [156] J.M. Varah, Stability restrictions on second order, three level finite difference schemes for parabolic equations, *SIAM Journal on Numerical Analysis* **17** (2) (1980), 300-309.
- [157] A. Verhoeven, A. El Guennouni, E.J.W. Ter Maten and R.M.M. Mattheij, A general compound multirate method for circuit simulation problems, *Scientific Computing in Electrical Engineering*, Springer (2006) pp. 143-149.
- [158] J. Verwer, Convergence and component splitting for the Crank-Nicolson–Leap-Frog integration method, *Modelling, Analysis and Simulation [MAS]* (E0902) (2009), 1-15.
- [159] P.K. Vijalapura, J. Stain and S. Govindjee, Fractional step methods for index-1 differential-algebraic equations, *Journal of Computational Physics* **203** (1) (2005), 305-320.
- [160] V. Volterra, Variazioni e fluttuazioni del numero d'individui in specie animali conviventi, *Memorie Accademia Nazionale Dei Lincei* **6** (2) (1926), 31-113.
- [161] V. Volterra, Variations and fluctuations of the number of individuals in animal species living together, *ICES Journal of Marine Science* **3** (1) (1928), 3-51.
- [162] H.F. Walker, C.S. Woodward and U.M. Yang, An accelerated fixed-point iteration for solution of variably saturated flow. In: J. Carrera, X.S. Villa and D.F. Garcia (eds.),

- Proceedings of the XVIII International Conference on Computational Methods in Water Resources (CMWR 2010)*, Int. Center for Numerical Methods in Engineering, Barcelona, Spain, (2010), pp. 216-223.
- [163] H.F. Walker and P. Ni, Anderson acceleration for fixed-point iterations, *SIAM Journal on Numerical Analysis* **49** (4) (2011), 1715-1735.
- [164] R. Weiner, M. Arnold, P. Rentrop and K. Strehmel, Partitioning strategies in Runge-Kutta type methods, *IMA Journal of Numerical Analysis* **13** (2) (1993), 303-319.
- [165] D.R. Wells, Multirate linear multistep methods for the solution of systems of ordinary differential equations, *Department of Computer Science, Illinois, Technical Report UIUCDCS-R-82-1093*, 1982.
- [166] T. Yoshida, L.E. Jones, S.P. Ellner, G.F. Fussmann and N.G.J. Hairston JR, Rapid evolution drives ecological dynamics in a predator-prey system, *Nature* **424** (6946) (2003), 303-306.
- [167] S. Zibaei and M. Namjoo, A nonstandard finite difference scheme for solving three-species food chain with fractional-order Lotka-Volterra model, *Iranian Journal of Numerical Analysis and Optimization* **6** (1) (2016), 53-79.
- [168] H. Zhang, A. Sandu and S. Blaise, High order implicit-explicit general linear methods with optimized stability regions, *SIAM Journal on Scientific Computing* **38** (3) (2016), A1430-A1453.
- [169] X. Zhong, Additive semi-implicit Runge-Kutta methods for computing high-speed nonequilibrium reactive flows, *Journal on Computational Physics* **128** (1) (1996), 19-31.